ABSTRACT

Investigating the Chemistry of the 9-Borataphenanthrene Anion

Tyler A. Bartholome, Ph.D.

Mentor: Caleb D. Martin, Ph.D.

Boron-containing analogues of unsaturated hydrocarbons exhibit a diverse array of reactivity modes that can be exploited for the synthesis of other more complex boron-containing compounds. Examples of such analogues include boroles, analogous with the cyclopentadienyl cation; boratabenzenes, analogous with benzene; and borataalkenes, analogous with olefins. A dibenzo-fused borole, 9-phenyl-9-borafluorene, was shown to undergo insertion of one or two carbene units upon reaction with trimethylsilyldiazomethane to produce six- or seven-membered nonaromatic boracycles. The six-membered product was found to undergo deprotonation to form the first example of a 9-borataphenanthrene anion, which exhibits structural features characteristic of boratabenzenes and borataalkenes. Its boratabenzene-like character was demonstrated through η^6 complexation with chromium(0), while its borataalkene-like character was demonstrated through protonation, *C*-methylation with iodomethane, B=C hydroboration with pinacolborane, and η^2 complexation with gold(I). The B=C bond at the 9- and 10-positions of the 9-borataphenanthrene anion was also shown to undergo a broad range of hydrofunctionalization reactivity, including hydroalkylation, hydroarylation,

hydroalkynylation, hydroamination, hydroalkoxylation, and hydration. The central BC_5 ring was demonstrated to form η^6 complexes with rhodium(I), iridium(I), and iron(II) centers. The wide array of boratabenzene- and borataalkene-like reactivity modes indicates the promising potential of 9-borataphenanthrene anions as reagents for inorganic and organic synthesis.

Investigating the Chemistry of the 9-Borataphenanthrene Anion

by

Tyler A. Bartholome, B.S.

A Dissertation

Approved by the Department of Chemistry and Biochemistry

_____

Patrick J. Farmer, Ph.D., Chairperson

Submitted to the Graduate Faculty of
Baylor University in Partial Fulfillment of the
Requirements for the Degree
of

Doctor of Philosophy

Approved by the Dissertation Committee

_____

Caleb D. Martin, Ph.D., Chairperson

_____

Patrick J. Farmer, Ph.D.

_____

Brian M. Lindley, Ph.D.

_____

John L. Wood, Ph.D.

_____

Kenneth S. Befus, Ph.D.

Accepted by the Graduate School

August 2021

_____

J. Larry Lyon, Ph.D., Dean

Page bearing signatures is kept on file in the Graduate School.

TABLE OF CONTENTS

LIST OF FIGURES

LIST OF TABLES

LIST OF SCHEMES

LIST OF NEW COMPOUNDS REPORTED

Compound	Structure	Page number for characterization details
2.8	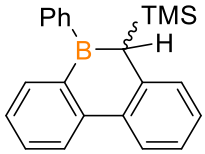	18
2.9	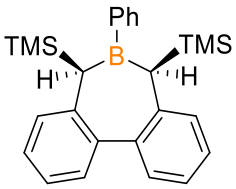	19
3.4	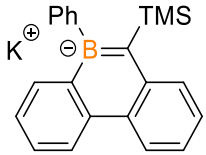	37
3.5	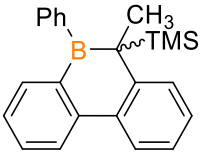	38
3.6a	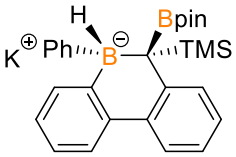	39
3.6b	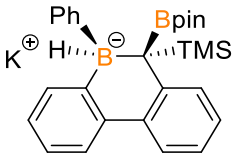	40

4.6	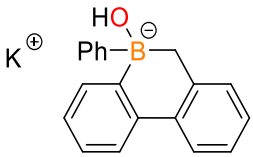	-
5.4a	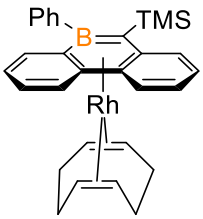	72
5.4b	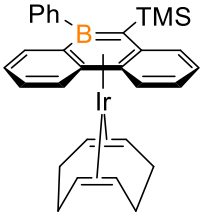	73
5.5	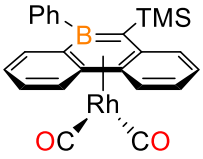	74
5.7	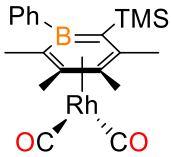	75
5.8	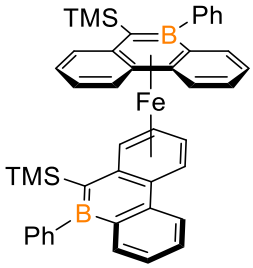	-

5.9	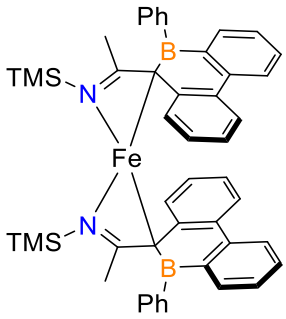	-
5.10	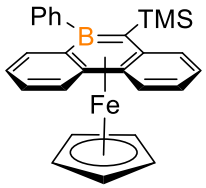	-

ACKNOWLEDGMENTS

I would like to begin by thanking my committee members, Drs. Caleb D. Martin, Patrick J. Farmer, Brian M. Lindley, John L. Wood, and Kenneth S. Befus. I greatly appreciate the time and effort that you have invested in evaluating my dissertation. I am especially grateful to my research advisor, Dr. Caleb D. Martin, whose leadership and guidance have enabled me to accomplish the work described in this document.

I would next like to thank all of my fellow members of the Martin group, current and former, for the support you have given me throughout my time at Baylor. Graduate school is by no means an easy thing to navigate, and I have only been able to do so because of the help and encouragement with which you have provided me. I am especially grateful to Dr. Sam Yruegas and Kristen R. Bluer for early mentorship during my first year of graduate school. The knowledge of laboratory techniques and chemistry in general with which you provided me has continued to serve me well throughout the entirety of my degree.

I am grateful to all of my relatives and friends outside of the Martin group for the lifetime of encouragement and guidance with which you have provided me. Without your aid, it is unlikely that I would have ever made the choice to attend graduate school in the first place. I am thankful to everyone who has served as an educator to me in any capacity. The knowledge you shared with me and the skills you taught me have been instrumental in enabling me to accomplish the work necessary for the completion of my degree.

I am grateful to Drs. Kevin K. Klausmeyer and Sam Yruegas for assistance with X-ray crystallography and Dr. Xianzhong Xu for assistance with $^{1}H\{^{11}B\}$ and $^{11}B\{^{1}H\}$ NMR spectroscopy. I am grateful to all who were coauthors with me on the manuscripts included in this dissertation: Dr. Caleb D. Martin, Kristen R. Bluer, Jesse J. Martinez, and computational collaborators Aishvaryadeep Kaur, Dr. David J. D. Wilson, and Dr. Jason L. Dutton. I am grateful to Katherine Rojales for the preparation of the reagent $Ir_2Cl_2(cod)_2$ used in Chapter Five of this dissertation. I am grateful to Baylor University for a Presidential Fellowship.

Soli Deo gloria.

DEDICATION

To the One who deserves a dedication more than anyone else.

"But God forbid that I should glory, save in the cross of our Lord Jesus Christ, by whom the world is crucified unto me, and I unto the world." – Galatians 6:14

CHAPTER ONE

Introduction

1.1 Boron-Containing Analogues of Unsaturated Hydrocarbons

Unsaturated hydrocarbyl functionalities, such as alkenes and benzene rings, are ubiquitous in the fields of organic and inorganic synthesis. Materials with unique physical and chemical properties can be obtained by replacement of a carbon center with boron or replacement of a C=C unit with an isoelectronic boron-containing unit such as B-N.[1-6] Examples of compounds that illustrate this principle are boroles, boratabenzenes, and borataalkenes (Figure 1.1). Boroles and boratabenzenes consist of cyclic conjugated π-systems and can be viewed as boron-containing analogues of the cyclopentadienyl cation and benzene, respectively.[4, 7-12] Borataalkenes consist of acyclic π-systems and can be viewed as boron-containing analogues of olefins.[13-16] These three key classes of compounds have found utility in a wide variety of applications in recent decades.

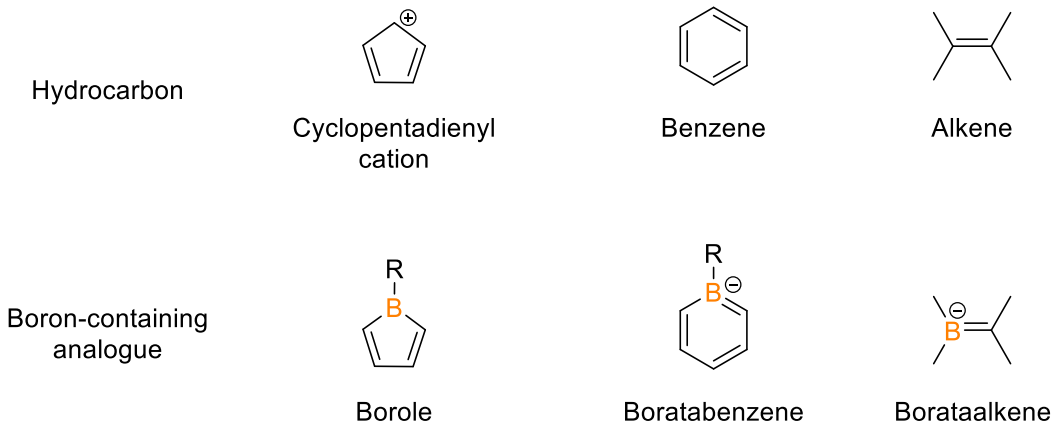

Figure 1.1. Unsaturated hydrocarbon species and their boron-containing analogues.

1.2 Boroles

Boroles, antiaromatic BC_4 heterocycles, can be viewed as neutral boron-containing analogues of the antiaromatic cyclopentadienyl cation.[4, 7, 11-12] The first monocyclic borole, pentaphenylborole (**1.1**), was synthesized in 1969 by Eisch and coworkers using two different routes.[7] The first consisted of transmetallation of 1,4-dilithio-1,2,3,4-tetraphenylbutadiene (**1.2**) with $PhBBr_2$, while the second consisted of transmetallation of 1,1-dimethyl-2,3,4,5-tetraphenylstannole (**1.3**) with $PhBCl_2$ (Scheme 1.1). Recent decades have seen numerous advances in borole research, with a variety of reactivity modes having been explored.[2, 4, 17-27] In particular, pentaphenylborole has been demonstrated to undergo a diverse set of ring expansion reactions to form aromatic and nonaromatic heterocycles, including oxygen- and sulfur-atom insertion,[25-26] carbene insertion,[19] nitrene and phosphinidene insertion,[2, 28-29] and 1,2-dipole insertion.[20-21] These insertion reactivity modes stem from the antiaromaticity of the BC_4 ring and lability of the endocyclic B-C bonds, which render boroles highly reactive.[4] The butadiene backbone of pentaphenylborole has also been demonstrated to act as a diene in Diels-Alder reactions with alkynes and olefins.[7, 30] Selected examples of pentaphenylborole reactivity are depicted in Scheme 1.2. Other less sterically hindered boroles, including 1-(diisopropylamino)borole and 1-phenyl-2,3,4,5-tetramethylborole, have also been prepared and exist as Diels-Alder dimers in contrast with the monomeric pentaphenylborole.[31-33] Such dimeric borole species have been demonstrated to be capable of many of the same modes of reactivity as pentaphenylborole, including Diels-Alder reactivity and ring expansion to form aromatic and nonaromatic boracycles.[30, 32, 34] In these reactions, elevated temperatures are necessary to “crack” the dimer.

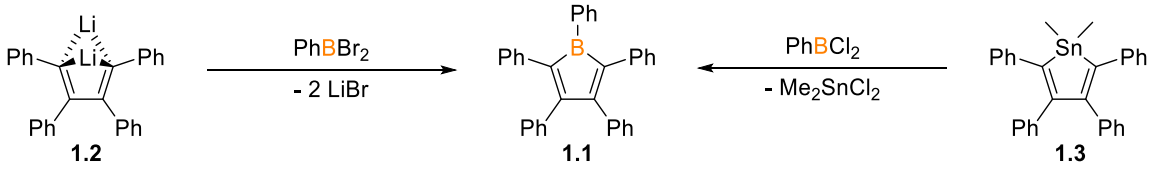

Scheme 1.1. Synthetic routes to pentaphenylborole.

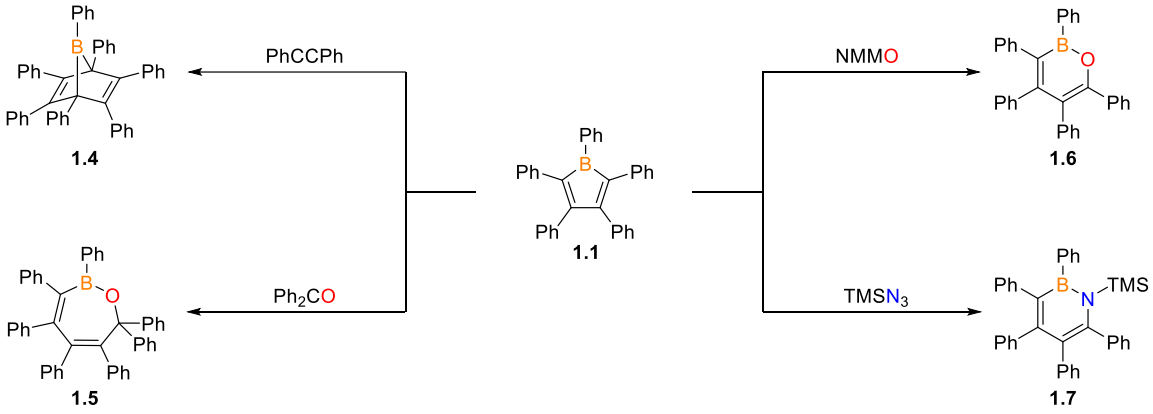

Scheme 1.2. Selected examples of pentaphenylborole reactivity (NMMO = *N*-methylmorpholine-*N*-oxide).

Although several types of fused polycyclic boroles are known, perhaps the most noteworthy are 9-borafluorenes, which consist of a central borole ring with two fused benzene rings.[35] The first 9-borafluorenes were synthesized by Köster and Benedikt in 1963 *via* thermolytic ring closing of boranes bearing 2-biphenylyl substituents (Scheme 1.3).[36] In recent years, 9-borafluorenes have been shown to undergo much of the same ring expansion reactivity as monocyclic boroles to form dibenzo-fused six- and seven-membered boracycles.[37-39] As in monocyclic boroles, the empty p orbital at boron renders 9-borafluorenes Lewis acidic, and the chemistry of 9-borafluorene Lewis acid-base adducts has been studied extensively.[35, 37, 40-45] Applications of 9-borafluorenes are broad in scope

and include fluorescent materials,[43, 46-48] molecular and ion sensors,[49-51] and thermochromic materials.[44]

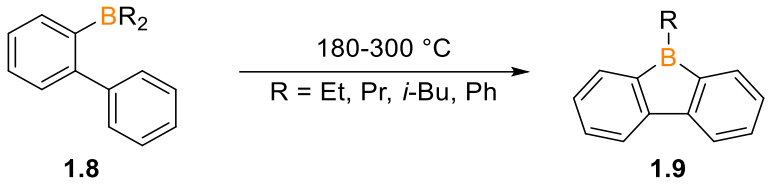

1.8 **1.9**

Scheme 1.3. Synthesis of 9-borafluorenes *via* ring closing of 2-biphenylylboranes.

1.3 Boratabenzenes

Boratabenzenes, anionic BC_5 heteroarenes, are isoelectronic analogues of benzene in which a C=C unit has been replaced by $[B=C]^-$.[8-10] Boratabenzenes have been known since the synthesis of the first boratabenzene transition-metal complex by Herberich and coworkers in 1970.[52] This complex was prepared by the reaction of cobaltocene with $PhBBr_2$ to produce intermediate **1.11**, which was then treated with $SnBr_4$ to produce the cationic boratabenzene/cyclopentadienide sandwich complex (**1.12**, Scheme 1.4). The first free alkali metal boratabenzene salt, lithium 1-phenylboratabenzene (**1.15a**), was synthesized one year later by Ashe and Shu.[8] This synthesis consisted of transmetallation of a 1,4-dihydrostannabenzene (**1.13**) with $PhBBr_2$ to form a 1,4-dihydroborabenzene (**1.14**), which was then deprotonated with *t*-BuLi to produce the lithium boratabenzene salt. In the decades since these early discoveries, boratabenzenes have been studied extensively as ligands, generally hexahaptic, in a wide variety of metal complexes.[8-9, 52-92] Because boratabenzenes are anionic and contain a cyclic 6-electron π-system, they are capable of serving as effective replacements for the cyclopentadienyl anion in sandwich and half-sandwich complexes.[57, 68-69, 88-91, 93] Such complexes are often prepared by reactions of

alkali metal boratabenzene salts with transition metal halides or other labile metal species.[9, 65, 76, 89] Selected examples of alkali metal boratabenzene reactivity are depicted in Scheme 1.5. The lithium boratabenzene salts **1.15** react with $ZrCl_4$ to produce the bis(boratabenzene)dichlorozirconium complexes **1.16**, which can be viewed as boron-containing analogues of zirconocene dichloride.[67-68] Similarly, the reactions of boratabenzene salts **1.15** with $FeCl_2$ produce the bis(boratabenzene)iron complexes **1.17**, which are boron-containing analogues of ferrocene.[57] The sodium salt of 1-methylboratabenzene reacts with $Cr(CO)_3(NH_3)_3$ to produce the anionic half-sandwich complex **1.18**.[62] Metal complexes of boratabenzenes have been applied in a variety of fields, but perhaps most notably in catalysis. Several zirconium(IV) bis(boratabenzene) complexes (including **1.16**) have been demonstrated to act as effective precatalysts for the polymerization of ethylene.[9, 67-70] In recent years, boratabenzene/cyclooctatetraenide sandwich complexes of erbium(III) have been demonstrated to act as single-ion magnets,[90] while a rhodium(I) phosphidoboratabenzene complex was demonstrated to act as an effective precatalyst for olefin hydrogenation.[91]

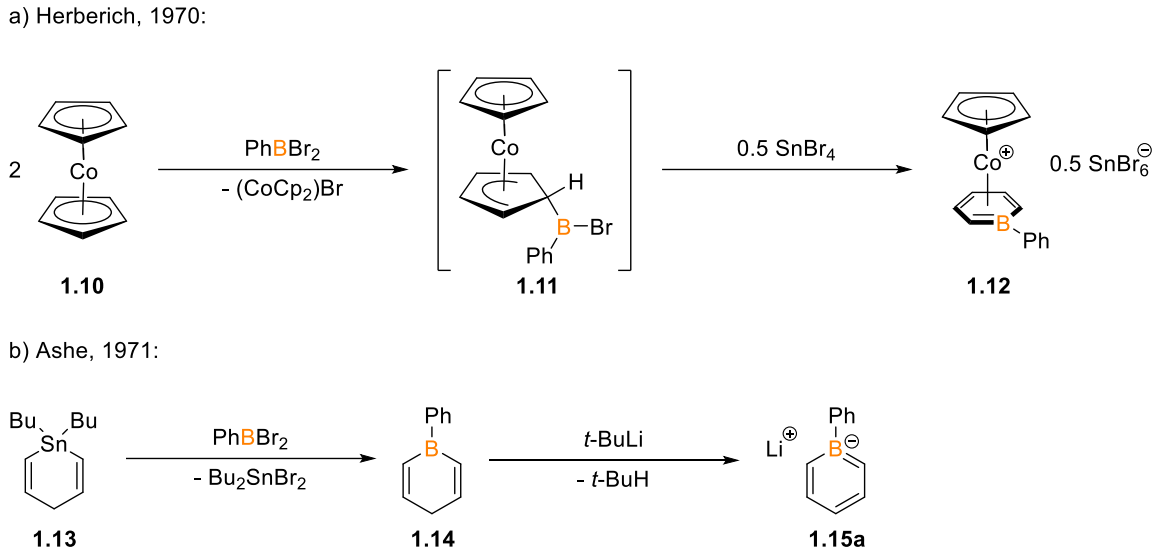

Scheme 1.4. a) Synthesis of a boratabenzene-containing Co(III) mixed sandwich complex and b) synthesis of lithium 1-phenylboratabenzene.

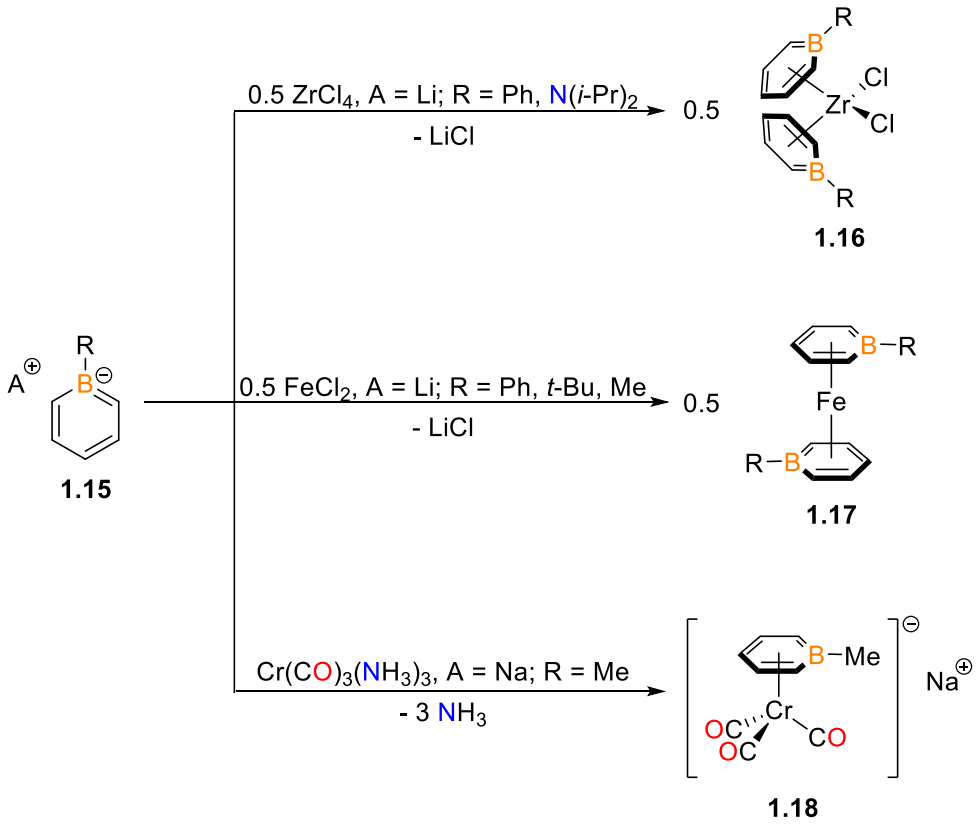

Scheme 1.5. Selected examples of alkali metal boratabenzene reactivity.

1.4 Borataalkenes

Borataalkenes, anionic boron-containing olefin analogues, consist of a $[B=C]^-$ system containing two π-electrons.[13-16] Borataalkenes have been known since 1972, when the first borataalkene was synthesized by Rathke and Kow *via* deprotonation of 9-methyl-9-borabicyclo[3.3.1]nonane (**1.19**) with lithium 2,2,6,6-tetramethylpiperidide (LiTMP, Scheme 1.6).[94] The resulting species **1.20** was described as a boron-stabilized carbanion, and the carbanionic nature was proven through a series of reactions including deuteronation with D_2O, *C*-alkylation with *n*-butyl bromide, and conversion of cyclohexanone to methylenecyclohexane. In contrast with boratabenzenes, for which research has primarily focused on metal complexes, borataalkene metal complexes are quite rare, with only a few known examples.[13-14, 95] However, borataalkenes have been shown to be effective reagents for a wide variety of organic transformations; this utility was studied extensively in the 1980s by Pelter and coworkers.[96-99] Selected examples of this work are depicted in Scheme 1.7. Reactions of lithium dimesitylboron methylidenide (**1.21**) with alkyl or benzylic halides resulted in alkylation at the borataalkene carbon to produce neutral dimesityl-substituted boranes **1.22**.[99] Reactions of borataalkenes with epoxides followed by oxidation with $NaOH/H_2O_2$ resulted in the formation of 1,3-diols.[98] Perhaps the most notable mode of borataalkene reactivity, however, is the "boron-Wittig" reaction in which borataalkenes react with aldehydes and ketones to produce alkenes with the elimination of borinate salts.[97, 100-101] The formation of the alkene product proceeds through an anionic 1,2-oxaboretanide intermediate (**1.24**), which in some cases can be isolated.[100-101] Overall, the variety of transformations observed for borataalkenes makes them promising as reagents in organic synthesis.

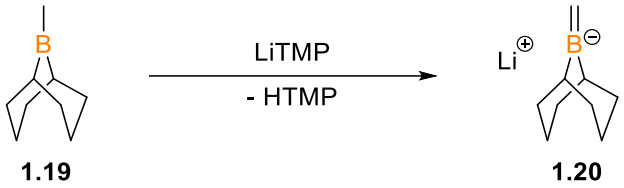

Scheme 1.6. Deprotonation of 9-methyl-9-borabicyclo[3.3.1]nonane to produce a borataalkene.

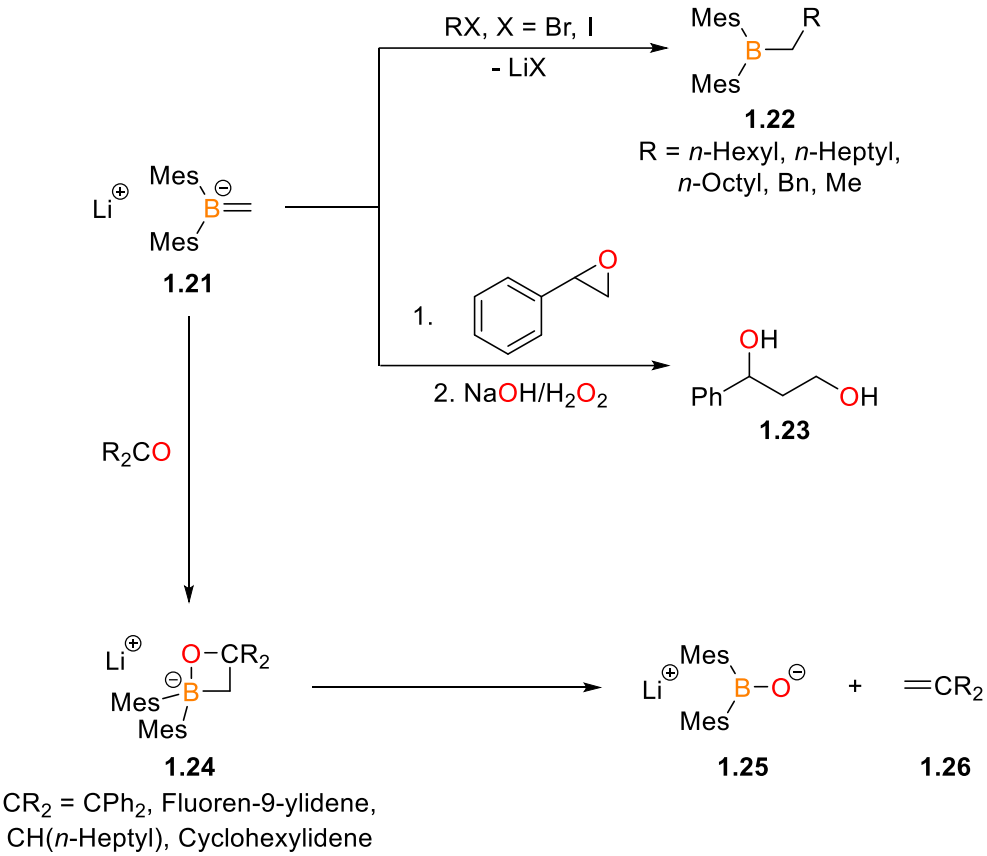

Scheme 1.7. Selected reactivity examples for lithium dimesitylboron methylidenide.

1.5 Scope of the Dissertation and Attributions

This dissertation details the synthesis and reactivity of the first known 9-borataphenanthrene anion. A wide variety of reactivity modes characteristic of

boratabenzenes and borataalkenes are described, and in some cases, the findings are supported by computational results.

Bartholome, T. A.; Bluer, K. R.; Martin, C. D., *Dalton Trans.* **2019**, *48*, 6319-6322.

Chapter Two describes the insertion of carbene units into 9-phenyl-9-borafluorene to produce six- and seven-membered nonaromatic boracycles. The project was conceived by C.D.M. and syntheses and characterizations carried out by T.A.B. X-ray crystallographic studies were conducted by K.R.B. All authors contributed to manuscript drafts.

Bartholome, T. A.; Kaur, A.; Wilson, D. J. D.; Dutton, J. L.; Martin, C. D., *Angew. Chem. Int. Ed.* **2020**, *59*, 11470-11476.

Chapter Three describes the synthesis of a 9-borataphenanthrene anion and preliminary reactivity studies indicating its boratabenzene- and borataalkene-like nature. The project was conceived by T.A.B. and C.D.M. All syntheses and characterizations were carried out by T.A.B., as were X-ray crystallographic studies. Computational studies were carried out by A.K., D.J.D.W., and J.L.D. All authors contributed to manuscript drafts.

Bartholome, T. A.; Martinez, J. J.; Kaur, A.; Wilson, D. J. D.; Dutton, J. L.; Martin, C. D.; *Organometallics* **2021**, *40*, 1966-1973.

Chapter Four details a variety of B=C bond hydrofunctionalization reactions of the 9-borataphenanthrene anion. The project was conceived by T.A.B. and C.D.M. The syntheses of compounds **4.1**-**4.3** and **4.6** were carried out by T.A.B. Preliminary syntheses for compounds **4.4** and **4.5** were carried out by J.J.M., while the final synthetic procedures were developed by T.A.B. All characterizations were carried out by T.A.B., as were X-ray

crystallographic studies. Computational studies were carried out by A.K., D.J.D.W., and J.L.D. Manuscript drafts were composed by T.A.B., A.K., D.J.D.W., J.L.D., and C.D.M.

Chapter Five describes the syntheses of a diverse array of metal complexes featuring 9-borataphenanthrene ligands. The project was conceived by T.A.B. and C.D.M. All syntheses and characterizations were carried out by T.A.B., as were X-ray crystallographic studies. Drafts were composed by T.A.B.

CHAPTER TWO

Successive Carbene Insertion into 9-Phenyl-9-Borafluorene

This chapter published as: Bartholome, T. A.; Bluer, K. R.; Martin, C. D., *Dalton Trans.* **2019**, *48*, 6319-6322. Reproduced by permission of the Royal Society of Chemistry.

2.1 Introduction

Unsaturated BC_4 heterocycles have recently been recognized as promising reagents for the synthesis of six- to eight-membered boracyclic systems *via* the formal insertion of one, two, or three atoms into the endocyclic B-C bond.[4-5, 102] Developing efficient methodologies to access heterocycles featuring tri-coordinate boron centers is of paramount interest as they have applications in electronic materials and pharmaceuticals.[3, 48-51, 103-107] In this vein, two types of unsaturated BC_4 systems have been focused upon, boroles (**1.1**)[5, 7] and their biphenyl-fused variants, 9-borafluorenes (**1.9**).[36, 108] Boroles are more reactive than 9-borafluorenes as they have greater anti-aromatic character and Lewis acidity.[23, 38, 41-42, 109-110] The intermolecular insertion chemistry of boroles has been investigated with a number of unsaturated molecules[2, 17-22, 24-29, 111-119] whereas the corresponding chemistry with 9-borafluorenes is less developed.[37-39, 45, 120-125]

The first intermolecular insertion reaction of a 9-borafluorene was reported in 2016 by Fukushima and coworkers with the insertion of alkynes into the endocyclic B-C bond of 9-chloro-9-borafluorene (**1.9a**) to furnish unsaturated BC_6 heterocycles (**2.1** and **2.2**; Fig 2.1a).[125] Our group, and He, discovered that 9-borafluorenes react with organic azides to generate 9,10-B,N-phenanthrenes (**2.3** and **2.4**, Fig 2.1b) *via* the insertion of either the α-

or γ-nitrogen atom.[38-39] Investigations with 1,2-dipolar substrates resulted in adducts (imine, nitrile, isocyanide) or seven membered rings (aldehyde, ketone, ketene, isocyanate, carbodiimide, phosphaalkyne) in which the negatively polarized atom is bound to boron and the positively polarized atom to carbon (Fig 2.1c).[37, 121-122]

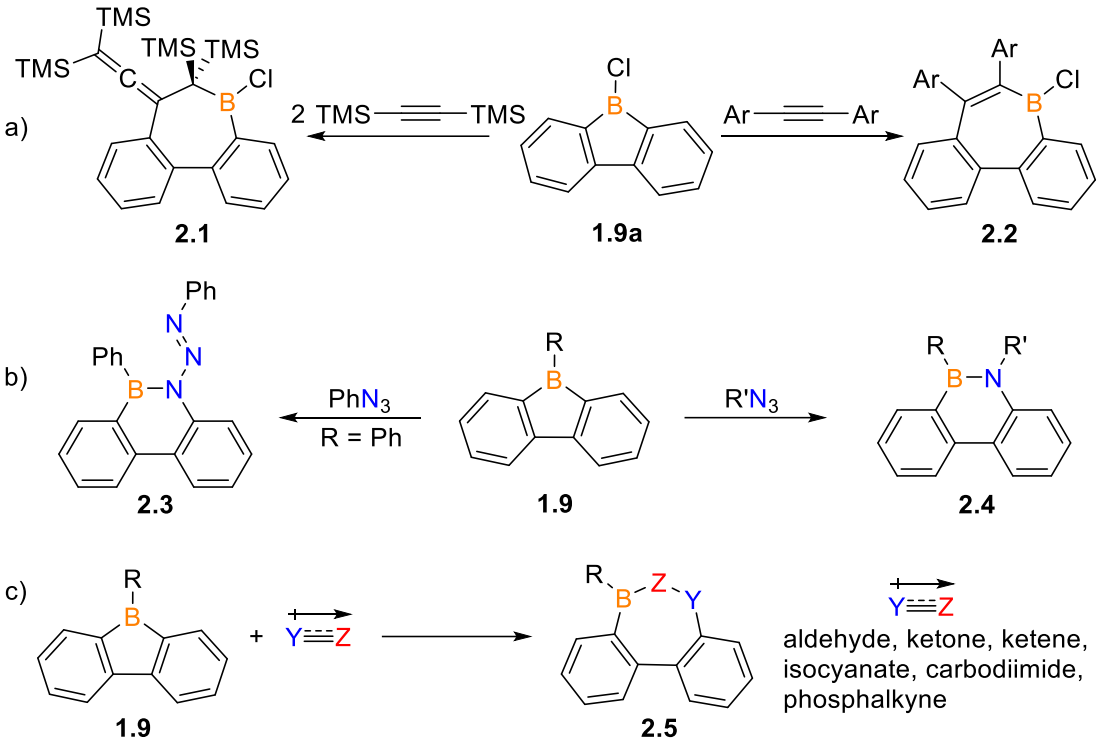

Figure 2.1. Reported intermolecular insertion reactions of alkynes (a), azides (b), and unsaturated 1,2-dipolar molecules (c) with 9-borafluorenes. TMS = trimethylsilyl.

The Ashe, Brown, and Matteson groups have demonstrated that the combination of halomethane/base can serve as a carbene source that inserts into B-C bonds.[126-134] The insertion of CR_2 units into boron-carbon bonds has also been reported using diazo reagents with notable recent work by the Stephan and Melen groups.[135-141] Braunschweig and coworkers investigated the reactions of boroles (**1.1**) with diazo reagents observing two outcomes (Fig 2.2).[19] The reaction with a bulky diazo species featuring two *para*-tolyl

groups on the α-carbon generated a 1,2-azaborine (**2.6**) *via* insertion of the terminal nitrogen into the B-C bond whereas the reaction with trimethylsilyldiazomethane resulted in insertion of a $CH(SiMe_3)$ unit into the endocyclic boron-carbon bond of **1.1** to provide a six-membered ring (**2.7**) with concomitant release of N_2 gas. Given the insertion chemistry of diazo compounds into boroles, we sought to examine the reactivity of trimethylsilyldiazomethane with 9-phenyl-9-borafluorene (**1.9b**).

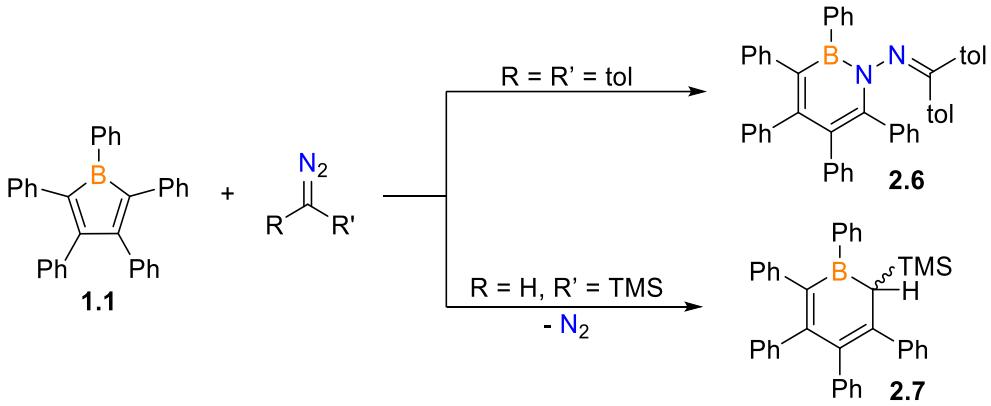

Figure 2.2. Reactions of pentaphenylborole (**1.1**) with diazo reagents (tol = *para*-tolyl).

2.2 Ring Expansion of 9-Phenyl-9-Borafluorene

The 1:1 stoichiometric reaction of **1.9b** with trimethylsilyldiazomethane at room temperature resulted in gas evolution accompanied by a color change from yellow to colorless (Scheme 2.1). No significant change was observed by *in situ* ^{11}B NMR spectroscopy; however, *in situ* ^{1}H NMR spectroscopy indicated complete consumption of trimethylsilyldiazomethane within 10 minutes by the disappearance of the trimethylsilyl peak at -0.04 ppm accompanied by the emergence of a singlet at -0.30 ppm. A diagnostic singlet in the aliphatic region at 3.88 ppm was assigned to the proton derived from the diazo α-carbon. Removing the volatiles *in vacuo* gave a pale yellow solid in quantitative

yield. An X-ray diffraction study on crystals grown revealed the product as the BC_5 heterocycle (**2.8**, Fig 2.3) from the formal insertion of a carbene unit into one of the B-C bonds. The product crystallizes in the P-1 space group, indicating a 50:50 racemate of **2.8** in the unit cell. The geometry about the boron center is trigonal planar [angular sum = 359.9(2)°] and the biphenyl backbone has a slight twist [interplanar angle = 9.9(2)°].

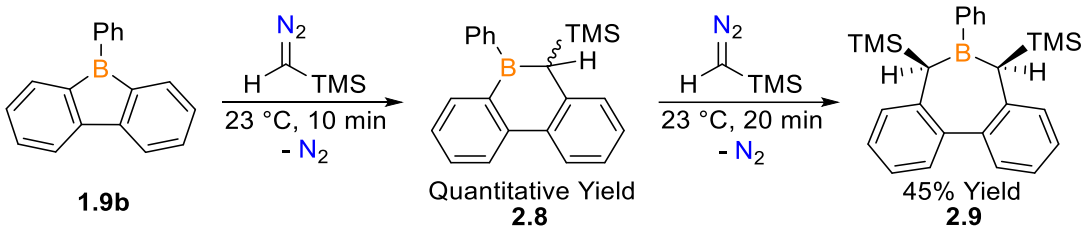

Scheme 2.1. Reaction of trimethylsilyldiazomethane with **1.9b**.

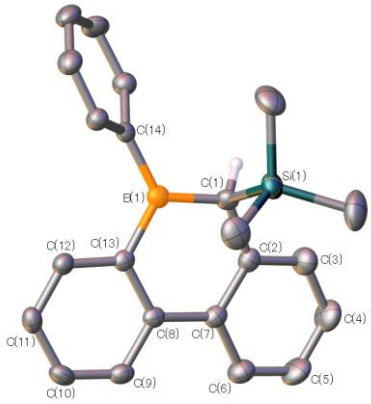

Figure 2.3. Solid-state structure of **2.8**. Hydrogen atoms are omitted for clarity (except at the chiral center), and ellipsoids are drawn at the 50% probability level. Selected bond lengths (Å) and angles (deg): B(1)-C(1) 1.541(3), C(1)-Si(1) 1.948(2), C(1)-C(2) 1.500(3), C(2)-C(7) 1.406(3), C(7)-C(8) 1.484(3), C(8)-C(13) 1.422(3), C(13)-B(1) 1.551(3), B(1)-C(14) 1.570(3), C(13)-B(1)-C(14) 122.26(18), C(13)-B(1)-C(1) 116.48(16), C(14)-B(1)-C(1) 121.17(16).

To determine if another equivalent of trimethylsilyldiazomethane would react with **1.9b**, the 1:1 reaction of trimethylsilyldiazomethane with **2.8** was conducted at room

temperature. Gas evolution was observed upon addition, and *in situ* ^{11}B NMR spectroscopy indicated conversion after 20 minutes to a new resonance at 75.4 ppm, shifted downfield from **2.8** (c.f. 65.8 ppm). After work up, colorless crystals were isolated in a 45% yield. Alternatively, the same product could be obtained by reacting **1.9b** with trimethylsilyldiazomethane directly in a 1:2 stoichiometric ratio. Redissolving the solids in C_6D_6 and acquiring an ^{1}H NMR spectrum revealed two singlets at -0.07 ppm and -0.59 ppm integrating in a 9:9 ratio, shifted upfield from trimethylsilyldiazomethane (-0.04 ppm). Singlets at 3.24 ppm and 2.70 ppm, each integrating to one, indicate the presence of two aliphatic protons. A single crystal X-ray diffraction study unambiguously identified the compound as the BC_6 heterocycle **2.9** from a second carbene insertion into the other B-$C_{biphenyl}$ bond of **1.9b**. The X-ray crystal structure revealed that the product is a single *meso* isomer in which the trimethylsilyl groups are oriented *cis* with respect to each other (Figure 2.4).[142] The BC_6 ring adopts a boat-like conformation which does not include a plane of symmetry about the boron heteroatom (Fig 2.5), rationalizing the presence of non-equivalent ^{1}H NMR signals for the two trimethylsilyl groups and the aliphatic protons assigned to those on the chiral carbon centers adjacent to boron.[143] The geometry at boron is trigonal planar [angular sum = 360.0(2)°], and the twist in the biphenyl group is significantly more pronounced with an interplanar angle of 48.7(2)° [c.f. **2.8** = 9.9(2)º].

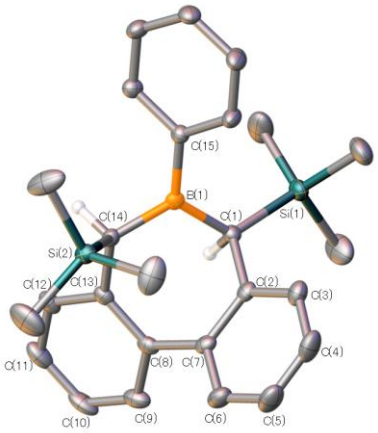

Figure 2.4. Solid-state structure of **2.9**. Hydrogen atoms are omitted for clarity (except at chiral centers), and ellipsoids are drawn at the 50% probability level. Selected bond lengths (Å) and angles (deg): B(1)-C(1) 1.587(3), C(1)-C(2) 1.523(2), C(2)-C(7) 1.409(3), C(7)-C(8) 1.486(3), C(13)-C(14) 1.509(2), C(14)-Si(2) 1.9302(17), C(14)-B(1) 1.567(3), B(1)-C(15) 1.568(3), C(14)-B(1)-C(15) 119.08(15), C(14)-B(1)-C(1) 117.36(15), C(15)-B(1)-C(1) 123.54(15).

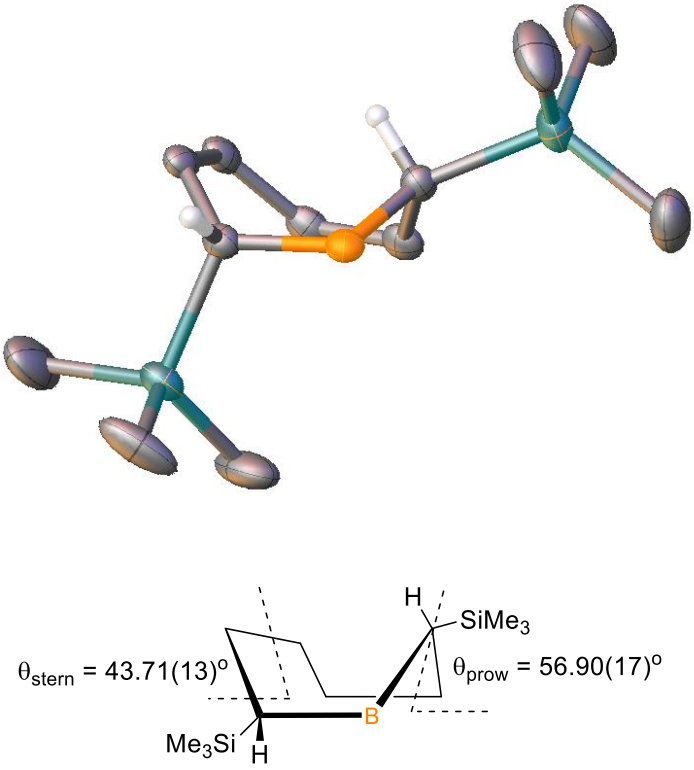

Figure 2.5: Diagram of **2.9** illustrating the dihedral planes θ_{prow} and θ_{stern} defining the deviation of the ring from planarity into a boat-like conformation.

The limit of the reactivity of **1.9b** was examined by conducting the reaction with excess trimethylsilyldiazomethane at 80 °C, upon which only the BC_6 product **2.9** was observed by ^{1}H and ^{11}B NMR spectroscopy. Examining the corresponding reaction of excess trimethylsilyldiazomethane with the borole variant, **1.1**, only gave the BC_5 product (**2.7**) from reaction with one equivalent. Upon heating at 80 °C for 24 hours, an indiscernible mixture was observed by *in situ* ^{11}B and ^{1}H NMR spectroscopy.

In summary, the reactions of trimethylsilyldiazomethane with 9-phenyl-9-borafluorene result in the sequential insertion of two carbene units, one into each of the endocyclic B-C bonds of the central BC_4 ring. This represents the first example in which insertion into both B-C bonds is observed for a 9-borafluorene. Interestingly, the chemistry of pentaphenylborole differs as only a single insertion occurs cleanly. The results further demonstrate the potential of 9-borafluorenes to serve as reagents for the preparation of polycyclic boron species.

2.3 Experimental Details

Benzene was purchased as ACS grade from Millipore Corporation, and dried by stirring for 3 days over CaH_2, distilling, and storing over 4 Å molecular sieves. 9-Phenyl-9-borafluorene (**1.9b**) was prepared by the literature procedure.[108] Trimethylsilyldiazomethane solution (2 M in hexanes) was purchased from Acros Organics and used as received.

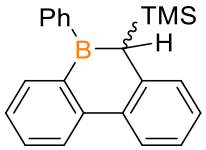

2.8

Synthesis of 2.8 (CCDC 1901552): To a solution of **1.9b** (28.0 mg, 0.117 mmol) in *n*-pentane (1 mL), trimethylsilyldiazomethane (2 M in hexanes, 0.067 mL, 0.134 mmol) was added dropwise at room temperature while stirring. The reaction mixture was stirred for an additional 10 min, after which the volatiles were removed *in vacuo*. The product, a pale yellow solid, was determined to be pure by ^{1}H NMR with no additional work-up. Single crystals for X-ray diffraction studies were grown from an *n*-pentane solution of **2.8** at -35 ºC. Yield: 38.0 mg (quantitative). d.p. 66-68 ºC;

^{1}H NMR (400 MHz, C_6D_6): δ 8.13 (dd, *J* = 7.5, 1.0 Hz, 1H), 8.07 (d, *J* = 8.0 Hz, 1H), 8.03-8.00 (m, 1H), 7.80 (dd, *J* = 7.5, 2.0 Hz, 2H), 7.46-7.42 (m, 1H), 7.35-7.29 (m, 3H), 7.26-7.12 (m, *C*$_6$*D*$_6$, 5H), 3.88 (s, 1H), -0.30 (s, 9H);

^{13}C{^{1}H} NMR (101 MHz, C_6D_6): δ 144.65, 140.59, 136.01, 135.15, 134.42, 133.37, 130.14, 129.80, 127.20, 126.76, 125.61, 124.79, 123.98, 48.87, -0.20;

^{11}B NMR (128 MHz, C_6D_6): δ 65.8;

FT-IR (cm^{-1} (ranked intensity)): 1593 (5), 1476 (12), 1439 (7), 1247 (2), 1038 (6), 952 (9), 826 (1), 766 (15), 746 (10), 730 (3), 702 (4), 659 (8), 544 (14), 486 (13), 439 (11);

High-resolution mass spectrometry (HRMS) chemical ionization (CI): calcd for $C_{22}H_{23}BSi$ $[M]^+$, 326.1662; found, 326.1667.

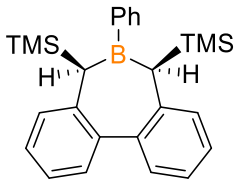

2.9

Synthesis of 2.9 (CCDC 1901553): To a solution of **2.8** (83.0 mg, 0.254 mmol) in benzene (1.5 mL), trimethylsilyldiazomethane (2 M in hexanes, 0.128 mL, 0.256 mmol) was added dropwise at room temperature while stirring. After 20 minutes of stirring, the volatiles were removed *in vacuo* to yield **2.9** as a white solid. The solid was then redissolved in a minimal amount of toluene, recrystallized at -35 ºC, and dried *in vacuo*. Yield: 47.0 mg (45%). d.p. 66-68 ºC;

Synthesis of 2.9 directly from 1.9b: To a solution of **1.9b** (429.0 mg, 1.787 mmol) in benzene (5 mL), trimethylsilyldiazomethane (2 M in hexanes, 1.787 mL, 3.574 mmol) was added dropwise at room temperature while stirring. The reaction mixture was then heated for 1 d at 80 ºC, after which the solvent was evaporated *in vacuo* to afford a pale yellow oil. Lyophilization of the crude oil from benzene (1 mL) provided a white powder, which was dissolved in a minimal amount of toluene and recrystallized at -35 ºC. Crystals for X-ray diffraction studies were grown from the crude product oil at -35 ºC. Yield: 136.0 mg (18%);

^{1}H NMR (400 MHz, C_6D_6): δ 7.66 (d, *J* = 8.0 Hz, 1H), 7.54 (dd, *J* = 7.0, 2.0 Hz, 1H), 7.46-7.43 (m, 3H), 7.25-7.20 (m, 3H), 7.19-7.13 (m, C_6D_6, 7H), 7.03 (dd, *J* = 7.0, 2.0 Hz, 1H), 3.24 (s, 1H), 2.70 (s, 1H), -0.07 (s, 9H), -0.59 (s, 9H);

^{13}C{^{1}H} NMR (101 MHz, C_6D_6): δ 144.32, 142.76, 140.12, 138.08, 130.77, 130.61, 129.53, 129.09, 128.96, 128.59, 127.54, 127.42, 126.00, 125.03, 49.78, 37.75, 0.61, 0.38;

^{11}B NMR (128 MHz, C_6D_6): δ 75.4;

FT-IR (cm^{-1} (ranked intensity)): 2954 (10), 1695 (5), 1596 (8), 1473 (14), 1436 (12), 1311 (9), 1247 (2), 1197 (11), 1026 (6), 834 (1), 749 (3), 700 (4), 579 (13), 499 (7), 479 (15);

High-resolution mass spectrometry (HRMS) chemical ionization (CI): calcd for $C_{26}H_{33}BSi_2$ $[M]^+$, 412.2214; found, 412.2218.

CHAPTER THREE

The 9-Borataphenanthrene Anion

This chapter published as: Bartholome, T. A.; Kaur, A.; Wilson, D. J. D.; Dutton, J. L.; Martin, C. D., *Angew. Chem. Int. Ed.* **2020**, *59*, 11470-11476. Reproduced by permission of John Wiley and Sons, Inc.

3.1 Introduction

Alkenyl and phenyl groups are ubiquitous unsaturated hydrocarbyl functionalities. Isoelectronic and isosteric analogues of such species are of interest because the substitution of a C=C unit with a heteroatom-containing two π-electron unit results in the introduction of a dipole moment, which can be used to alter the physical and chemical properties of the molecule.[1-2, 5-6, 144-146] Boron-containing analogues of alkenes include aminoboranes and borataalkenes in which B-N and $[B=C]^-$ units serve as two π-electron systems (Figure 3.1).[5, 13, 96, 144] The respective benzene analogues containing B-N or $[B=C]^-$ in place of two carbon atoms are 1,2-azaborines and boratabenzenes. [1-2, 5-6, 9, 65, 76, 89, 144, 147]

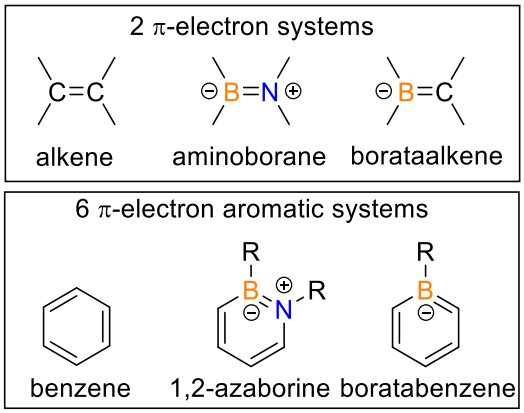

Figure 3.1. Isoelectronic relationship of an alkene and benzene to row two boron-containing species.

Boratabenzenes have been extensively studied as polyhaptic ligands for transition metals since their discovery in 1970 by Herberich and coworkers.[8-9, 52-92] The corresponding complexes and related compounds have been applied in fields that span olefin polymerization catalysis,[9, 67-69, 86, 148] asymmetric synthesis,[149-151] and single-ion magnets.[90] Research has primarily focused on monocyclic systems, with three types of polycyclic boratabenzene-containing frameworks reported to date: 1-boratanaphthalenes,[93] 2-boratanaphthalenes,[66, 75, 152] and 9-borataanthracenes[70, 153-155] (**3.1**-**3.3**, Figure 3.2). Analogues of phenanthrene with a boron atom at the 9-position are a particularly interesting target since they contain a distinct B=C moiety at the 9- and 10-positions that may be best described as a borataalkene in contrast to the fused polycyclic boratabenzenes that are currently known. This expectation is founded on the known ability of phenanthrene to act as a biphenyl-substituted alkene, as evidenced by its alkene-like reactivity toward Br_2 via 9,10-dibromination,[156] ozonolysis at the 9- and 10-positions,[157-159] and diminished aromaticity in the central ring relative to the two peripheral rings.[160] Borataalkenes were first reported in 1972 by Rathke and Kow, who described them as boron-stabilized carbanions.[94] For nearly five decades, boratabenzene chemistry and borataalkene chemistry have remained separate fields. We herein report the first example of a 9-borataphenanthrene, a compound that features reactivity patterns of both boratabenzenes and borataalkenes.

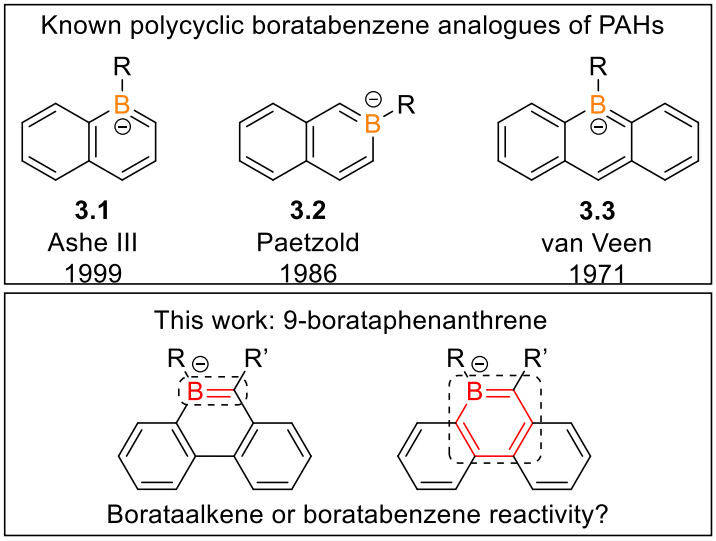

Figure 3.2. Known examples of boratabenzene analogues of polycyclic aromatic hydrocarbons and 9-borataphenanthrene disclosed in this work.[161]

3.2 Synthesis and Reactivity of a 9-Borataphenanthrene Anion

The synthesis of 9,10-dihydro-9-boraphenanthrene **2.8** via carbene insertion into the endocyclic B-C bond of 9-phenyl-9-borafluorene was reported in Chapter Two (Scheme 2.1).[162] The compound bears a proton on an sp^3 carbon adjacent to a tricoordinate boron atom, making it a viable precursor to a boratabenzene-containing species by deprotonation. Potassium hexamethyldisilazide (KHMDS) proved to be a suitable base to deprotonate **2.8** as confirmed by single crystal X-ray diffraction studies (Figure 3), and the resulting yellow borataphenanthrene **3.4** was isolated in high yield (86%, Scheme 3.1). The ^{1}H NMR spectrum of **3.4** lacks the aliphatic C-H singlet at 3.88 ppm for the proton at the 10-position and features a diagnostic singlet at -0.01 ppm for the trimethylsilyl group, shifted downfield from -0.30 ppm for **2.8**. ^{11}B NMR spectroscopy revealed an upfield shift from 65.8 ppm for **2.8** to 40.4 ppm for **3.4**, consistent with boratabenzene and borataalkene species.[16, 93, 151-152, 163-168]

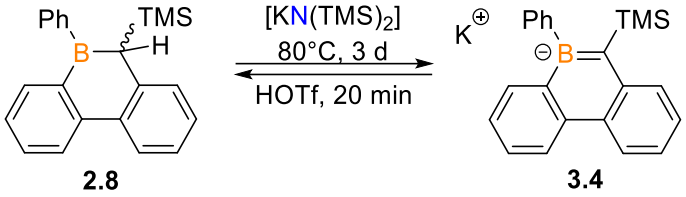

2.8 **3.4**

Scheme 3.1. Interconversion of **2.8** and 9-borataphenanthrene **3.4**.

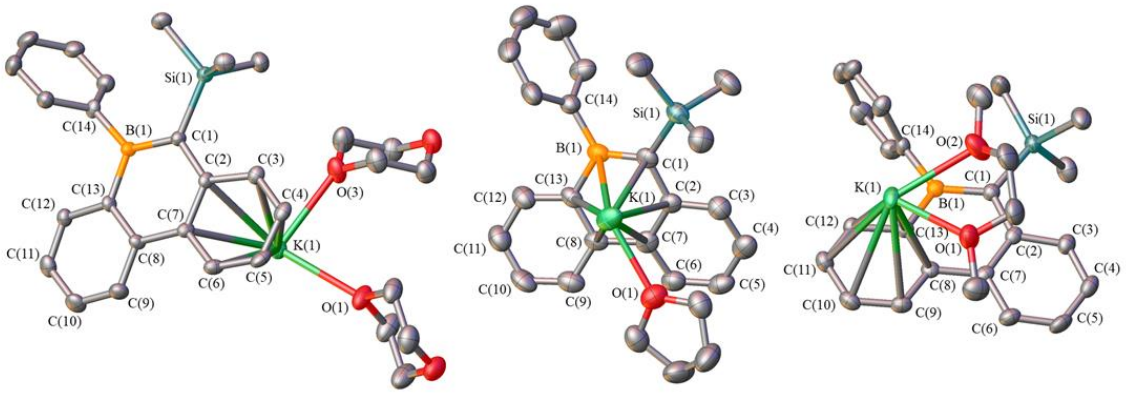

Figure 3.3. Solid-state structures of **3.4•dioxane**, **3.4•THF**, and **3.4•DME** (left to right) showing the coordination of the potassium cation with each of the three aromatic rings of the 9-borataphenanthrene anion. Hydrogen atoms are omitted for clarity, and thermal ellipsoids are drawn at the 50% probability level. The asymmetric units are displayed, but the solvates of **3.4** exist as polymeric species (Figures B-60-62).

Theoretical calculations examining the electronic structure of **1** yield a geometry (as a free anion) in agreement with the X-ray diffraction structure (Table 3.1). The calculated HOMO is π-symmetric with the largest coefficients on the endocyclic B-C bond, while the LUMO does not have any contribution at the boron atom (Figure 3.4). The Wiberg bond index (WBI) of the B-C bond in **3.4** is calculated to be 1.248, which indicates multiple bond character. For comparison, the WBI is 0.929 for the analogous B-C single bond in precursor **2.8**, and the B-C bond to the biphenyl backbone in **3.4** has a WBI value of 0.937. Nucleus-independent chemical shift scan (NICS-Scan) calculations indicate that

the boron-containing ring has significant aromatic character, with a minimum NICS value of -17 ppm at 1.3 Å above the plane of the ring (NICS plots are depicted in Figure 3.5). For comparison, the minima for benzene, the central ring of phenanthrene,[160] and 1-*H*-boratabenzene are -30 ppm, -21 ppm, and -26 ppm, respectively, all at 1.0 Å above the ring plane. These NICS values indicate that incorporating boron into the ring, as well as fusing rings, reduces aromaticity. The NICS calculations confirm aromatic character in the central ring, while the localization of the HOMO on the B=C functionality indicates that **3.4** can be described as either a dibenzo-fused boratabenzene or a biphenyl-substituted borataalkene. The borataalkene carbon atom has the largest partial negative NBO charge in **3.4** at -0.99, suggesting that this carbon atom has potential to act as a nucleophilic site.

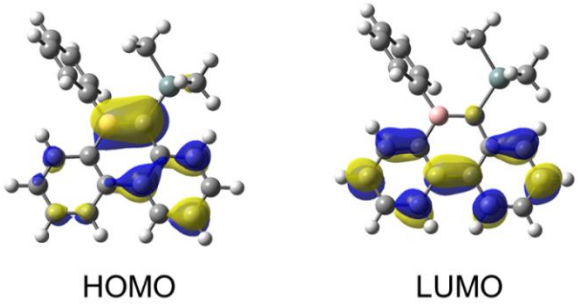

Figure 3.4. Frontier molecular orbitals of **3.4**.

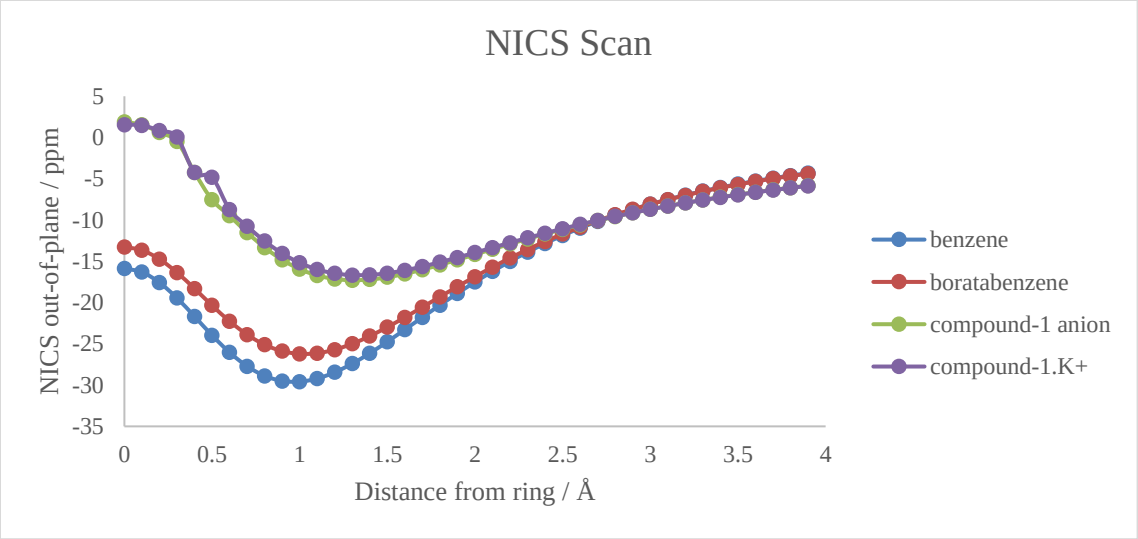

Figure 3.5: NICS plots for **3.4** (free anion), **3.4•K**$^{+}$, benzene, boratabenzene. B3LYP-D3(BJ)/def2-TZVP in THF solvent. NICS calculations are at points perpendicular to the plane of the ring. In the case of **3.4**.K+, the NICS points are on the opposite side to the K^{+} ion. Neighboring atoms/groups can disrupt the smooth convergence of the NICS-scan plots.

To examine if 9-borataphenanthrene anion **3.4** acts as a nucleophile, in accordance with the calculated negative charge localized on the borataalkene carbon, protonation was attempted with triflic acid at room temperature. The reaction regenerated the protonated borataphenanthrene species **2.8** with potassium triflate as the byproduct (Scheme 3.1). C-alkylation was attempted by reaction with iodomethane at room temperature, resulting in a change in color from yellow to a colorless slurry (Scheme 3.2). In situ ^{11}B NMR spectroscopy indicated a downfield shift in the boron resonance from 40.4 ppm to 67.2 ppm, indicative of the formation of a tricoordinate boron center, with conversion completed in 20 minutes. The isolated compound exhibits a diagnostic singlet at 1.86 ppm in its ^{1}H NMR spectrum that integrates in a 3:9 ratio with the trimethylsilyl singlet, confirming the addition of the methyl group to **3.4**. The structure of the compound was determined by X-

ray crystallography to be the C-methylated derivative **3.5**, indicating that alkylation occurs at the borataalkene carbon of **3.4**.

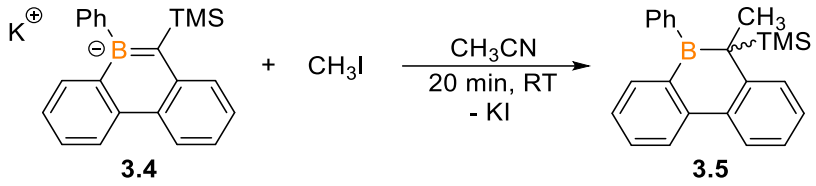

3.4 **3.5**

Scheme 3.2. Alkylation of **3.4** with iodomethane.

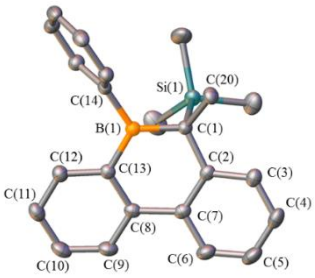

Figure 3.6. Solid-state structure of **3.5**. Hydrogen atoms are omitted for clarity, and thermal ellipsoids are drawn at the 50% probability level.

To determine if the borataalkene moiety of **3.4** can exhibit olefin-like behavior, hydroboration with pinacolborane (HBpin) was attempted at room temperature (Scheme 3.3). In situ ^{11}B NMR spectroscopy indicated the consumption of **3.4** and HBpin after 21 hours. The spectrum consisted of a broad singlet at 34.5 ppm and two distinct doublets, a major species at -11.1 ppm and minor species at -12.1, the latter consistent with hydride-substituted tetracoordinate boron centers. Both species were crystallized and identified as the *syn* (major) and *anti* (minor) isomers of the B=C hydroboration product (Figure 3.7). In their respective proton NMR spectra, broad quartets were observed at 2.62 and 2.69 ppm, with matching coupling constants to the doublets in the ^{11}B NMR spectrum (J = 88.5

Hz and 87.5 Hz) confirming the presence of a boron-bound hydride. This was further supported by a $^{1}H\{^{11}B\}$ NMR experiment in which the quartets became singlets and a $^{11}B\{^{1}H\}$ NMR experiment in which the doublets became singlets. This differs from the limited known B=C hydroboration reactions in that the hydride is not bridged between the two boron centers and the *anti* B=C hydroboration product is observed.[166, 169-171]

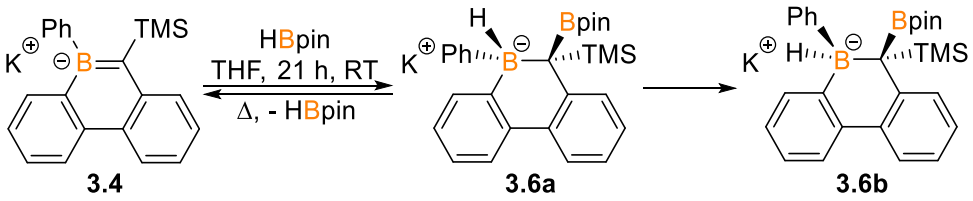

Scheme 3.3. Hydroboration of **3.4** with pinacolborane to produce diastereomers **3.6a** and **3.6b** (pin = pinacolate).

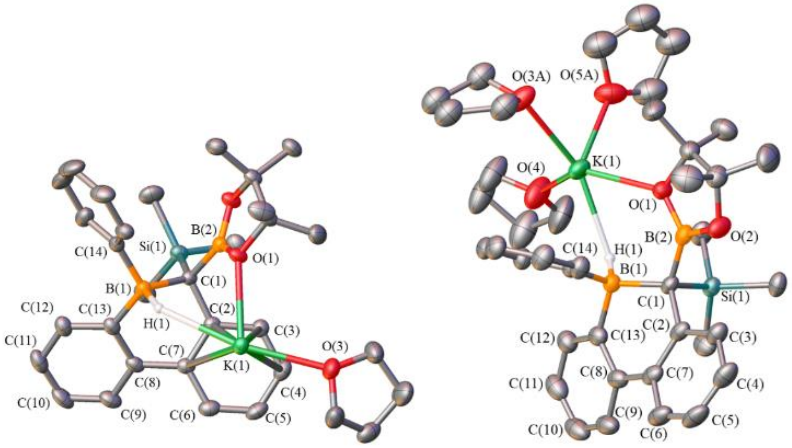

Figure 3.7. Solid-state structures of **3.6a** and **3.6b**. Hydrogen atoms (except for boron-bound hydrides) and non-coordinated solvates are omitted for clarity, and thermal ellipsoids are drawn at the 50% probability level. For disordered atoms, only the component with the highest occupancy is shown. The complete dimeric representation of **3.6a** is shown in Figure B-59).

Allowing the reaction to proceed for longer periods of time showed a decrease in the intensity of the doublet at -11.1 ppm accompanied by an increase in the intensity of the

doublet at -12.1 ppm in the in situ ^{11}B NMR spectra. Conducting variable-temperature ^{1}H NMR studies with a 1:1 mixture of **3.6a** and **3.6b** did not result in any interconversion of the two diastereomers; instead at 70 ºC, the intensity of the trimethylsilyl singlet for **3.6a** decreased with the emergence of a trimethylsilyl singlet at -0.01 ppm that corresponds to **3.4**. In addition, the Bpin methyl singlets for **3.4a** decreased in intensity and a singlet at 1.28 ppm corresponding to pinacolborane emerged. The methyl and trimethylsilyl singlets for **3.6b**, however, remained unchanged, thus confirming that the *syn* diastereomer, **3.6a**, is capable of thermal *syn* elimination of HBpin in a reverse hydroboration process while **3.6b** is not. Calculation of the reaction pathway shows that **3.6a** lies 11 kJ/mol below the starting materials, and isomerization to **3.6b** is a further 17 kJ/mol lower in energy. Modeling a simplified system bearing an -SiH_3 group on **3.4** showed that the transition state barrier for the conversion of **3.4** to **3.6a** is 84 kJ/mol (ΔG), and the reverse barrier is similar in magnitude for the model system at 85 kJ/mol. These data and the relatively flat ΔG of reaction at 11 kJ/mol are consistent with reversion of **3.6a** to **3.4** at elevated temperatures, driven by entropy. The ability of **3.4** to undergo hydroboration presents a potential new route to geminal bis(boron)-functionalized organic species.

The nucleophilicity at carbon and addition reactivity with HBpin provide evidence for a borataalkene description of **3.4**.[96, 99, 172] Given the resemblance of the HOMO on the B=C bond to the HOMO of an olefin, we postulated that η^2 coordination with the π-bond could occur, reminiscent of an olefin.[173-175] Reaction of **3.4** with (Ph_3P)AuCl at room temperature resulted in a color change from yellow to colorless (Scheme 3.4), and in situ $^{31}P\{^{1}H\}$ NMR spectroscopy showed the emergence of a singlet at 39.7 ppm along with the disappearance of the singlet at 33.2 ppm corresponding to (Ph_3P)AuCl with the reaction

complete in an hour. The in situ ^{11}B NMR spectrum contained a single broad peak at 42.4 ppm, slightly downfield from **3.4** (40.4 ppm). Single-crystal X-ray crystallography identified the product as the η^2-borataalkene complex **3.7** (Figure 3.8). The solid-state structure of **3.7** is disordered but clearly reveals that the gold center preferentially occupies a position closer to the borataalkene carbon rather than boron (88% site occupancy). The gold center is closer to the borataalkene carbon than to boron [Au-C = 2.188(7) Å vs. Au-B = 2.427(8) Å]. This is consistent with known examples of η^2-borataalkene complexes; two previously reported borataalkene tantalum complexes were determined to have Ta-C bond distances of 2.337(5) Å and 2.348(5) Å, for Ta-B bond distances of 2.728(6) Å and 2.738(6) Å, respectively.[13, 95] Theoretical calculations reproduce this trend, with Au-C and Au-B bond distances of 2.227 and 2.491 Å, respectively. The geometry about the gold(I) center is approximately linear with respect to the borataalkene carbon as shown by its P-Au-C bond angle of 172.1(2)º. The ligand geometries about the borataalkene boron and carbon centers remain trigonal planar with angular sums of 359.6(9)º and 359.0(8)º. This is a unique mononuclear η^2-borataalkene metal complex as it originates from a free borataalkene and is of a late transition metal. The other species reported are of early transition metals and prepared by the modification of pre-existing ligands.[13, 95, 176]

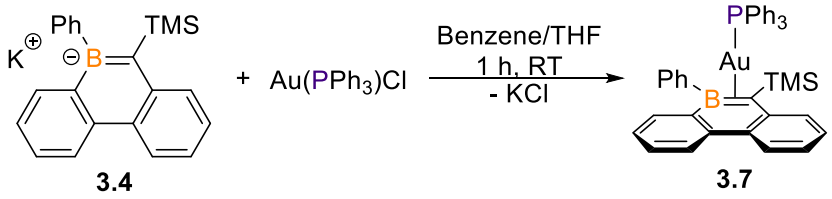

Scheme 3.4. Reaction of **1** with $(Ph_3P)AuCl$ to produce η^2-borataalkene complex **3.7**.

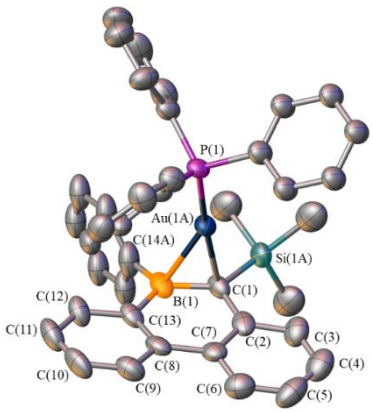

Figure 3.8. Solid-state structure of **3.7**. Hydrogen atoms are omitted for clarity, and thermal ellipsoids are drawn at the 50% probability level. For disordered atoms, only the component with the highest occupancy is shown. Selected bond lengths (Å) and angles (º): Au(1A)-B(1) 2.427(8), Au(1A)-C(1) 2.188(7), Au(1A)-P(1) 2.2618(18), B(1)-Au(1A)-P(1) 146.8(2), C(1)-Au(1A)-P(1) 172.1(2).

With the borataalkene reactivity of **3.4** established, the boratabenzene character was investigated next. To determine if the central BC_5 ring in 9-borataphenanthrene **3.4** exhibits boratabenzene reactivity, complexation with chromium was attempted by reacting **3.4** with tris(acetonitrile)tricarbonylchromium at room temperature in THF (Scheme 3.5). Upon mixing, the solution color immediately changed from yellow to red. In situ ^{11}B NMR spectroscopy revealed an upfield shift of the boron resonance from 40.4 ppm to 30.5 ppm, consistent with the formation of an η^6-boratabenzene complex[87-88, 91] with complete conversion of **3.4** in 75 minutes. Coordination of dibenzo-18-crown-6 to the potassium ion allowed for the isolation and crystallographic characterization of the piano-stool complex **3.8** (Figure 3.9). The borataphenanthrene ligand coordinates to the chromium center through the central BC_5 ring. The FT-IR spectrum of the piano-stool complex **3.8** exhibits carbonyl stretching bands at 1903, 1821, and 1769 cm^{-1}, which are similar to the chromium boratabenzene complex $Na[(MeBC_5H_5)Cr(CO)_3]$ (υ_{CO} = 1910, 1820, 1776 cm^{-1}).[62] The η^6

complexation of the central boratabenzene ring of **3.4** is consistent with the aromatic character determined in the NICS calculations.

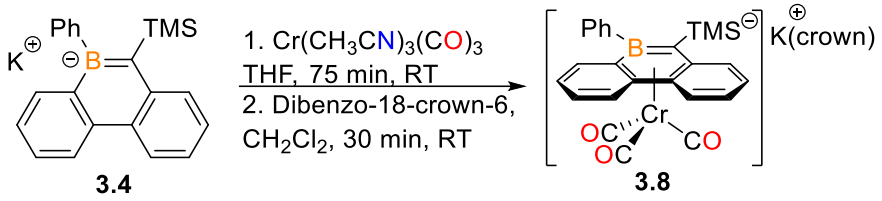

Scheme 3.5. Reaction of **3.4** with tris(acetonitrile)tricarbonylchromium to form η^6-boratabenzene complex **3.8** (crown = dibenzo-18-crown-6).

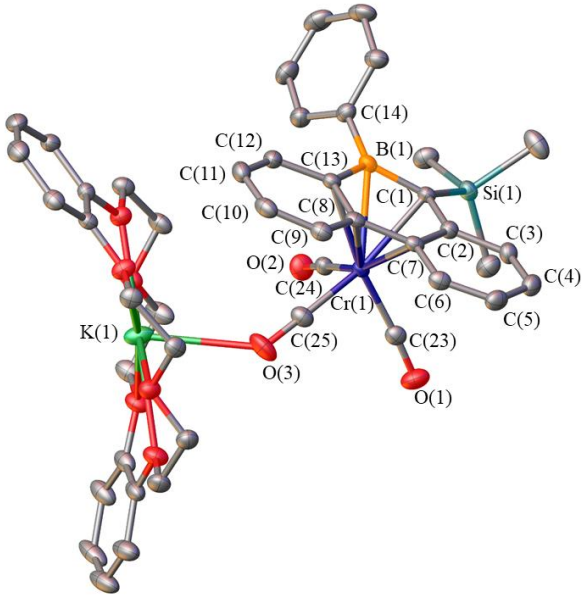

Figure 3.9. Solid-state structure of **3.8**. Hydrogen atoms and dichloromethane solvate are omitted for clarity, and thermal ellipsoids are drawn at the 50% probability level. Selected bond lengths (Å) and angles (º): B(1)-Cr(1) 2.410(4), C(1)-Cr(1) 2.294(3), C(2)-Cr(1) 2.306(4), C(7)-Cr(1) 2.294(3), C(8)-Cr(1) 2.329(3), C(13)-Cr(1) 2.349(3), Cr(1)-C(23) 1.821(4), C(23)-O(1) 1.171(5), Cr(1)-C(24) 1.813(4), C(24)-O(2) 1.163(5), Cr(1)-C(25) 1.809(4), C(25)-O(3) 1.174(5), O(3)-K(1) 2.849(4).

All compounds share the fused tricyclic framework, enabling a comparison of their common metrical parameters from X-ray diffraction data (Table 1). The structure of **3.4** was determined with three different solvates, THF, 1,4-dioxane, and dimethoxyethane

(DME), with the closest contacts of the potassium cation with the borataphenanthrene anion differing in each. In the THF solvate, coordination of the potassium ion to the central boratabenzene ring occurs, while in the dioxane solvate, the potassium ion coordinates to the carbonaceous ring adjacent to the trimethylsilyl-substituted carbon, and in the DME solvate, the potassium ion coordinates to the carbonaceous ring adjacent to boron. The heteroatom bonds to the deprotonated carbon are notably shortened with the B-C bond of 1.541(3) Å of **2.8** contracting to 1.487(10)-1.495(2) Å in the structures of **3.4** and the C-Si bond contracting from 1.948(2) Å to 1.856(7)-1.8736(18) Å. The boron-carbon and carbon-silicon bond lengths of the methylated product are similar to **2.8** [**3.5**: B-C = 1.5481(18) Å and C-Si = 1.9721(12) Å] while the metal complexes are similar to those of **3.4** [**3.7**: B-C = 1.504(11) Å and C-Si = 1.891(12) Å, **3.8**: B-C = 1.517(5) Å and C-Si = 1.888(4) Å], indicating that metal complexation has minimal effect on the bonding in the borataphenanthrene. The hydroboration products have significantly lengthened boron-carbon bonds [**3.6a** = 1.702(3) Å, **3.6b** = 1.674(5) Å] that are consistent with quaternization of the boron center. In all the structures, there is minimal perturbation of the biphenyl framework.

Table 3.1. Selected bond lengths (Å) for **2.8**,[162] **3.4** (free anion, calculated), **3.4•dioxane**, **3.4•THF**, **3.4•DME**, **3.5**, **3.6a**, **3.6b**, **3.7**, and **3.8**.

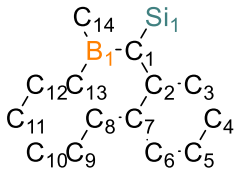

	2.8	**3.4**	**3.4•dioxane**	**3.4•THF**	**3.4•DME**	**3.5**	**3.6a**	**3.6b**	**3.7**	**3.8**
B(1)-C(1)	1.541(3)	1.497	1.495(2)	1.487(10)	1.489(3)	1.5481(18)	1.702(3)	1.674(5)	1.504(11)	1.517(5)
C(1)-Si(1)	1.948(2)	1.877	1.8736(18)	1.856(7)	1.8643(18)	1.9721(12)	1.9010(17)	1.906(3)	1.891(12)	1.888(4)
C(1)-C(2)	1.500(3)	1.453	1.450(2)	1.480(8)	1.456(2)	1.5129(16)	1.522(2)	1.525(4)	1.501(12)	1.441(5)
C(2)-C(3)	1.402(3)	1.432	1.434(2)	1.407(10)	1.429(2)	1.4052(18)	1.406(3)	1.412(5)	1.411(11)	1.444(5)
C(2)-C(7)	1.406(3)	1.448	1.444(2)	1.426(9)	1.440(3)	1.4182(18)	1.423(2)	1.415(5)	1.435(11)	1.449 (5)
C(3)-C(4)	1.372(3)	1.383	1.376(3)	1.382(10)	1.373(3)	1.382(2)	1.387(3)	1.385(5)	1.362(14)	1.357(5)
C(4)-C(5)	1.375(3)	1.407	1.397(3)	1.393(11)	1.392(3)	1.386(2)	1.388(3)	1.389(7)	1.376(15)	1.407(6)
C(5)-C(6)	1.370(3)	1.386	1.380(3)	1.367(10)	1.371(3)	1.381(2)	1.382(3)	1.372(6)	1.377(14)	1.364(5)
C(6)-C(7)	1.405(3)	1.417	1.415(2)	1.412(9)	1.416(3)	1.4087(18)	1.403(3)	1.412(5)	1.401(13)	1.436(5)
C(7)-C(8)	1.484(3)	1.466	1.471(2)	1.462(10)	1.463(2)	1.4839(18)	1.483(3)	1.491(5)	1.485(11)	1.468(5)
C(8)-C(9)	1.401(3)	1.421	1.418(2)	1.412(10)	1.419(3)	1.4095(18)	1.402(3)	1.406(5)	1.398(11)	1.431(5)
C(8)-C(13)	1.422(3)	1.430	1.419(2)	1.422(9)	1.421(2)	1.4170(17)	1.413(3)	1.409(5)	1.424(12)	1.429(5)
C(9)-C(10)	1.377(3)	1.387	1.370(3)	1.366(12)	1.380(3)	1.381(2)	1.389(3)	1.372(7)	1.377(13)	1.370(6)
C(10)-C(11)	1.379(3)	1.407	1.394(3)	1.382(10)	1.397(3)	1.388(2)	1.380(3)	1.386(7)	1.383(15)	1.411(6)
C(11)-C(12)	1.378(3)	1.387	1.375(3)	1.392(11)	1.376(3)	1.3846(19)	1.393(3)	1.389(5)	1.383(12)	1.353(6)
C(12)-C(13)	1.403(3)	1.419	1.420(2)	1.400(10)	1.419(2)	1.4108(18)	1.404(3)	1.398(5)	1.400(11)	1.441(5)
C(13)-B(1)	1.551(3)	1.560	1.553(3)	1.563(9)	1.562(3)	1.5496(18)	1.618(3)	1.605(5)	1.545(11)	1.546(5)
B(1)-C(14)	1.570(3)	1.594	1.603(3)	1.604(9)	1.601(3)	1.5782(17)	1.628(3)	1.636(4)	1.597(12)	1.586(6)

The synthesis of the 9-borataphenanthrene anion enabled a reactivity study that revealed surprisingly diverse reaction modes. The feature compound readily undergoes protonation to regenerate its charge-neutral precursor or methylation at carbon with iodomethane, consistent with the B=C bond polarization and borataalkene reactivity. Hydroboration of the B=C bond with pinacolborane demonstrated the potential for addition reactions in the system and provided a B=C hydroboration product that does not have a three-center two-electron bond with the hydride and boron atoms. Accordingly, this is also the first observation of an *anti* hydroboration product and provides a potential route to geminal bis(boron)-functionalized organic molecules. An η^2-borataalkene complex with gold was synthesized and is atypical in that it features a late transition metal center and is synthesized directly from a free borataalkene anion rather than by modification of an existing ligand. The 9-borataphenanthrene species coordinates to chromium in an η^6 fashion from the central BC_5 ring to underscore the diverse reactivity. Although several unusual transformations were disclosed in this manuscript, we are merely scratching the surface of the chemistry of the 9-borataphenanthrene anion. Overall the new class of compound demonstrates alkylation at carbon along with olefinic and aromatic behavior and reactivity within a single heterocyclic ring system.

3.3 Experimental Details

Dimethoxyethane was purchased from Acros Organics and dried by stirring for 3 days over CaH_2, distilling, and storing over molecular sieves. 1,4-Dioxane was purchased from Beantown Chemical and stored over molecular sieves. 9-Phenyl-9-borafluorene and $(Ph_3P)AuCl$ were prepared by the literature procedures.[108, 177] The following reagents were

purchased from the listed sources and used as received: Trimethylsilyldiazomethane 2 M solution in hexanes (Acros Organics), pinacolborane (Acros Organics), triflic acid (Beantown Chemical), potassium bis(trimethylsilyl)amide (Aldrich), tris(acetonitrile)tricarbonylchromium (Aldrich), dibenzo-18-crown-6 (TCI). Iodomethane was purchased from Acros Organics and stored over molecular sieves.

Computational Methods

Unless noted, all calculations were performed with the Gaussian 16 program.[178] Geometry optimizations were carried out in a THF solvent forcefield using B3LYP-D3(BJ)[179] with a def2-SVP basis set.[180] Frequency calculations were performed analytically at the same level of theory to characterize the stationary points as minima or transition states. NBO analysis was carried out with NBO 6.0.[181] Plots of molecular orbitals were obtained by performing MO analysis at B3LYP-D3(BJ)/def2-SVP in THF solvent. NICS scan calculations were carried out with the AROMA program[160, 182-184] coupled to Gaussian. NICS calculations were carried out with the B3LYP[185-186] method, def2-TZVP basis set,[180] and THF solvation.

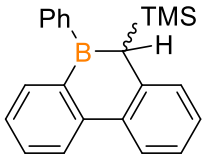

2.8

Synthesis of 2.8 (CCDC 1901552): **2.8** was prepared using a modified version of the literature procedure to accommodate a larger scale.[162] Trimethylsilyldiazomethane (2 M in hexanes, 2.67 mL, 5.34 mmol) was added dropwise to a solution of 9-phenyl-9-

borafluorene (1.12 g, 4.65 mmol) in *n*-pentane (25 mL) while stirring at room temperature. The reaction mixture was then stirred for an additional hour, after which the volatile components were removed *in vacuo*. The resulting solid was then recrystallized from *n*-pentane at -35 ºC to yield **2.8** as a colorless solid. Yield: 1.15 g (75%). The characterization details match the literature data.[162]

Synthesis of 2.8 from 3.4: A solution of triflic acid (25 μL, 0.28 mmol) in THF (2.5 mL) was added dropwise to a solution of **3.4** (102 mg, 0.281 mmol) in THF (2.5 mL) while stirring at room temperature. After 15 minutes of stirring, the volatile components were removed *in vacuo*, and the residue was extracted with benzene (3 mL). The supernatant was then filtered and lyophilized to yield **2.8** as a white powder. Yield: 72 mg (79%). The characterization details match the literature data.[15]

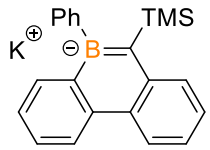

3.4

Synthesis of 3.4 (CCDC 1981968-1981970): A solution of potassium bis(trimethylsilyl)amide (0.630 g, 3.16 mmol) in benzene (15 mL) was added dropwise to a solution of **2.8** (0.964 g, 2.95 mmol) in benzene (5 mL) while stirring at room temperature. The resulting yellow solution was then transferred to a pressure tube with a Teflon cap and heated at 80 ºC for 3 d, resulting in the formation of a yellow precipitate. The precipitate was collected by vacuum filtration, washed with additional benzene (40 mL), and dried *in vacuo* to yield **3.4** as a yellow powder. Yield: 0.922 g (86%). M.p. 99-102 ºC. Crystals for X-ray diffraction studies were grown by vapor diffusion of *n*-pentane

into a 1,4-dioxane solution of **3.4** (**3.4•dioxane**), by vapor diffusion of *n*-pentane into a THF solution of **3.4** (**3.4•THF**), or by vapor diffusion of hexanes into a dimethoxyethane solution of **3.4** (**3.4•DME**);

^{1}H NMR (400 MHz, CD_3CN): δ 8.59 (d, *J* = 8.0 Hz, 1H), 8.55 (dd, *J* = 8.0, 2.5 Hz, 1H), 7.84 (dd, *J* = 8.5, 1.0 Hz, 1H), 7.64 (dd, *J* = 7.5, 1.5 Hz, 1H), 7.50-7.48 (m, 2H), 7.39-7.35 (m, 1H), 7.29-7.25 (m, 2H), 7.20-7.11 (m, 3H), 6.91-6.87 (m, 1H), -0.01 (s, 9H);

^{13}C{^{1}H} NMR (101 MHz, CD_3CN): δ 148.13, 138.50, 134.99, 134.45, 128.63, 127.82, 126.67, 125.04, 124.61, 124.46, 124.11, 122.53, 122.50, 115.49, 4.61;

^{11}B NMR (128 MHz, CD_3CN): δ 40.4;

FT-IR (cm^{-1} (ranked intensity)): 1467 (9), 1417 (15), 1298 (6), 1256 (14), 1243 (8), 1229 (13), 930 (7), 863 (10), 828 (1), 761 (2), 748 (3), 727 (5), 710 (4), 676 (12), 622 (11);

High-resolution mass spectrometry (HRMS) electrospray ionization (ESI): calcd for $C_{22}H_{22}BSi$ $[M]^-$, 325.1583; found, 325.1578.

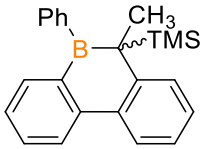

3.5

Synthesis of 3.5 (CCDC 1981971): Iodomethane (55 μL, 0.88 mmol) was added dropwise to a solution of **3.4** (107 mg, 0.293 mmol) in acetonitrile (3 mL) while stirring at room temperature. After 20 minutes, the reaction mixture was extracted with *n*-pentane (3 × 5 mL). The volatile components were then evaporated *in vacuo* from the *n*-pentane extract to afford **2** as a colorless oil, which was lyophilized from benzene to produce a white

powder. This powder was then further purified by recrystallization from *n*-pentane at -35 ºC. Yield: 63 mg (63%). d.p. 82 ºC. Crystals for X-ray diffraction studies were grown by storing an *n*-pentane solution of **3.5** at -35 ºC;

^{1}H NMR (400 MHz, C_6D_6): δ 8.10 (t, *J* = 8.0 Hz, 2H), 7.84 (dd, *J* = 7.5, 1.0 Hz, 1H), 7.43-7.39 (m, 4H), 7.34-7.21 (m, 5H), 7.16-7.12 (m, 1H), 1.86 (s, 3H), -0.33 (s, 9H);

^{13}C{^{1}H} NMR (101 MHz, C_6D_6): δ 144.37, 143.82, 136.99, 134.28, 133.62, 132.21, 127.44, 127.41, 126.75, 126.60, 125.55, 124.56, 123.23, 17.91, -1.07;

^{11}B NMR (128 MHz, C_6D_6): δ 67.2;

FT-IR (cm^{-1} (ranked intensity)): 1591 (15), 1437 (13), 1247 (4), 1226 (12), 950 (14), 835 (1), 766 (8), 752 (5), 744 (7), 732 (2), 707 (3), 690 (11), 671 (6), 663 (9), 636 (10);

High-resolution mass spectrometry (HRMS) chemical ionization (CI): calcd for $C_{23}H_{25}BSi$ $[M]^+$, 340.1819; found, 340.1821;

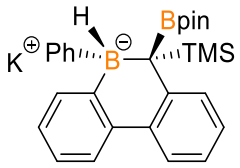

3.6a

Synthesis of 3.6a (CCDC 1981972): Pinacolborane (212 µL, 1.46 mmol) was added to a solution of **3.4** (354 mg, 0.972 mmol) in THF (5 mL) while stirring at room temperature. After 21 hours of stirring, the solution was concentrated to a volume of 2 mL, resulting in the formation of a cloudy yellow precipitate. The precipitate was isolated by decantation and dried *in vacuo* to yield **3.6a** as a pale yellow powder. Yield: 308 mg (64%, minimum

7:1 diastereomer ratio). d.p. 167 ºC. Crystals for X-ray diffraction studies were grown by slow evaporation of a solution of **3.6a** in THF/benzene (5:1);

^{1}H NMR (400 MHz, CD_3CN): δ 7.57-7.55 (m, 1H), 7.43 (d, *J* = 7.5 Hz, 1H), 7.20-7.17 (m, 2H), 7.01-6.93 (m, 4H), 6.88 (td, *J* = 7.5, 1.5 Hz, 1H), 6.80 (td, *J* = 7.0, 1.5 Hz, 1H), 6.67-6.64 (m, 3H), 2.62 (q, *J* = 88.0 Hz, 1H), 0.87 (s, 6H), 0.69 (s, 6H), -0.08 (s, 9H);

^{1}H{^{11}B} NMR (400 MHz, CD_3CN): δ 7.57-7.55 (m, 1H), 7.43 (d, *J* = 7.5 Hz, 1H), 7.20-7.18 (m, 2H), 7.00-6.93 (m, 4H), 6.88 (td, *J* = 7.0, 1.5 Hz, 1H), 6.81-6.78 (m, 1H), 6.68-6.65 (m, 3H), 2.62 (s, 1H), 0.87 (s, 6H), 0.68 (s, 6H), -0.08 (s, 9H);

^{13}C{^{1}H} NMR (101 MHz, CD_3CN): δ 151.88, 142.70, 136.09, 134.35, 131.16, 126.13, 125.52, 125.45, 125.34, 124.02, 123.76, 122.95, 122.78, 81.31, 25.39, 24.50, 2.69;

^{11}B NMR (128 MHz, CD_3CN): δ 34.5 (s, br), -11.1 (d, *J* = 88.5 Hz);

^{11}B{^{1}H} NMR (128 MHz, CD_3CN): δ 34.9 (s, br), -11.1 (s);

FT-IR (cm^{-1} (ranked intensity)): 2974 (9), 1426 (10), 1297 (6), 1241 (4), 1140 (2), 973 (7), 891 (14), 828 (1), 762 (13), 737 (3), 716 (5), 674 (8), 620 (15), 600 (12), 510 (11);

High-resolution mass spectrometry (HRMS) electrospray ionization (ESI): calcd for $C_{28}H_{35}B_2O_2Si$ $[M]^-$, 453.2592; found, 453.2614.

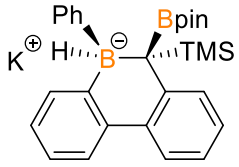

3.6b

Synthesis of 3.6b (CCDC 1981973): Pinacolborane (52 μL, 0.36 mmol) was added to a solution of **3.4** (87 mg, 0.24 mmol) in THF (3 mL) while stirring at room temperature.

After 17 days of stirring, the volatile components were removed *in vacuo* to produce a colorless oil. The oil was then redissolved in a mixture of THF (1 mL) and *n*-pentane (2 mL) and recrystallized at -35 ºC to yield colorless crystals of **3.6b**. Yield: 72 mg (61%). d.p. 151 ºC. Crystals for X-ray diffraction studies were grown by storing an *n*-pentane/THF (2:1) solution of **3.6b** at -35 ºC;

^{1}H NMR (400 MHz, CD_3CN): δ 7.66-7.64 (m, 1H), 7.56-7.53 (m, 1H), 7.44-7.40 (m, 1H), 7.26 (s, br, 1H), 7.13-7.12 (m, 2H), 7.00-6.92 (m, 2H), 6.85-6.81 (m, 2H), 6.70-6.66 (m, 2H), 6.64-6.59 (m, 1H), 2.69 (q, br, *J* = 87.5 Hz, 1H), 0.98 (s, 6H), 0.82 (s, 6H), -0.34 (s, 9H);

^{1}H{^{11}B} NMR (400 MHz, CD_3CN): δ 7.66-7.64 (m, 1H), 7.56-7.53 (m, 1H), 7.44-7.40 (m, 1H), 7.27-7.24 (m, 1H), 7.14-7.11 (m, 2H), 7.00-6.92 (m, 2H), 6.86-6.81 (m, 2H), 6.70-6.66 (m, 2H), 6.64-6.60 (m, 1H), 2.68 (s, 1H), 0.98 (s, 6H), 0.82 (s, 6H), -0.34 (s, 9H);

^{13}C{^{1}H} NMR (101 MHz, CD_3CN): δ 141.10, 135.44, 135.37, 126.13, 125.82, 125.34, 124.27, 123.80, 123.28, 122.72, 122.69, 81.39, 25.65, 25.52, 0.63;

^{11}B NMR (128 MHz, CD_3CN): δ 35.4 (s, br), -12.1 (d, *J* = 87.5 Hz);

^{11}B{^{1}H} NMR (128 MHz, CD_3CN): δ 35.1 (s, br), -12.1 (s);

FT-IR (cm^{-1} (ranked intensity)): 2975 (12), 1477 (9), 1425 (11), 1371 (15), 1303 (6), 1238 (4), 1143 (3), 1023 (14), 972 (8), 833 (1), 742 (2), 712 (7), 677 (5), 620 (10), 596 (13);

High-resolution mass spectrometry (HRMS) electrospray ionization (ESI): calcd for $C_{28}H_{35}B_2O_2Si$ $[M]^-$, 453.2592; found, 453.2521.

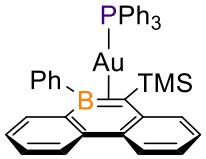

3.7

Synthesis of 3.7 (CCDC 1981974): A solution of (Ph_3P)AuCl (52 mg, 0.11 mmol) in benzene (4 mL) was added to a solution of **3.4** (39 mg, 0.11 mmol) in THF (1 mL) while stirring at room temperature. After 60 minutes, the volatile components were evaporated *in vacuo* to produce a colorless oily residue, which was then extracted with benzene (10 mL). The benzene extract was then filtered and lyophilized to yield **3.7** as a white powder. Yield: 73 mg (88%). d.p. 57 ºC. Crystals for X-ray diffraction studies were grown by vapor diffusion of *n*-pentane into a toluene solution of **3.7**;

^{1}H NMR (400 MHz, $CDCl_3$): δ 8.53 (dd, *J* = 8.0, 1.0 Hz, 1H), 8.48 (d, *J* = 8.0 Hz, 1H), 8.06 (d, *J* = 8.0 Hz, 1H), 7.62-7.57 (m, 2H), 7.52-7.42 (m, 6H), 7.34-7.29 (m, 8H), 7.24-7.20 (m, 3H), 7.10-7.05 (m, 6H), 0.16 (s, 9H);

^{13}C{^{1}H} NMR (101 MHz, $CDCl_3$): δ 149.70, 143.20, 143.14, 141.33, 139.75, 134.70, 134.06 (d, *J* = 14.0 Hz), 132.77, 131.56, 131.53, 129.54, 129.17 (d, *J* = 11.0 Hz), 129.07, 129.01, 128.83, 126.46, 125.55, 125.27, 125.20, 124.73, 122.83, 122.12, 4.65;

^{11}B NMR (128 MHz, $CDCl_3$): δ 42.4;

^{31}P{^{1}H} NMR (162 MHz, $CDCl_3$): δ 39.7;

FT-IR (cm^{-1} (ranked intensity)): 1476 (9), 1435 (5), 1243 (8), 1099 (7), 928 (10), 829 (3), 745 (6), 729 (12), 691 (1), 676 (14), 639 (13), 619 (11), 593 (15), 532 (2), 498 (4);

High-resolution mass spectrometry (HRMS) electrospray ionization (ESI): calcd for $C_{40}H_{37}AuBKPSi$ $[M+K]^+$, 823.1798; found, 823.1802.

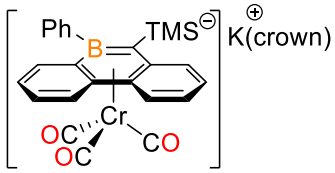

3.8

Synthesis of 3.8 (CCDC 1981975): A solution of tris(acetonitrile)tricarbonylchromium (76 mg, 0.29 mmol) in THF (6 mL) was added dropwise to a solution of **3.4** (108 mg, 0.296 mmol) in THF (2 mL) while stirring at room temperature under low-light conditions. After 75 minutes, dibenzo-18-crown-6 (107 mg, 0.296 mmol) in dichloromethane (4 mL) was added to the reaction mixture. The reaction mixture was then stirred for an additional 30 minutes, after which the volatile components were evaporated *in vacuo*. The resulting solid was then washed with dichloromethane (1 mL) to yield **3.8** as a bright red powder. Yield: 189 mg (75%). d.p. 131 ºC. Crystals for X-ray diffraction studies were grown by vapor diffusion of a dichloromethane solution of **3.8** into toluene;

^{1}H NMR (400 MHz, CD_3CN): δ 8.75 (d, *J* = 8.5 Hz, 1H), 8.50 (d, *J* = 8.5 Hz, 1H), 8.37 (s, br, 1H), 7.83 (d, *J* = 8.5 Hz, 1H), 7.47-7.24 (m, 8H), 7.02 (t, *J* = 8 Hz, 1H), 6.95 (s, 8H), 4.14-4.12 (m, 8H), 3.92-3.90 (m, 8H), 0.13 (s, 9H);

^{13}C{^{1}H} NMR (101 MHz, CD_3CN): δ 147.83, 138.68, 135.75, 135.38, 133.81, 129.97, 129.29, 129.18, 127.34, 125.99, 124.47, 123.42, 122.33, 122.23, 122.10, 115.49, 112.29, 97.83, 70.01, 68.00, 4.53;

^{11}B NMR (128 MHz, CD_3CN): δ 30.5;

FT-IR (cm^{-1} (ranked intensity)): 1903 (7), 1821 (13), 1769 (3), 1503 (5), 1453 (9), 1245 (2), 1211 (10), 1120 (4), 1061 (12), 942 (6), 830 (8), 743 (1), 702 (15), 683 (14), 634 (11);

High-resolution mass spectrometry (HRMS) chemical ionization (CI): calcd for $C_{25}H_{23}BCrO_3Si$ $[M+H]^-$, 462.0915; found, 462.0912.

CHAPTER FOUR

Borataalkene Hydrofunctionalization Reactions

This chapter published as: Bartholome, T. A.; Martinez, J. J.; Kaur, A.; Wilson, D. J. D.; Dutton, J. L.; Martin, C. D.; *Organometallics* **2021**, *40*, 1966-1973. Reprinted with permission.

4.1 Introduction

Hydrofunctionalization reactions of alkenes are a valuable synthetic tool and, accordingly, have been studied extensively in recent decades.[187-193] This class of reactions consists of the addition of an element-hydrogen bond across a carbon-carbon double bond (Scheme 4.1). Prominent examples of hydrofunctionalization reactions for olefins include hydroboration,[191, 194-200] hydrosilylation,[191, 199, 201-204] hydroamination,[205-208] hydroalkoxylation,[209-210] and hydrocarbonation.[193, 201, 211-221] Intriguingly, some examples of hydrofunctionalization reactions, specifically hydroboration, hydrophosphination, and hydroamination, have recently been realized for boron-boron double and triple bonds by Braunschweig and coworkers.[222-226]

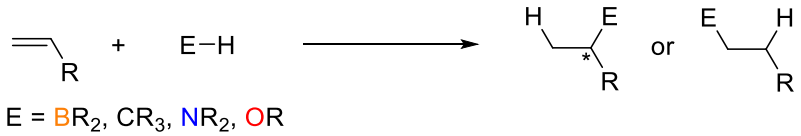

Scheme 4.1. Hydrofunctionalization reactions of an olefin with an α-olefin as an example.

Borataalkenes, anionic boron-containing analogues of olefins, have been known since 1972 and, although somewhat rare,[168, 227] have been demonstrated to undergo a

variety of transformations,[94, 96, 228] including alkylation at carbon,[94, 99, 172] epoxide ring opening,[98, 229] and the "boron-Wittig" reaction.[94, 97, 100-101] Despite the abundance of literature on olefin hydrofunctionalization, the hydrofunctionalization reactivity of borataalkenes has remained largely unexplored. The Erker and Yamashita groups have demonstrated that zwitterionic borataalkenes react with hydroboranes to form species containing four-membered BHBC rings (Scheme 4.2).[166, 169-171] The anionic borataalkene moiety of 9-borataphenanthrene anion **3.4** undergoes hydroboration with pinacolborane (HBpin) to produce a tetracoordinate boron species in which the hydride is not bridged between the two boron centers.[230] Aside from the aforementioned hydroboration reactivity, examples of borataalkene hydrofunctionalization reactions are generally absent from the literature.[231] Given the vast utility of alkene hydrofunctionalization chemistry and limited precedent for B=C bond hydrofunctionalization, we herein investigate the potential of a B=C system for hydrofunctionalization reactivity.

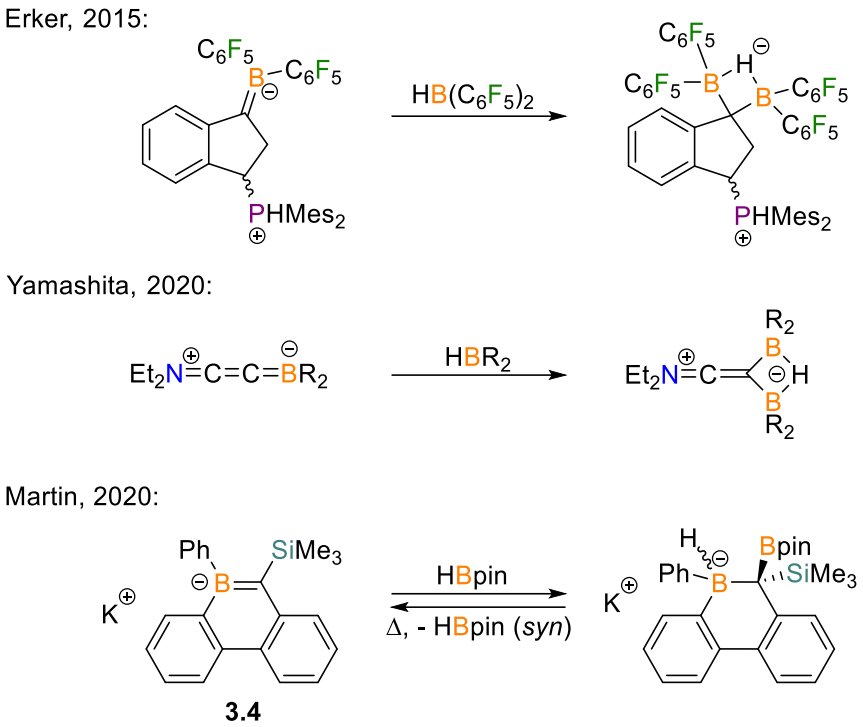

Scheme 4.2. Selected examples of reactions of borataalkene-containing species with hydroboranes (Mes = 2,4,6-trimethylphenyl, BR_2 = 9-borabicyclo[3.3.1]nonyl, pin = pinacolate).

4.2 Hydrofunctionalization of a 9-Borataphenanthrene B=C Bond

Addition reactions of C-H bonds across unactivated olefins are generally challenging transformations.[189, 212, 216-217] However, given that the polarization of the B=C bond results in an electron-rich carbon center, we envisioned that a borataalkene might engage in C-H bond addition reactivity. The reaction of **3.4** with neat acetonitrile at room temperature led to a new singlet in the tetracoordinate region at -12.8 ppm in the *in situ* ^{11}B NMR spectrum after 4 days (c.f. **3.4** = 40.4 ppm). Complete conversion could be achieved upon heating at 80 °C for 16 hours. Sequestration of the potassium counter-cation with dibenzo-18-crown-6 enabled isolation in 66% yield of the major product, determined by X-ray crystallography to be the cyanomethyl-substituted tetracoordinate boron species **4.1**

(Figure 4.1). *Syn* addition of an acetonitrile C-H bond across the borataalkene B=C bond occurred rather than insertion of the cyano group into the C-Si bond of **3.4** (Scheme 4.3). This differs from nitrile/silyl carbanion reactivity observed for trimethylsilyl-substituted alkyllithium reagents, which undergo cyano group insertion into the C-Si bond to produce *N*-trimethylsilyl-1-azaallyl anions.[232-233] The ^{1}H NMR spectrum of **4.1** contains three signals integrating in a 1:1:1 ratio for the three aliphatic protons derived from acetonitrile: a singlet at 1.19 ppm assigned to the proton added to the borataalkene carbon and two multiplets at 1.31-1.27 ppm and 1.02-0.98 ppm assigned to the two diastereotopic protons of the cyanomethyl group. An absorption band at 2212 cm^{-1} in the FT-IR spectrum confirms the presence of the pendant nitrile.

Given the unusual C-H bond activation with acetonitrile (sp^3 C-H substrate), the activation of sp^2 and sp C-H bonds was targeted using pentafluorobenzene and phenylacetylene, respectively (Scheme 4.3). The reactions of **3.4** with excess pentafluorobenzene and phenylacetylene were monitored by *in situ* ^{11}B NMR spectroscopy and resulted in complete consumption of **3.4** within 2 days at 60 °C for both reactions with signals in the tetracoordinate region observed at -9.7 ppm (**4.2**) and -15.4 ppm (**4.3**), respectively. Compound **4.2** was isolated as the [K(18-crown-6)]$^{+}$ salt in 45% yield and **4.3** as the free potassium salt in 84% yield.[234] Single-crystal X-ray diffraction studies identified both species as the *syn* C-H addition products **4.2** and **4.3** for pentafluorobenzene and phenylacetylene, respectively (Figure 4.1). Aliphatic singlets at 2.23 ppm and 1.42 ppm corresponding to the protonated borataalkene carbon were observed in the ^{1}H NMR spectra of **4.2** and **4.3**, respectively. The reactivity of **3.4** with phenylacetylene differs from

that of a tantalum-bound η^2-borataalkene ligand, which underwent cyclization with the alkyne moiety of phenylacetylene to form a five-membered BC_3Ta ring.[14]

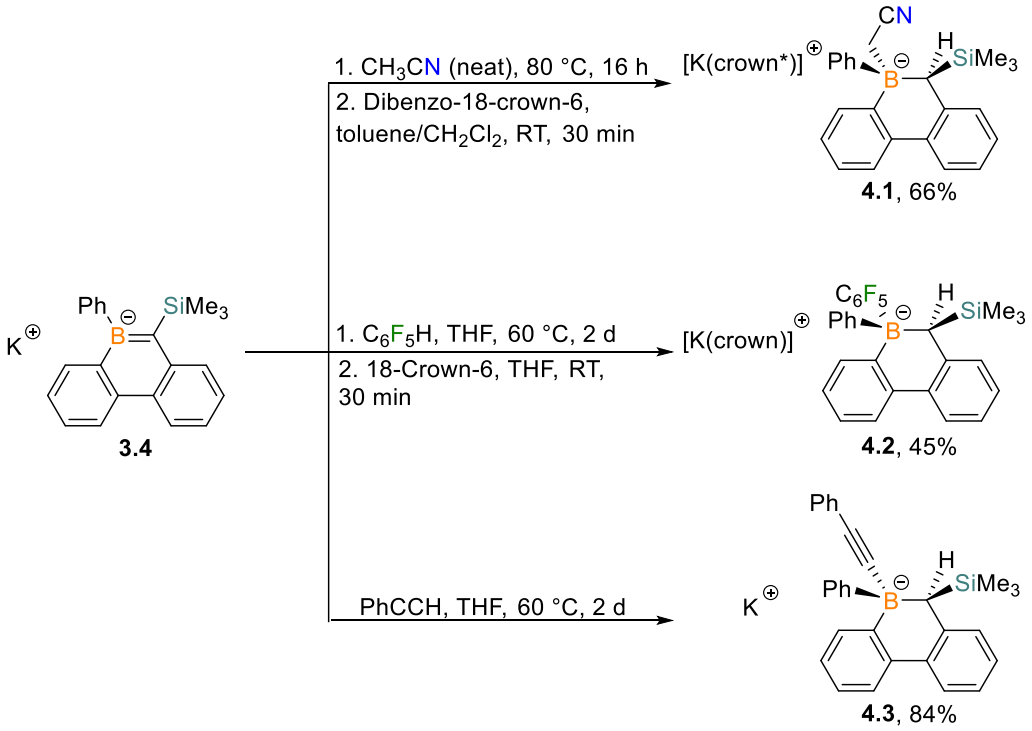

Scheme 4.3. C-H activation reactivity of **3.4** with acetonitrile, pentafluorobenzene, and phenylacetylene (relative stereochemistry depicted).

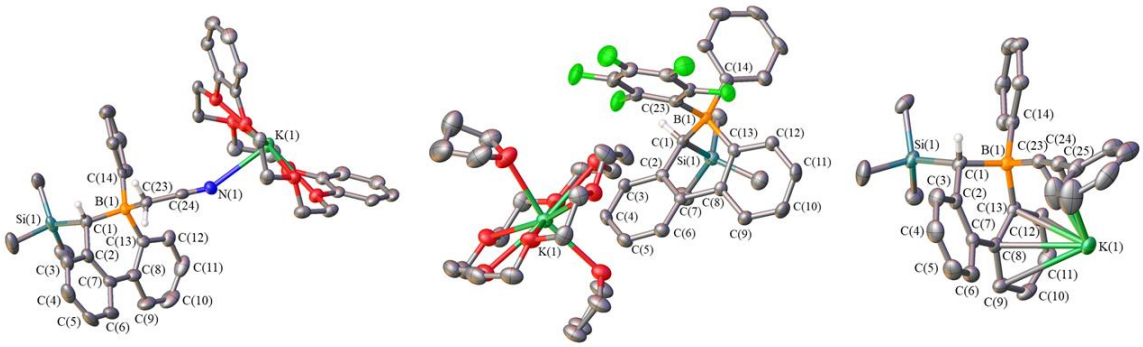

Figure 4.1. Solid state structures of **4.1**, **4.2**, and **4.3** (left to right). Hydrogen atoms (except those from the C-H addition event) and non-coordinated solvates are omitted for clarity, and thermal ellipsoids are drawn at the 50% probability level. For disordered atoms, only the component with the higher occupancy is shown. Only the asymmetric unit is displayed for **3**; the full dimeric structure is shown in Figure C-36.

The uncatalyzed series of sp^3, sp^2, and sp regioselective C-H addition reactivity is noteworthy and suggests that the borataphenanthrene B=C bond could react with other element-hydrogen bonds.[235] Accordingly, we examined the reactivity of **3.4** with N-H and O-H bond-containing substrates. The reaction of **3.4** with excess diphenylamine at room temperature in THF resulted in complete conversion after 24 hours to a tetracoordinate boron-containing product as indicated by *in situ* ^{11}B NMR spectroscopy (δ = -4.1 ppm, Scheme 4.4). The product was isolated in 58% yield and identified as the *syn* hydroamination product **4.4** by a single crystal X-ray diffraction study (Figure 2). A diagnostic aliphatic singlet at 2.05 ppm in the ^{1}H NMR spectrum was assigned as the proton derived from the N-H unit in diphenylamine, further confirming hydroamination of the B=C bond.

The reaction of **3.4** with phenol resulted in a different outcome than the N-H and C-H substrates. In this case, the 1:1 stoichiometric reaction did not result in an isolable product, but heating a 2:1 mixture at 60 °C for 24 hours generated a single product exhibiting a tetracoordinate ^{11}B NMR signal at -1.5 ppm. X-ray crystallography revealed that in addition to hydroalkoxylation of the borataalkene B=C bond, desilylation at the borataalkene carbon also occurred with the elimination of phenyl trimethylsilyl ether (**4.5**, Scheme 4.4, Figure 4.2). This structural assignment was corroborated by the absence of a trimethylsilyl singlet in the product ^{1}H NMR spectrum and the presence of two aliphatic multiplets at 2.11-2.07 ppm and 2.00-1.96 ppm corresponding to the diastereotopic protons at the 10-position. Additionally, generation of phenyl trimethylsilyl ether was indicated by the presence of a trimethylsilyl singlet (δ = 0.16 ppm in C_6D_6) in the crude ^{1}H NMR spectrum. The reactivity of **3.4** with O-H containing substrates was explored further by

exposing a THF solution of **3.4** to water. This resulted in hydration of the B=C bond and hydrolysis of the C-Si bond with the elimination of trimethylsilanol (**4.6**, Scheme 4.4), similar to the reaction with phenol. Although this species could not be cleanly isolated, X-ray crystallography confirmed its generation (Figure 4.2).

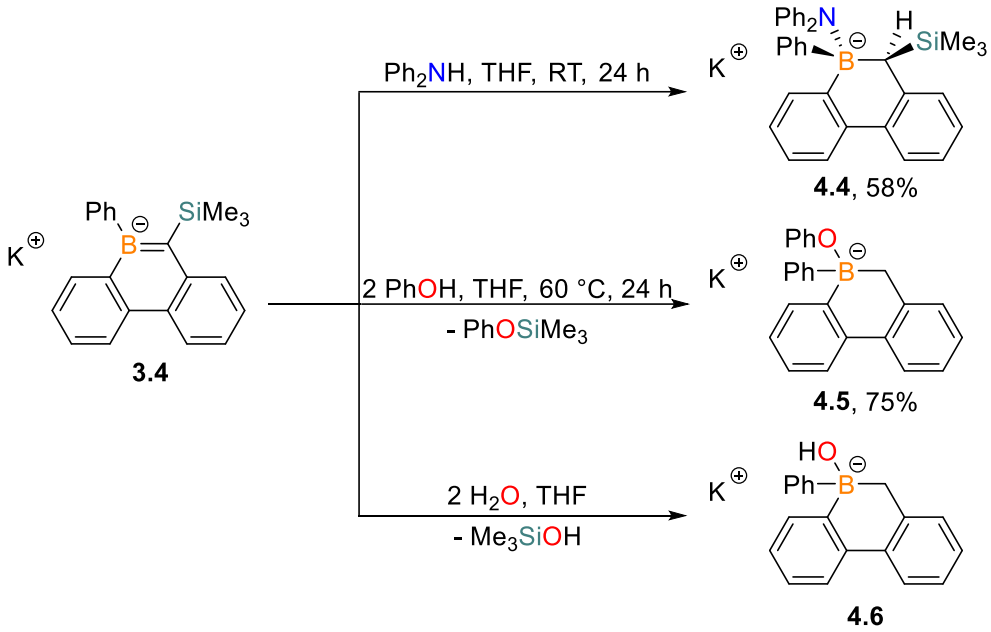

Scheme 4.4. Reactions of **3.4** with N-H and O-H containing substrates (relative stereochemistry depicted).

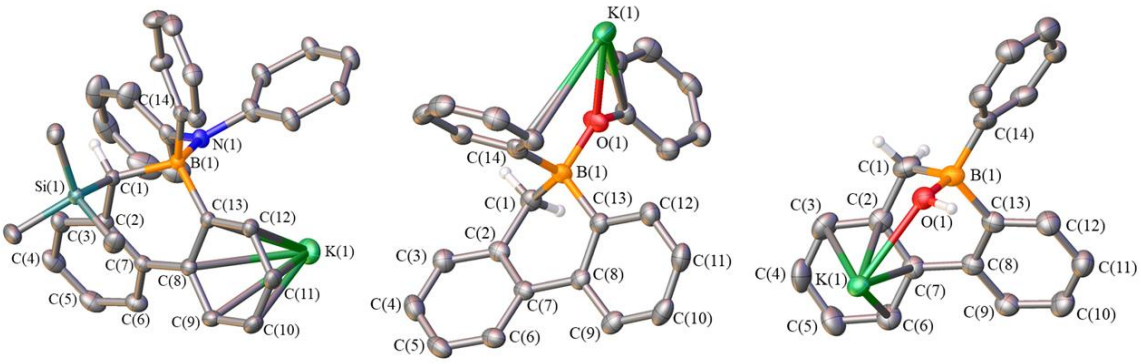

Figure 4.2. Solid-state structures of **4.4**, **4.5**, and **4.6** (left to right). Hydrogen atoms (except those derived from N-H or O-H bonds) and solvates are omitted for clarity. Thermal ellipsoids are drawn at the 50% probability level. Only the asymmetric units are displayed; the full polymeric structures are shown in Figures C-37-39. For disordered atoms, only the component with the higher occupancy is shown.

4.3 Mechanism of B=C Bond Hydrofunctionalization

The mechanism for the hydrofunctionalization reactivity of **3.4** with the various substrates was investigated using density functional theory (DFT) calculations for two different pathways (Scheme 4.5): one in which a simple addition event occurs (observed for **4.1**-**4.4**), and another that includes desilylation (observed for **4.5** and **4.6**). In the formation of **4.1**-**4.4**, the first step consists of deprotonation of the substrate by the borataalkene carbon to produce a 9,10-dihydro-9-boraphenanthrene (**Int4.1**). This is consistent with the Hirshfeld charge of -0.25 at carbon versus -0.08 at boron. The barrier for this step (**TS4.1**) was found to be higher for the three C-H addition reactions (120.2, 111.0, and 108.7 kJ/mol for acetonitrile, pentafluorobenzene, and phenylacetylene, respectively) than for the hydroamination with diphenylamine (82.2 kJ/mol). The difference in barrier height is consistent with the experimental observation that the hydroamination proceeds to completion at room temperature while the three C-H activation reactions require elevated temperatures. The second step consists of coordination of the

deprotonated substrate to the Lewis acidic boron center of **Int4.1**. Although a transition state could not be located for this step, a scan of the reaction energy surface with constrained geometry optimizations at a series of fixed B-$C_{substrate}$ bond distances (CH_3CN substrate reaction) indicates that product formation may be considered a barrierless process (without a transition state), while the loss of planarity around the boron atom (from sp^2 to sp^3) occurs very late on the reaction energy surface and requires minimal energy change. For all four substrates, formation of the B=C hydrofunctionalization product **Prod4.1** was found to be thermodynamically favorable (Table 4.1).

For the formation of **4.5** and **4.6**, protonation of the borataalkene carbon initially occurs as in the formation of **4.1-4.4**, with barrier heights of 48.2 and 86.5 kJ/mol (consistent with the observed room-temperature reactivity) for the reactions with phenol and water, respectively. Although modeling the H_2O reaction with a single H_2O molecule was problematic, addition of an explicit water solvent molecule in the form a water dimer (H_2O-H_2O) yielded more appropriate transition state and minimum energy structures. Following the formation of protonated borataphenanthrene **Int4.1**, however, nucleophilic attack by the deprotonated substrate occurs at silicon rather than boron. The electrophilicity at silicon is corroborated by a Hirshfeld charge of +0.38, which is considerably greater than that of boron at +0.11 in **Int4.1**. Desilylation subsequently produces the *C*-unsubstituted 9-borataphenanthrene anion **Int4.2**. Hydrofunctionalization of the B=C bond in **Int4.2** then occurs in a manner analogous with that observed for **A** in the mechanism for the formation of **4.1-4.4** by deprotonation of the substrate by the borataalkene carbon to produce 9,10-dihydro-9-boraphenanthrene **Int4.3**, which subsequently undergoes nucleophilic attack by the deprotonated substrate to form **Prod4.2** in a barrierless process.

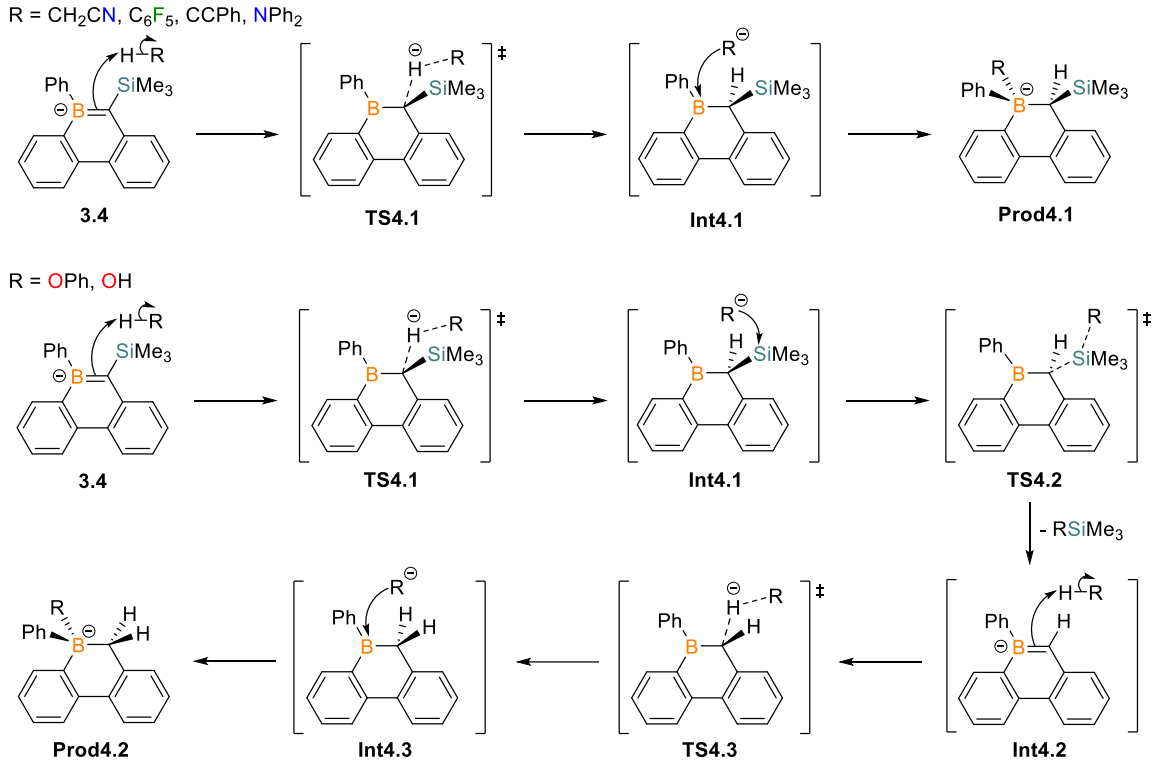

Scheme 4.5. General reaction pathways modeled for hydrofunctionalization reactions with **3.4**.

Table 4.1. Calculated reaction free energies (Δ*G*, kJ/mol) for pathways arising from proton abstraction of the substrate by **3.4**, together with experimental pK_a (DMSO) of substrates.[a]

Substrate	pK_a [b]	TS4.1	Int4.1	Prod4.1	TS4.2	Int4.2	TS4.3	Int4.3	Prod4.2
H_2O	31.4	86.5	55.6	-47.3	103.6	-106.3	14.1	-9.7	-143.3
CH_3CN	31.3	120.2	55.6	-11.2	151.1	-27.0	103.4	69.6	-25.7
C_6F_5H	29.0	111.0	37.2	-10.0	160.4	-27.0	100.0	51.2	-34.6
PhCCH	28.8	108.7	33.8	-52.2	123.0	-70.7	44.9	4.1	-113.5
Ph_2NH	25.0	82.2	21.9	-10.6	161.2	-58.6	26.0	4.4	-60.3
PhOH	18.0	48.2	-16.7	-71.6	64.3	-117.0	-70.6	-92.5	-171.2

[a]B3LYP-D3(BJ)/def2-TZVP(THF)//B3LYP-D3(BJ)/def2-SVP(THF) results, with energies given relative to the reactants. H_2O modeled as a hydrogen-bonded dimer H_2O-H_2O.
[b]pK_a in DMSO.[236-241]

Further analysis of the desilylation pathway indicated that the formation of **Prod4.2** is more thermodynamically favorable than the formation of **Prod4.1** for all six substrates examined. This, combined with the large positive Hirshfeld charge at silicon in **Int4.1**, suggests that the system is kinetically controlled. Evidence supporting kinetic control is found when the barrier heights for **TS4.2** and **TS4.3** are compared with that of **TS4.1** across all six reactions. For the three C-H substrates, the largest barrier is associated with **TS4.3**, which is greater than the **TS4.1** barrier by 10.3, 16.1, and 6.8 kJ/mol for CH_3CN, C_6F_5H, and PhCCH, respectively. With Ph_2NH the largest barrier is for **TS4.2** (139.3 kJ/mol), which is 57.1 kJ/mol larger than for **TS4.1**. In contrast, the largest barrier on the **Prod4.2** pathway for phenol (**TS4.2**, 80.9 kJ/mol) is smaller in magnitude than the **TS4.1** barrier for PhCCH and C_6F_5H, which is consistent with PhOH forming **Prod4.2** despite the fact that PhCCH and C_6F_5H form **Prod4.1** under similar experimental conditions. For water, the calculated barrier for **TS4.3** of 120.5 kJ/mol is larger than for **TS4.1** (86.5 kJ/mol), although the **TS4.3** barrier is at the top of the range of barriers that can be crossed at room temperature. Comparison of the pK_a of the substrate (Table 1) with the **TS4.1** barrier height indicates a near-perfect linear relationship (r^2 = 0.992 excluding H_2O, Figure 4.3), which confirms the importance of the acidic proton character of the substrate. Water is an outlier to this trend, with a lower barrier than expected from the relationship to pK_a in DMSO, with the caveat that the pK_a of water varies widely depending on solvent.[238] Since water does not follow the trend for **TS4.1** barriers, it is possible that similar factors influence the **TS4.2** and **TS4.3** barrier heights, with the true barrier potentially being lower in energy. Modeling the system with larger water clusters could alter the calculated energetics;

however, the results presented here for a water dimer provide qualitative agreement with experiment.

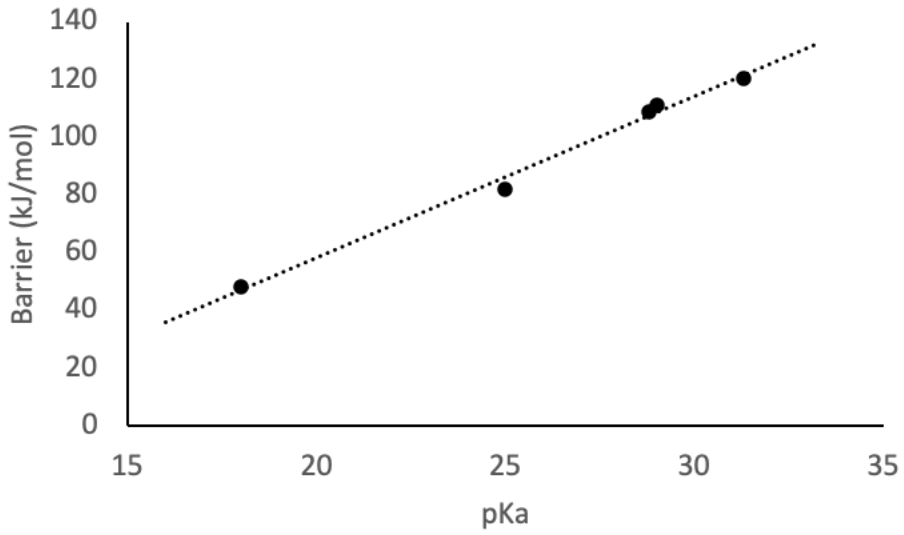

Figure 4.3. Relationship between substrate pK_a and TS1 barrier height. Water is omitted as a substrate.

The borataalkene moiety at the 9- and 10-positions of the 9-borataphenanthrene anion was demonstrated to undergo a variety of hydrofunctionalization reactions, including hydroalkylation, hydroarylation, hydroalkynylation, hydroamination, hydroalkoxylation, and hydration. Such hydrofunctionalization reactions were previously unexplored for borataalkenes, which is surprising given the extensively studied hydrofunctionalization reactivity of alkenes. The ability of the anionic B=C bond to undergo diverse hydrofunctionalization reactivity presents B=C hydrofunctionalization as a potentially promising technique for the synthesis of tetracoordinate borates.

4.4 Experimental Details

THF-d_8 for NMR spectroscopy was purchased from Cambridge Isotope Laboratories and stored over molecular sieves. Compound **3.4** was prepared by the literature procedure.[230] The following reagents were purchased from the listed manufacturers and used as received: dibenzo-18-crown-6 (TCI), pentafluorobenzene (TCI), 18-crown-6 (Oakwood Chemical), phenol (Sigma-Aldrich), diphenylamine (Alfa Aesar). Phenylacetylene was purchased from Chem-Impex International and stored over molecular sieves.

Computational Methods

Geometry optimization of reactants, products, intermediates, and TS structures were carried out at the B3LYP-D3(BJ)[179, 185-186, 242-243]/def2-SVP[180] level of theory inclusive of solvation (SMD model,[244] tetrahydrofuran solvent). Frequency calculations were also performed analytically at the same level of theory to characterize all stationary points and to calculate thermodynamic corrections. Subsequent electronic energy calculations were carried out at the B3LYP-D3(BJ)[179, 185-186, 242-243]/def2-TZVP[180] (SMD model,[244] tetrahydrofuran solvent) using the Gaussian 16 suite of programs.[178] Extended Hirshfeld method CM5[245] partial charges were calculated at the B3LYP-D3(BJ)[179, 185-186, 242-243]/def2-TZVP[180] (SMD model,[244] tetrahydrofuran solvent) level. Single point calculations with wB97X-D[246]/def2-TZVP[180] (SMD model,[244] tetrahydrofuran solvent) were also carried out and yielded equivalent results. All calculations were carried out in Gaussian 16.[178]

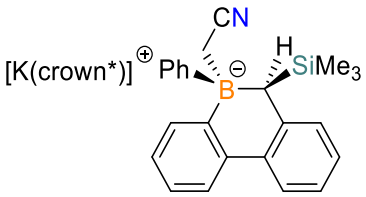

4.1

Synthesis of 4.1 (CCDC 2055588): **3.4** (74 mg, 0.20 mmol) was dissolved in acetonitrile (3 mL) and heated to 80 ºC in a pressure tube with a Teflon cap. After 16 hours of heating, the volatile components were removed from the solution *in vacuo*, and the resulting pale yellow oil was redissolved in toluene (2 mL). A solution of dibenzo-18-crown-6 (74 mg, 0.20 mmol) in dichloromethane (2 mL) was then added to the product solution while stirring at room temperature. After an additional 30 minutes of stirring, the volatile components were removed from the solution *in vacuo*, and the residue was washed with toluene (10 mL) and dried *in vacuo* to yield **4.1** as a white powder. Yield: 103 mg (66%). d.p. 173 °C. Crystals for X-ray diffraction studies were grown by vapor diffusion of *n*-pentane into a 1,4-dioxane solution of **4.1**;

^{1}H NMR (400 MHz, CD_3CN): δ 7.68 (d, *J* = 7.0 Hz, 2H), 7.64-7.60 (m, 2H), 7.57-7.55 (m, 1H), 7.17-7.14 (m, 2H), 7.10-7.05 (m, 2H), 7.03-6.99 (m, 1H), 6.97-6.95 (m, 10H), 6.94-6.90 (m, 1H), 4.17-4.15 (m, 8H), 3.94-3.92 (m, 8H), 1.31-1.27 (m, 1H), 1.19 (s, 1H), 1.02-0.98 (m, 1H), -0.75 (s, 9H);

^{13}C{^{1}H} NMR (101 MHz, CD_3CN): δ 149.21, 147.86, 142.81, 138.51, 135.48, 134.27, 132.03, 128.66, 127.12, 125.84, 125.81, 125.71, 125.07, 123.97, 123.31, 123.27, 122.33, 112.31, 70.03, 68.03, 0.53;

^{11}B NMR (128 MHz, CD_3CN): δ -12.8;

FT-IR (cm^{-1} (ranked intensity)): 2212 (14), 1504 (6), 1455 (10), 1247 (2), 1213 (4), 1120 (3), 1052 (7), 942 (5), 908 (11), 854 (8), 779 (15), 739 (1), 705 (9), 603 (12), 466 (13);

High-resolution mass spectrometry (HRMS) electrospray ionization (ESI): calcd for $C_{24}H_{25}BNSi$ $[M]^-$, 366.1849; found, 366.1864.

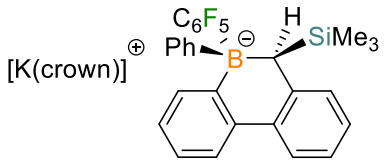

4.2

Synthesis of 4.2 (CCDC 2055589): Pentafluorobenzene (0.423 mL, 3.81 mmol) was added to a solution of **3.4** (278 mg, 0.762 mmol) in THF (5 mL) while stirring at room temperature. The resulting solution was then transferred to a pressure tube with a Teflon cap and heated at 60 °C for 2 d, after which the solution was cooled to room temperature and filtered. A solution of 18-crown-6 (211 mg, 0.799 mmol) in THF (2 mL) was then added to the solution while stirring at room temperature. After 30 minutes of stirring, the volatile components were removed *in vacuo* to produce a red-orange oil, which was washed with 1:1 THF/*n*-pentane (5 mL) at -35 °C and dried *in vacuo* to yield **4.2** as a yellow-orange solid. Yield: 273 mg (45%). d.p. 78 °C. Crystals for X-ray diffraction studies were grown by storing the crude product oil at -35 °C;

^{1}H NMR (400 MHz, $CDCl_3$): δ 7.93 (d, *J* = 7.0 Hz, 1H), 7.65 (d, *J* = 7.0 Hz, 2H), 7.51 (d, *J* = 7.0 Hz, 1H), 7.41 (d, *J* = 7.0 Hz, 1H), 7.15-7.05 (m, 5H), 7.00-6.97 (m, 1H), 6.91-6.82 (m, 2H), 3.48 (s, 24H), 2.23 (s, 1H), -0.63 (s, 9H);

$^{13}C\{^{1}H\}$ NMR (101 MHz, $CDCl_3$): δ 150.69, 143.07, 138.87, 135.29, 134.04, 133.99, 133.95, 130.07, 125.98, 124.59, 124.21, 123.86, 123.26, 122.81, 121.47, 70.09, 1.03;

^{11}B NMR (128 MHz, $CDCl_3$): δ -9.7;

$^{19}F\{^{1}H\}$ NMR (376 MHz, $CDCl_3$): δ -129.64 (d, br, *J* = 1728 Hz, 2F), -166.42 (t, *J* = 20.5 Hz, 1F), -167.70-167.87 (m, 2F);

FT-IR (cm^{-1} (ranked intensity)): 2886 (12), 1503 (11), 1434 (3), 1350 (6), 1240 (8), 1104 (1), 1067 (10), 960 (2), 829 (4), 746 (5), 708 (7), 678 (13), 650 (14), 607 (9), 471 (15);

High-resolution mass spectrometry (HRMS) electrospray ionization (ESI): calcd for $C_{28}H_{23}BF_5Si$ $[M]^-$, 493.1582; found, 493.1539.

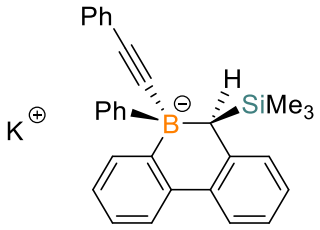

4.3

Synthesis of 4.3 (CCDC 2055590): Phenylacetylene (33 µL, 0.30 mmol) was added to a solution of **3.4** (101 mg, 0.276 mmol) in THF (5 mL) while stirring at room temperature. The resulting solution was then transferred to a pressure tube with a Teflon cap and heated at 60 °C for 2 d, after which the volatile components were removed *in vacuo* to produce a yellow oil. The oil was then washed with benzene (5 mL) to produce a white precipitate, which was dried *in vacuo* to yield **4.3** as a white powder. Yield: 108 mg (84%). d.p. 114 °C. Crystals for X-ray diffraction studies were grown by storing a dichloromethane solution of **4.3** at -35 °C;

^{1}H NMR (400 MHz, CD_3CN): δ 7.85 (d, *J* = 7.0 Hz, 2H), 7.62-7.59 (m, 1H), 7.56-7.52 (m, 1H), 7.50-7.49 (m, 1H), 7.15-6.90 (m, 13H), 1.42 (s, 1H), -0.70 (s, 9H);

^{13}C{^{1}H} NMR (101 MHz, CD_3CN): δ 150.34, 143.47, 136.40, 133.66, 131.76, 131.51, 129.66, 129.55, 128.76, 126.78, 125.97, 125.88, 124.84, 123.80, 123.31, 122.98, 0.76;

^{11}B NMR (128 MHz, CD_3CN): δ -15.4;

FT-IR (cm^{-1} (ranked intensity)): 1593 (13), 1485 (8), 1425 (7), 1240 (3), 1054 (10), 897 (15), 828 (2), 741 (1), 712 (5), 692 (12), 676 (4), 613 (6), 578 (14), 529 (9), 466 (11);

High-resolution mass spectrometry (HRMS) electrospray ionization (ESI): calcd for $C_{30}H_{28}BSi$ $[M]^-$, 427.2053; found, 427.2071.

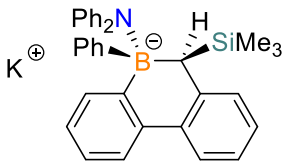

4.4

Synthesis of 4.4 (CCDC 2055591): A solution of diphenylamine (171 mg, 1.01 mmol) in THF (2 mL) was added to a solution of **A** (74 mg, 0.20 mmol) in THF (2 mL) while stirring at room temperature. After 24 hours of stirring, the volatile components were removed *in vacuo* to produce a yellow oil, which was lyophilized from benzene (3 mL) and washed with *n*-pentane (8 × 10 mL) to yield **4.4** as a yellow powder. Yield: 63 mg (58%). d.p. 109 °C. Crystals for X-ray diffraction studies were grown by vapor diffusion of a dichloromethane solution of **4.4** into benzene;

^{1}H NMR (400 MHz, THF-d_8): δ 7.82-7.80 (m, 2H), 7.41 (dd, *J* = 7.5, 1.5 Hz, 1H), 7.32-7.30 (m, 1H), 7.23 (d, *J* = 7.0 Hz, 1H), 7.03-7.00 (m, 3H), 6.94-6.92 (m, 1H), 6.89-6.84

(m, 1H), 6.83-6.81 (m, 1H), 6.78-6.74 (m, 1H), 6.71 (td, *J* = 7.5, 1.5 Hz, 1H), 6.58-6.53 (m, 4H), 6.46 (td, *J* = 7.5, 1.5 Hz, 1H), 6.39 (s, br, 3H), 6.21 (s, br, 1H), 6.16-6.14 (m, 1H), 2.05 (s, 1H), -0.65 (s, 9H);

$^{13}C\{^{1}H\}$ NMR (101 MHz, THF-d_8): δ 154.70, 149.30, 143.78, 140.01, 136.82, 135.94, 131.63, 129.62, 127.28, 126.23, 125.16, 124.74, 124.58, 124.49, 123.32, 123.12, 121.88, 117.97, 1.65;

^{11}B NMR (128 MHz, THF-d_8): δ -4.1;

FT-IR (cm^{-1} (ranked intensity)): 3044 (15), 2951 (13), 1591 (3), 1493 (4), 1425 (10), 1307 (7), 1241 (5), 1174 (11), 1027 (9), 842 (2), 783 (14), 741 (1), 690 (6), 612 (8), 466 (12)

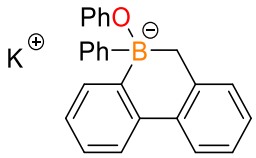

4.5

Synthesis of 4.5 (CCDC 2055592): A solution of phenol (42 mg, 0.45 mmol) in THF (1 mL) was added to a solution of **3.4** (83 mg, 0.23 mmol) in THF (2 mL) while stirring at room temperature. The resulting solution was transferred to a pressure tube with a Teflon cap and heated at 60 °C for 24 h, after which the volatile components were removed *in vacuo*. The residue was then washed with 1:1 dichloromethane/*n*-pentane (2 × 3 mL) and dried *in vacuo* to yield **5** as a white solid. Yield: 65 mg (75%). d.p. 173 °C. Crystals for X-ray diffraction studies were grown by vapor diffusion of a dichloromethane solution of **4.5** into hexanes;

^{1}H NMR (400 MHz, $CDCl_3$): δ 7.57 (d, *J* = 7.5 Hz, 1H), 7.35 (d, *J* = 7.0 Hz, 1H), 7.29-7.27 (m, 1H), 7.23-7.19 (m, 1H), 7.17-7.14 (m, 1H), 7.08-7.06 (m, 3H), 6.95-6.87 (m, 4H), 6.81 (t, *J* = 7.5 Hz, 2H), 6.69-6.66 (m, 1H), 6.59 (t, *J* = 7.5 Hz 1H), 6.42 (d, *J* = 8.0 Hz, 2H), 2.11-2.07 (m, 1H), 2.00-1.96 (m, 1H);

^{13}C{^{1}H} NMR (101 MHz, $CDCl_3$): δ 160.92, 145.38, 139.36, 137.86, 132.98, 131.09, 130.68, 129.24, 127.78, 127.34, 126.97, 126.36, 125.21, 124.83, 124.17, 123.98, 120.44, 118.22;

^{11}B NMR (128 MHz, $CDCl_3$): δ -1.5;

FT-IR (cm^{-1} (ranked intensity)): 3045 (14), 1590 (5), 1486 (2), 1426 (8), 1255 (4), 1167 (9), 1070 (13), 1023 (15), 998 (12), 903 (3), 752 (1), 699 (6), 619 (10), 598 (11), 564 (7)

CHAPTER FIVE

Metal Complexes Featuring 9-Borataphenanthrene Ligands[247]

5.1 Introduction

Transition-metal complexes of boratabenzenes have been known since 1970, when a cobalt(III) boratabenzene complex was synthesized by Herberich and coworkers.[52] In the decades since then, a vast array of boratabenzene metal complexes has been prepared,[8-9, 52-92] including several complexes containing fused polycyclic boratabenzene ligands.[66, 70, 75, 93] The simplest examples of fused polycyclic boratabenzenes are the bicyclic 1- and 2-boratanaphthalenes.[66, 75, 93, 152] The first 1-boratanaphthalenes were synthesized by Ashe and coworkers in 1999 and were demonstrated to undergo complexation with RuCp* and $ZrCl_2Cp^*$ upon reaction with $[Cp^*RuCl]_4$ and Cp^*ZrCl_3, respectively.[93] The ability of 2-boratanaphthalenes to serve as η^6 ligands was explored extensively by Paetzold and coworkers in 1986, with coordination to iron, rhodium, and lithium being reported.[66] A fused tricyclic boratabenzene, the 9-borataanthracene anion, was shown by Bazan and coworkers in 1998 to form complexes with $ZrCl_2Cp^*$ and $ZrMe_2Cp^*$ upon reaction with Cp^*ZrCl_3 and Cp^*ZrMe_2Cl, respectively.[70] Additionally, the complex with $ZrCl_2Cp^*$ was shown to act as a precatalyst for the oligomerization of ethylene. Selected examples of fused polycyclic boratabenzene complexes are depicted in Figure 5.1.

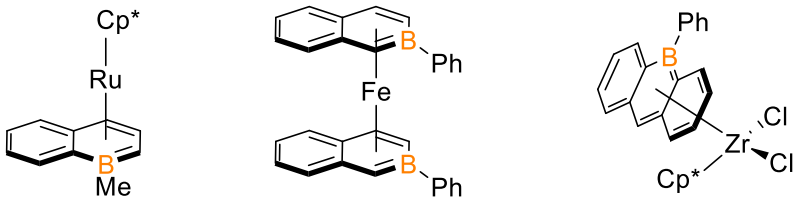

5.1 **5.2** **5.3**

Figure 5.1. Selected examples of transition-metal complexes of fused polycyclic boratabenzenes.

The synthesis of a 9-borataphenanthrene anion (**3.4**) *via* deprotonation of a 9,10-dihydro-9-boraphenanthrene precursor was reported in Chapter Three (Scheme 3.1).[230] The resulting species represents a new class of fused polycyclic boratabenzene and was demonstrated to form an anionic η^6 complex with $Cr(CO)_3$ and a charge-neutral η^2 complex with $Au(PPh_3)$ (**3.8** and **3.7**, Scheme 5.1). Given the abundance of monocyclic boratabenzene metal complexes in the literature and the lack of known charge-neutral η^6-borataphenanthrene complexes, we sought to prepare neutral complexes of a 9-borataphenanthrene ligand with a variety of metal centers.

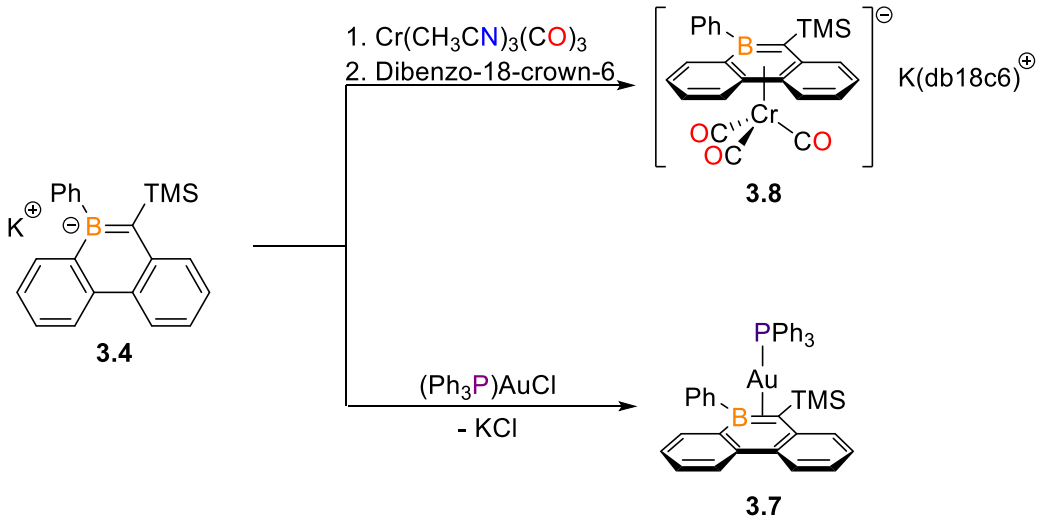

Scheme 5.1. Previous syntheses of 9-borataphenanthrene transition-metal complexes.

5.2 9-Borataphenanthrene Complexes of Rhodium(I) and Iridium(I)

In an effort to prepare charge-neutral complexes containing η^6-borataphenanthrene ligands, **3.4** was reacted in a 2:1 stoichiometry with the reagents $M_2Cl_2(cod)_2$ (M = Rh, Ir; cod = 1,5-cyclooctadiene) in THF (Scheme 5.2). Within one hour at room temperature, complete disappearance of the ^{11}B NMR singlet at 40.4 ppm corresponding to **3.4** was observed along with the emergence of new singlets at 31.4 ppm and 28.8 ppm for the reactions with $Rh_2Cl_2(cod)_2$ and $Ir_2Cl_2(cod)_2$, respectively. In both cases, the formation of a precipitate (presumably potassium chloride) was observed over the course of the reaction. Single-crystal X-ray crystallography revealed the identity of the products to be the η^6-borataphenanthrene complexes of Rh(cod) and Ir(cod) (**5.4**, Figure 5.2). The products were isolated as yellow solids with yields of 82% for **5.4a** and 98% (minimum purity 93%) for **5.4b**.

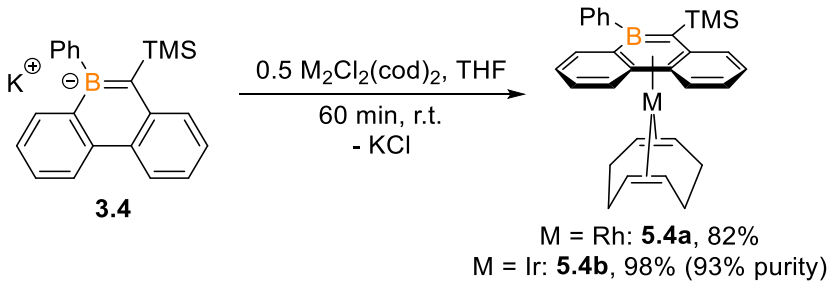

Scheme 5.2. Reactions of **3.4** with $M_2Cl_2(cod)_2$ reagents to produce **5.4**.

To gain insight into the electron-donating properties of **3.4** as a ligand, complexation with $Rh(CO)_2$ was attempted *via* reaction of **3.4** with $Rh_2Cl_2(CO)_4$ in THF (Scheme 5.3). Complete consumption of **3.4** and emergence of a new singlet at 35.1 ppm were observed by *in situ* ^{11}B NMR spectroscopy within 30 minutes at room temperature.

The resulting species was isolated as an orange solid in 88% yield and determined by X-ray crystallography to be complex **5.5** in which η^6-coordination of the borataphenanthrene ligand to rhodium is observed (Figure 5.2). Reaction of the monocyclic boratabenzene ligand **5.6** with $Rh_2Cl_2(CO)_4$ in THF yielded the analogous η^6-boratabenzene complex **5.7** with the reaction proceeding to completion within 45 minutes at room temperature (Scheme 5.3). The resulting species was isolated as a yellow solid in 81% yield and exhibits a singlet at 26.1 ppm in its ^{11}B NMR spectrum. Generation of an η^6 complex was further confirmed by single-crystal X-ray diffraction studies (Figure 5.2). The FT-IR spectrum of **5.5** exhibits carbonyl stretching bands at 2049 and 1990 cm^{-1} *versus* 2032 and 1971 cm^{-1} for **5.7**, indicating that the fused polycyclic ligand **3.4** is a weaker donor than the monocyclic ligand **5.6**. This is likely a result of retention of aromaticity in the fused benzene rings of **3.4** accompanied by reduction of aromaticity in the central boratabenzene ring.

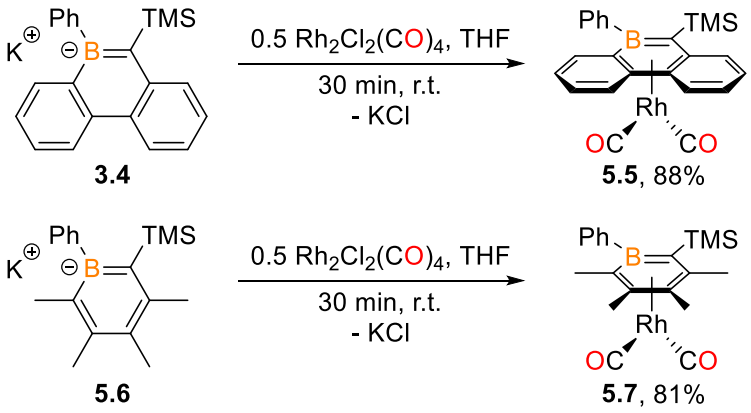

Scheme 5.3. Synthesis of $Rh(CO)_2$ complexes of **3.4** and **5.6**.

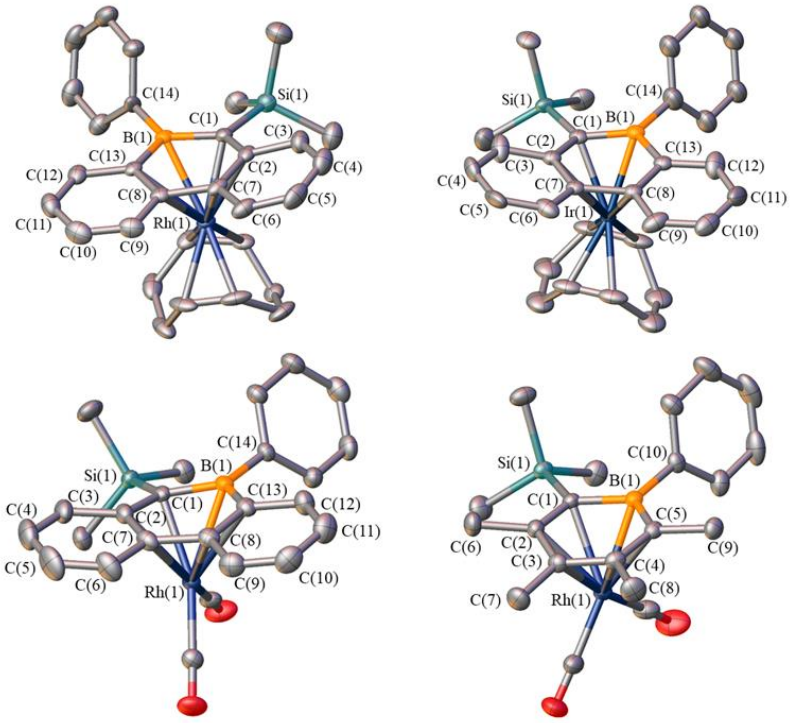

Figure 5.2. Solid-state structures of **5.4a**, **5.4b**, **5.5**, and **5.7**. Hydrogen atoms are omitted for clarity, and thermal ellipsoids are drawn at the 50% probability level.

5.3 9-Borataphenanthrene Complexes of Iron(II)

In addition to the aforementioned Rh(I) and Ir(I) complexes, a series of Fe(II) complexes with **3.4** was prepared. These complexes could not be isolated due to decomposition at room temperature; however, their formation was confirmed by X-ray crystallography (Figure 5.3). The reaction of **3.4** with $FeBr_2$ resulted in two different outcomes depending on whether acetonitrile was present in the reaction mixture. In the absence of acetonitrile, the bis(borataphenanthrene) complex **5.8** is formed within 7 days at room temperature in THF (Scheme 5.4). In this complex, coordination of two different ligand rings to the iron center is observed; one borataphenanthrene ligand coordinates by the central boratabenzene ring while the other coordinates by the carbonaceous ring

opposite from boron. In the presence of acetonitrile, however, insertion of the acetonitrile cyano group into the borataphenanthrene C-Si bond is observed within 18 hours at room temperature in THF (**5.9**, Scheme 5.4). The resulting boron-substituted 1-azaallyl ligand coordinates to the iron center in a bidentate fashion with both ligands exhibiting the same coordination mode. This nitrile insertion is likely a result of the carbanionic character of the borataalkene carbon of the 9-borataphenanthrene anion, as nitrile insertion into C-Si bonds has been previously reported by Lappert and coworkers for trimethylsilyl-substituted alkyllithium compounds.[232-233] In addition to these homoleptic Fe(II) complexes, a heteroleptic borataphenanthrene/cyclopentadienide complex of Fe(II) could be generated. Upon reaction of **3.4** with $CpFe(CO)_2I$, the formation of heteroleptic sandwich complex **5.10** was observed within 3 days at room temperature in THF (Scheme 5.4). In this complex, the borataphenanthrene ligand is observed to coordinate by the central boratabenzene ring as in the Rh(I) and Ir(I) complexes.

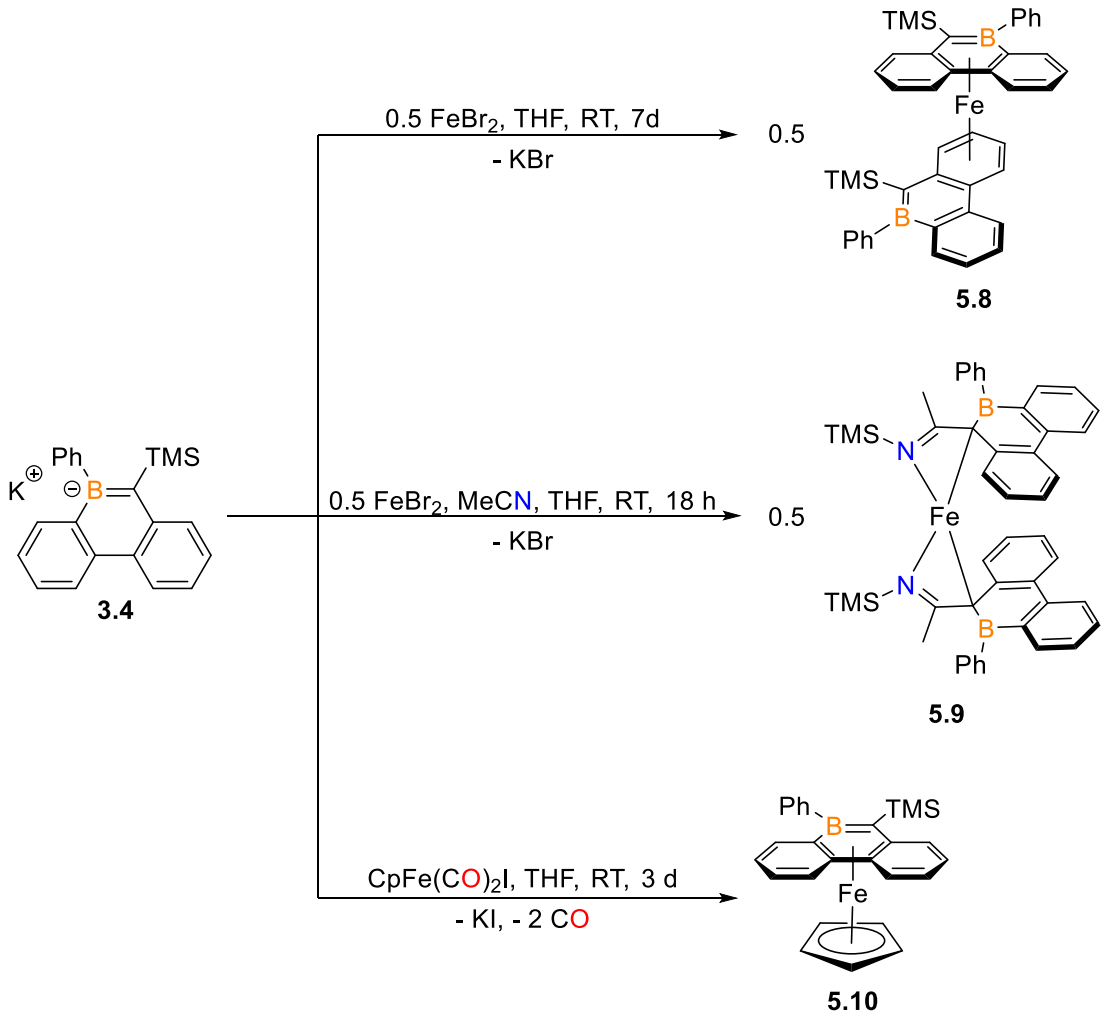

Scheme 5.4. Synthesis of Fe(II) complexes from **3.4**. Products characterized by X-ray crystallography but not isolated.

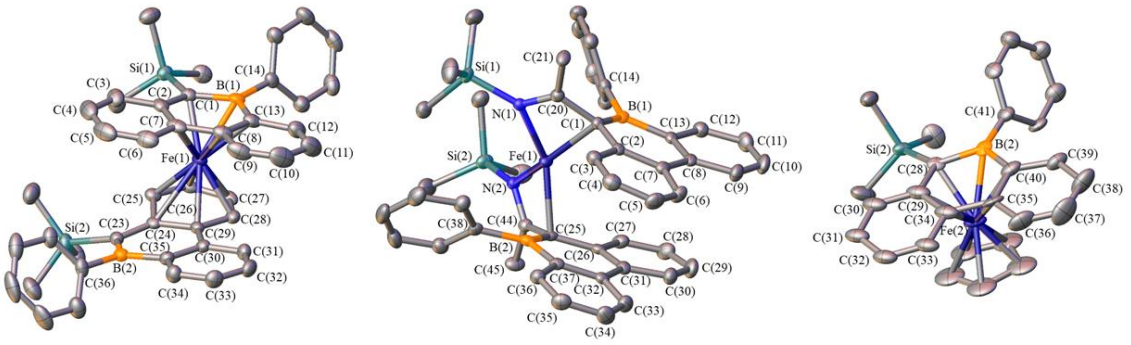

Figure 5.3. Solid-state structures of **5.8-5.10**. Hydrogen atoms (and benzene solvate for **5.7**) are omitted for clarity, and thermal ellipsoids are drawn at the 50% probability level.

A variety of transition-metal complexes containing the 9-borataphenathrene anion were synthesized. Charge-neutral complexes of η^6-borataphenanthrene ligands with Rh(cod), Ir(cod), and $Rh(CO)_2$ were prepared from the respective $M_2Cl_2L_n$ reagents [M = Rh, Ir; L_n = $(cod)_2$, $(CO)_4$] in high yields. Comparison of the FTIR spectra of $Rh(CO)_2$ complex **5.5** with the analogous monocyclic boratabenzene complex indicated that the fused polycyclic boratabenzene ligand **3.4** is a weaker electron donor than the monocyclic boratabenzene ligand **5.6**. Additionally, a series of Fe(II) complexes were synthesized and, although not isolable, were characterized by X-ray crystallography. These included a bis(borataphenanthrene) sandwich complex exhibiting two different ligand coordination modes, a boron-substituted 1-azaallyl complex, and a heteroleptic borataphenanthrene/cyclopentadienide sandwich complex. The series of complexes represents a vast expansion of the scope of known 9-borataphenanthrene metal complexes.

5.4 Experimental Details

3.4,[230] chloro(1,5-cyclooctadiene)rhodium(I) dimer,[248-249] chloro(1,5-cyclooctadiene)iridium(I) dimer,[250] and **5.6**[251] were prepared by the literature procedures.

The following reagents were purchased from commercial sources and used as received: chlorodicarbonylrhodium(I) dimer (Strem Chemicals), iron(II) bromide (Alfa Aesar), and cyclopentadienyliron dicarbonyl iodide (Aldrich). For the crystal structure of compound **5.5**, a solvated acetonitrile molecule disordered across a symmetry site was removed using the SQUEEZE function in PLATON.[252]

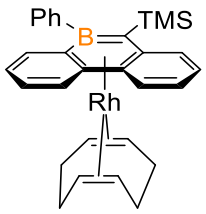

5.4a

Synthesis of 5.4a: A solution of $Rh_2Cl_2(cod)_2$ (26 mg, 0.052 mmol) in THF (1 mL) was added to a solution of **3.4** (39 mg, 0.11 mmol) in THF (2 mL) while stirring at room temperature. After an hour of stirring, the volatile components were removed *in vacuo*, and the resulting solid was extracted with benzene (5 mL). The benzene extract was then filtered and lyophilized to yield **5.4a** as a yellow powder. Yield: 45 mg (82%). D.p. 207 °C. Crystals for X-ray diffraction studies were grown by vapor diffusion of a chloroform solution of **5.4a** into toluene;

^{1}H NMR (400 MHz, $CDCl_3$): δ 8.26 (d, *J* = 8.5 Hz, 1H), 7.94 (t, *J* = 9.0 Hz, 2H), 7.82 (s, br, 1H), 7.75 (d, *J* = 8.0 Hz, 1H), 7.55-7.34 (m, 7H), 7.23 (t, *J* = 7.5 Hz, 1H), 4.02-3.99 (m, 2H), 2.97-2.95 (m, 2H), 2.05-1.88 (m, 4H), 1.72-1.63 (m, 2H), 1.43-1.34 (m, 2H), 0.10 (s, 9H);

^{13}C{^{1}H} NMR (101 MHz, $CDCl_3$): δ 135.86, 134.95, 134.31, 133.10, 131.09, 129.49, 127.85, 127.45, 127.24, 127.03, 126.88, 125.94, 125.40, 124.83, 124.62, 124.60, 120.50,

114.08, 114.06, 104.73, 104.72, 78.09 (d, J = 13.0 Hz), 74.54 (d, J = 13.0 Hz), 33.01, 29.24, 3.78;

^{11}B NMR (128 MHz, $CDCl_3$): δ 31.4;

FT-IR (cm^{-1} (ranked intensity)): 1426 (7), 1329 (13), 1252 (4), 996 (15), 927 (6), 828 (2), 754 (10), 740 (1), 704 (3), 678 (12), 626 (9), 609 (5), 593 (14), 481 (11), 452 (8);

High-resolution mass spectrometry (HRMS) electrospray ionization (ESI): calcd for $C_{30}H_{35}BRhSi$ $[M+H]^+$, 537.1656; found, 537.1648.

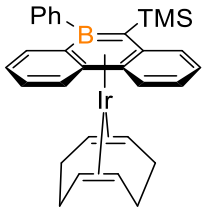

5.4b

Synthesis of 5.4b: A solution of $Ir_2Cl_2(cod)_2$ (30. Mg, 0.045 mmol) in THF (2 mL) was added to a solution of **3.4** (33 mg, 0.091 mmol) in THF (1 mL) while stirring at room temperature. After an hour of stirring, the volatile components were evaporated *in vacuo*, and the residue was extracted with benzene (5 mL). The benzene extract was then filtered and lyophilized to yield **5.4b** as a dark yellow powder. Yield: 56 mg (98%, minimum purity 93%). D.p. 168 °C. Crystals for X-ray diffraction studies were grown by vapor diffusion of an *n*-pentane solution of **5.4b** into toluene;

^{1}H NMR (400 MHz, $CDCl_3$): δ 8.29 (d, J = 8.5 Hz, 1H), 7.91-7.89 (m, 2H), 7.77 (d, J = 7.0 Hz, 1H), 7.63-7.59 (m, 1H), 7.56-7.52 (m, 2H), 7.49-7.43 (m, 3H), 7.40-7.32 (m, 2H), 7.17-7.13 (m, 1H), 3.98-3.94 (m, 2H), 2.57 (td, J = 8.0, 4.0 Hz, 2H), 1.92-1.80 (m, 4H), 1.66-1.56 (m, 2H), 1.22-1.14 (m, 2H), 0.08 (s, 9H);

$^{13}C\{^{1}H\}$ NMR (101 MHz, $CDCl_3$): δ 135.87, 134.29, 134.23, 131.62, 129.08, 128.84, 127.28, 127.04, 125.98, 125.93, 125.20, 124.45, 120.78, 120.32, 106.01, 102.15, 62.35, 57.37, 34.80, 30.17, 3.91;

^{11}B NMR (128 MHz, $CDCl_3$): δ 28.8;

FT-IR (cm^{-1} (ranked intensity)): 2881 (13), 1427 (8), 1261 (4), 1025 (12), 923 (10), 903 (5), 865 (9), 827 (2), 755 (6), 739 (1), 702 (3), 673 (14), 625 (15), 606 (7), 484 (11).

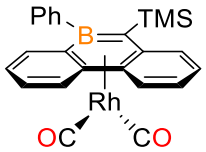

5.5

Synthesis of 5.5: A solution of $Rh_2Cl_2(CO)_4$ (26 mg, 0.067 mmol) in THF (2 mL) was added to a solution of **3.4** (50. mg, 0.14 mmol) in THF (2 mL) while stirring at room temperature. After 30 minutes of stirring, the volatile components were evaporated *in vacuo*, and the resulting brown oil was extracted with *n*-pentane (4 mL). The pentane extract was then filtered, and the volatile components were evaporated *in vacuo* from the filtrate to yield **5.5** as an orange solid. Yield: 57 mg (88%). d.p. 44 °C. Crystals for X-ray diffraction studies were grown by storing an acetonitrile solution of **5.5** at -35 °C;

^{1}H NMR (400 MHz, C_6D_6): δ 8.12-8.10 (m, 1H), 7.83-7.74 (m, 4H), 7.68 (d, J = 8.0 Hz, 1H), 7.41-7.37 (m, 2H), 7.33-7.30 (m, 1H), 7.26-7.22 (m, 1H), 7.13-7.09 (m, 2H), 7.02 (t, J = 7.5 Hz, 1H), 0.29 (s, 9H);

$^{13}C\{^{1}H\}$ NMR (101 MHz, C_6D_6): δ 134.85, 132.18, 129.96, 129.95, 128.77, 128.73, 128.66, 127.71, 127.31, 127.10, 126.99, 122.09, 118.25, 118.24, 99.89, 99.87, 3.01;

^{11}B NMR (128 MHz, C_6D_6): δ 35.1;

FT-IR (cm^{-1} (ranked intensity)): 2049 (2), 1990 (1), 1427 (11), 1249 (5), 927 (10), 832 (3), 745 (4), 721 (13), 702 (7), 612 (8), 593 (14), 580 (15), 549 (6), 492 (9), 423 (12);

High-resolution mass spectrometry (HRMS) chemical ionization (CI): calculated for $C_{24}H_{22}BO_2RhSi$ $[M]^+$, 484.0537; found, 484.0533.

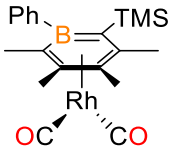

5.7

Synthesis of 5.7: A solution of $Rh_2Cl_2(CO)_4$ (22 mg, 0.055 mmol) in THF (1 mL) was added to a solution of **5.6** (41 mg, 0.13 mmol) in THF (2 mL) while stirring at room temperature. After 45 minutes of stirring, the volatile components were evaporated *in vacuo*, and the resulting brown oil was extracted with *n*-pentane (5 mL). The pentane extract was then filtered, and the volatile components were evaporated *in vacuo* from the filtrate to yield **5.7** as a yellow solid. Yield: 39 mg (81%). d.p. 46 °C. Crystals for X-ray diffraction studies were grown by storing an acetonitrile solution of **5.7** at -35 °C;

^{1}H NMR (400 MHz, C_6D_6): δ 7.79-7.46 (m, br, 2H), 7.35-7.31 (m, 2H), 7.25-7.20 (m, 1H), 2.05 (s, 3H), 1.83 (s, 3H), 1.79 (s, 3H), 1.78 (s, 3H), 0.10 (s, 9H);

^{13}C{^{1}H} NMR (101 MHz, C_6D_6): δ 191.21, 190.39, 133.19, 133.15, 127.76, 126.51, 97.70, 97.67, 23.40, 19.58, 18.79, 16.37, 3.23;

^{11}B NMR (128 MHz, C_6D_6): δ 26.1;

FT-IR (cm^{-1} (ranked intensity)): 2032 (5), 1971 (1), 1383 (14), 1295 (15), 1246 (6), 1015 (9), 881 (12), 830 (2), 759 (11), 741 (8), 702 (3), 624 (10), 591 (13), 548 (7), 506 (4); **High-resolution mass spectrometry** (HRMS) chemical ionization (CI): calculated for $C_{20}H_{26}BO_2RhSi$ $[M]^+$, 440.0850; found, 440.0862.

CHAPTER SIX

Synopsis and Future Work

6.1 Synopsis

The synthesis and reactivity of the first 9-borataphenanthrene anion, **3.4**, have been described in this dissertation. Chapter Two describes the insertion of carbene units into the endocyclic B-C bonds of 9-phenyl-9-borafluorene (**1.9b**), a precursor to the 9-borataphenanthrene anion. The reaction of **1.9b** with trimethylsilyldiazomethane resulted in the formation of a six-membered, nonaromatic BC_5 ring *via* carbene insertion into the borole B-C bond. The resulting species, **2.8**, was found to react with an additional equivalent of diazo compound to produce the seven-membered BC_6 species **2.9** *via* carbene insertion into the other endocyclic B-C_{sp2} bond (Scheme 6.1).

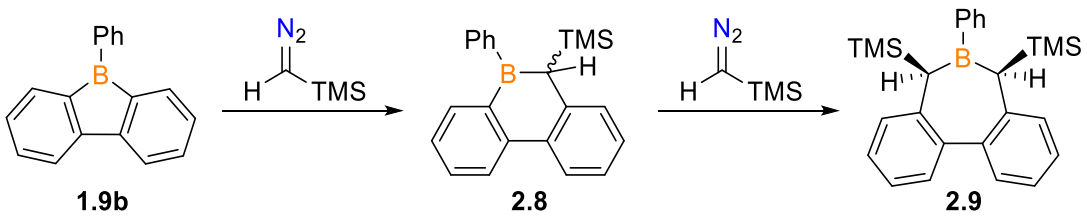

Scheme 6.1. Ring expansion of 9-phenyl-9-borafluorene with trimethylsilyldiazomethane. T. A. Bartholome, K. R. Bluer, C. D. Martin, *Dalton Trans.* **2019**, *48*, 6319-6322. Adapted by permission of the Royal Society of Chemistry.

Chapter Three describes the synthesis of a 9-borataphenanthrene anion and several preliminary examples of its boratabenzene- and borataalkene-like reactivity. The 9-borataphenanthrene anion, **3.4**, was synthesized *via* deprotonation of compound **2.8** with

potassium bis(trimethylsilyl)amide (KHMDS). The ability of **3.4** to act as a base and nucleophile was demonstrated by protonation with triflic acid to regenerate **2.8** and methylation with iodomethane to produce **3.5**. Reaction of **3.4** with pinacolborane (HBpin) resulted in hydroboration of the B=C bond at the 9- and 10-positions, with isomerization from the *syn* diastereomer to the *anti* diastereomer being observed over time. The olefin-like behavior of **3.4** was further demonstrated by its η^2-coordination to gold upon reaction with $(Ph_3P)AuCl$. Finally, the aromatic character of **3.4** was demonstrated by η^6-coordination with chromium upon reaction with $(MeCN)_3Cr(CO)_3$ (Scheme 6.2). Additionally, computational studies indicated that the central BC_5 ring is aromatic, indicating boratabenzene character, while the HOMO is localized on the B=C moiety at the 9- and 10-positions, indicating borataalkene character.

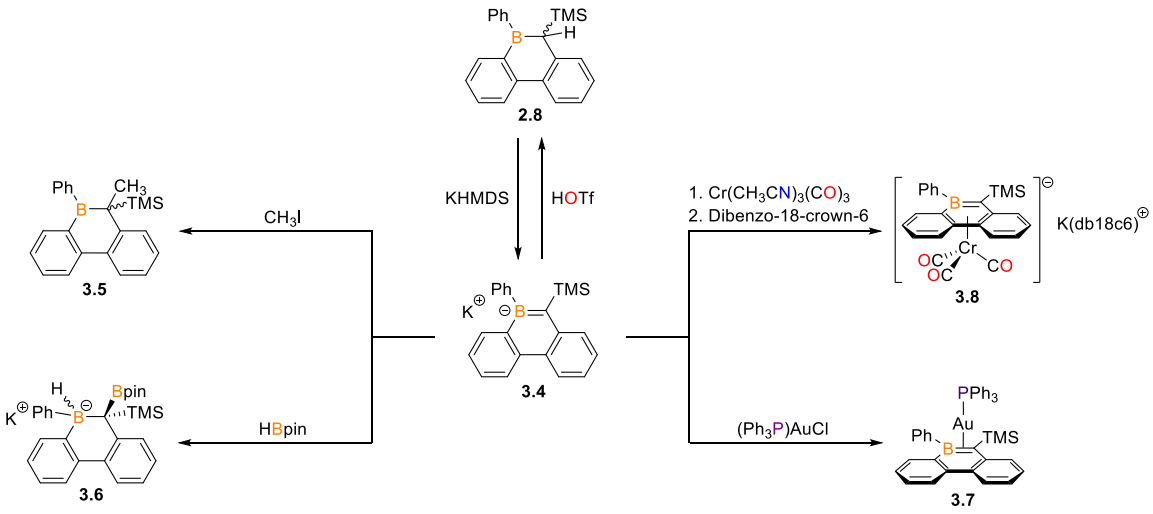

Scheme 6.2. Synthesis of the first 9-borataphenanthrene anion and examples of boratabenzene- and borataalkene-like reactivity.

Chapter Four describes the hydrofunctionalization reactivity of 9-borataphenanthrene **3.4**. Activation of C-H bonds in sp^3, sp^2, and sp substrates was

demonstrated by the reactions of **3.4** with acetonitrile, pentafluorobenzene, and phenylacetylene, respectively. In all cases, *syn* addition of the C-H bond across the B=C bond at the 9- and 10-positions was observed. Similarly, hydroamination of **3.4** was achieved upon reaction with diphenylamine and resulted in *syn* addition analogous to that observed for the three C-H substrates. However, the reactions of **3.4** with the O-H bond-containing substrates phenol and water resulted in desilylation at carbon in addition to hydrofunctionalization of the B=C bond (Scheme 6.3). Mechanistic calculations were carried out for two different pathways: one in which desilylation occurs and one in which only hydrofunctionalization occurs.

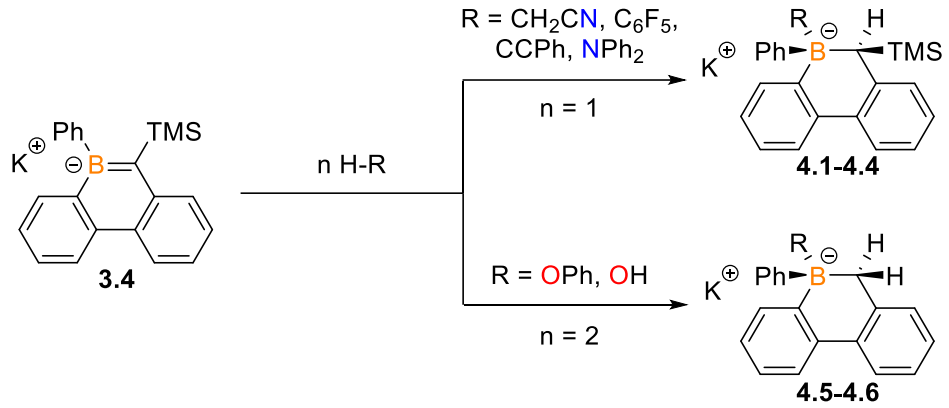

Scheme 6.3. Hydrofunctionalization reactivity of the 9-borataphenanthrene anion.

Chapter Five described the preparation of a wide variety of metal complexes featuring 9-borataphenanthrene ligands. The reactions of **3.4** with $Rh_2Cl_2(cod)_2$ and $Ir_2Cl_2(cod)_2$ resulted in η^6-complexation of the borataphenanthrene ligand with Rh(cod) and Ir(cod), respectively (cod = 1,5-cyclooctadiene). Similarly, the reaction of **3.4** with $Rh_2Cl_2(CO)_4$ resulted in η^6-complexation with $Rh(CO)_2$. Upon comparison of the FT-IR carbonyl bands of the resulting complex, **5.5**, with an analogous monocyclic boratabenzene

complex, the polycyclic ligand was found to be a weaker electron donor. A series of complexes of **3.4** with iron were observed by X-ray crystallography but not isolated. These included a bis(borataphenanthrene) sandwich complex in which two different ligand coordination modes are observed, a mixed borataphenanthrene/cyclopentadienide sandwich complex, and a boron-substituted 1-azaallyl complex resulting from nitrile insertion into the borataphenanthrene C-Si bond (Scheme 6.4).

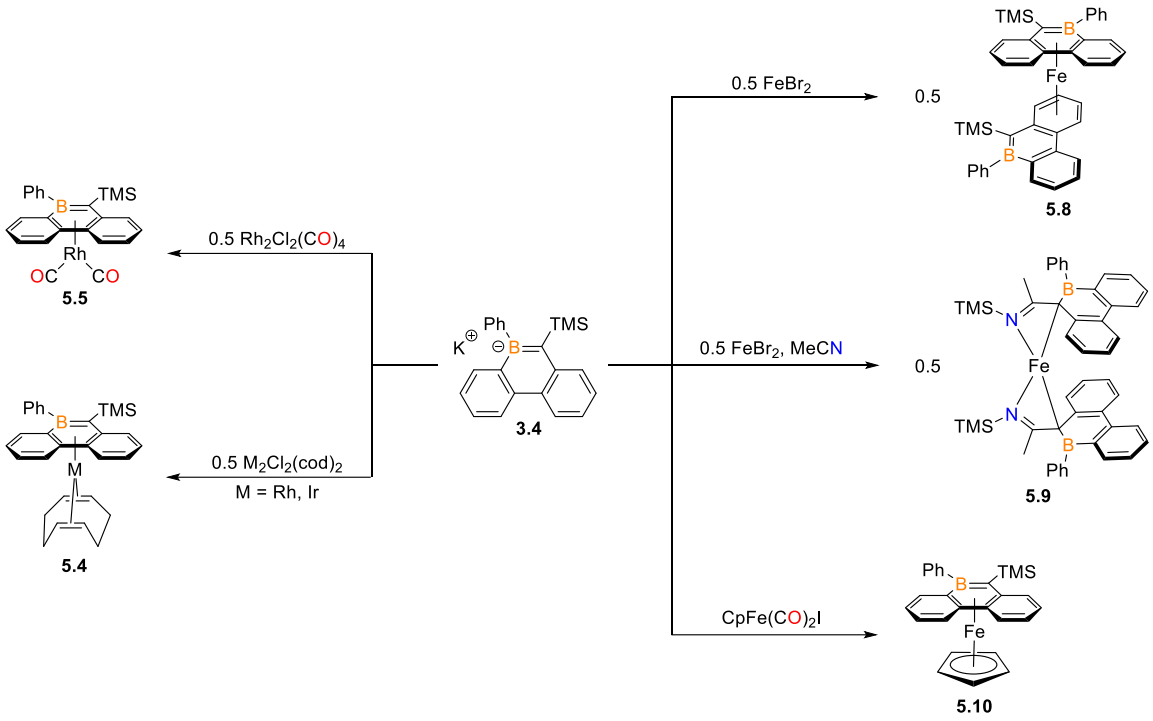

Scheme 6.4. Synthesis of 9-borataphenanthrene metal complexes.

6.2 Future Work

It is likely that the methods used to synthesize the 9-borataphenanthrene anion can also be applied to the syntheses of other fused polycyclic boratabenzenes. A potential precursor for such a compound is phenanthrene-fused stannole **6.1**, first synthesized by Toste and coworkers in 2018.[253] The reaction of **6.1** with $PhBCl_2$ at room temperature in

chloroform resulted in disappearance of the ^{11}B singlet at 55.4 ppm corresponding to $PhBCl_2$ accompanied by the emergence of a singlet at 64.8 ppm, similar to that of 9-phenyl-9-borafluorene.[108] Although the reaction did not proceed to completion within 5 days at room temperature, complete conversion was observed within 3 days when the temperature was increased to 80 °C in benzene. The resulting product has not yet been isolated or characterized crystallographically; however, the ^{11}B NMR shift indicates promising potential for the synthesis of phenanthrene-fused borole **6.2** *via* a tin/boron transmetallation route similar to that used by Piers and coworkers to synthesize 9-phenyl-9-borafluorene.[108] The resulting species could potentially be capable of undergoing ring expansion reactions analogous with other boroles.[2, 4, 19-21, 25-26, 34-35, 37-39, 116, 121, 125] Accordingly, nitrene insertion with phenyl azide will be attempted with phenyl azide to produce a 4,5-azaborapyrene (**6.3**), and carbene insertion will be attempted with trimethylsilyldiazomethane to produce a 4,5-dihydro-4-borapyrene (**6.4**). Both reactions closely resemble known reactions of 9-borafluorenes.[38-39, 162] Compound **6.4** will then be deprotonated with KHMDS to produce a 4-boratapyrene anion (**6.5**) in a manner analogous with that used to prepare the 9-borataphenanthrene anion.[230]

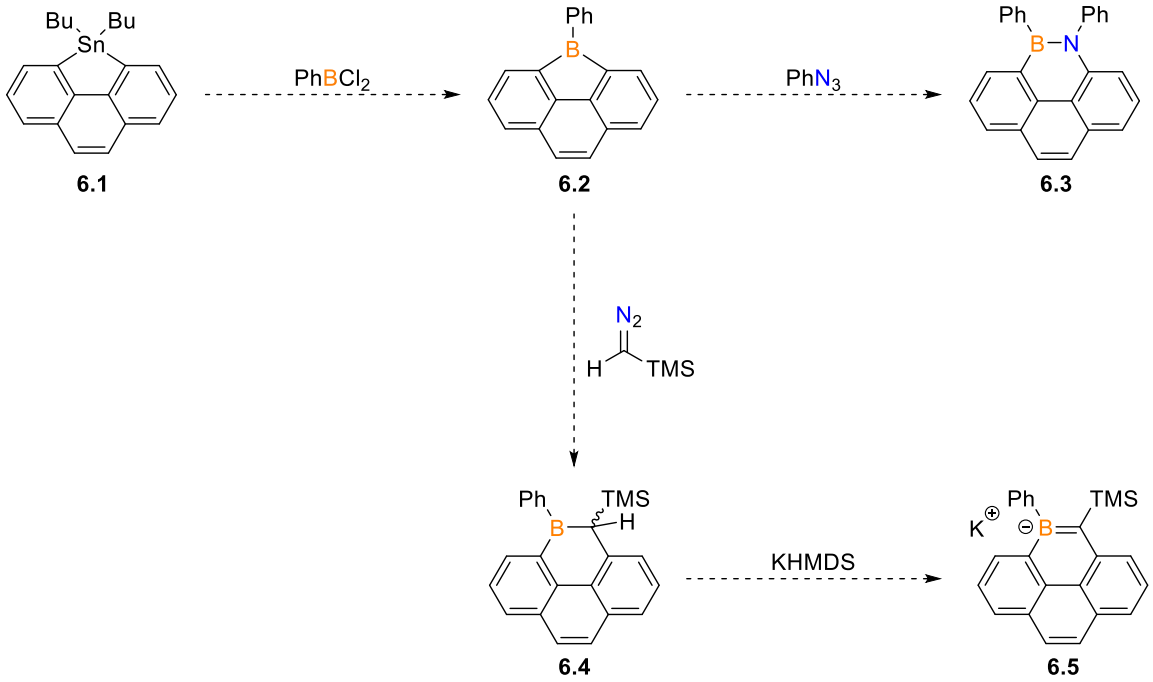

Scheme 6.5. Proposed syntheses of a 4-boratapyrene and a 4,5-azaborapyrene.

The 9-borataphenanthrene anion and proposed 4-boratapyrene anion represent fascinating new additions to the family of anionic boron-doped polycyclic aromatic hydrocarbons. The 9-borataphenanthrene anion has been shown to exhibit an intriguing dual boratabenzene/borataalkene nature lending to a diverse range of reactivity modes. The boratabenzene-like character of the 9-borataphenanthrene anion allows for usage as a ligand in transition-metal complexes, while its borataalkene-like character makes it viable as a precursor to tetracoordinate borates. The combined reactivity modes make 9-borataphenanthrenes and their structural relatives promising as reagents in inorganic and organic synthesis.

APPENDICES

APPENDIX A

General Experimental Details and Supplementary Information for Chapter Two

General Experimental Details

All manipulations were performed under an inert atmosphere in a nitrogen-filled MBraun Unilab glove box or using standard Schlenk techniques. $CDCl_3$, C_6D_6, and CD_3CN for NMR spectroscopy were purchased from Cambridge Isotope Laboratories and dried by stirring for 3 days over CaH_2, distilling, and storing over molecular sieves. All other solvents (unless otherwise specified) were purchased from commercial sources as anhydrous grade, dried further using a JC Meyer Solvent System with dual columns packed with solvent-appropriate drying agents, and stored over molecular sieves.

Multinuclear NMR spectra (^1H, $^1H\{^{11}B\}$, $^{13}C\{^1H\}$, ^{11}B, $^{11}B\{^1H\}$, $^{31}P\{^1H\}$, $^{19}F\{^1H\}$) were recorded on a Bruker Ascend 400 MHz instrument. High resolution mass spectra (HRMS) were obtained at the Baylor University Mass Spectrometry Center on a Thermo Scientific LTQ Orbitrap Discovery spectrometer using ESI or at the University of Texas at Austin Mass Spectrometry Center on a Micromass Autospec Ultima spectrometer using CI. Melting points were measured with a Thomas Hoover Uni-melt capillary melting point apparatus and are uncorrected. FT-IR spectra were recorded on a Bruker Alpha ATR FT-IR spectrometer on solid samples. Single crystal X-ray diffraction data were collected on a Bruker Apex II-CCD detector using Mo-Kα radiation (λ = 0.71073 Å). Crystals were selected under paratone oil, mounted on MiTeGen micromounts, and immediately placed in a cold stream of N_2. Structures were solved and refined using SHELXTL and figures produced using OLEX2.[254-255]

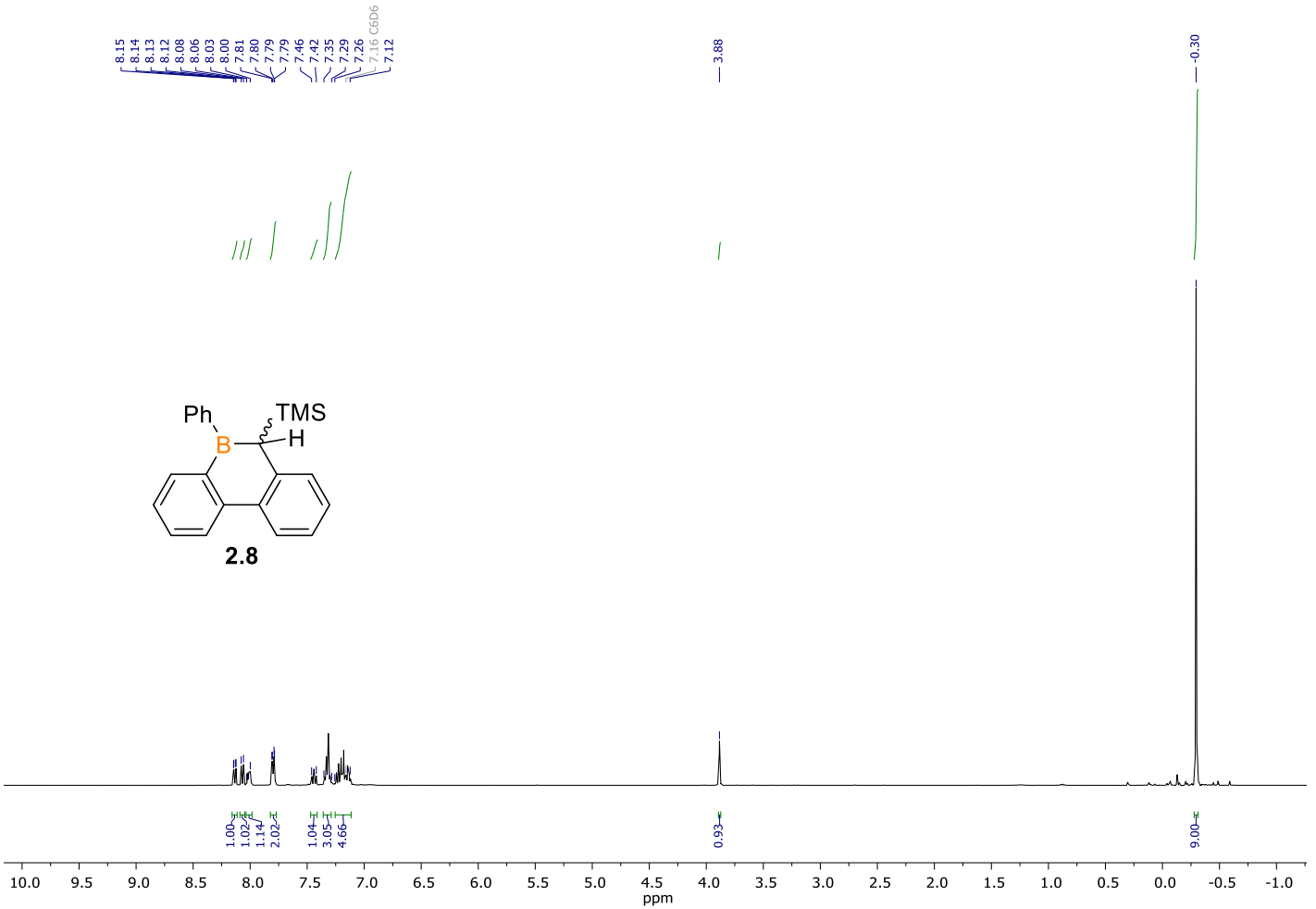

Figure A-1: ^{1}H NMR spectrum of **2.8** in C_6D_6.

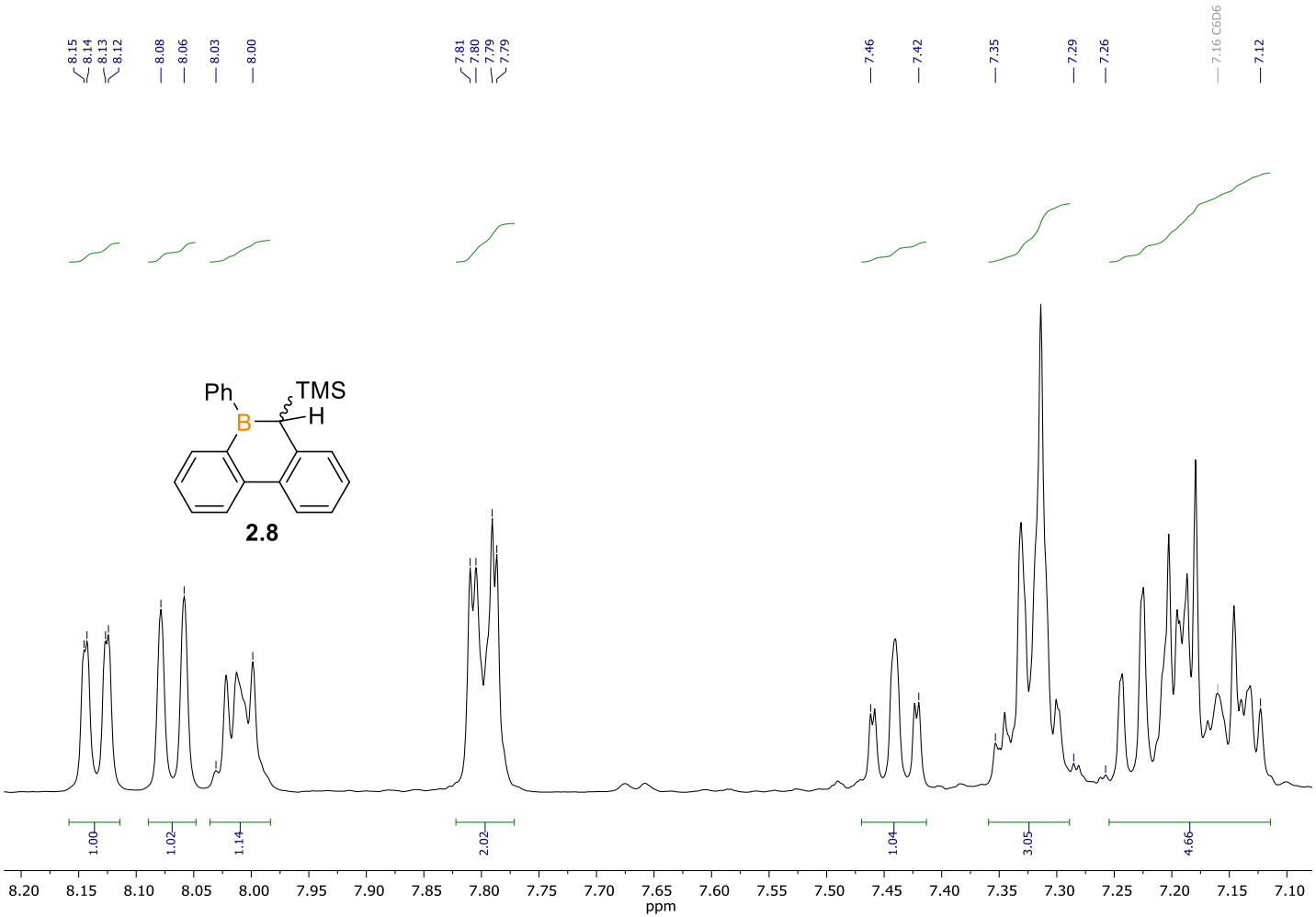

Figure A-2: Expansion of ^{1}H NMR spectrum of **2.8** in C_6D_6 (aryl region).

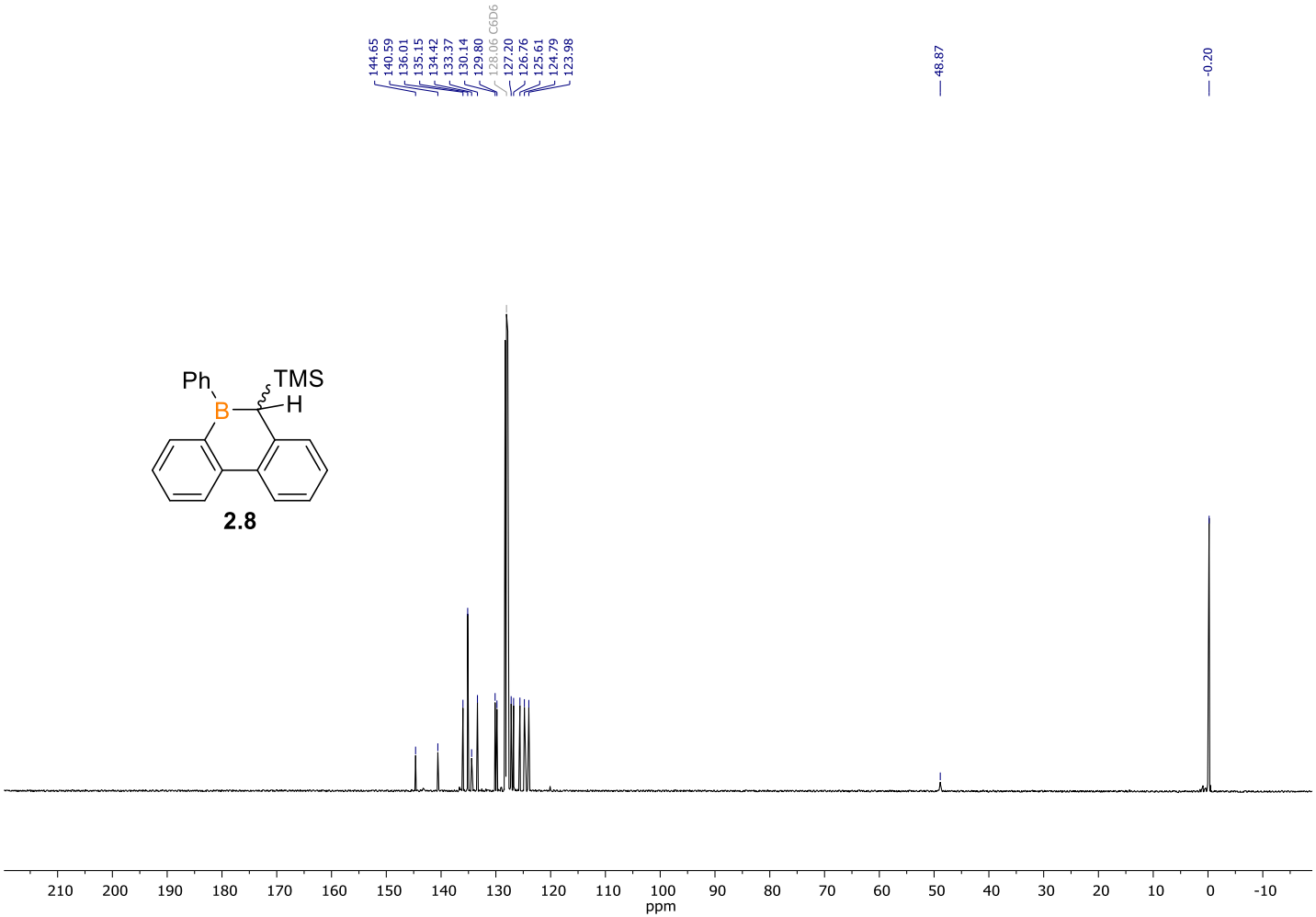

Figure A-3: $^{13}C\{^{1}H\}$ NMR spectrum of **2.8** in C_6D_6.

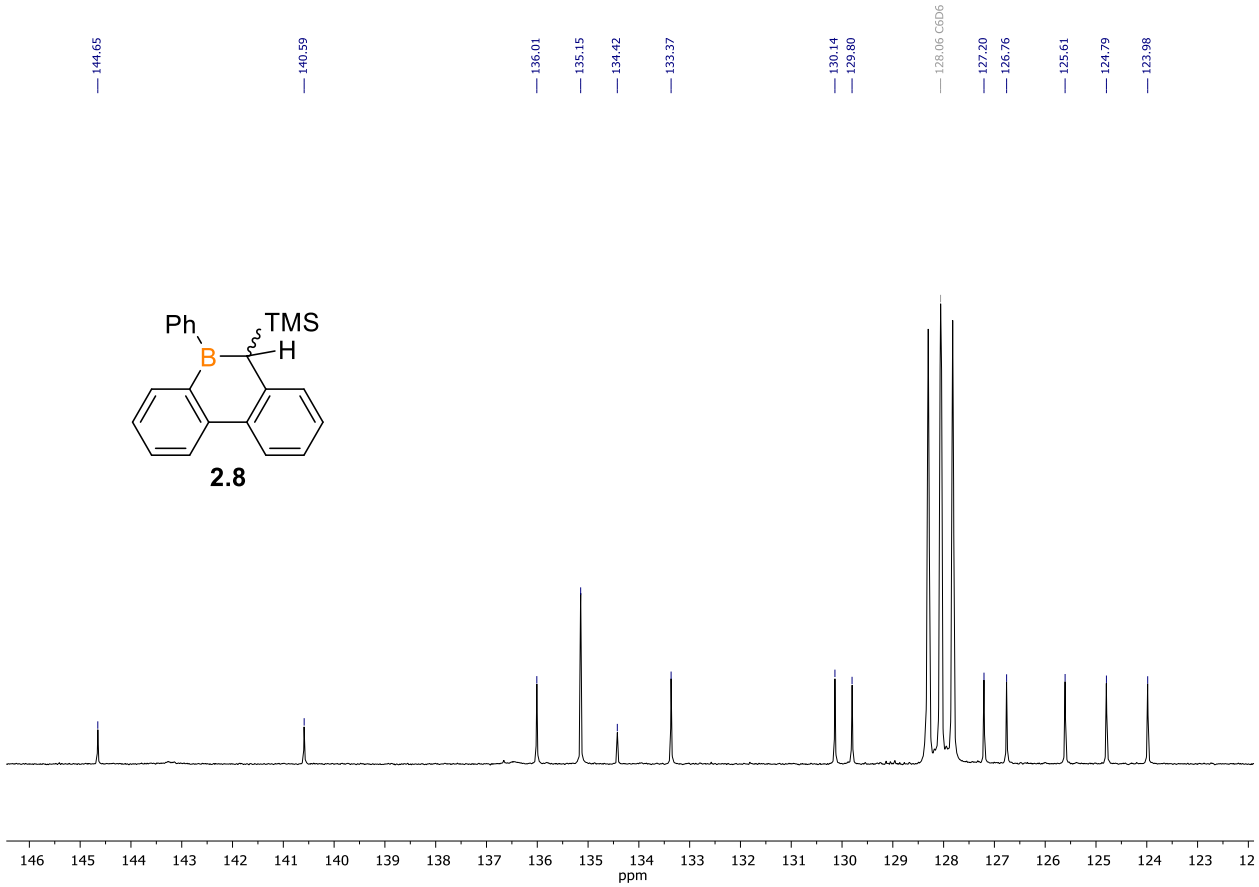

Figure A-4: Expansion of $^{13}C\{^{1}H\}$ NMR spectrum of **2.8** in C_6D_6 (aryl region).

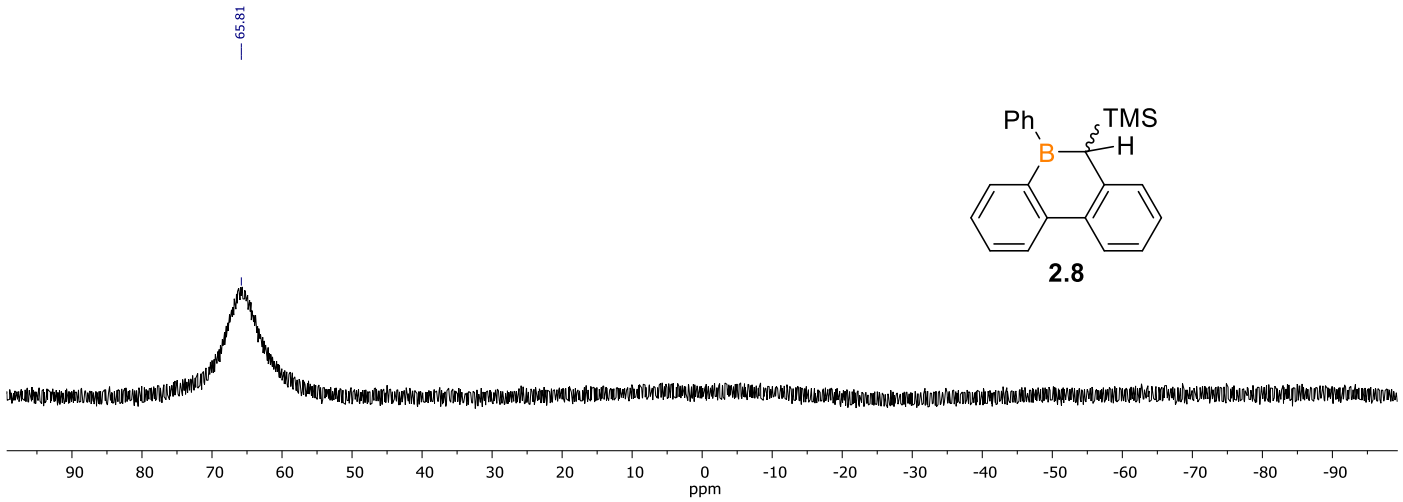

Figure A-5: ^{11}B NMR spectrum of **2.8** in C_6D_6.

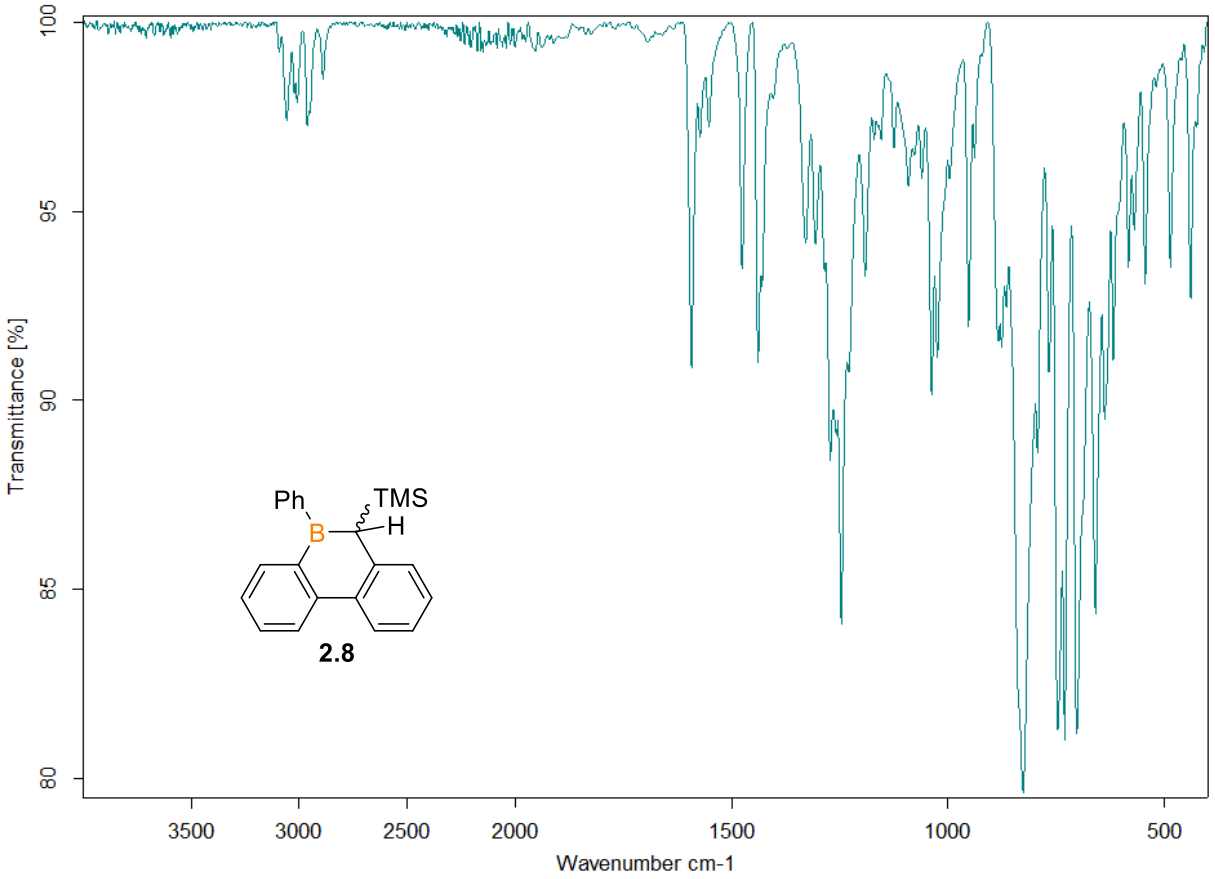

Figure A-6: FT-IR spectrum of **2.8**.

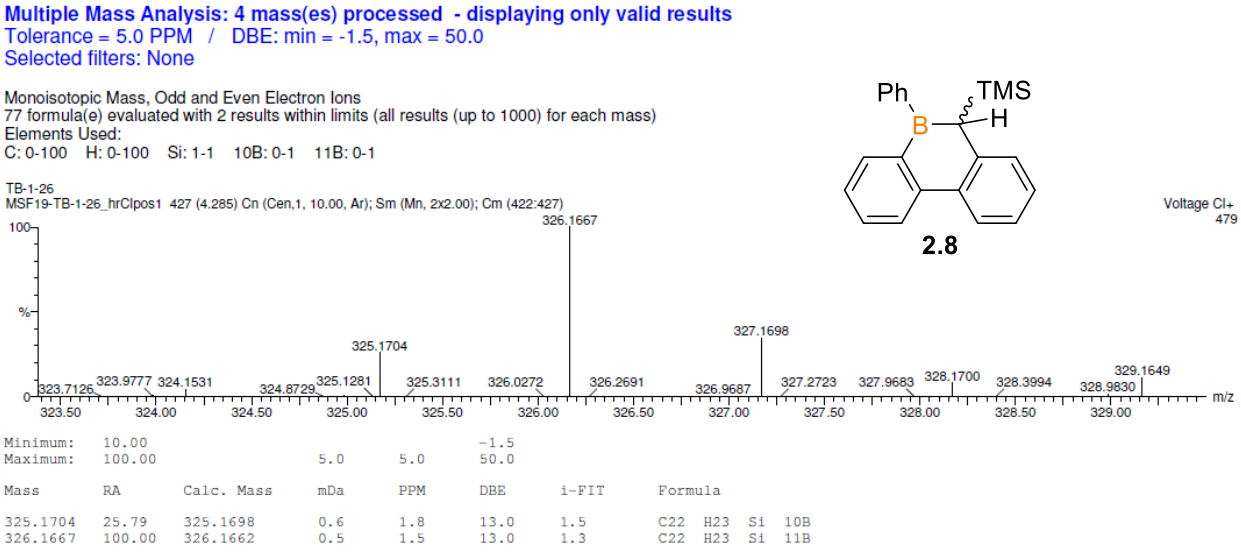

Figure A-7: High resolution mass spectrum of **2.8**.

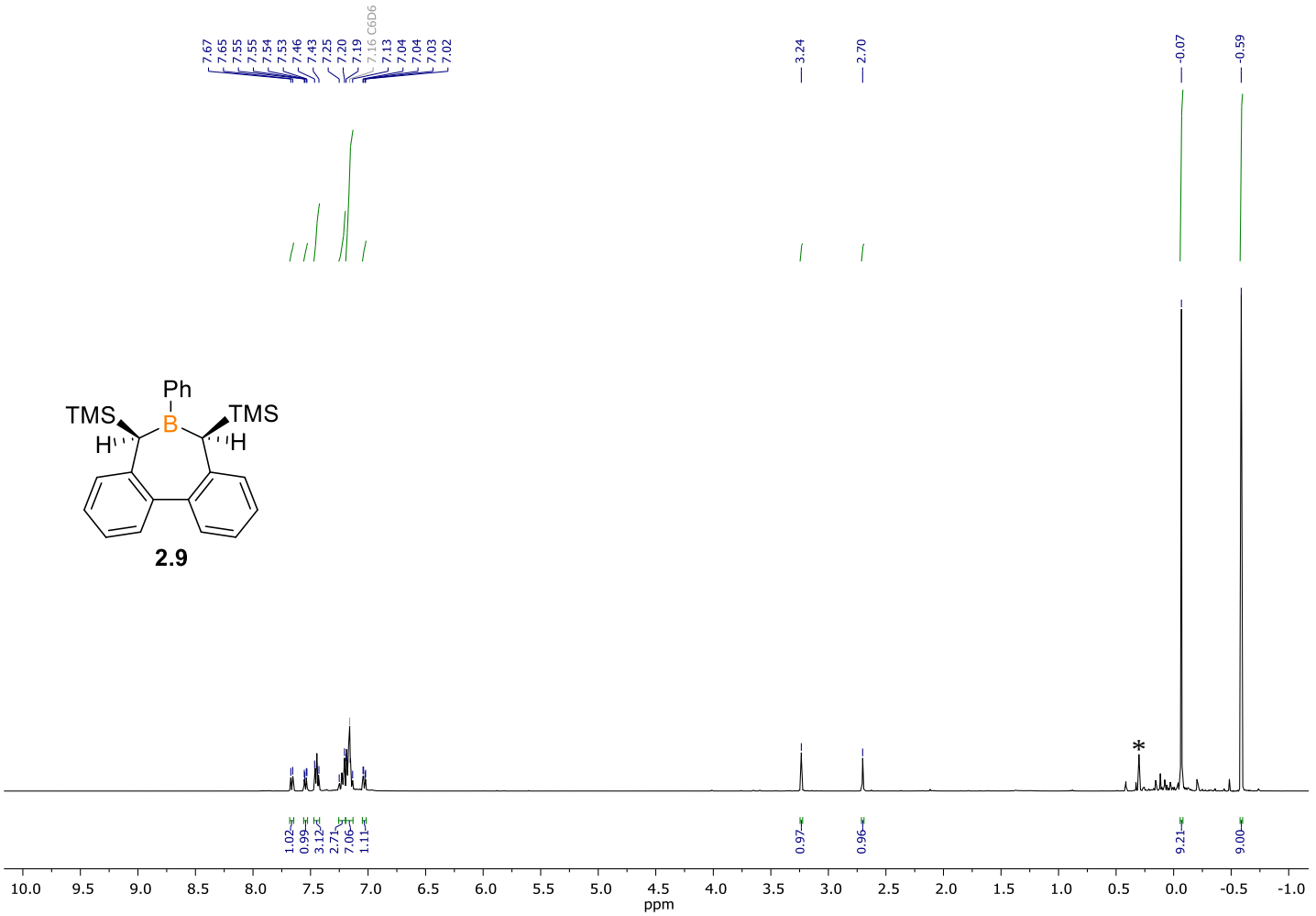

Figure A-8: ^{1}H NMR spectrum of **2.9** in C_6D_6 (* indicates grease).

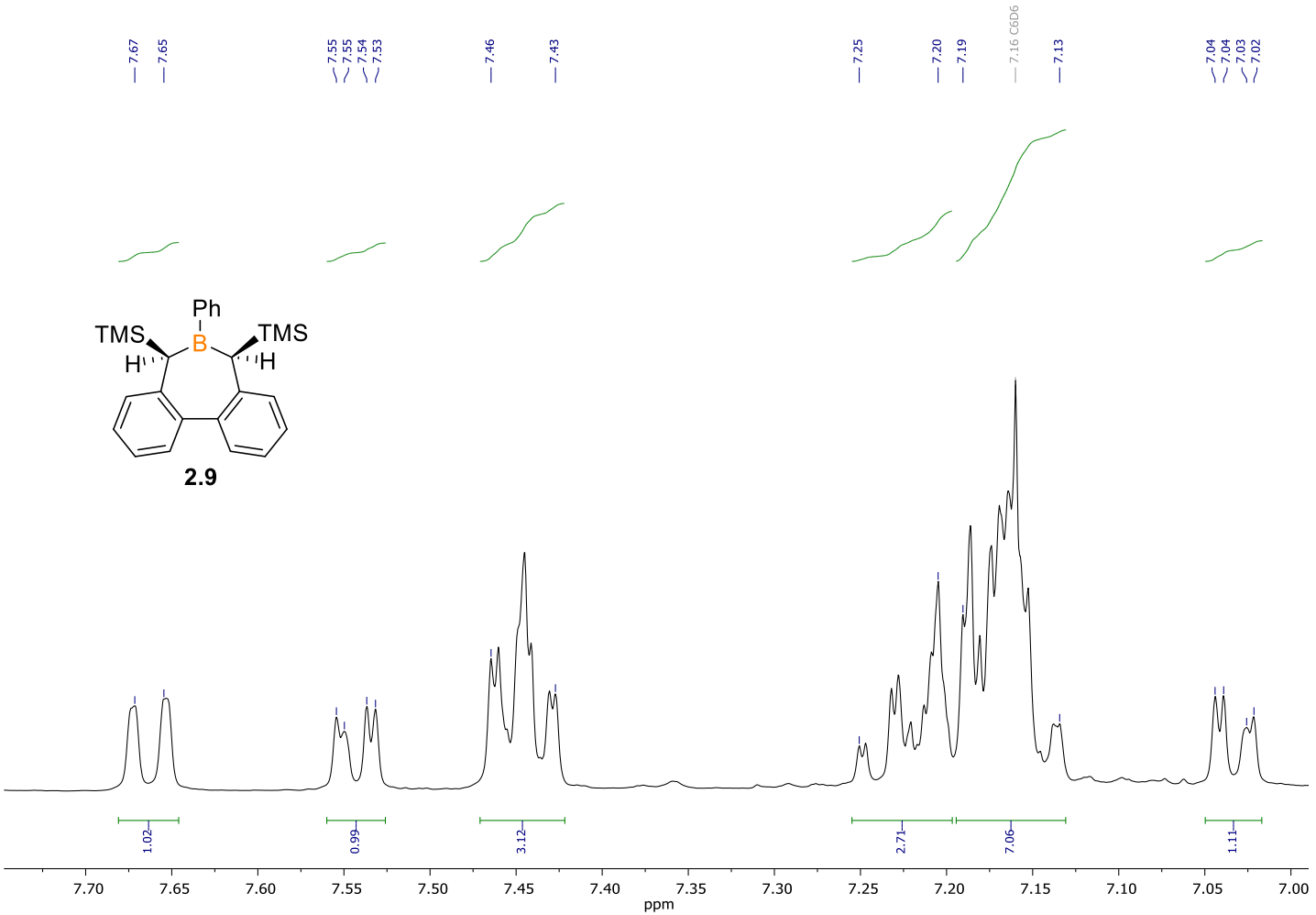

Figure A-9: Expansion of ^{1}H NMR spectrum of **2.9** in C_6D_6 (aryl region).

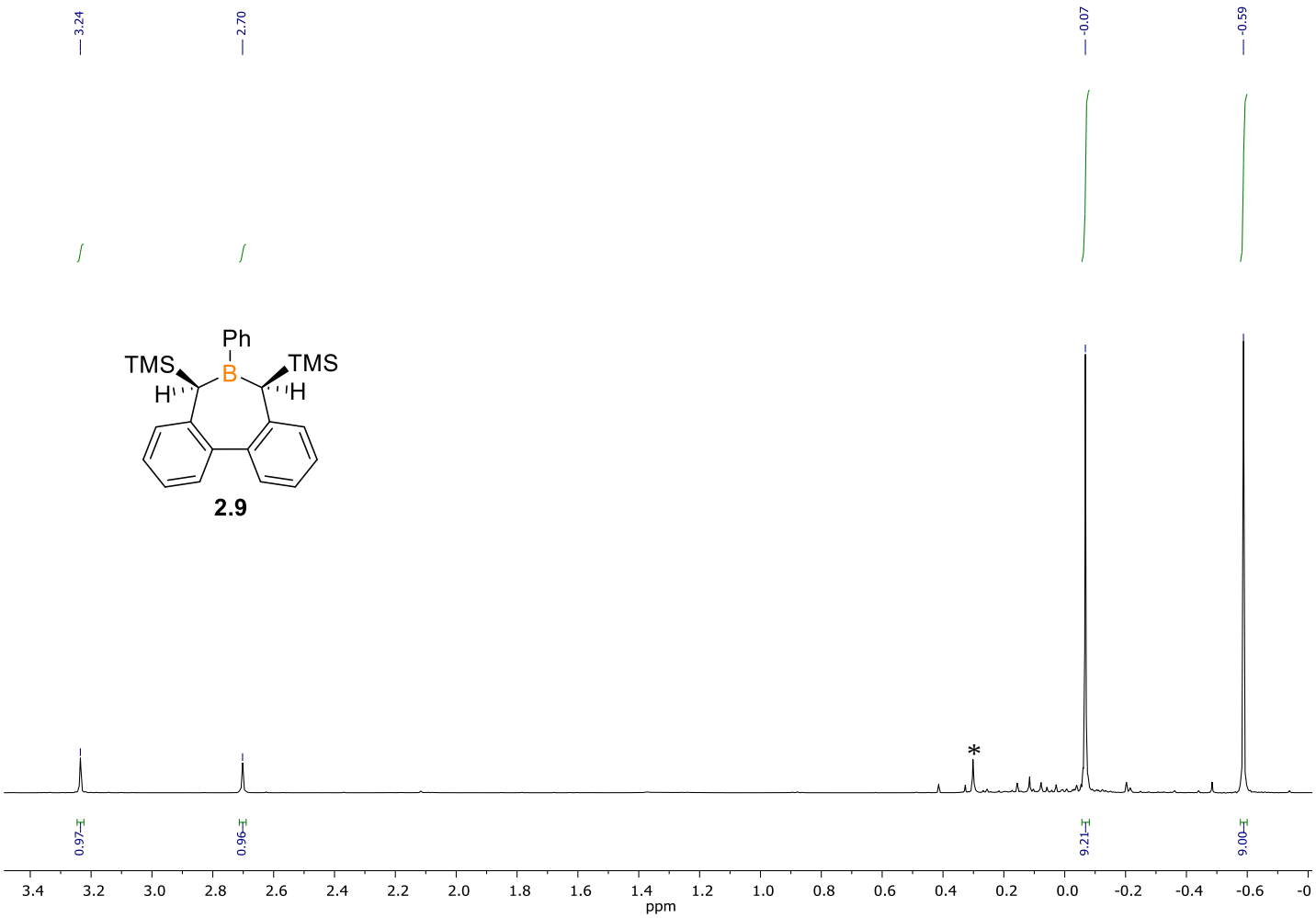

Figure A-10: Expansion of ^{1}H NMR spectrum of **2.9** in C_6D_6 (aliphatic region, * indicates grease).

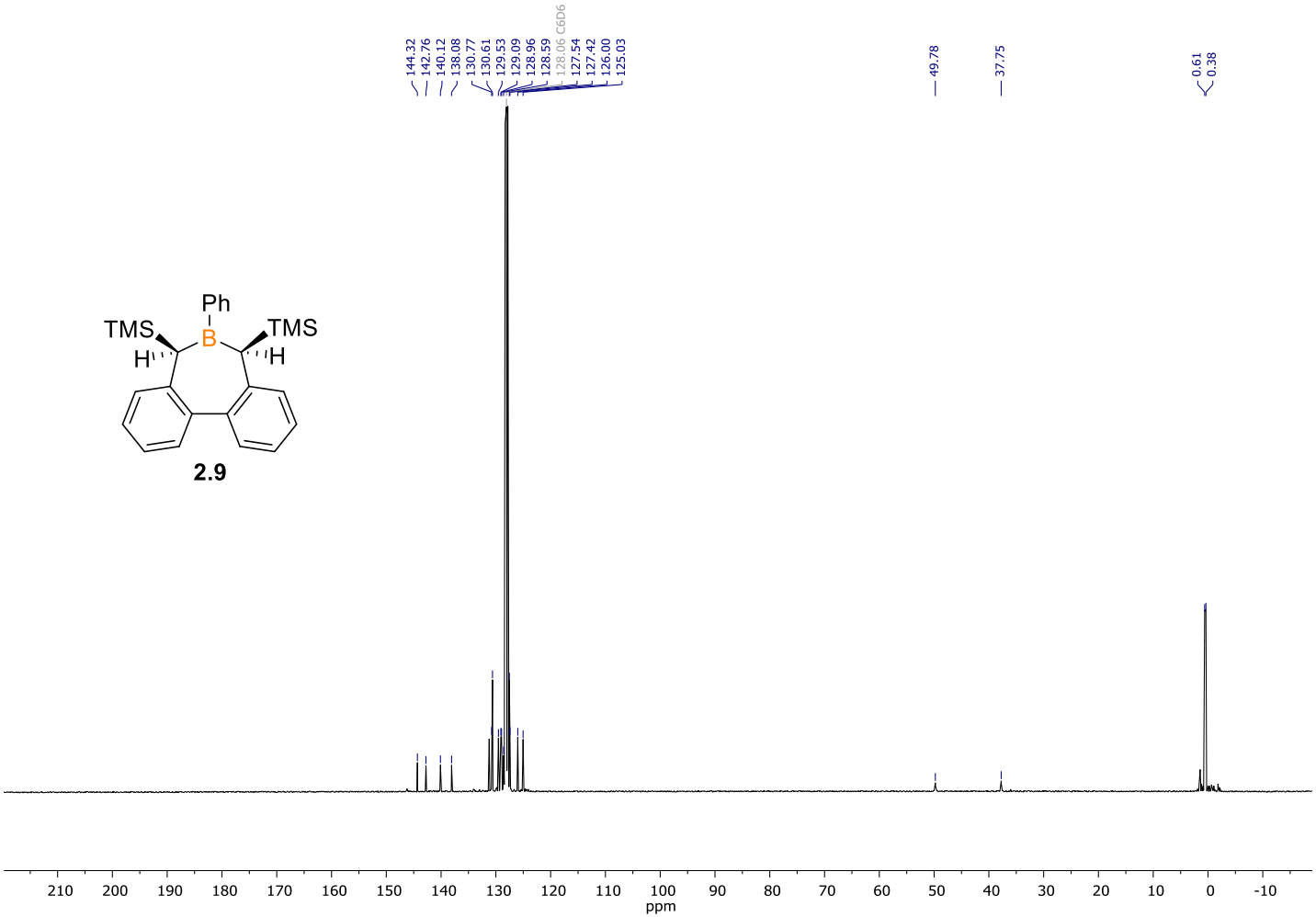

Figure A-11: $^{13}C\{^{1}H\}$ NMR spectrum of **2.8** in C_6D_6 (* indicates grease).

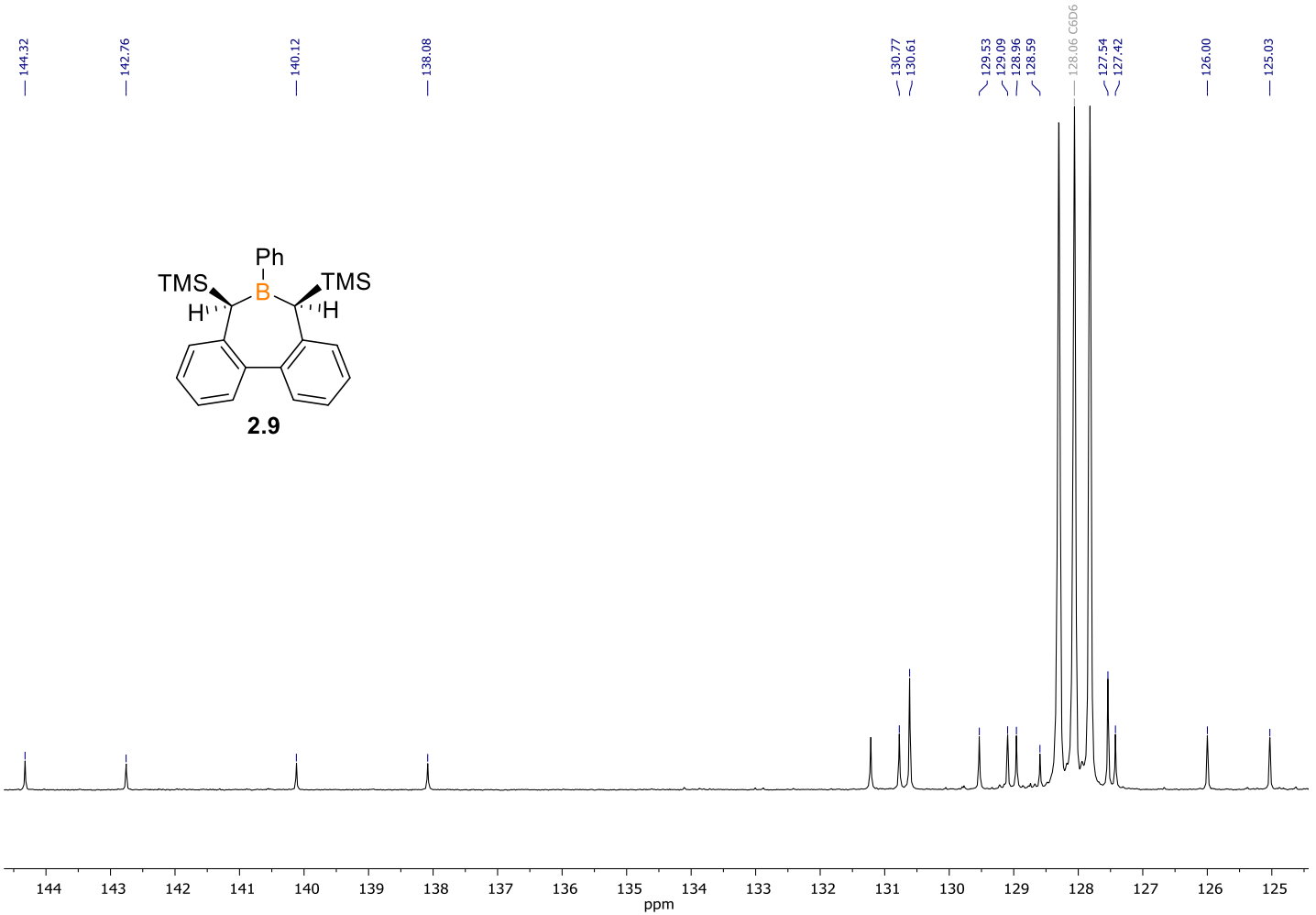

Figure A-12: Expansion of $^{13}C\{^{1}H\}$ NMR spectrum of **2.8** in C_6D_6 (aryl region).

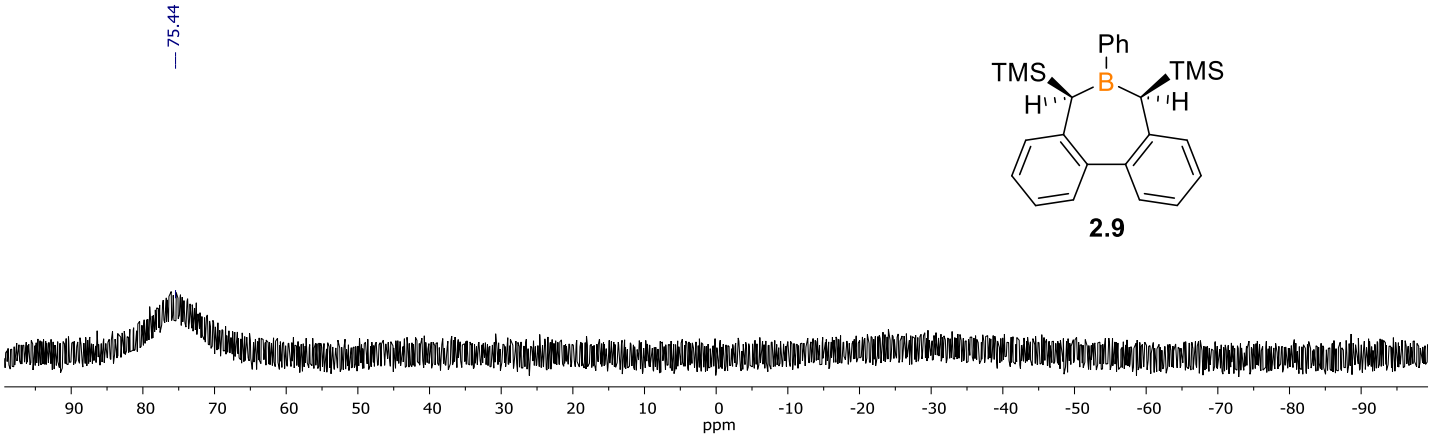

Figure A-13: ^{11}B NMR spectrum of **2.8** in C_6D_6.

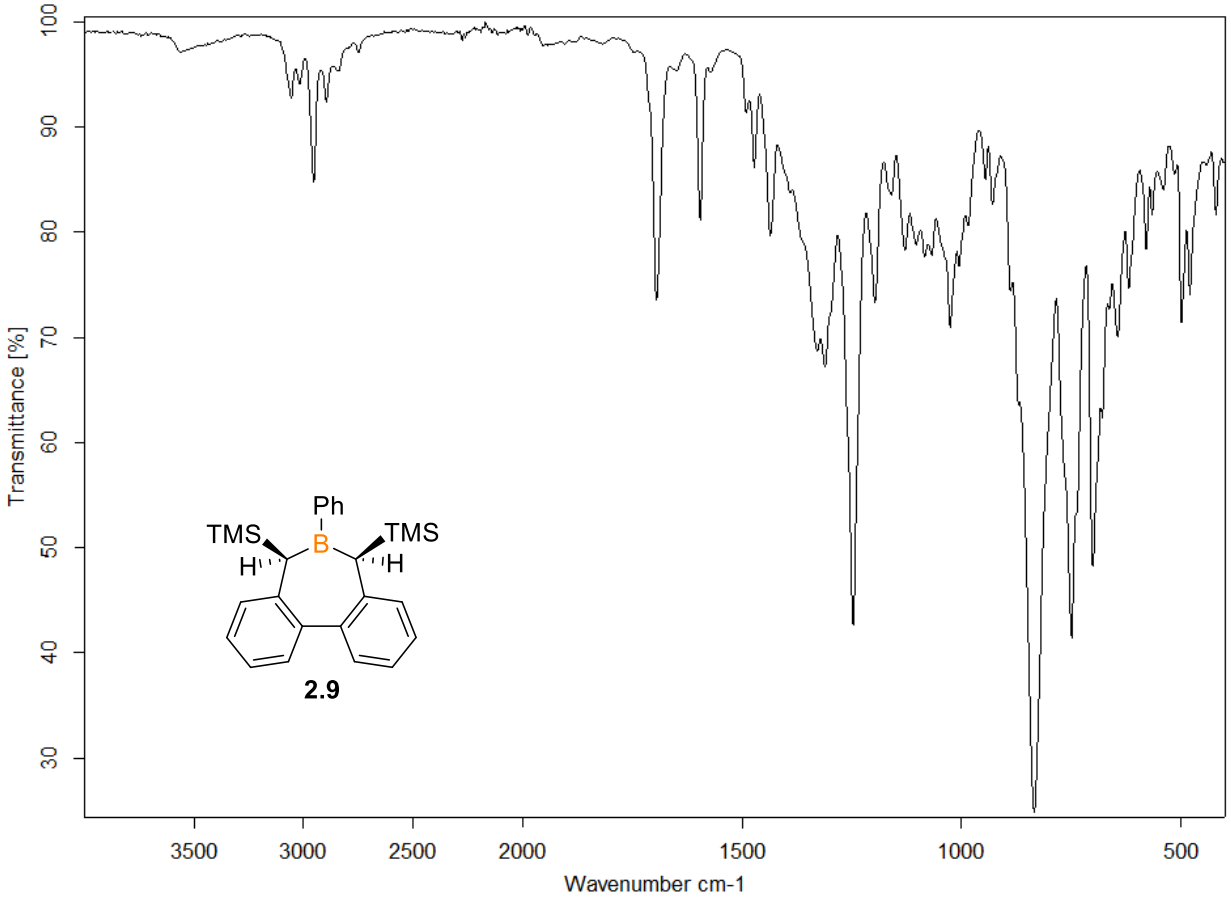

Figure A-14: FT-IR spectrum of **2.8**.

Multiple Mass Analysis: 6 mass(es) processed - displaying only valid results
Tolerance = 5.0 PPM / DBE: min = -1.5, max = 50.0
Selected filters: None

Monoisotopic Mass, Odd and Even Electron Ions
123 formula(e) evaluated with 4 results within limits (all results (up to 1000) for each mass)
Elements Used:
C: 0-100 H: 0-100 10B: 0-1 11B: 0-1 Si: 2-2

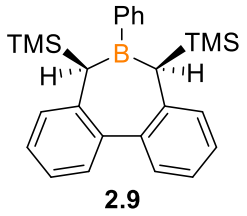

2.9

TB-1-15-10
MSF19-TB-1-15-10_hrClpos1 1361 (13.677) Cn (Cen,1, 20.00, Ar); Sm (Mn, 2x2.00); Cm (1358:1444)

Voltage CI+
91.3

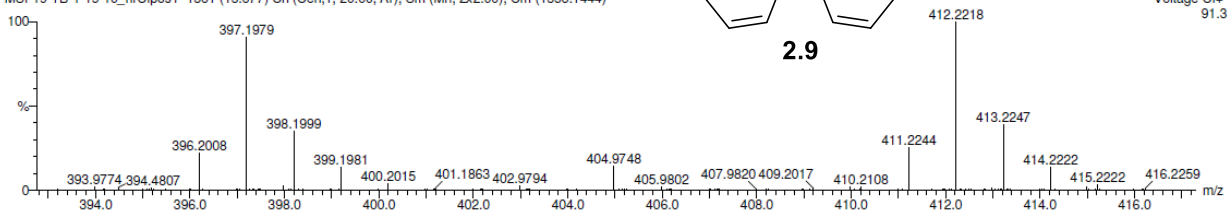

Minimum:	20.00				-1.5		
Maximum:	100.00		5.0	5.0	50.0		
Mass	RA	Calc. Mass	mDa	PPM	DBE	i-FIT	Formula
396.2008	21.96	396.2015	-0.7	-1.8	13.5	0.0	C25 H30 10B Si2
397.1979	90.79	397.1979	0.0	0.0	13.5	0.1	C25 H30 11B Si2
411.2244	25.43	411.2250	-0.6	-1.5	13.0	0.1	C26 H33 10B Si2
412.2218	100.00	412.2214	0.4	1.0	13.0	0.0	C26 H33 11B Si2

Figure A-15: High resolution mass spectrum of **2.8**.

Table A-1: X-ray crystallographic details for **2.8** and **2.9**.

Compound	**2.8**	**2.9**
CCDC	1901552	1901553
Empirical Formula	$C_{22}H_{23}BSi$	$C_{26}H_{33}BSi_2$
FW (g/mol)	326.30	412.51
Crystal System	Triclinic	Monoclinic
Space Group	P -1	I 2/a
a (Å)	7.2004(11)	17.718(4)
b (Å)	9.8166(16)	10.3253(17)
c (Å)	13.857(2)	28.130(7)
α (deg)	86.856(5)	90
β (deg)	79.281(5)	103.693(10)
γ (deg)	74.582(5)	90
V (Å^3)	927.7(3)	4999.9(19)
Z	2	8
D_c (g cm^{-3})	1.168	1.096
Radiation λ (Å)	0.71073	0.71073
Temp (K)	150	150
R1 [I>2(σ)I][a]	0.0487	0.0406
wR2 (F^2)[a]	0.1068	0.1066
GOF (S)[a]	1.029	1.056

[a] $R1(F[I > 2(I)]) = \sum||F_o| - |F_c||/\sum|F_o|$; $wR2(F^2\ [\text{all data}]) = [w(F_o^2 - F_c^2)^2]^{1/2}$; $S(\text{all data}) = [w(F_o^2 - F_c^2)^2/(n-p)]^{1/2}$ (n = no. of data; p = no. of parameters varied; $w = 1/[^2(F_o^2) + (aP)^2 + bP]$ where $P = (F_o^2 + 2F_c^2)/3$ and a and b are constants suggested by the refinement program.

APPENDIX B

Supplementary Information for Chapter Three

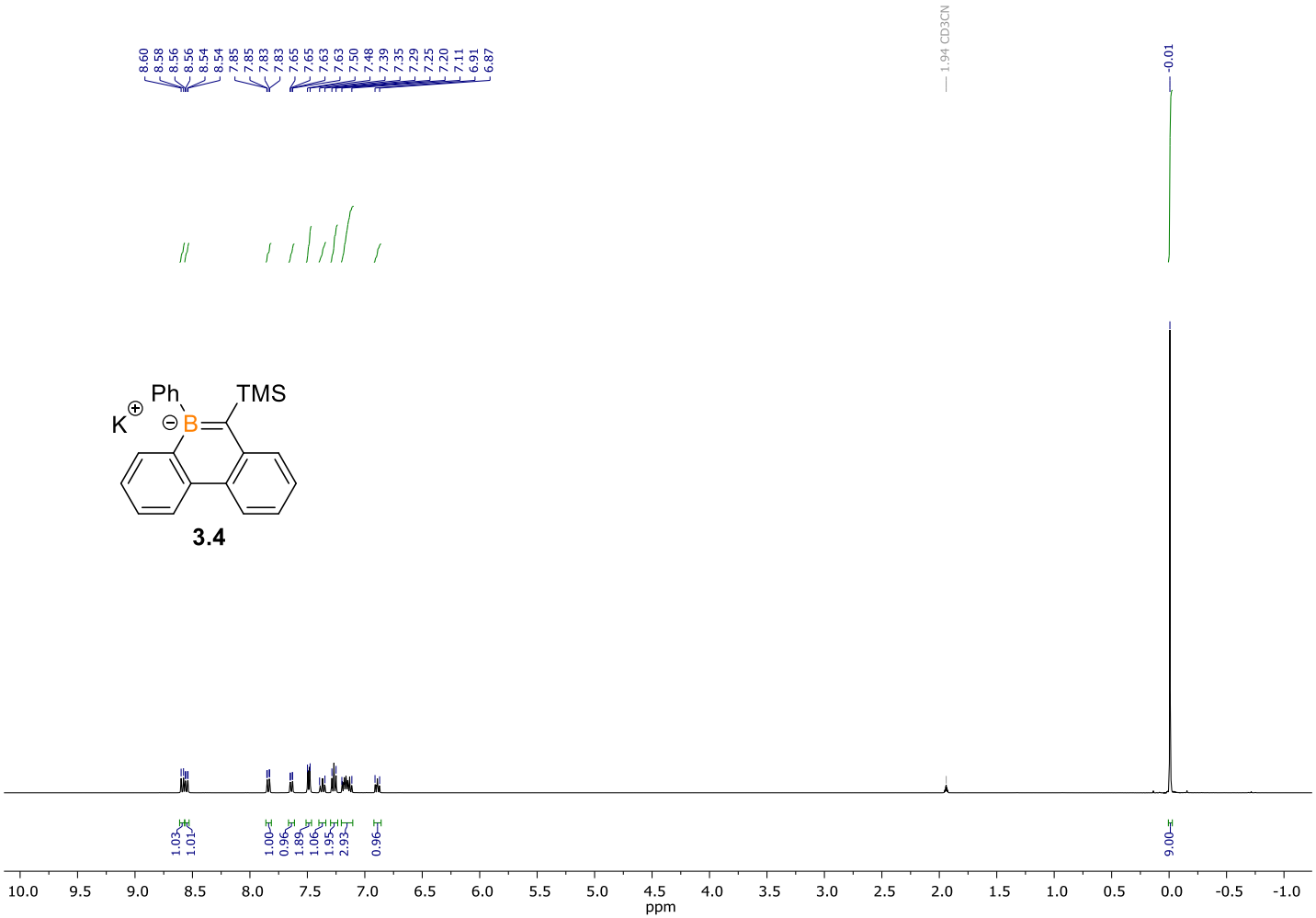

Figure B-1: ^{1}H NMR spectrum of **3.4** in CD_3CN.

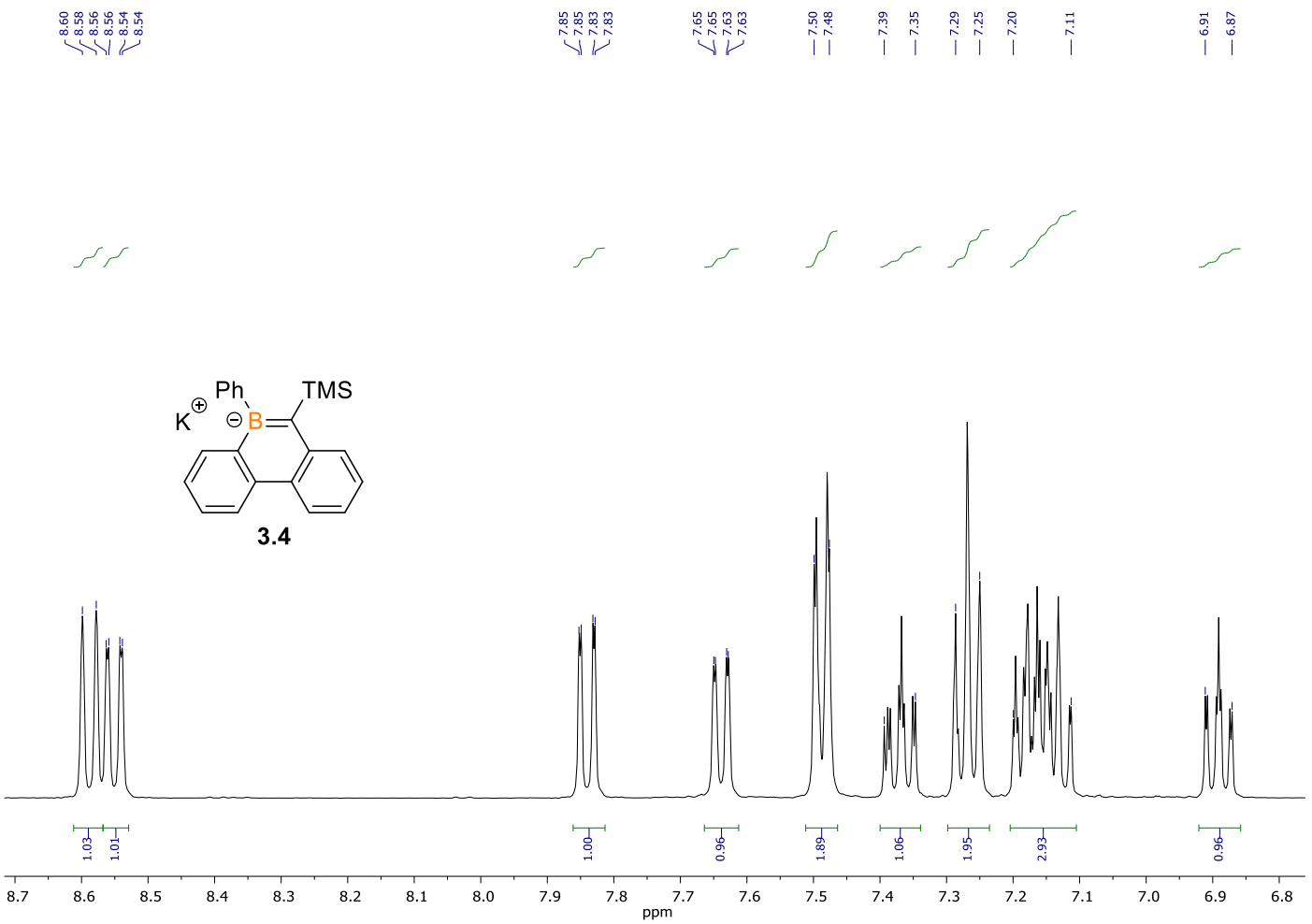

Figure B-2: Expansion of ^{1}H NMR spectrum of **3.4** in CD_3CN (aryl region).

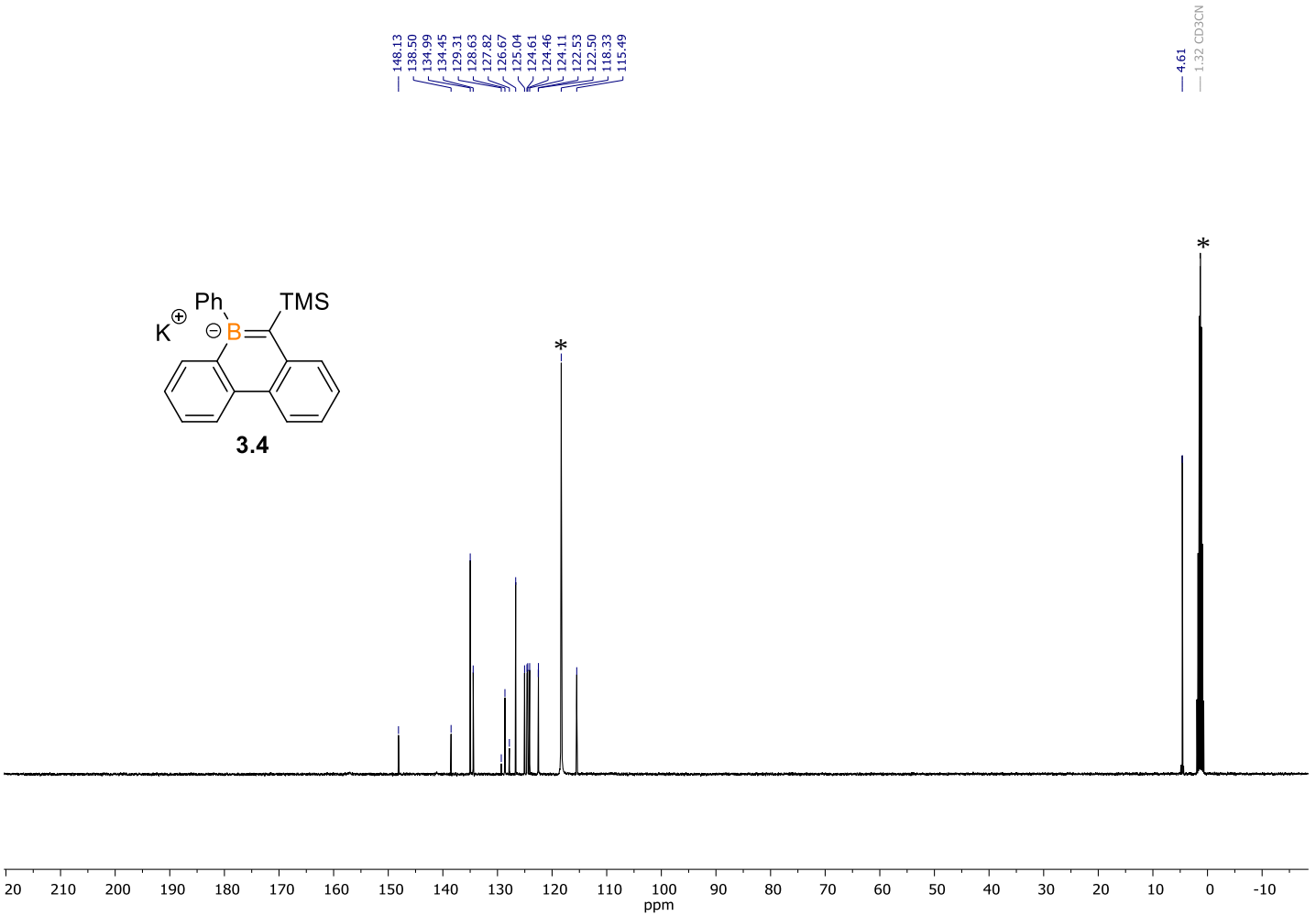

Figure B-3: $^{13}C\{^{1}H\}$ NMR spectrum of **3.4** in CD_3CN (* indicates CD_3CN).

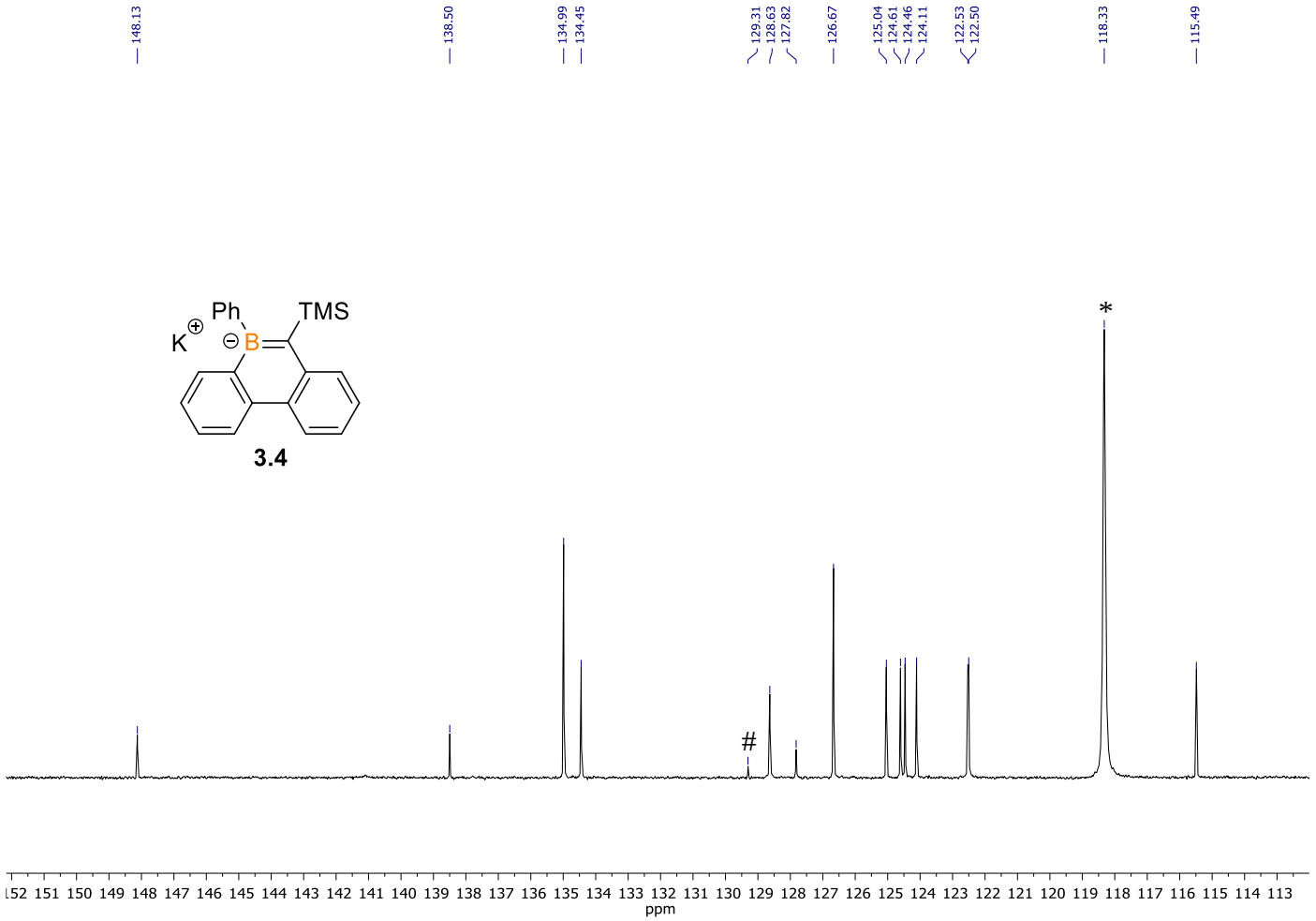

Figure B-4: Expansion of $^{13}C\{^{1}H\}$ NMR spectrum of **3.4** in CD_3CN (aryl region, * indicates CD_3CN, # indicates benzene).

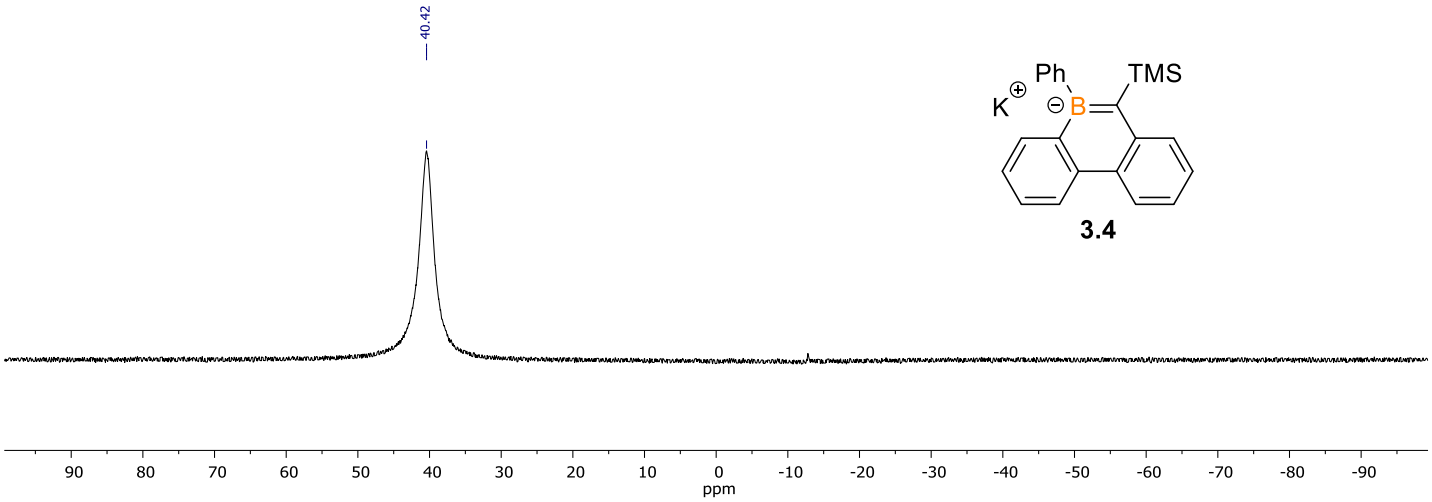

Figure B-5: ^{11}B NMR spectrum of **3.4** in CD_3CN.

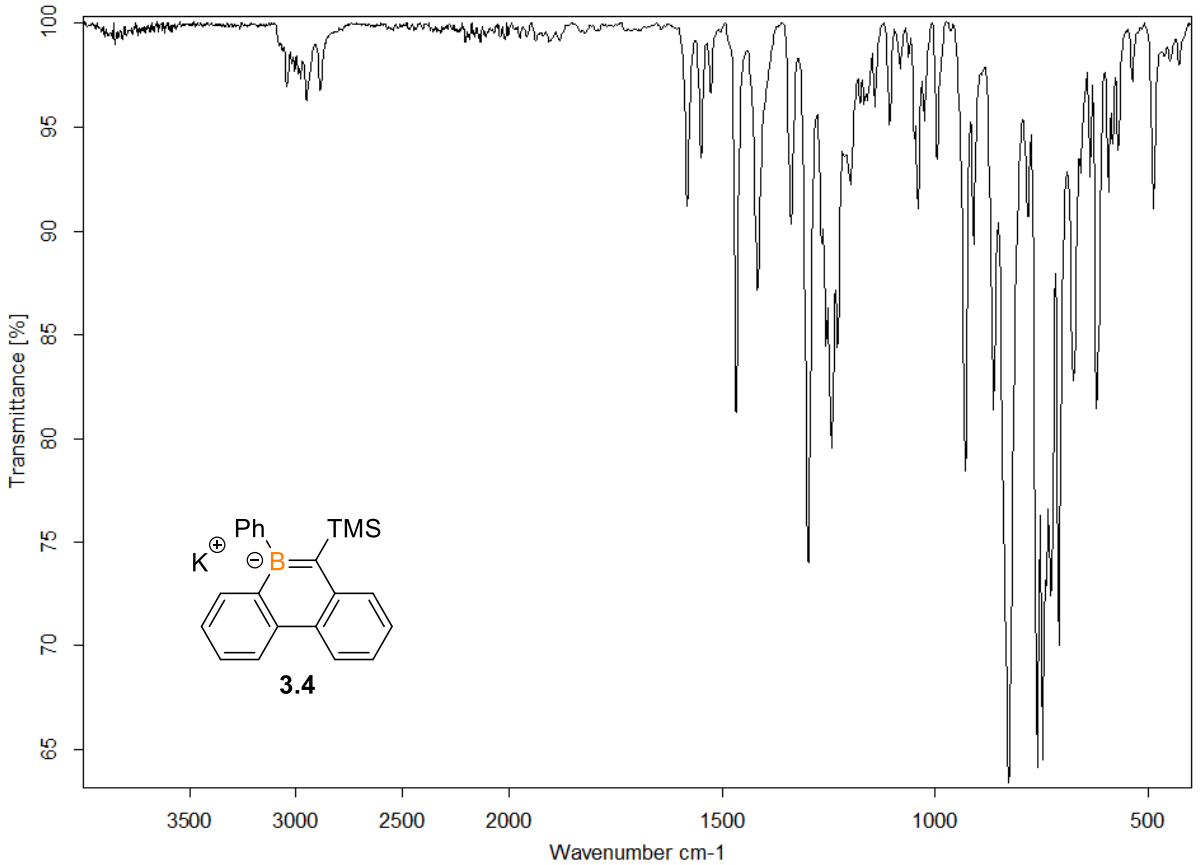

Figure B-6: FT-IR spectrum of **3.4**.

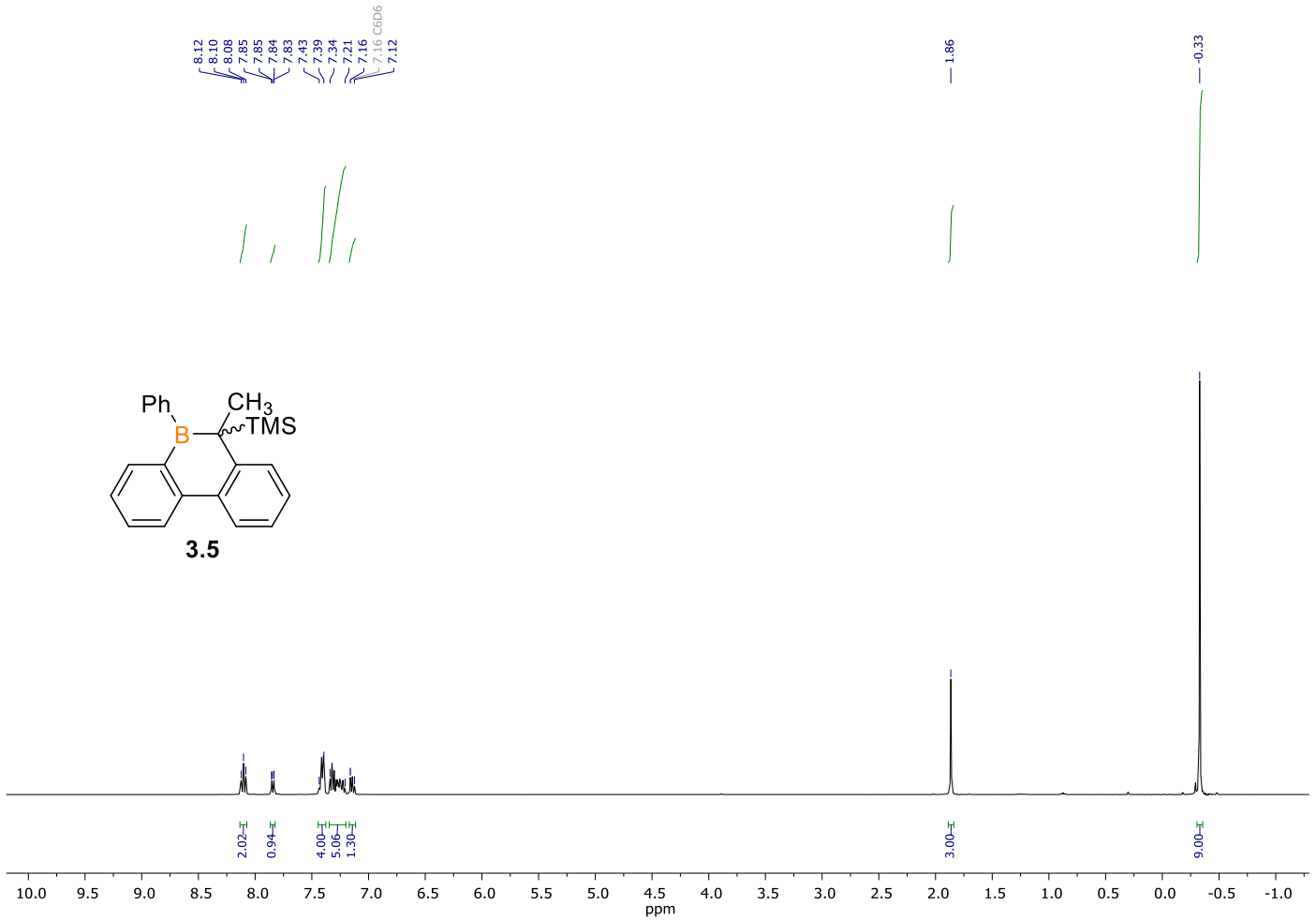

Figure B-7: ^{1}H NMR spectrum of **3.5** in C_6D_6.

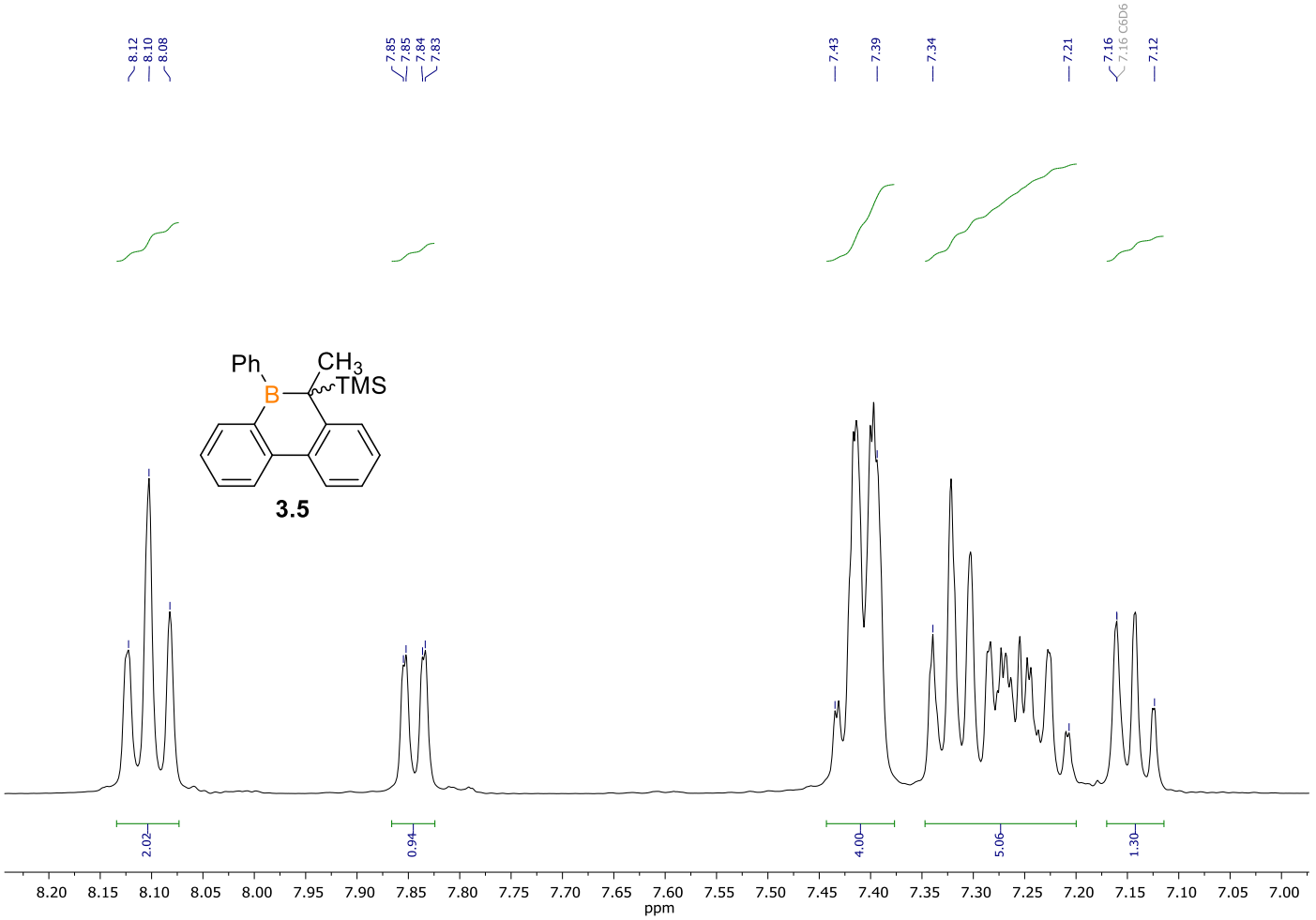

Figure B-8: Expansion of ^{1}H NMR spectrum of **3.5** in C_6D_6 (aryl region).

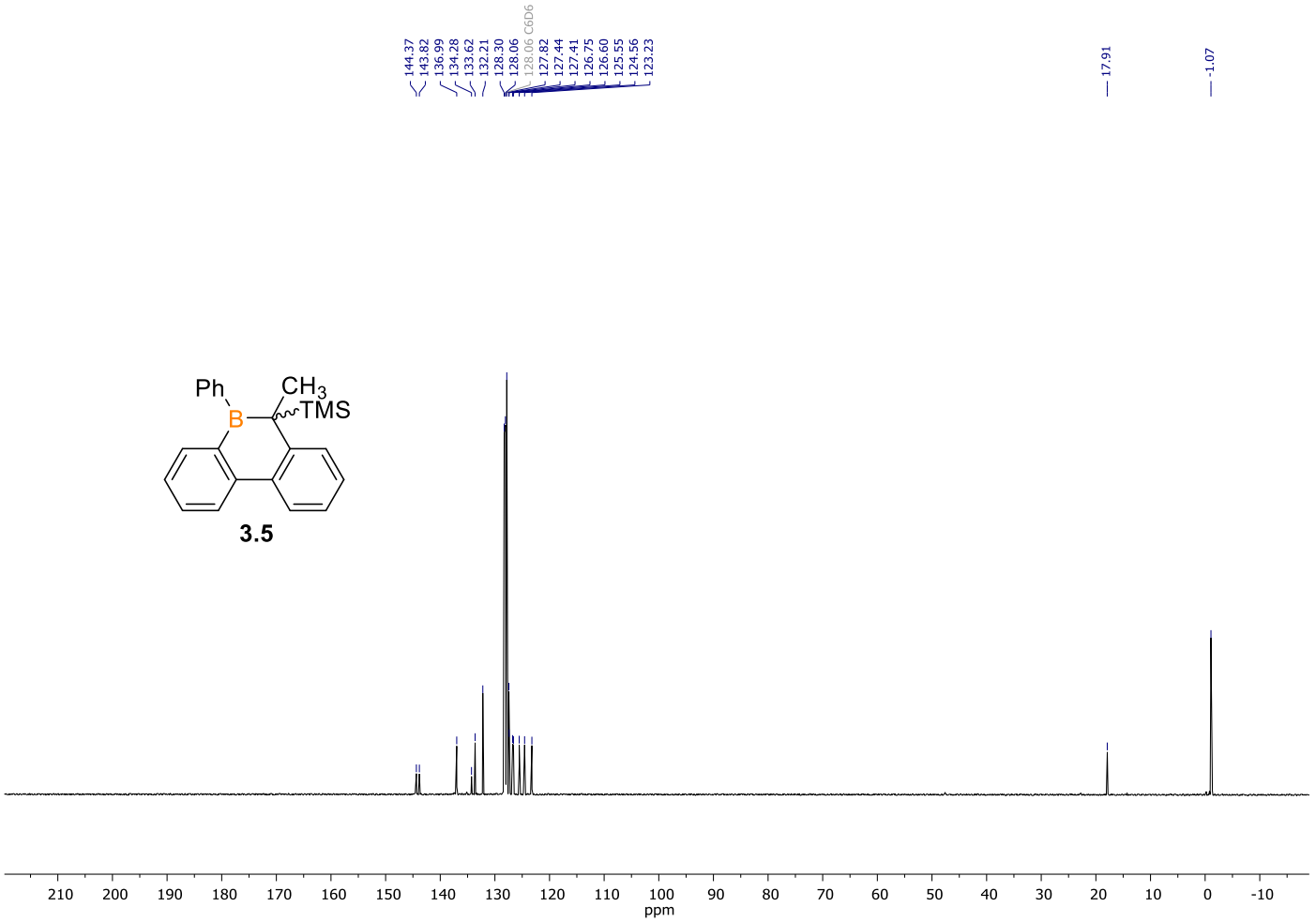

Figure B-9: $^{13}C\{^{1}H\}$ NMR spectrum of **3.5** in C_6D_6.

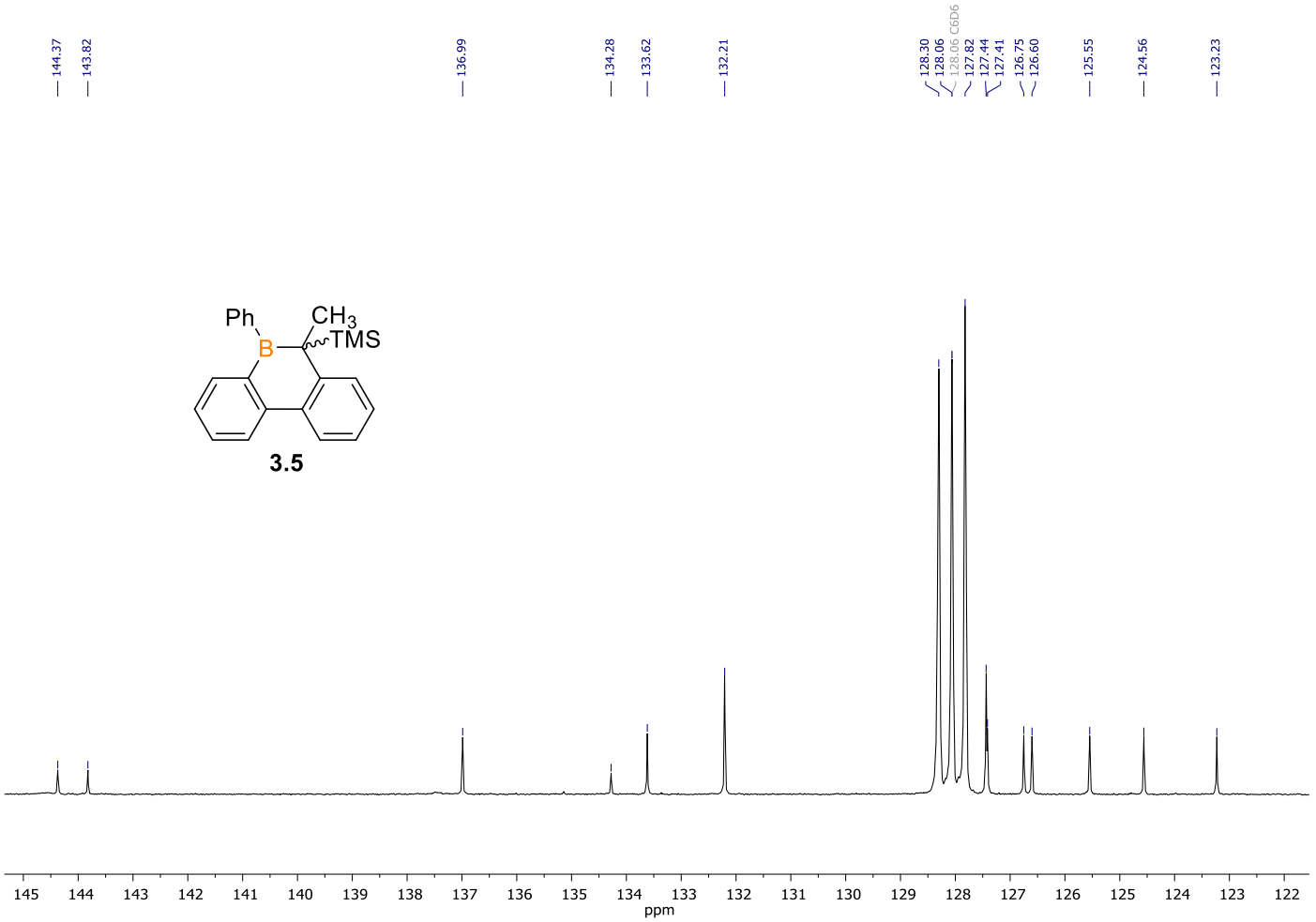

Figure B-10: Expansion of $^{13}C\{^{1}H\}$ NMR spectrum of **3.5** in C_6D_6 (aryl region).

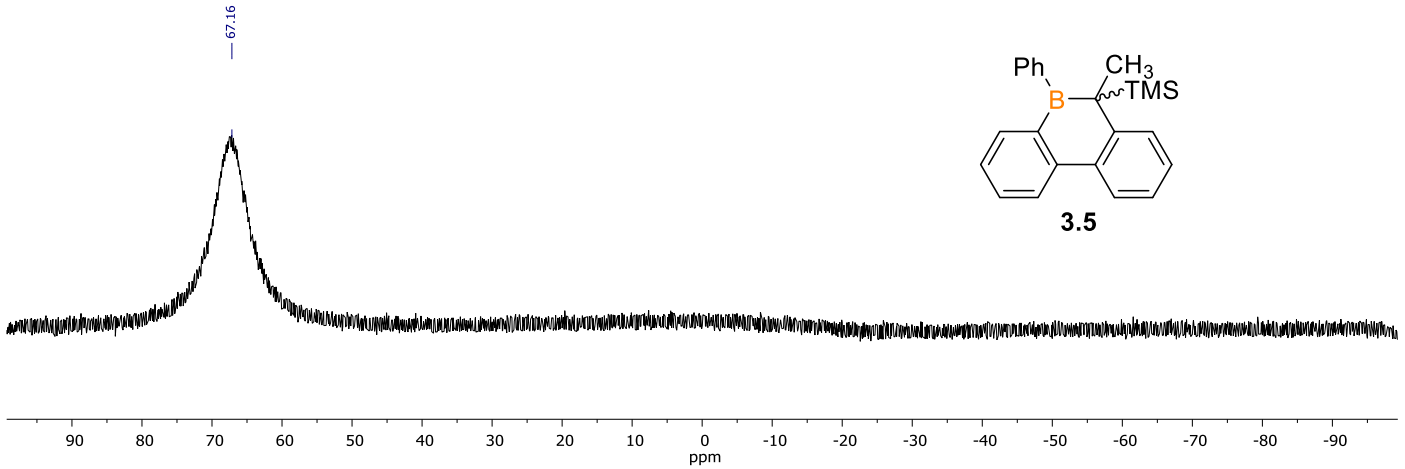

Figure B-11: ^{11}B NMR spectrum of **3.5** in C_6D_6.

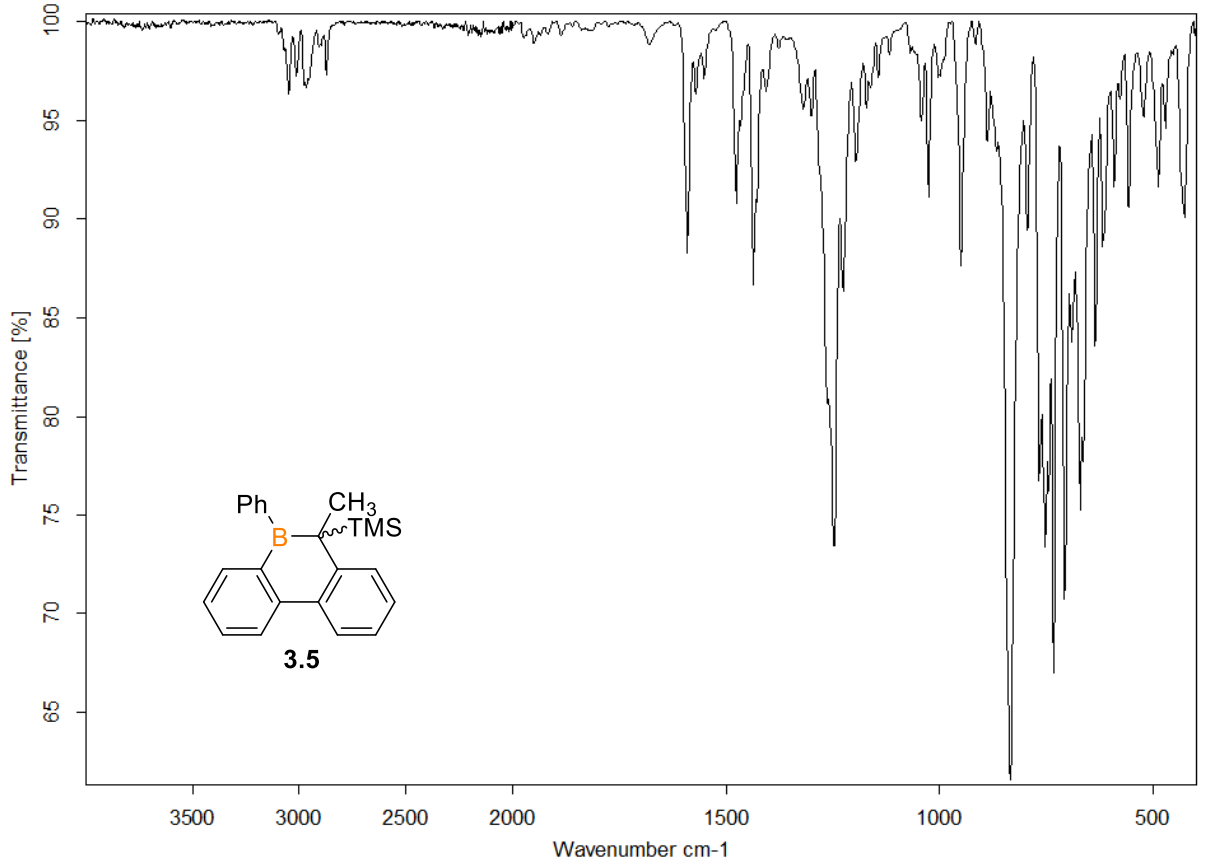

Figure B-12: FT-IR spectrum of **3.5**.

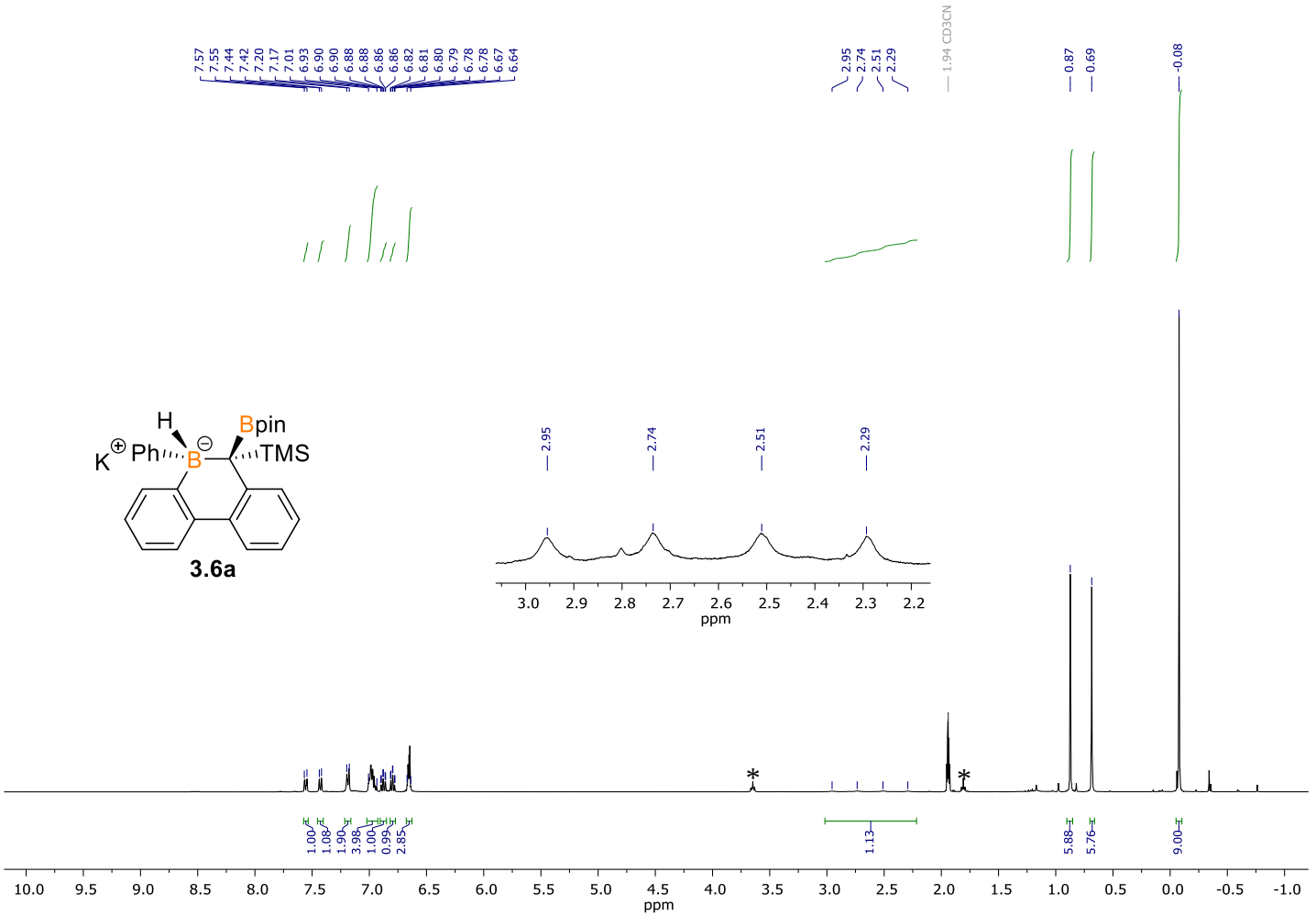

Figure B-13: ^{1}H NMR spectrum of **3.6a** in CD_3CN (* indicates THF).

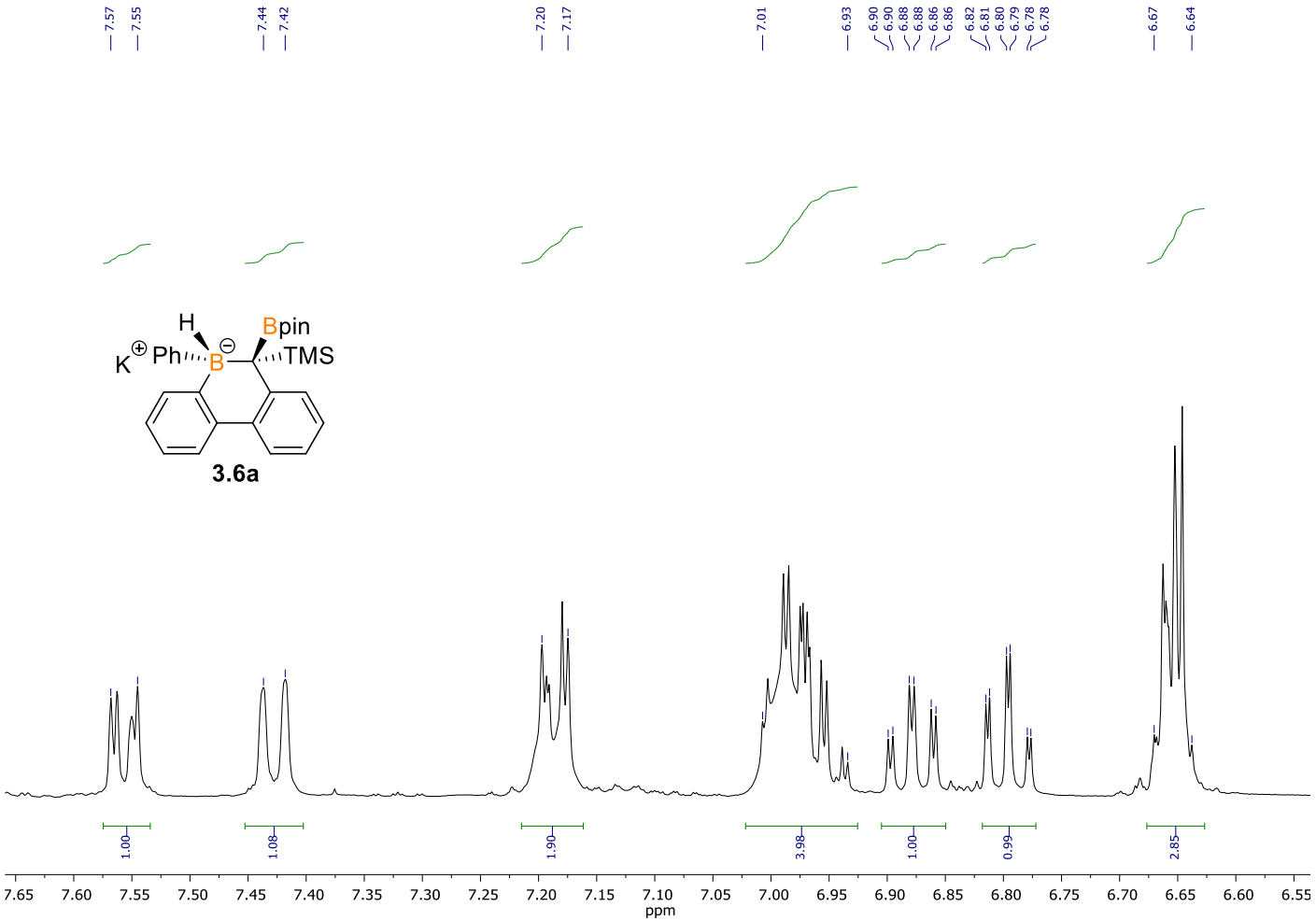

Figure B-14: Expansion of ^{1}H NMR spectrum of **3.6a** in CD_3CN (aryl region).

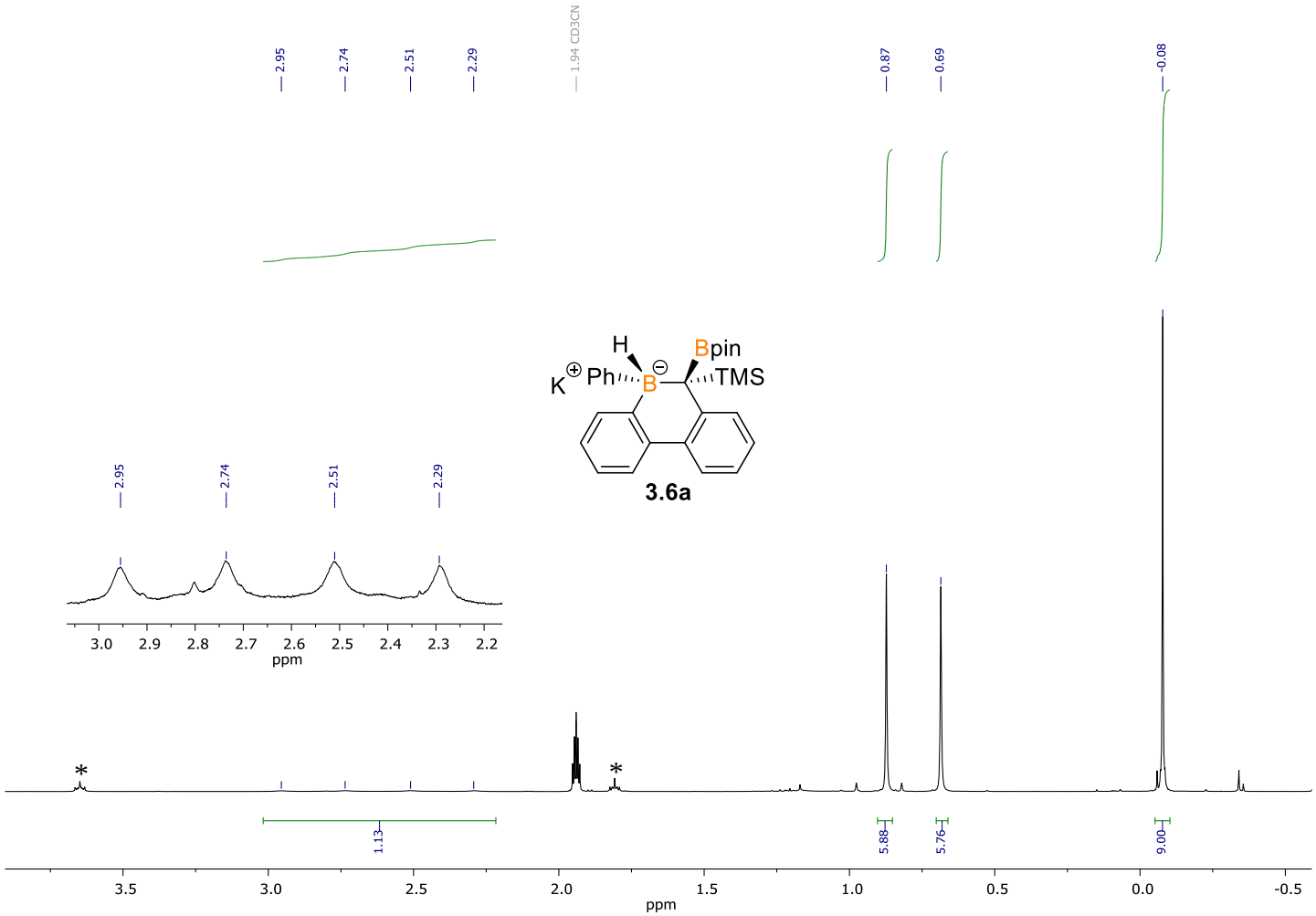

Figure B-15: Expansion of ^{1}H NMR spectrum of **3.6a** in CD_3CN (aliphatic region, * indicates THF).

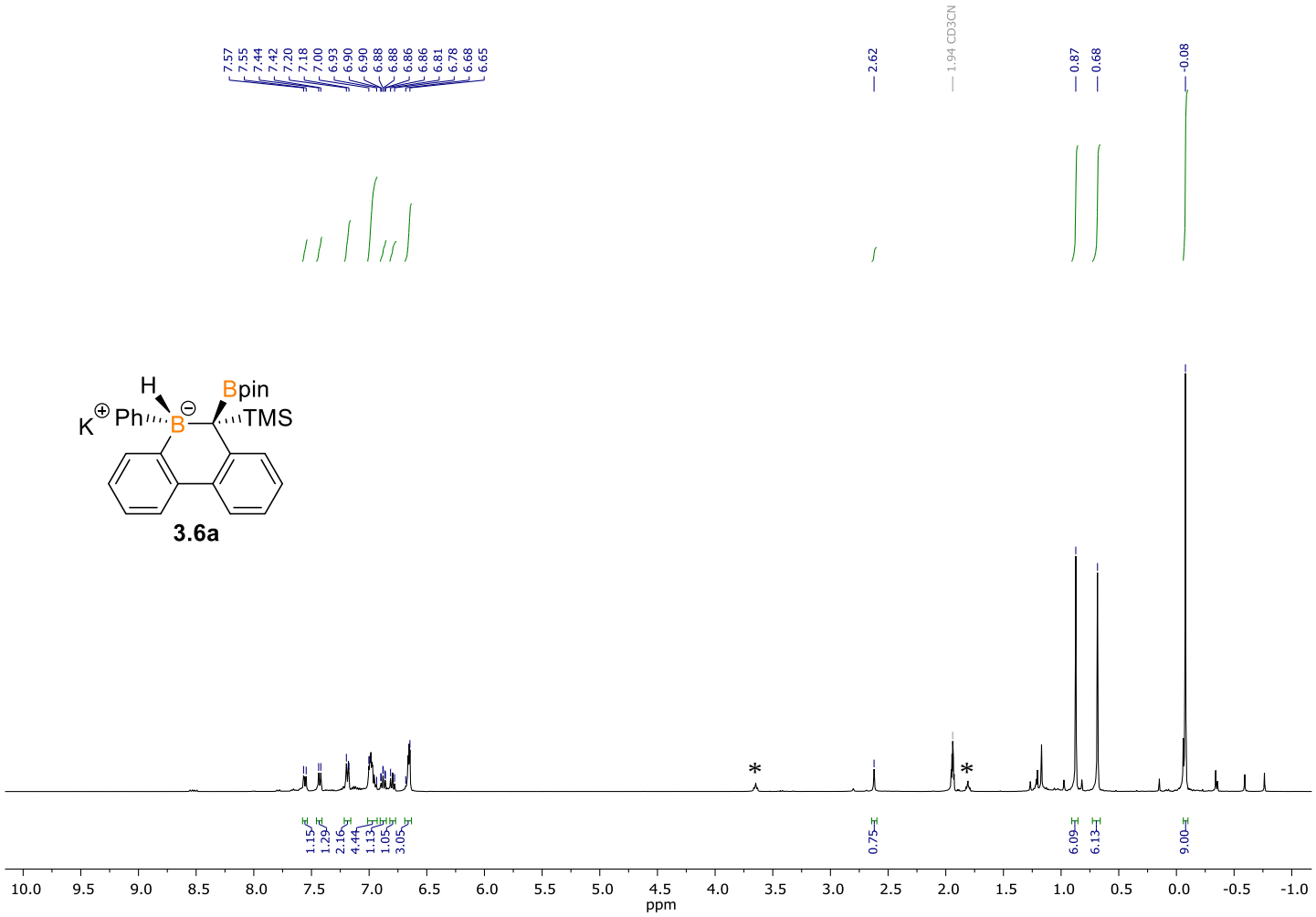

Figure B-16: $^{1}H\{^{11}B\}$ NMR spectrum of **3.6a** in CD_3CN (* indicates THF).

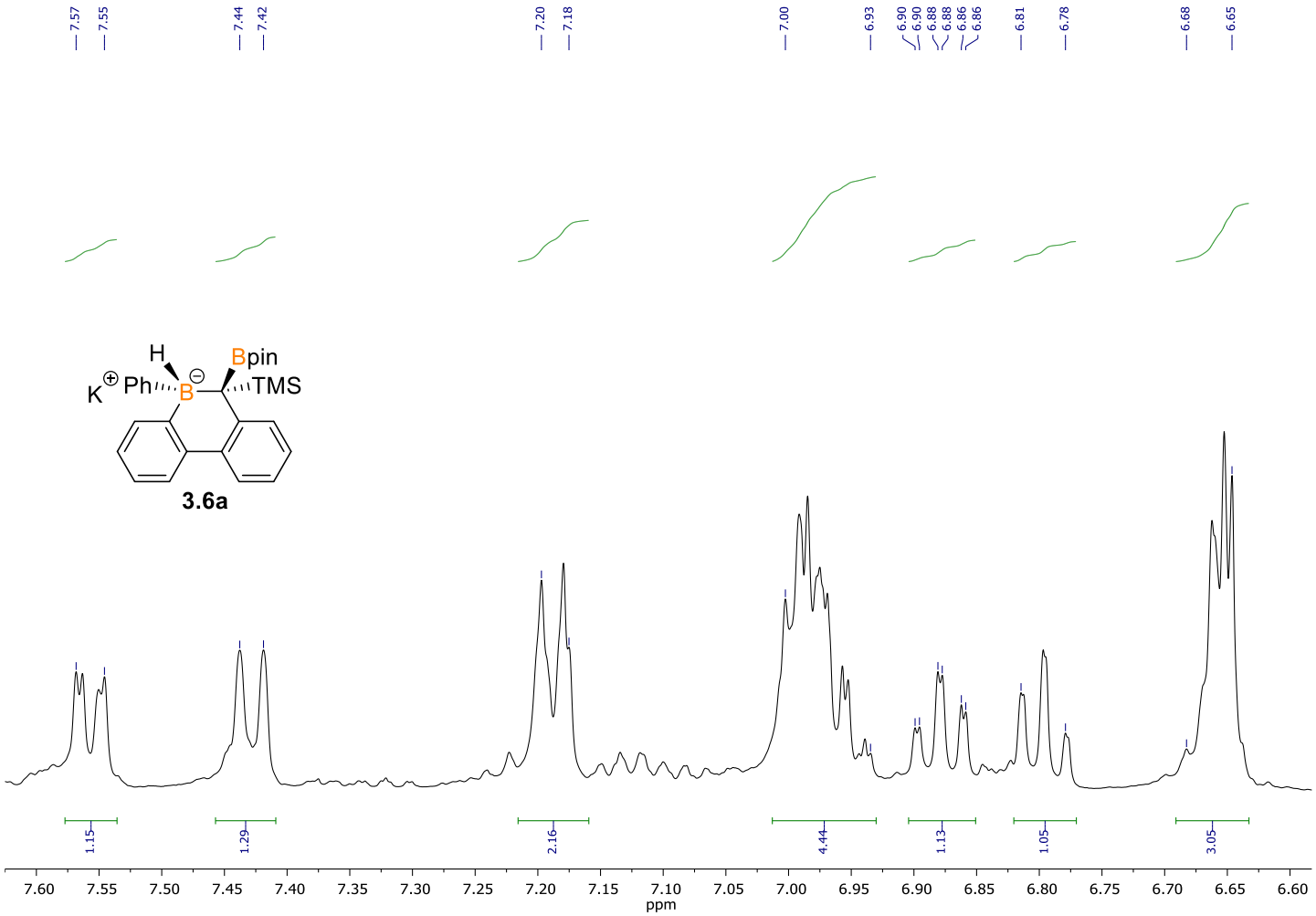

Figure B-17: Expansion of $^{1}H\{^{11}B\}$ NMR spectrum of **3.6a** in CD_3CN (aryl region).

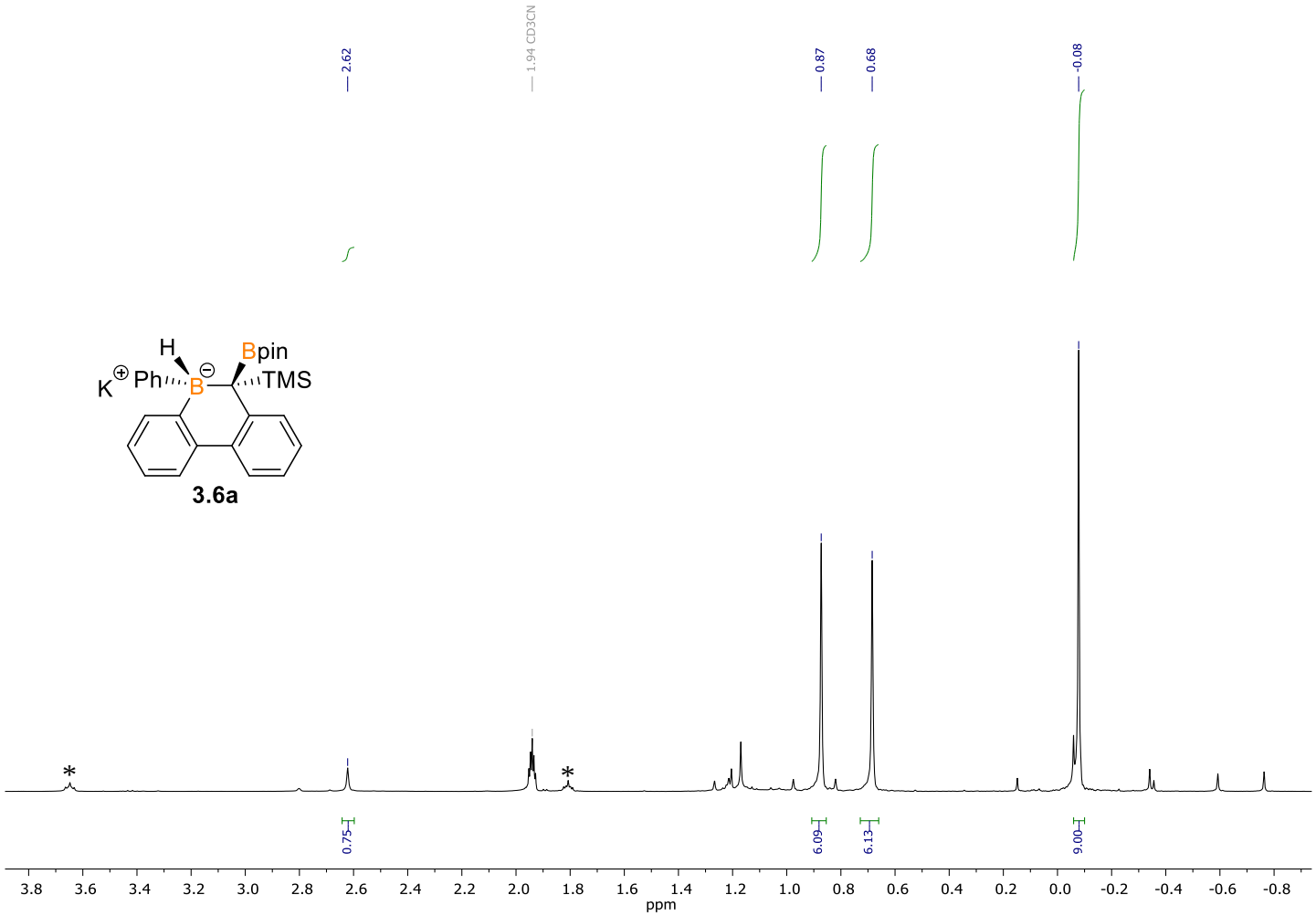

Figure B-18: Expansion of $^{1}H\{^{11}B\}$ NMR spectrum of **3.6a** in CD_3CN (aliphatic region, * indicates THF).

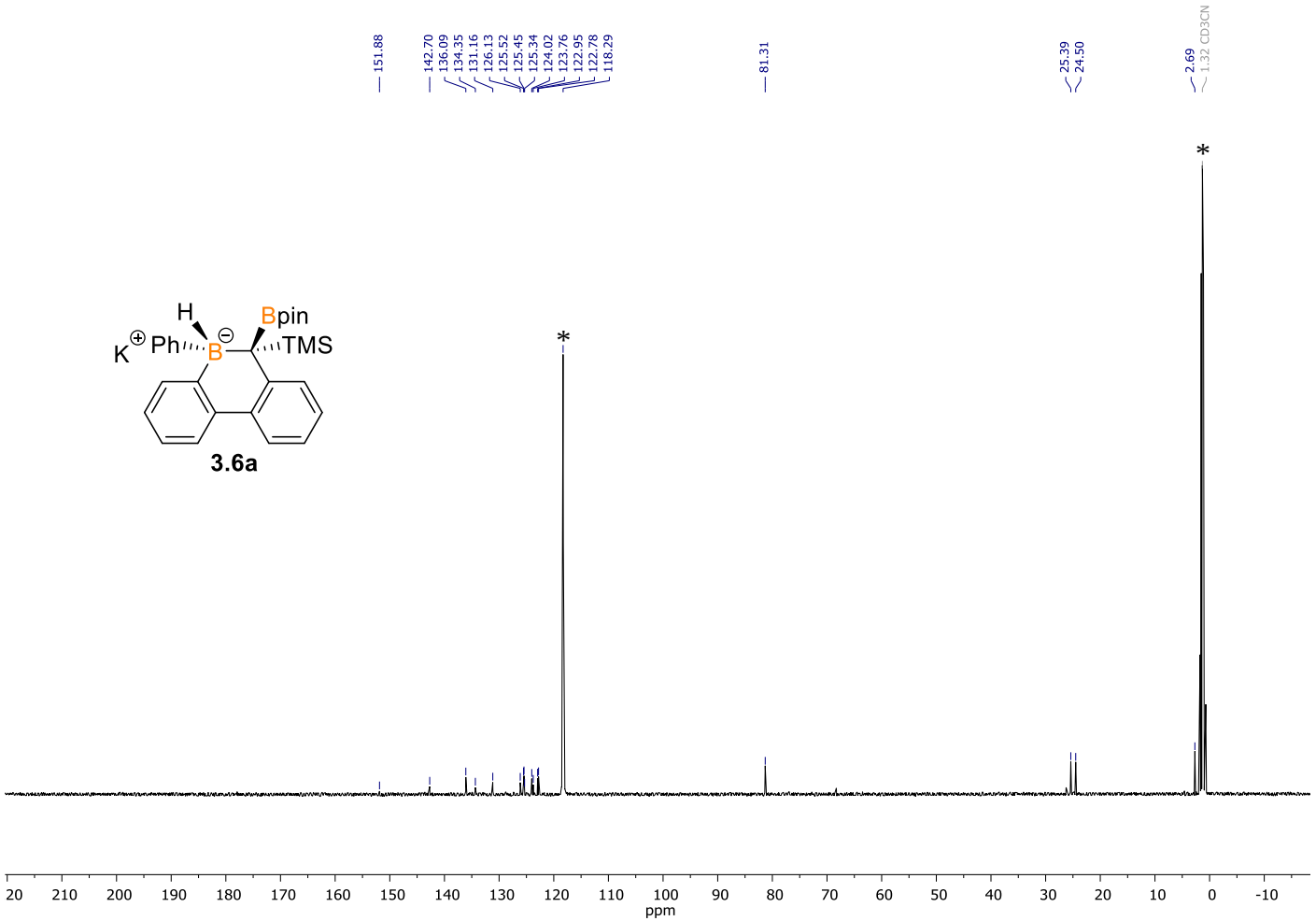

Figure B-19: $^{13}C\{^{1}H\}$ NMR spectrum of **3.6a** in CD_3CN (* indicates CD_3CN).

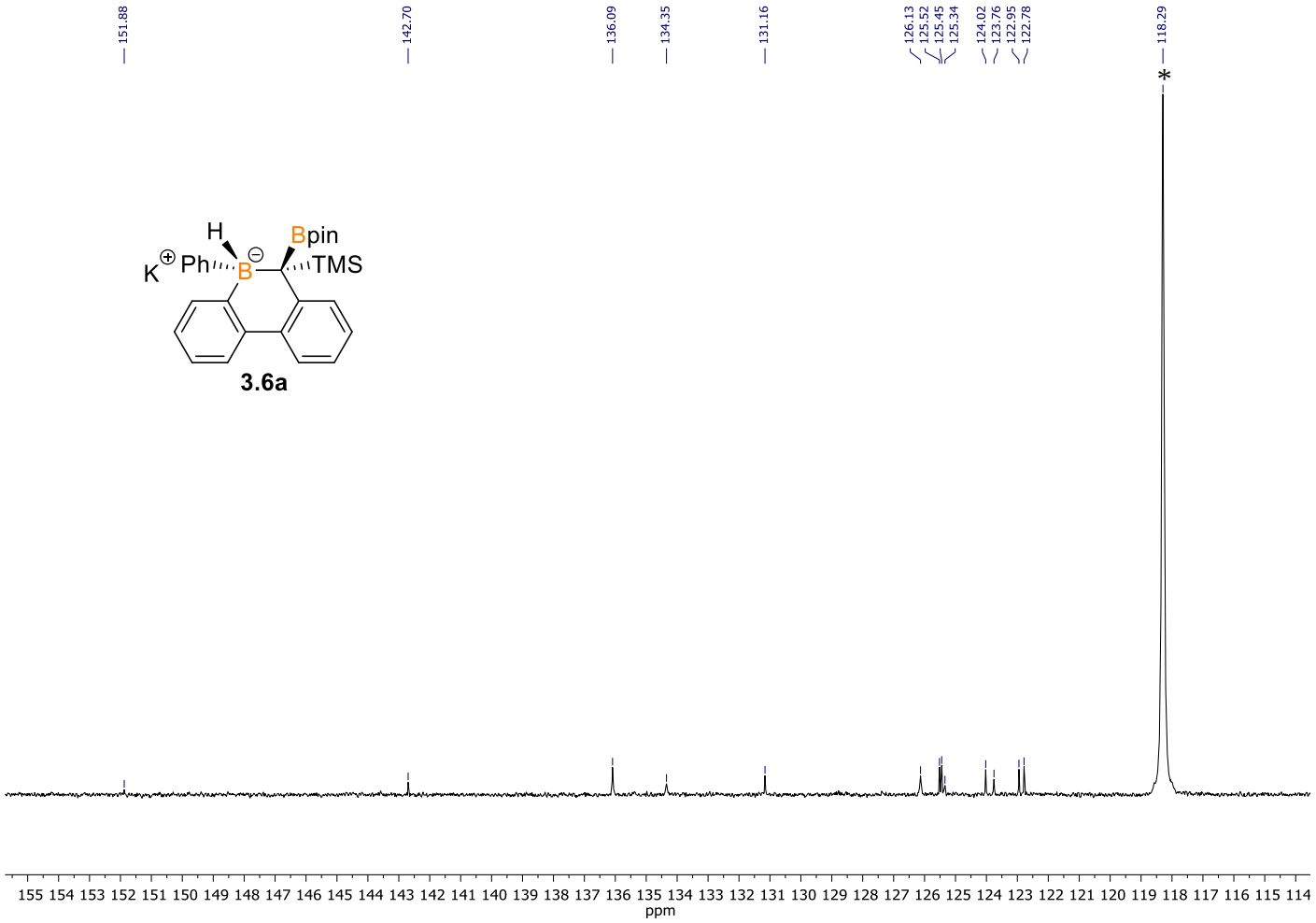

Figure B-20: Expansion of $^{13}C\{^{1}H\}$ NMR spectrum of **3.6a** in CD_3CN (aryl region, * indicates CD_3CN).

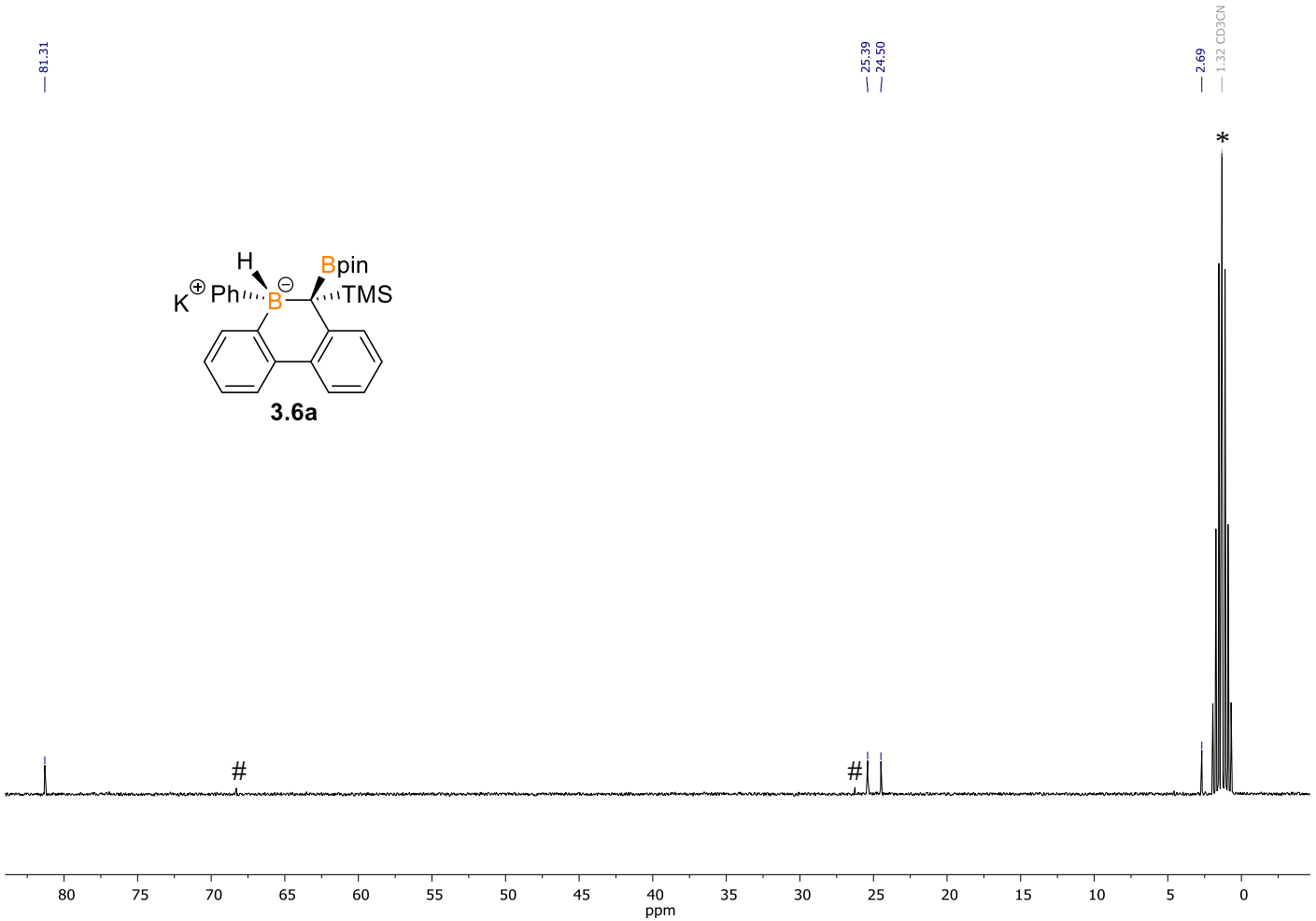

Figure B-21: Expansion of $^{13}C\{^{1}H\}$ NMR spectrum of **3.6a** in CD_3CN (aliphatic region, * indicates CD_3CN, # indicates THF).

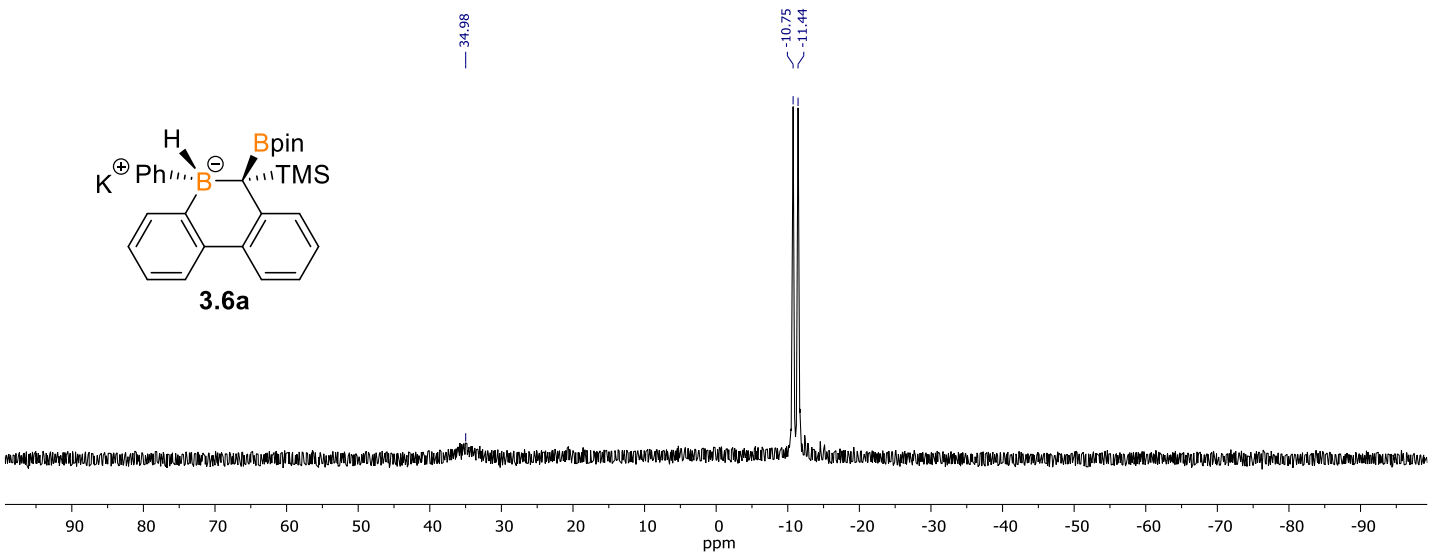

Figure B-22: ^{11}B NMR spectrum of **3.6a** in CD_3CN.

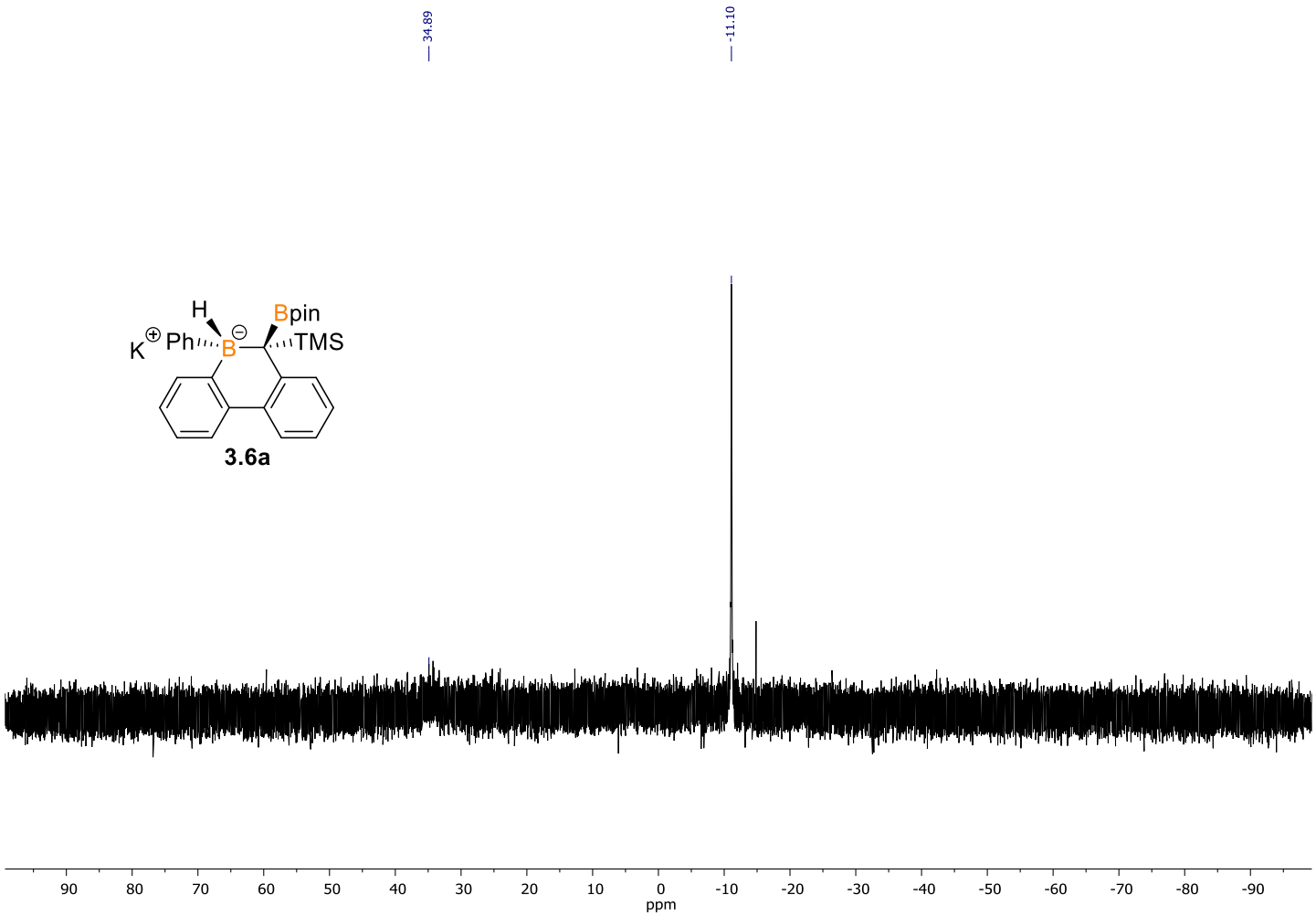

Figure B-23: $^{11}B\{^{1}H\}$ NMR spectrum of **3.6a** in CD_3CN.

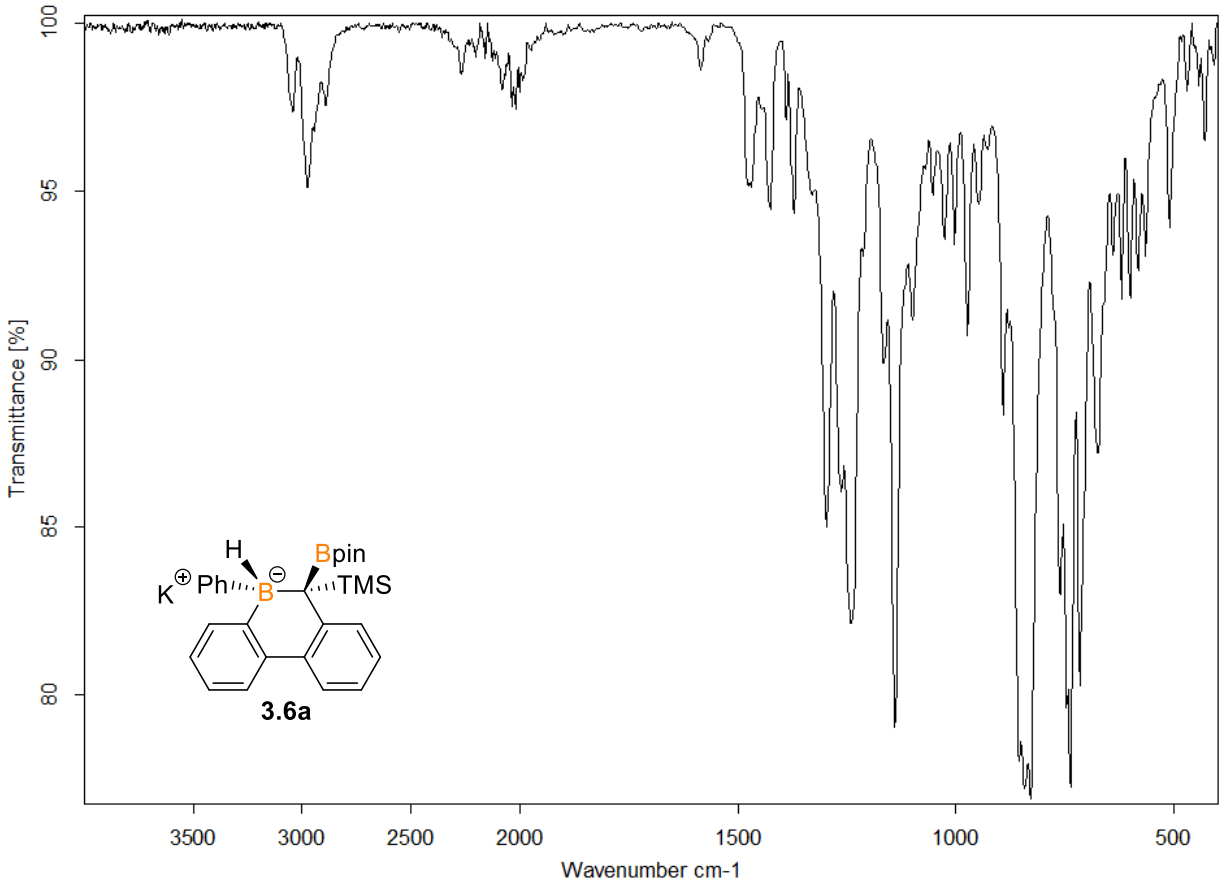

Figure B-24: FT-IR spectrum of **3.6a**.

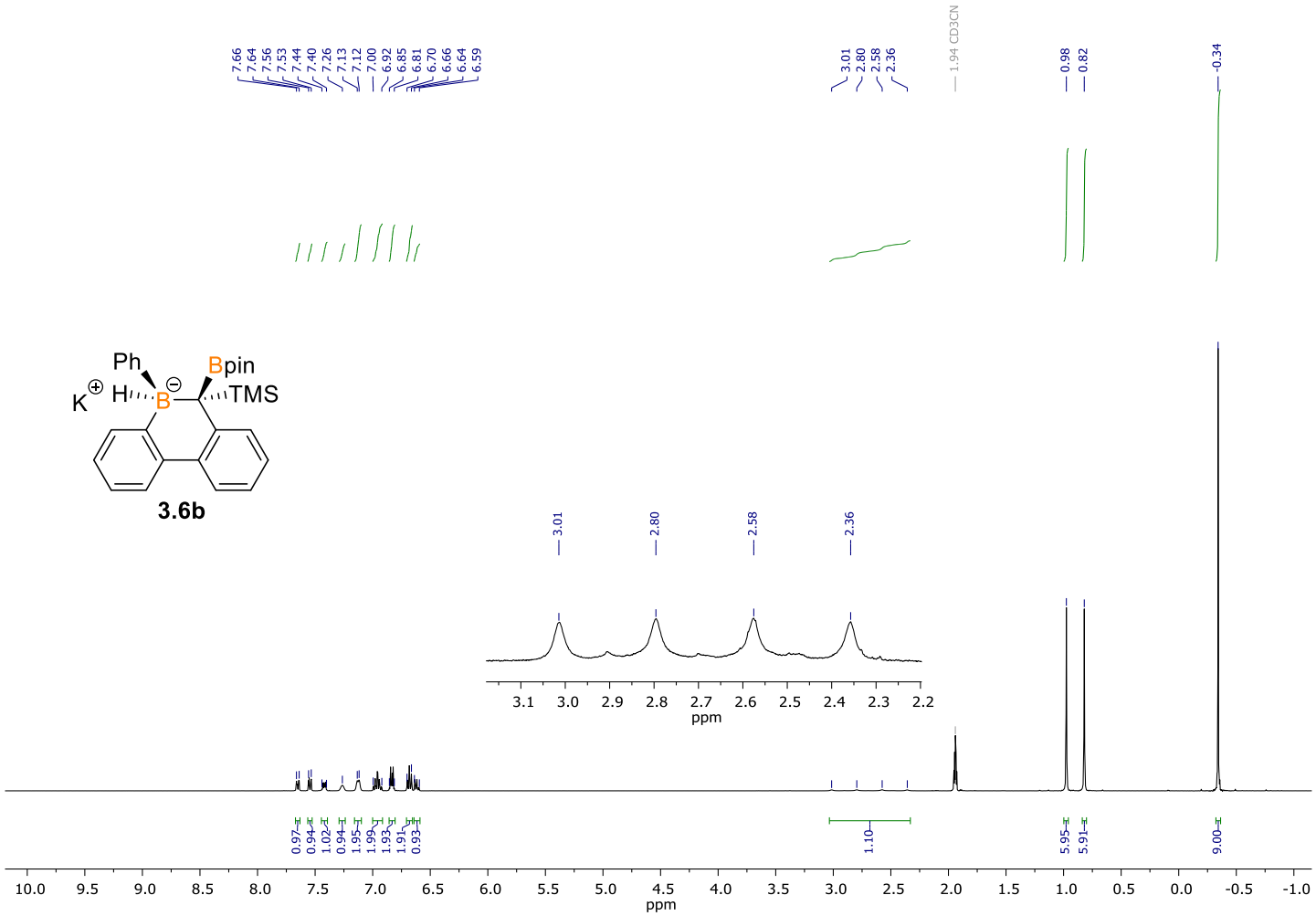

Figure B-25: ^{1}H NMR spectrum of **3.6b** in CD_3CN.

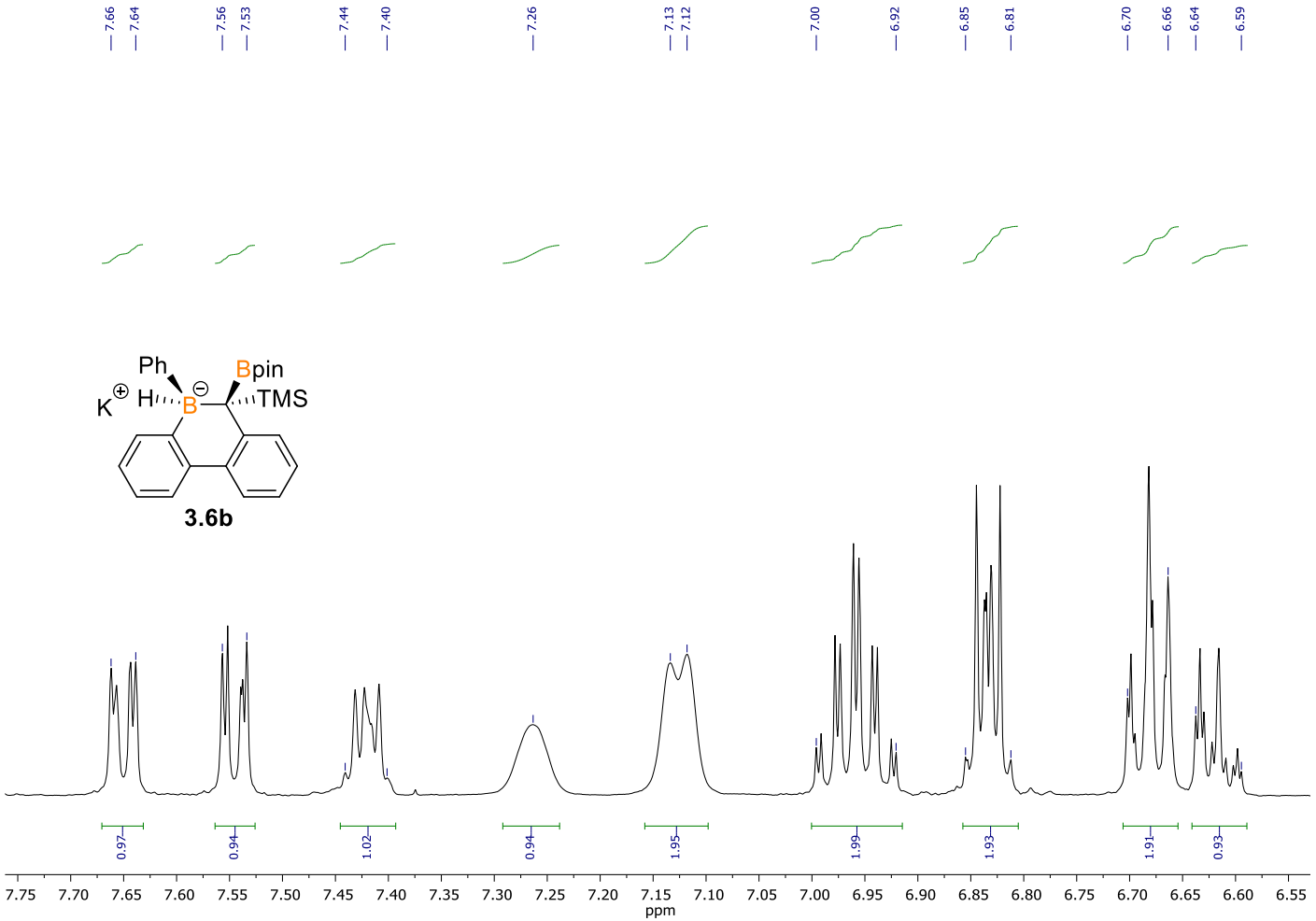

Figure B-26: Expansion of ^{1}H NMR spectrum of **3.6b** in CD_3CN (aryl region).

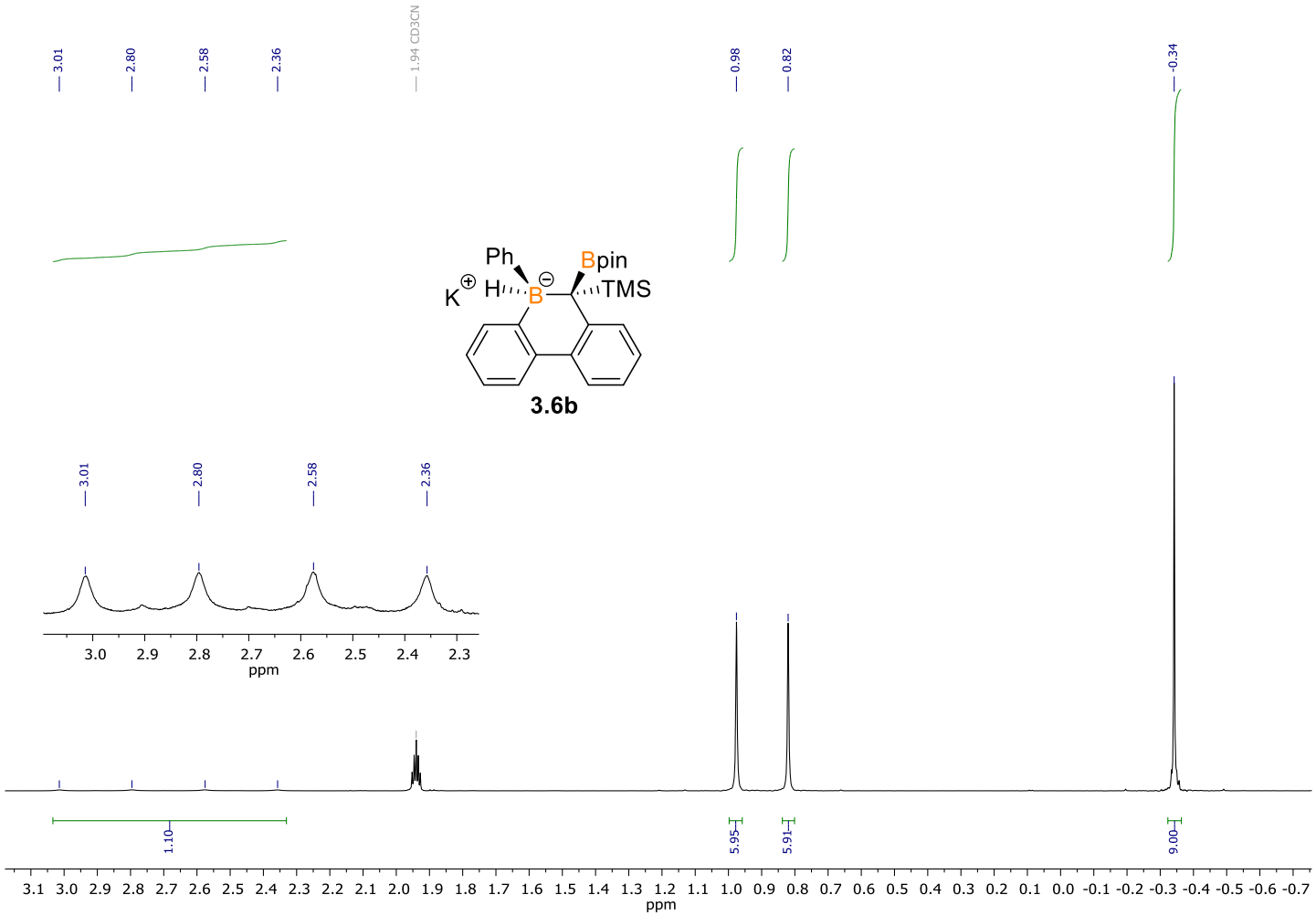

Figure B-27: Expansion of ^{1}H NMR spectrum of **3.6b** in CD_3CN (aliphatic region).

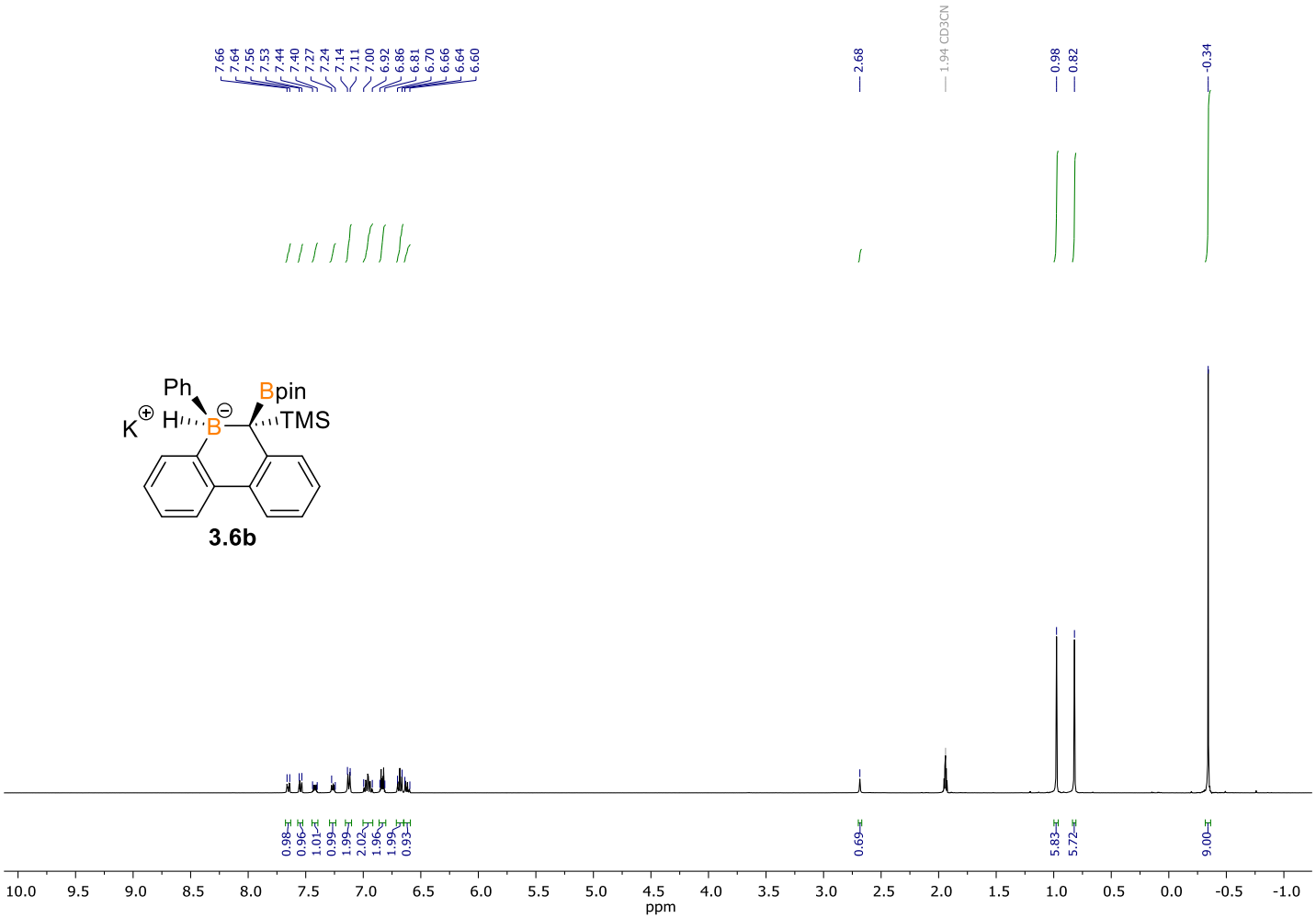

Figure B-28: $^{1}H\{^{11}B\}$ NMR spectrum of **3.6b** in CD_3CN.

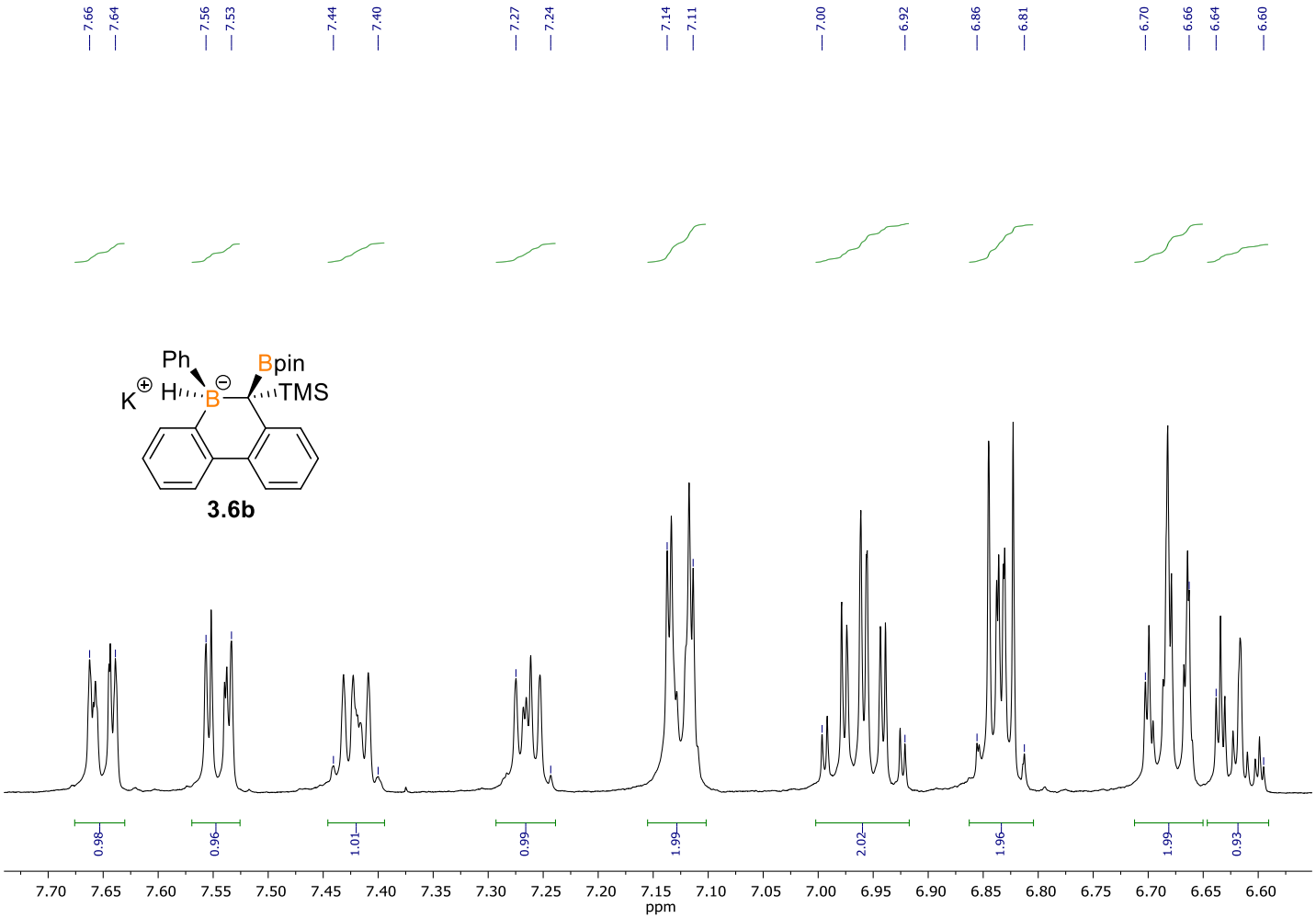

Figure B-29: Expansion of $^{1}H\{^{11}B\}$ NMR spectrum of **3.6b** in CD_3CN (aryl region).

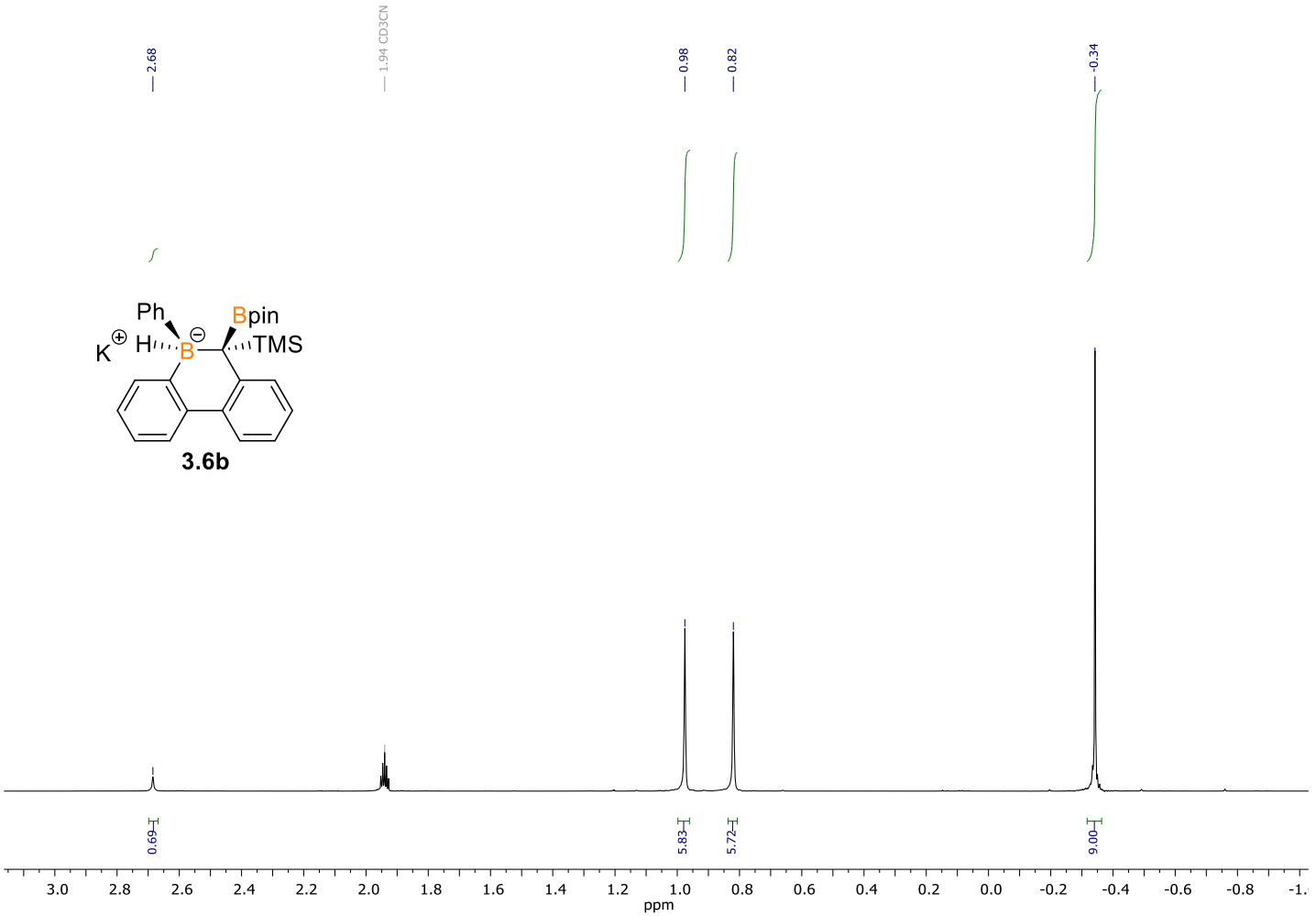

Figure B-30: Expansion of $^{1}H\{^{11}B\}$ NMR spectrum of **3.6b** in CD_3CN (aliphatic region).

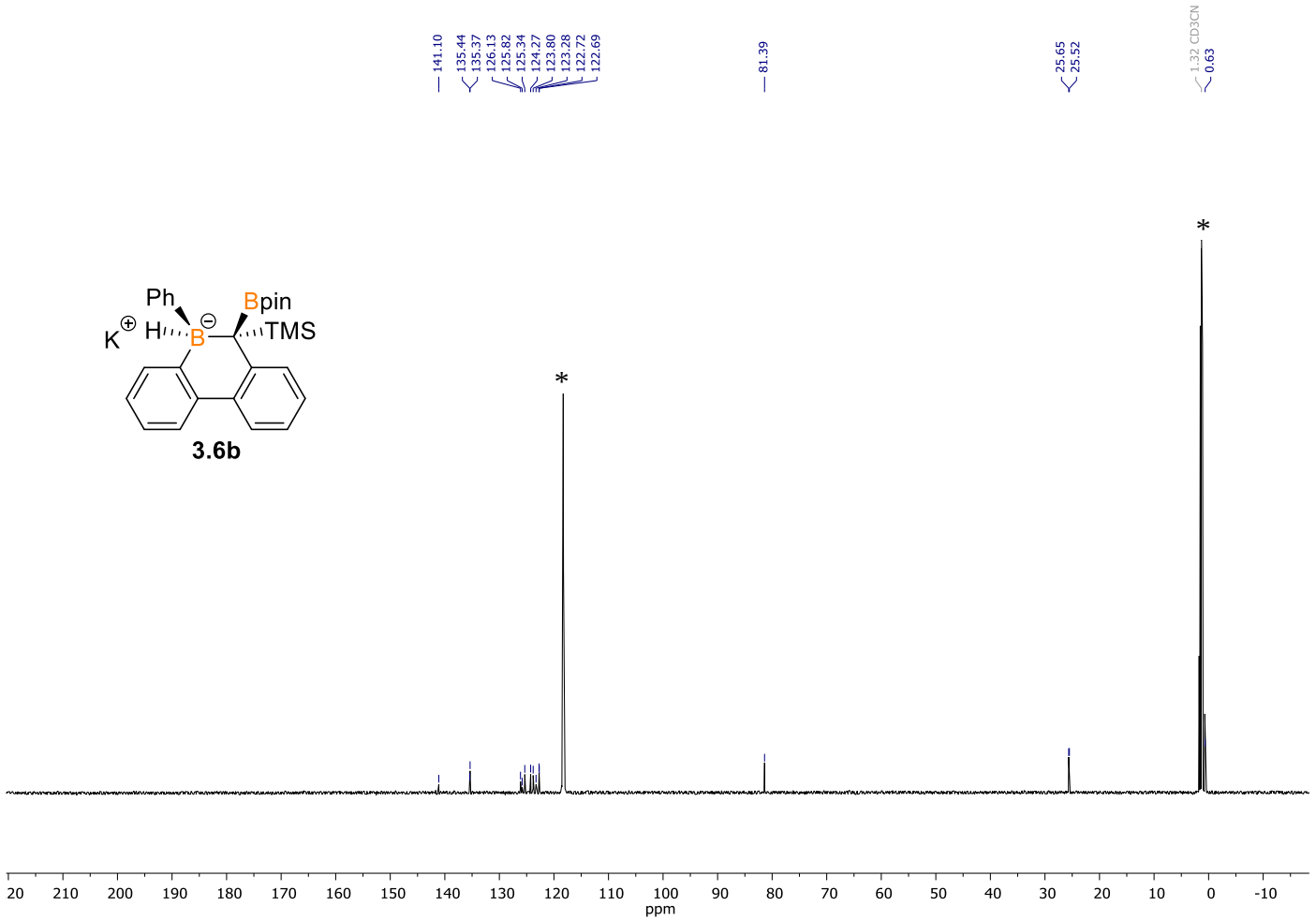

Figure B-31: $^{13}C\{^{1}H\}$ NMR spectrum of **3.6b** in CD_3CN (* indicates CD_3CN).

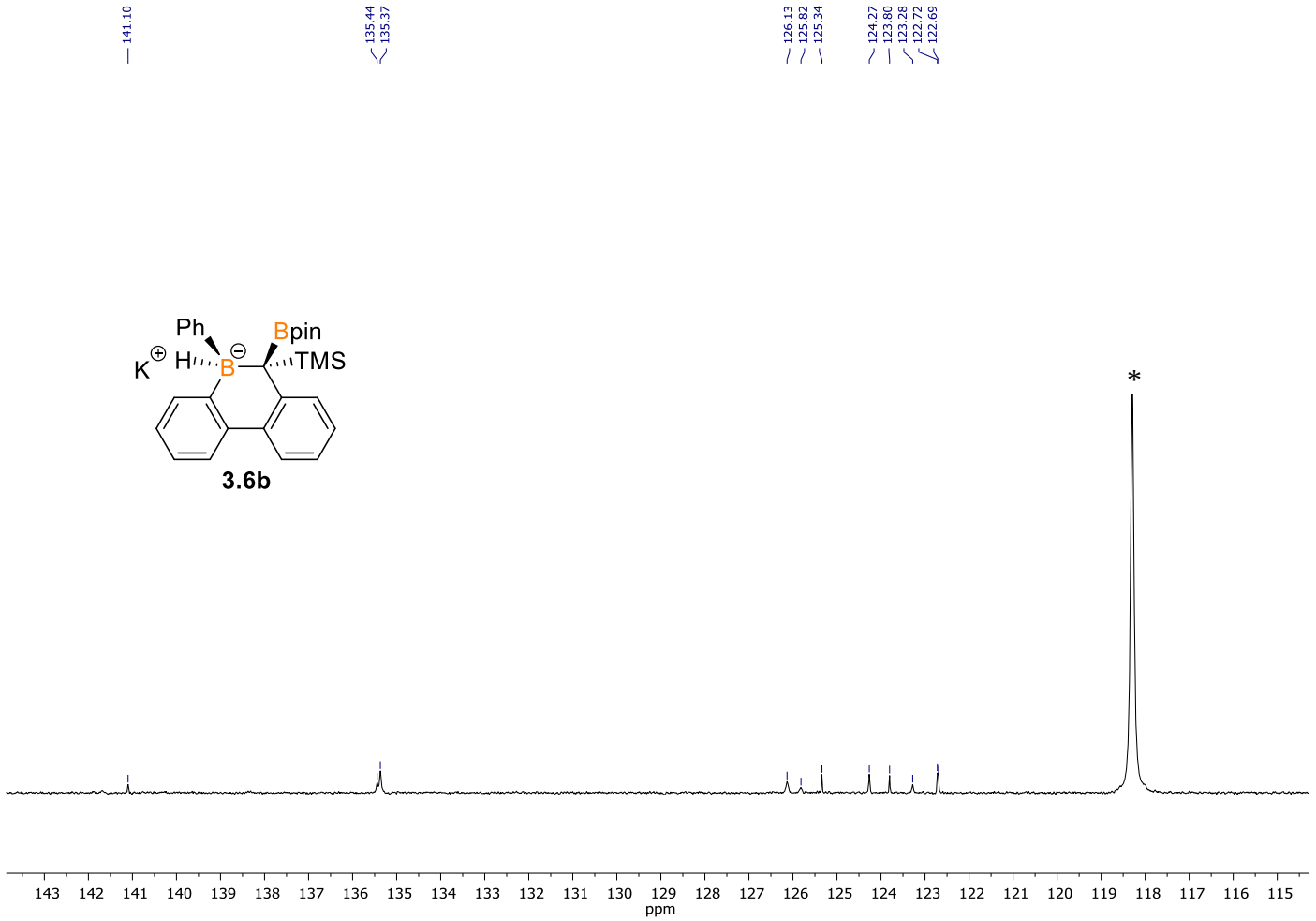

Figure B-32: Expansion of $^{13}C\{^{1}H\}$ NMR spectrum of **3.6b** in CD_3CN (aryl region, * indicates CD_3CN).

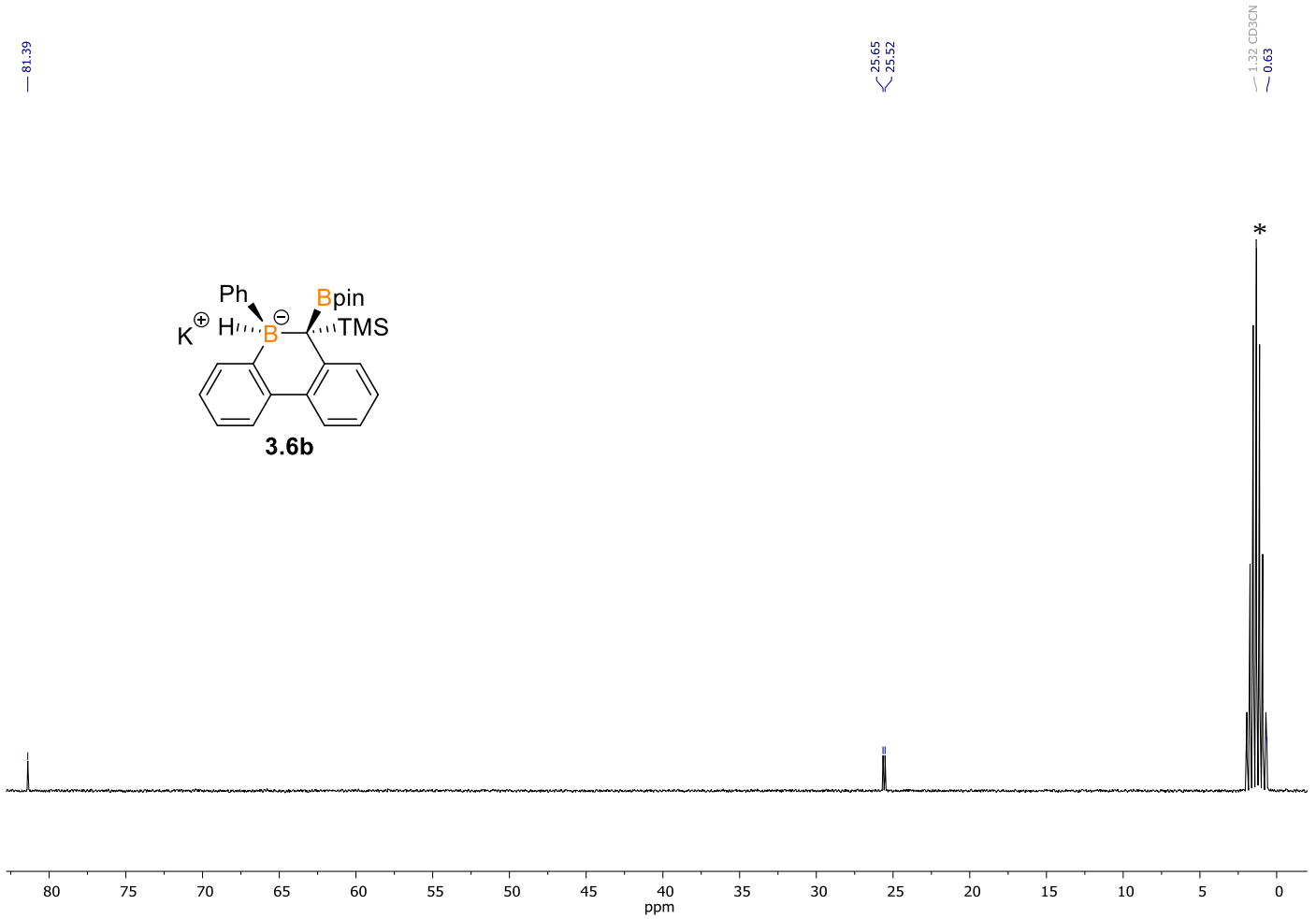

Figure B-33: Expansion of $^{13}C\{^{1}H\}$ NMR spectrum of **3.6b** in CD_3CN (aliphatic region, * indicates CD_3CN).

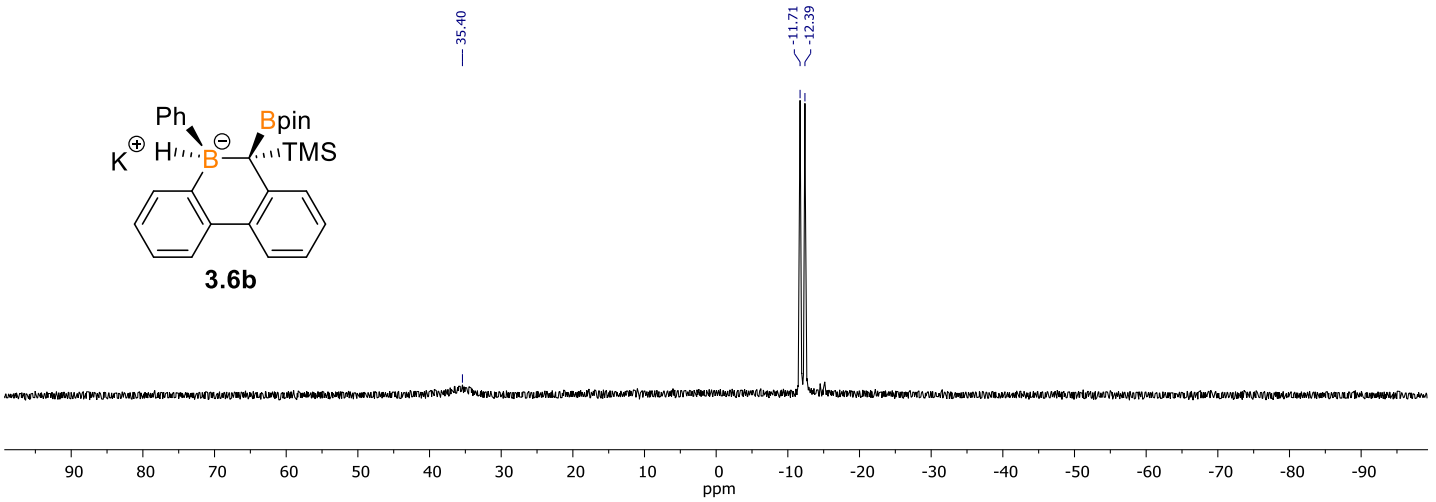

Figure B-34: ^{11}B NMR spectrum of **3.6b** in CD_3CN.

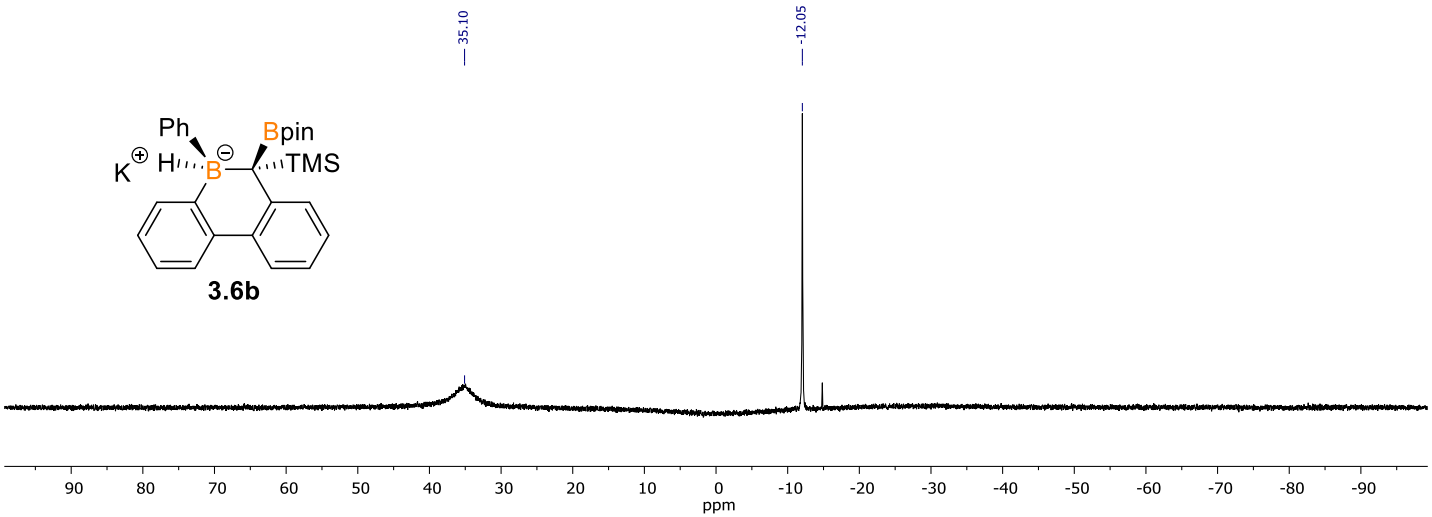

Figure B-35: $^{11}B\{^{1}H\}$ NMR spectrum of **3.6b** in CD_3CN.

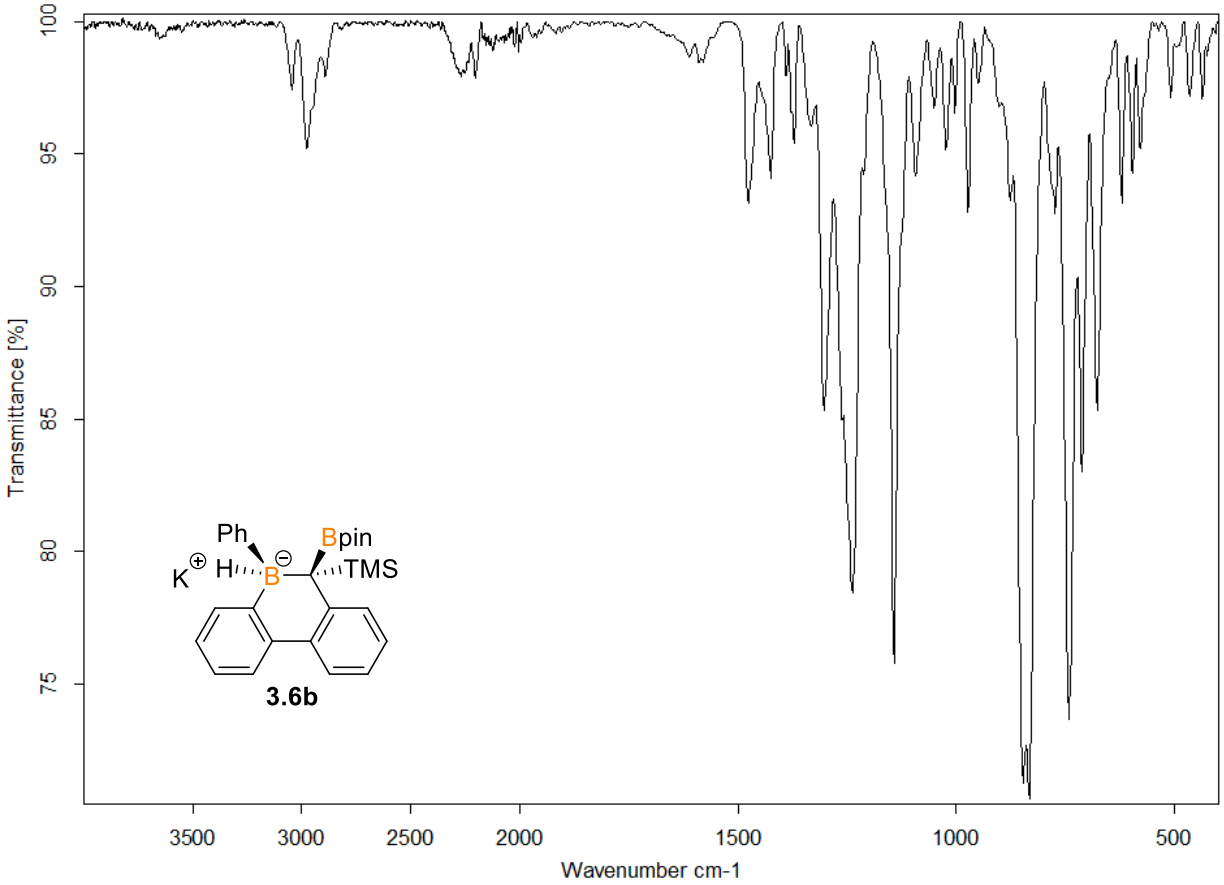

Figure B-36: FT-IR spectrum of **3.6b**.

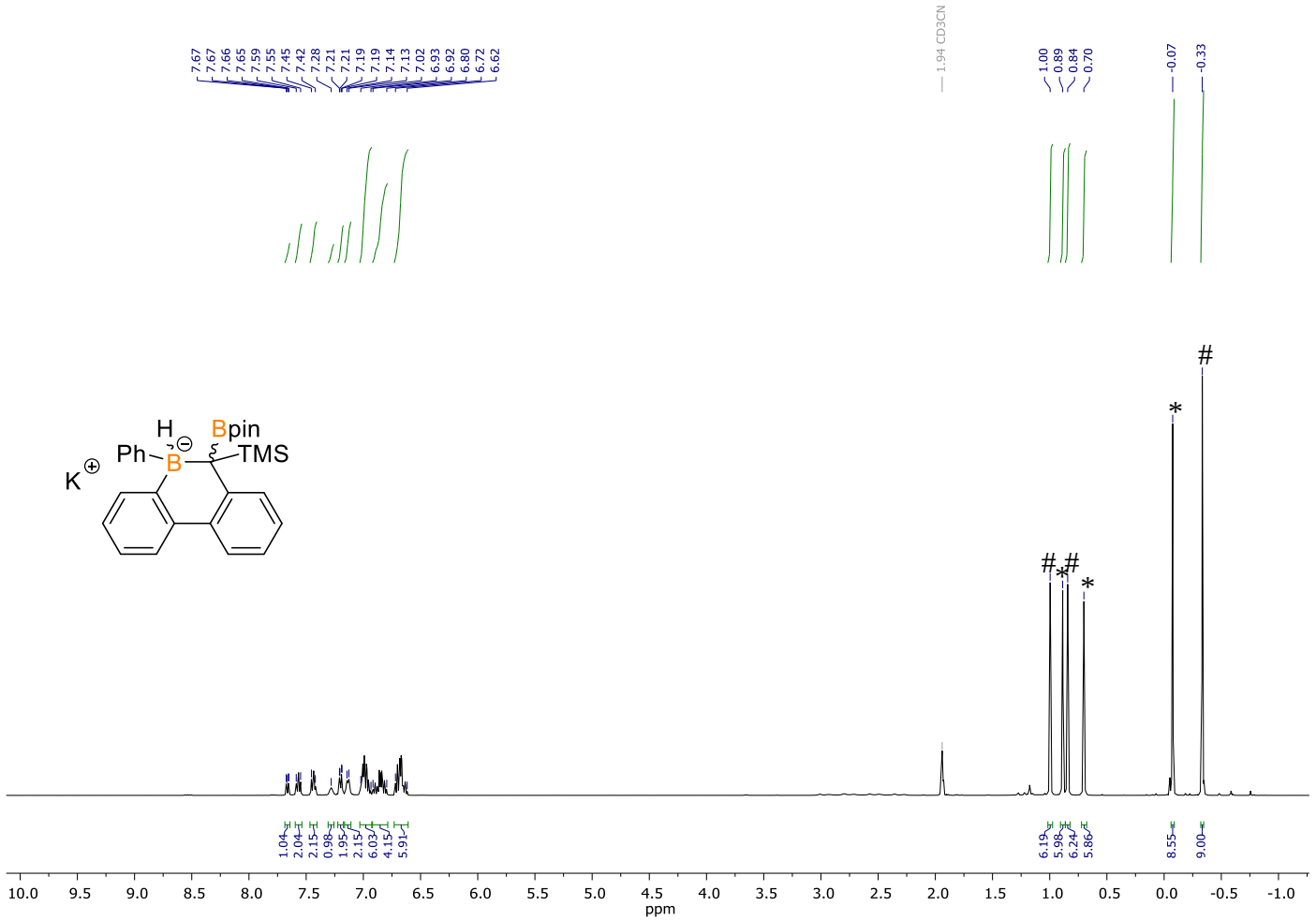

Figure B-37: ^{1}H NMR spectrum of 1:1 **3.6a/3.6b** in CD_3CN at 27 ºC (* indicates **3.6a**, # indicates **3.6b**).

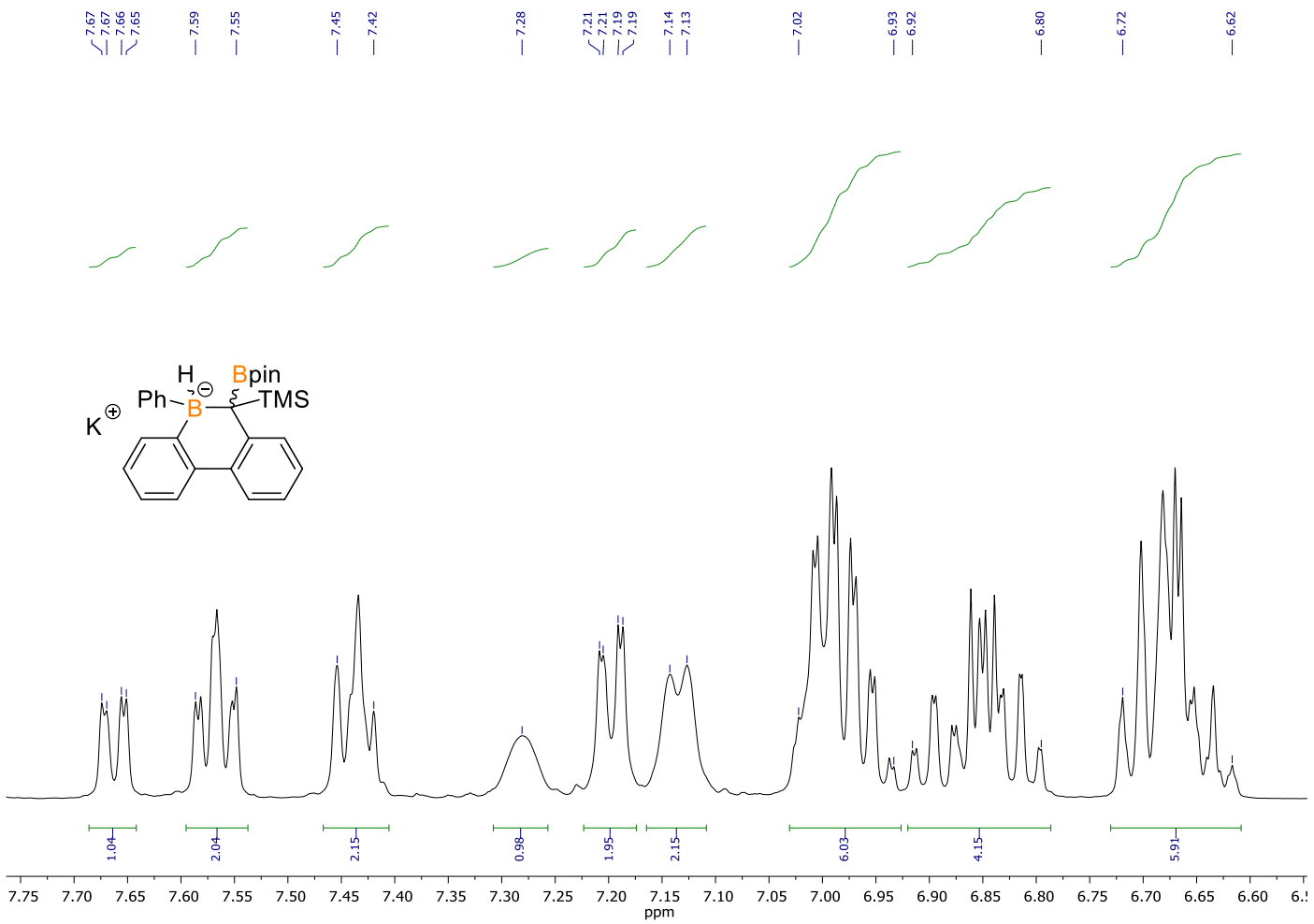

Figure B-38: Expansion of ^{1}H NMR spectrum of 1:1 **3.6a/3.6b** in CD_3CN at 27 ºC (aryl region).

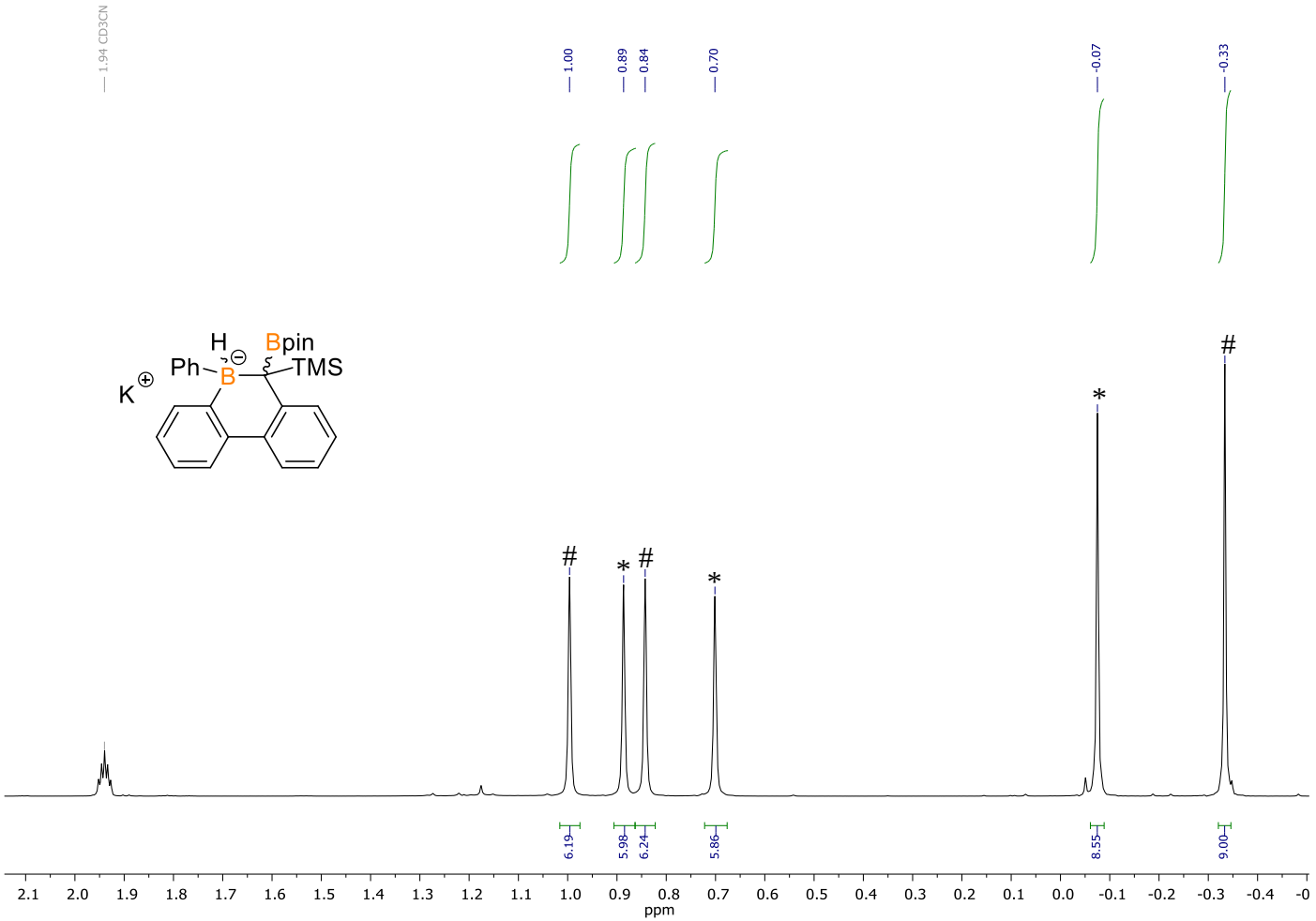

Figure B-39: Expansion of ^{1}H NMR spectrum of 1:1 **3.6a/3.6b** in CD_3CN at 27 ºC (aliphatic region, * indicates **3.6a**, # indicates **3.6b**).

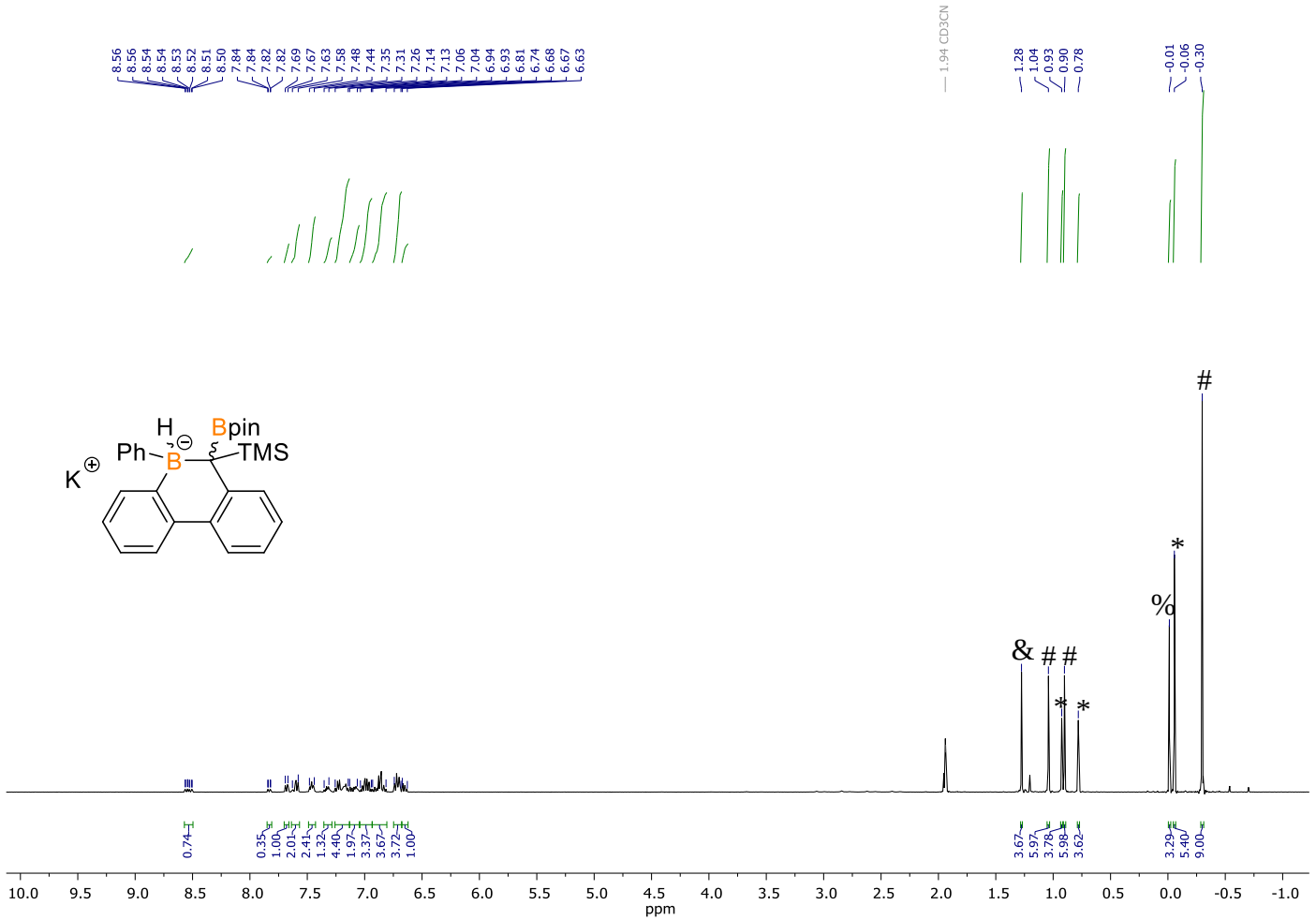

Figure B-40: ^{1}H NMR spectrum of 1:1 **3.6a/3.6b** in CD_3CN at 70 ºC (* indicates **3.6a**, # indicates **3.6b**, % indicates **3.4**, & indicates HBpin).

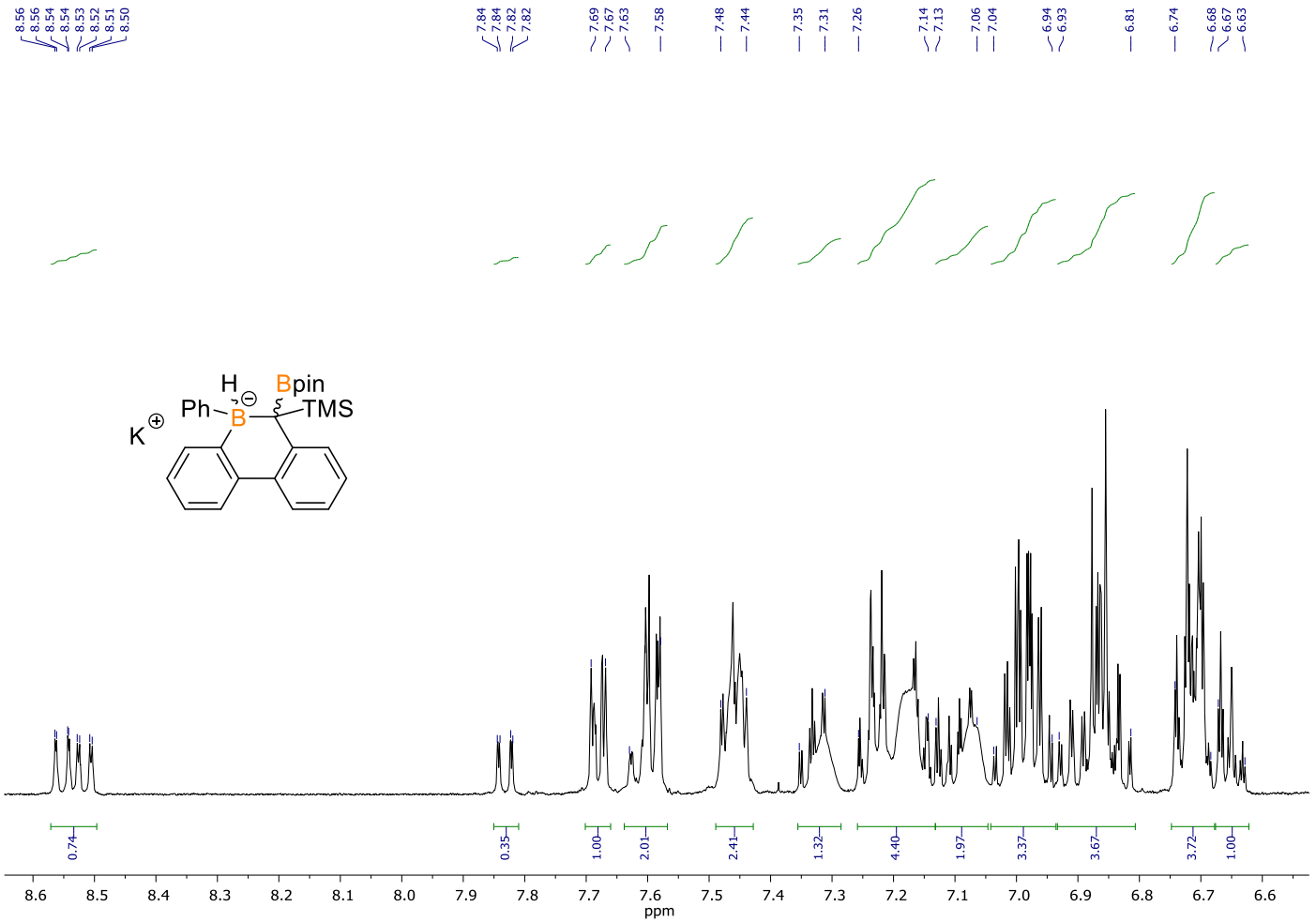

Figure B-41: Expansion of ^{1}H NMR spectrum of 1:1 **3.6a/3.6b** in CD_3CN at 70 ºC (aryl region).

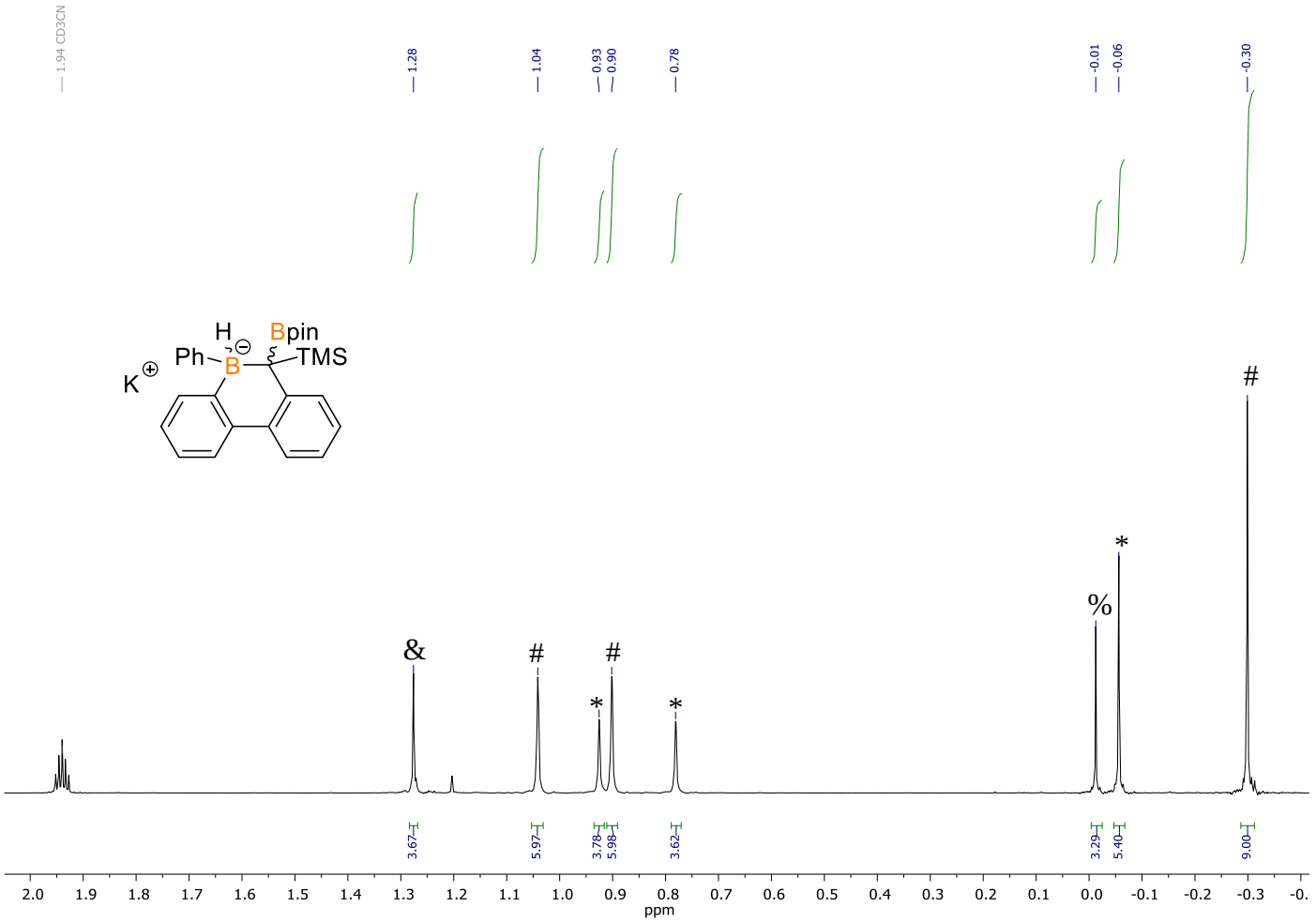

Figure B-42: Expansion of ^{1}H NMR spectrum of 1:1 **3.6a**/**3.6b** in CD_3CN at 70 ºC (aliphatic region, * indicates **3.6a**, # indicates **3.6b**, % indicates **3.4**, & indicates HBpin).

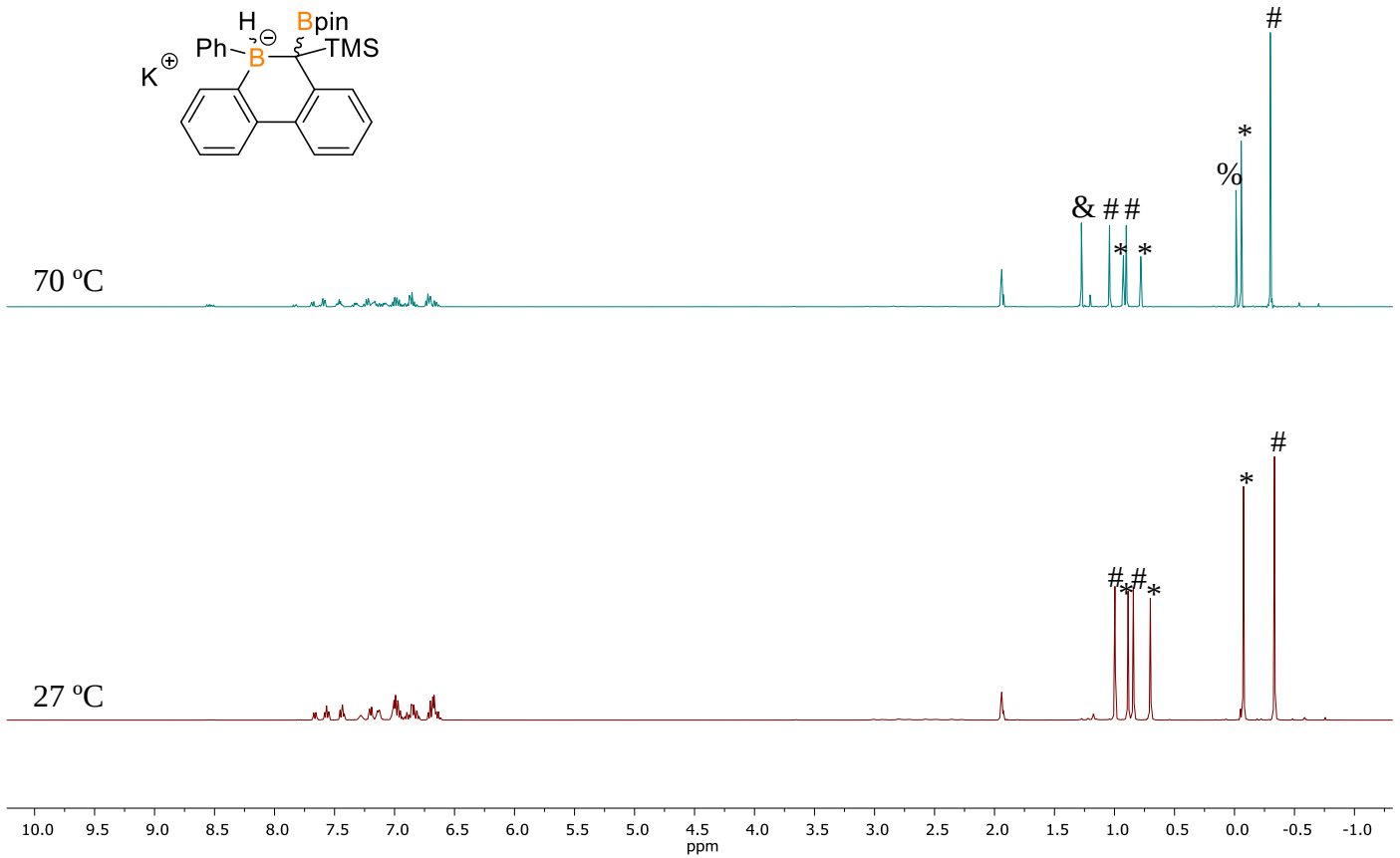

Figure B-43: Stacked plot of variable-temperature ^{1}H NMR spectra for 1:1 **3.6a/3.6b** in CD_3CN (* indicates **3.6a**, # indicates **3.6b**, % indicates **3.4**, & indicates HBpin).

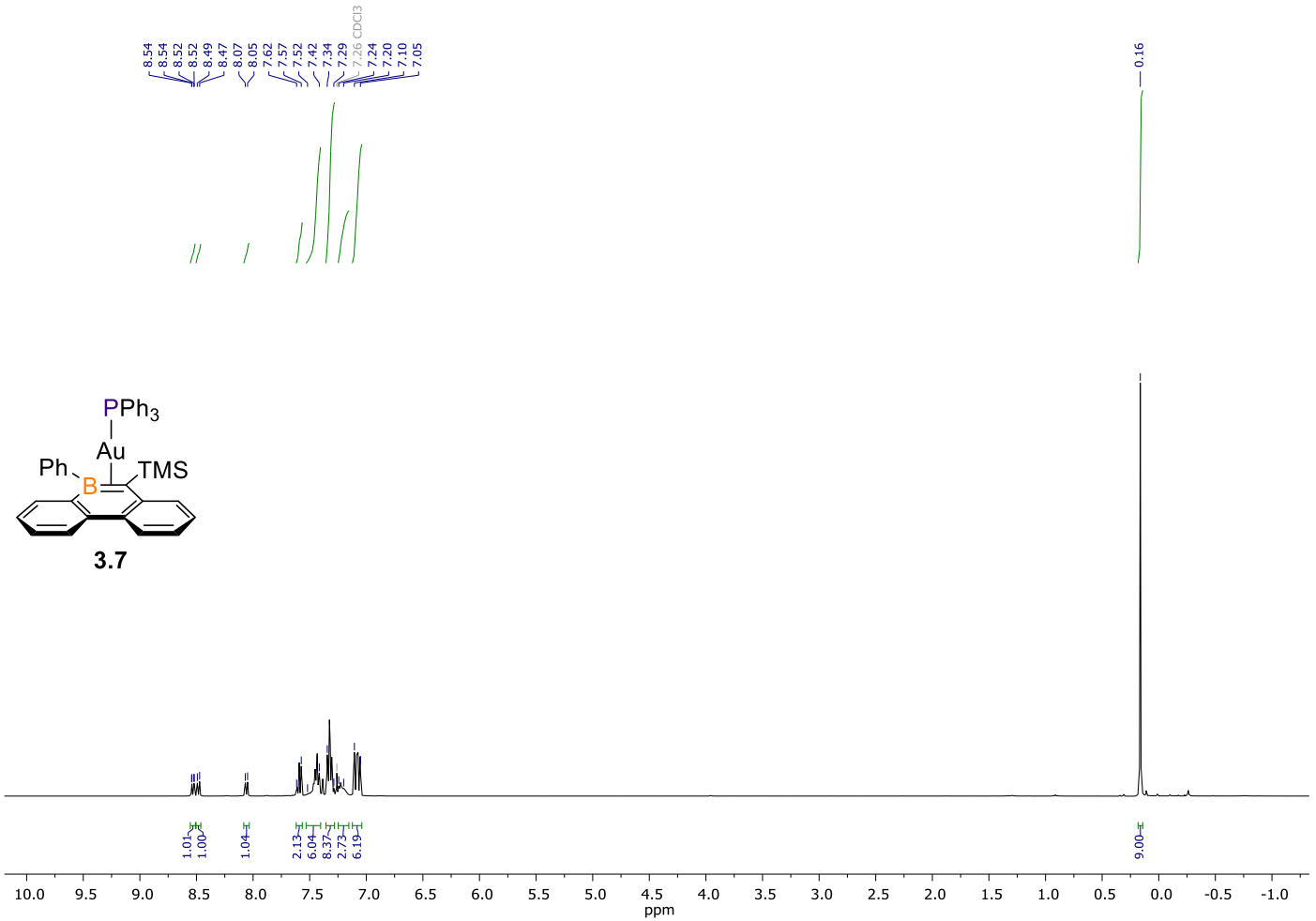

Figure B-44: ^{1}H NMR spectrum of **3.7** in $CDCl_3$.

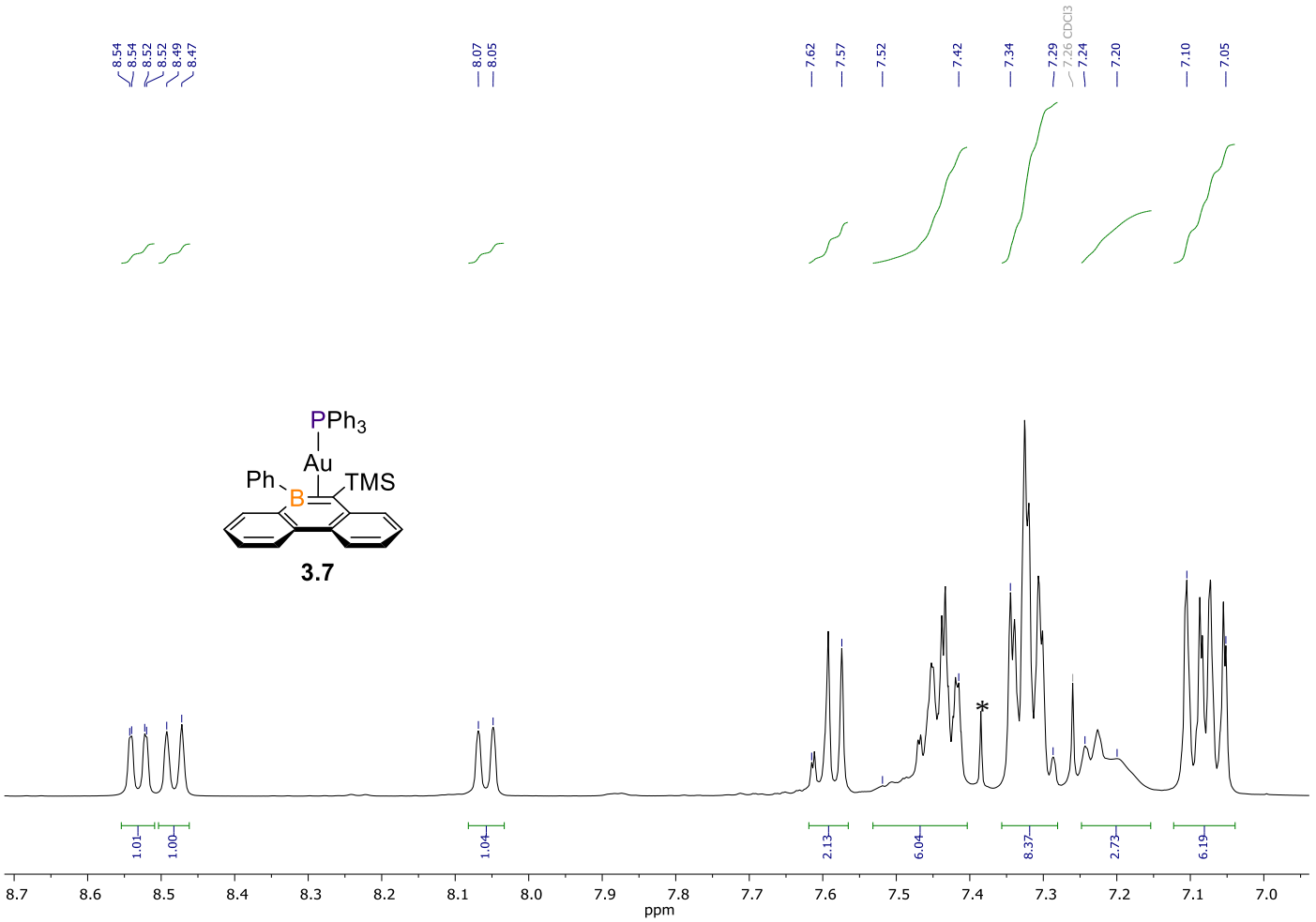

Figure B-45: Expansion of ^{1}H NMR spectrum of **3.7** in $CDCl_3$ (aryl region, * indicates benzene).

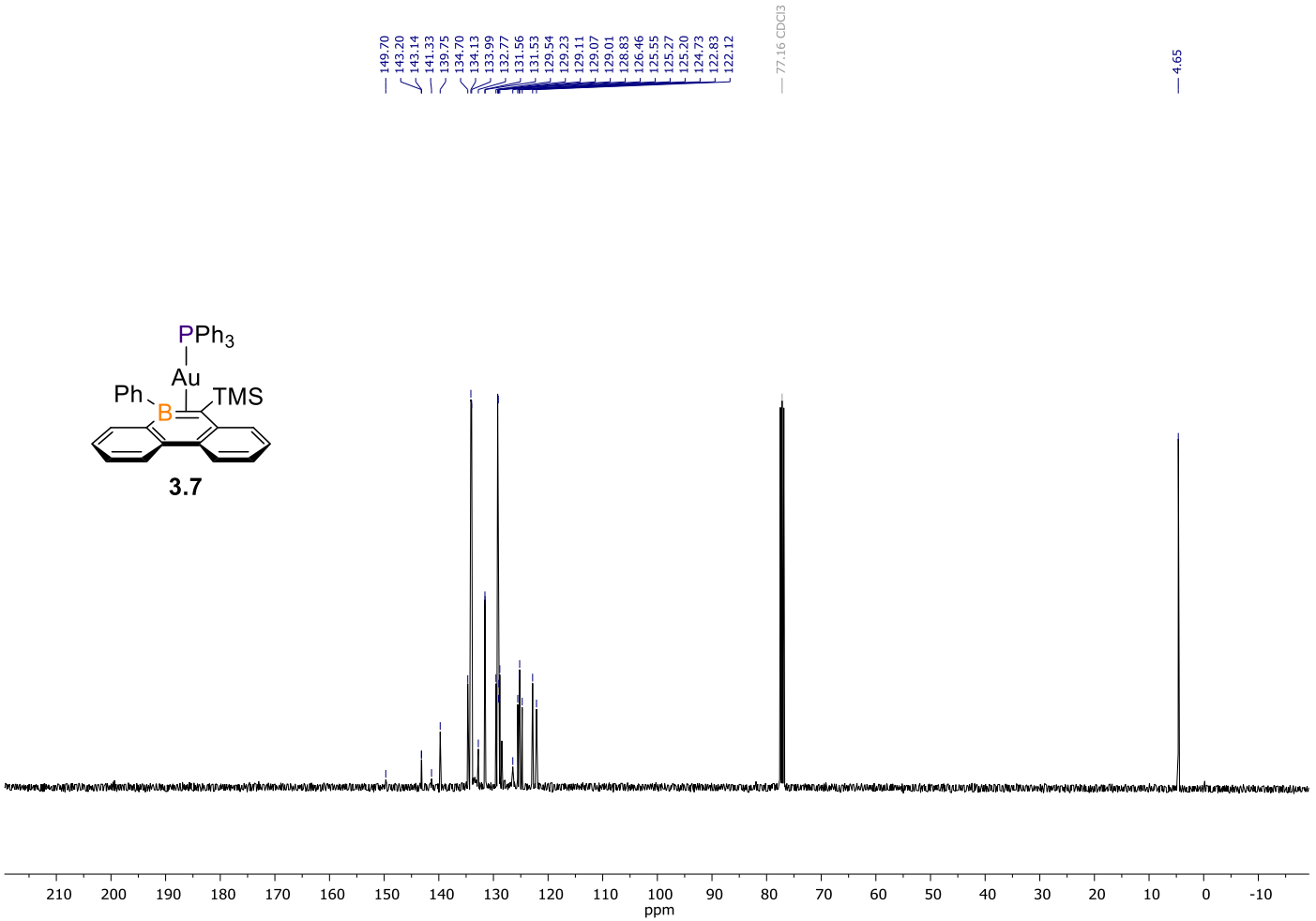

Figure B-46: $^{13}C\{^{1}H\}$ NMR spectrum of **3.7** in $CDCl_3$.

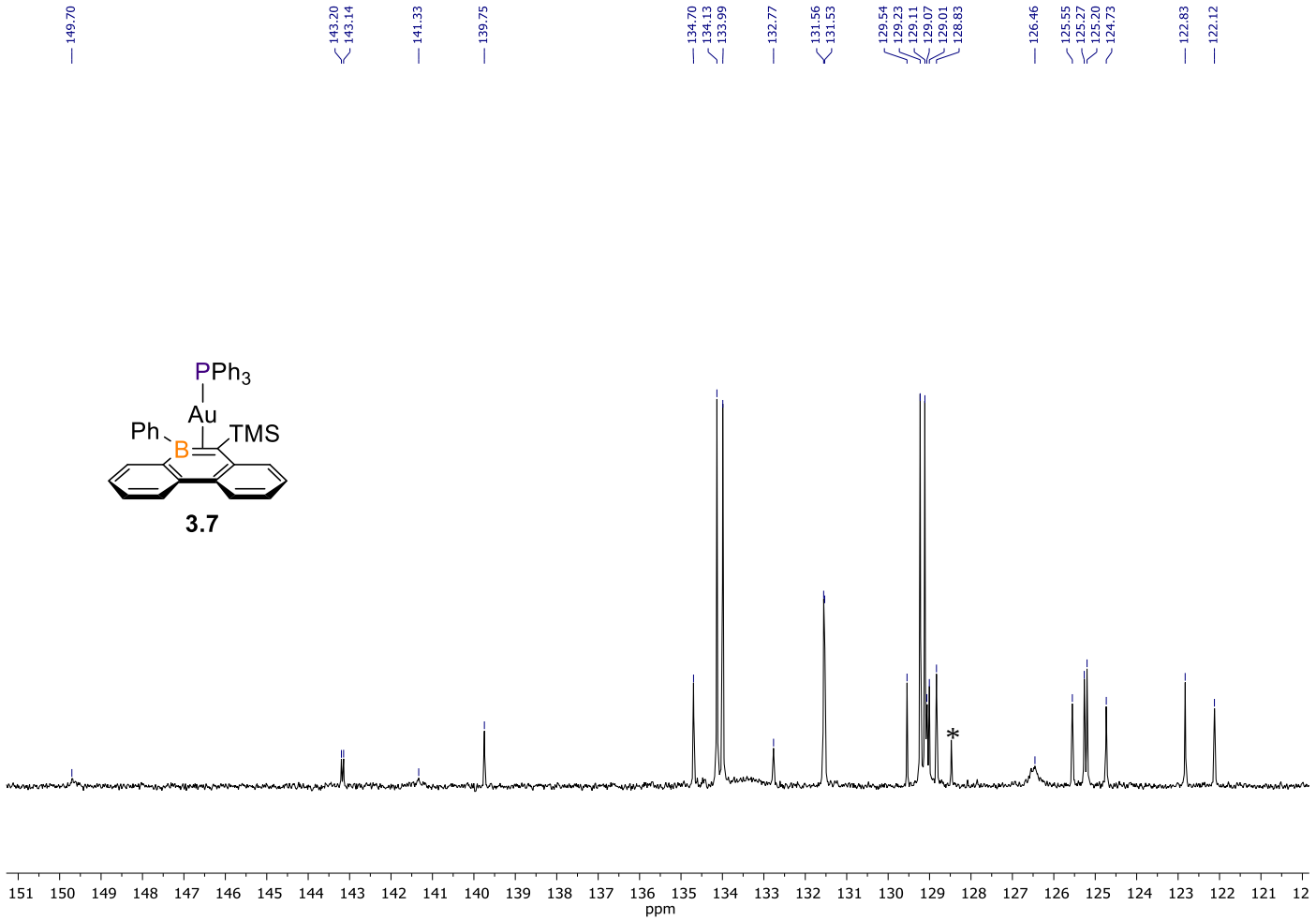

Figure B-47: Expansion of $^{13}C\{^{1}H\}$ NMR spectrum of **3.7** in $CDCl_3$ (aryl region, * indicates benzene).

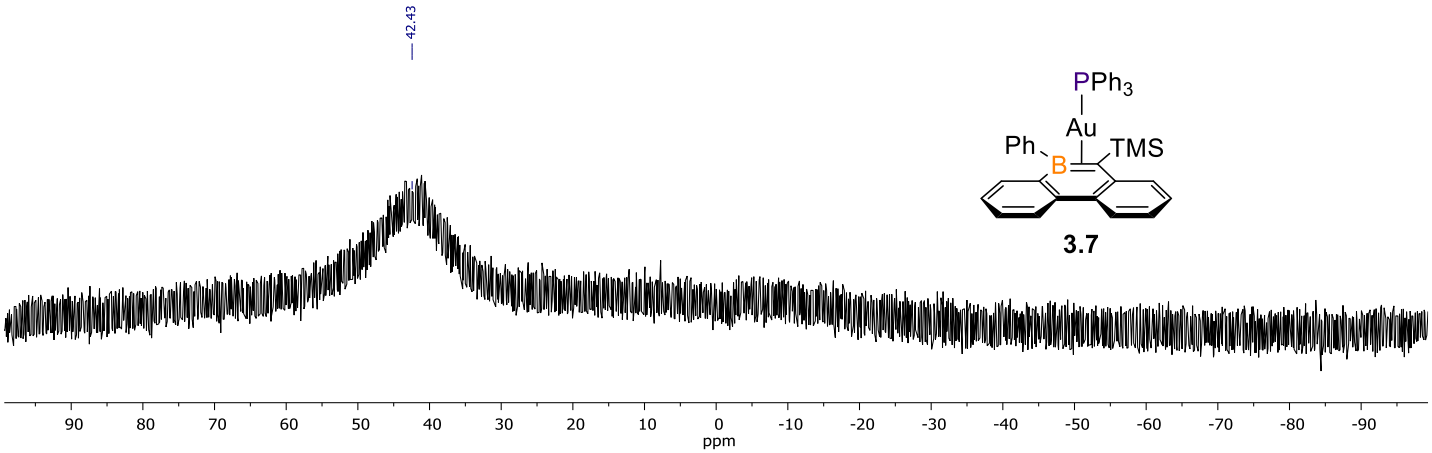

Figure B-48: ^{11}B NMR spectrum of **3.7** in $CDCl_3$.

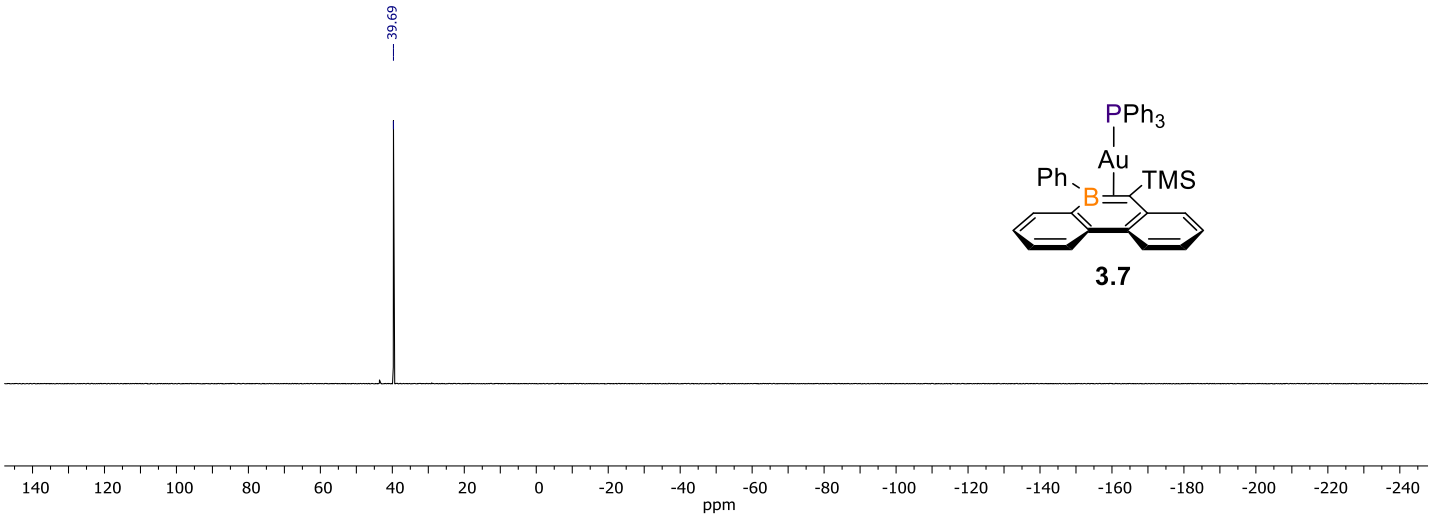

Figure B-49: $^{31}P\{^{1}H\}$ NMR spectrum of **3.7** in $CDCl_3$.

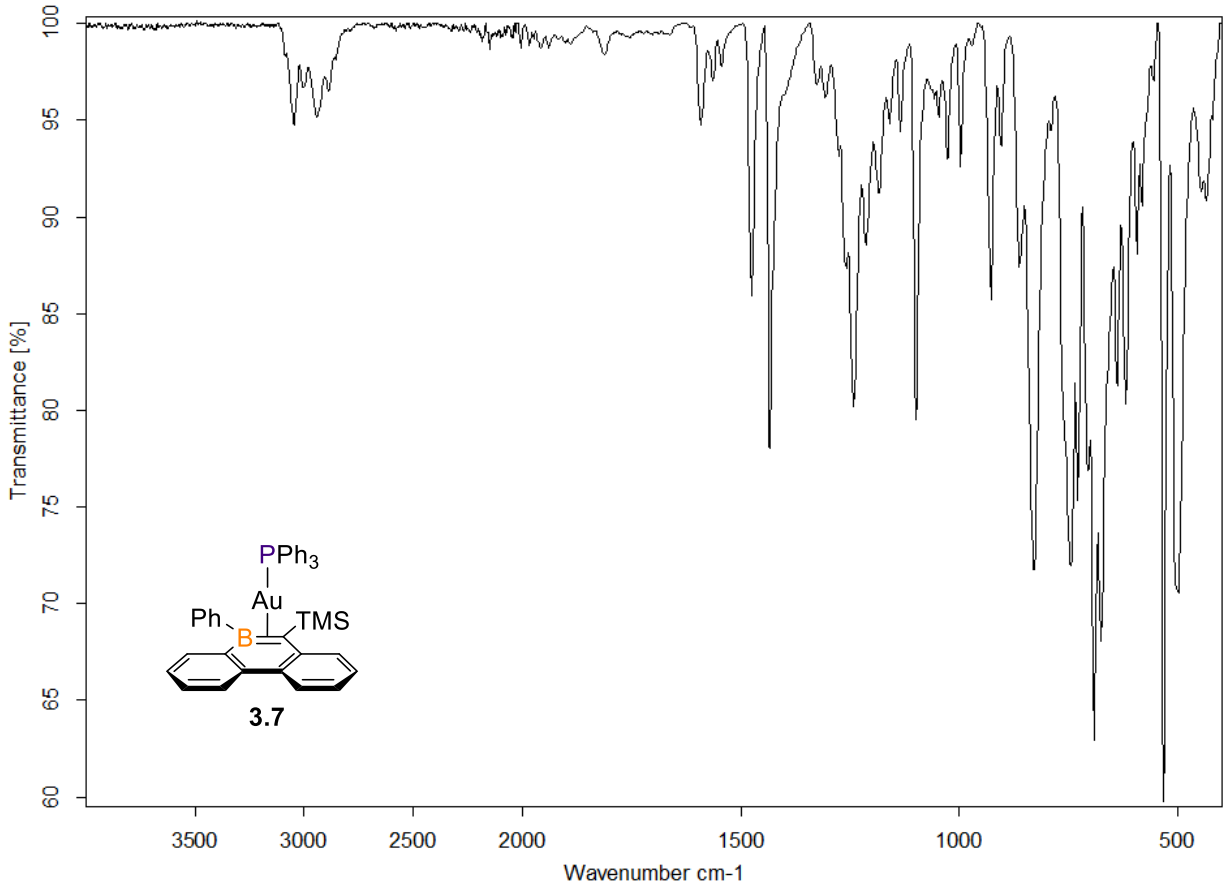

Figure B-50: FT-IR spectrum of **3.7**.

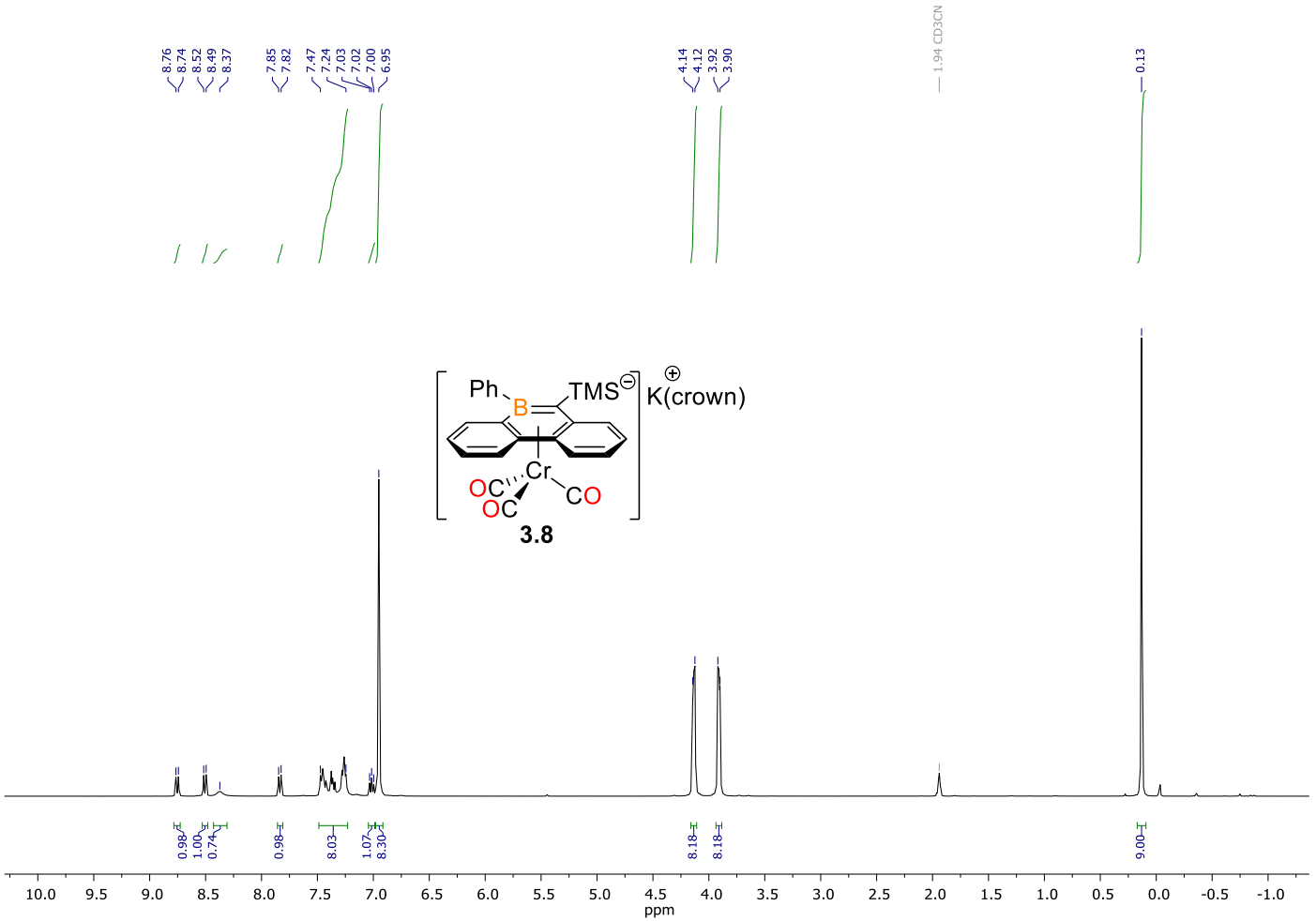

Figure B-51: ^{1}H NMR spectrum of **3.8** in CD_3CN.

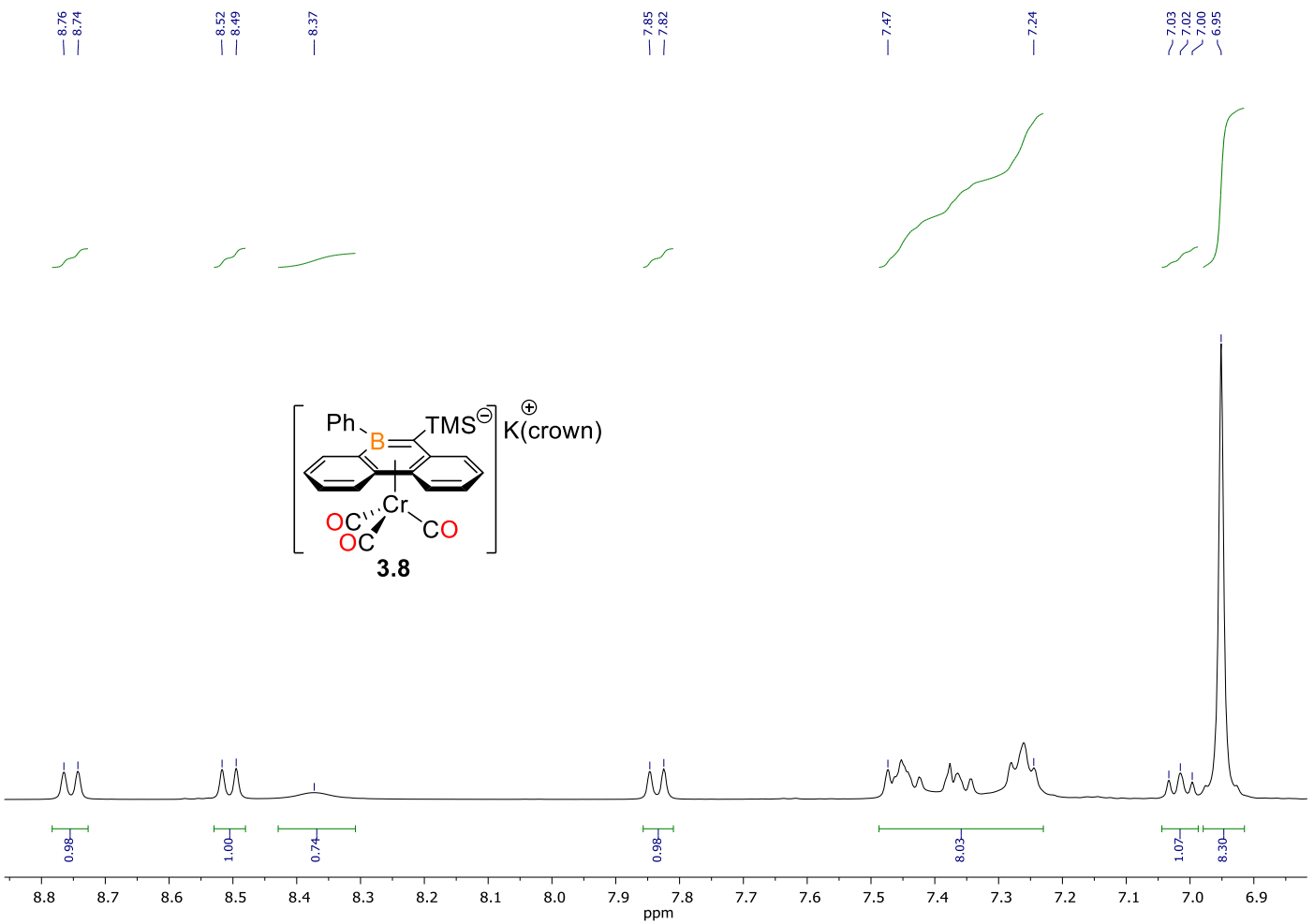

Figure B-52: Expansion of ^{1}H NMR spectrum of **3.8** in CD_3CN (aryl region).

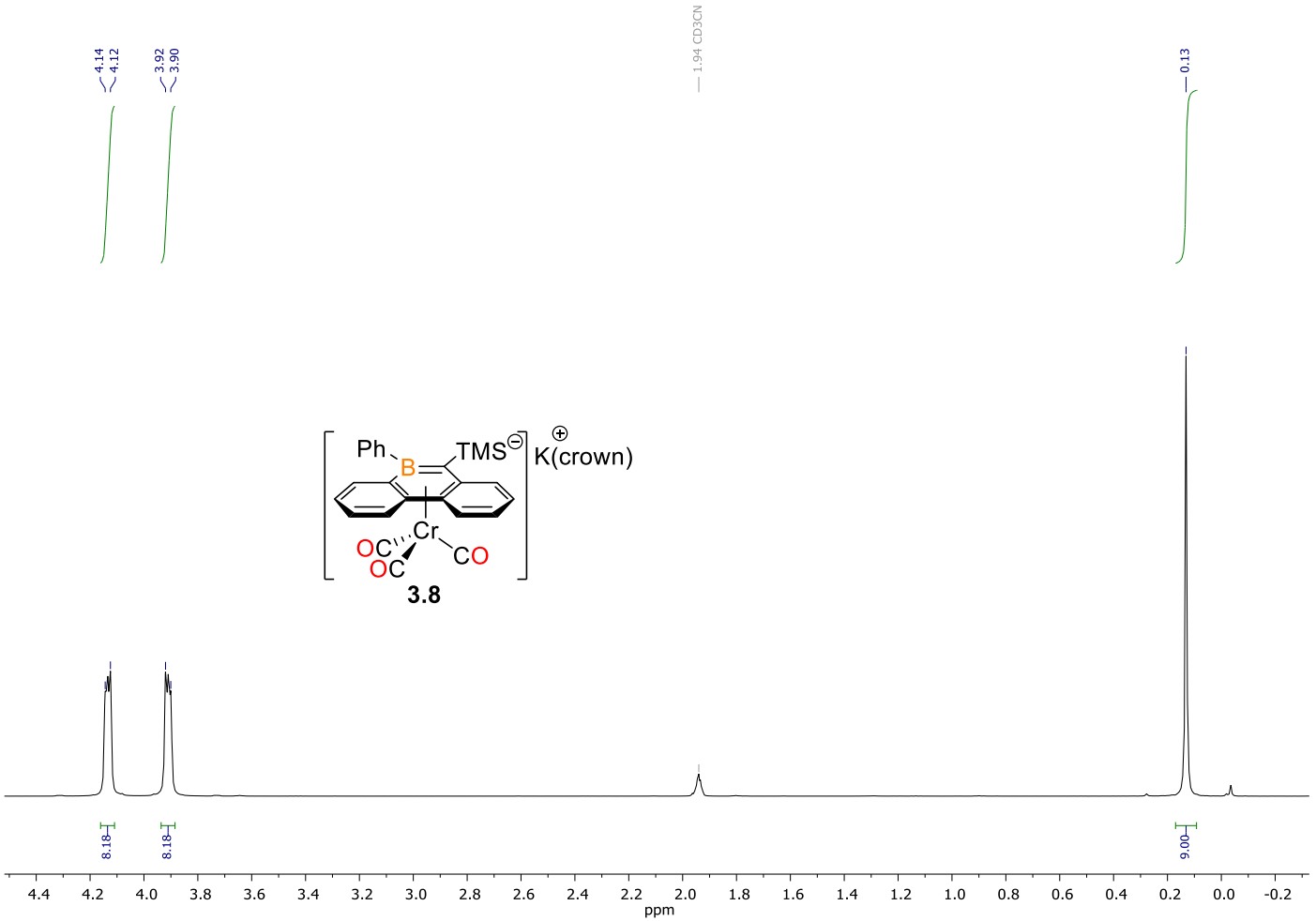

Figure B-53: Expansion of ^{1}H NMR spectrum of **3.8** in CD_3CN (aliphatic region).

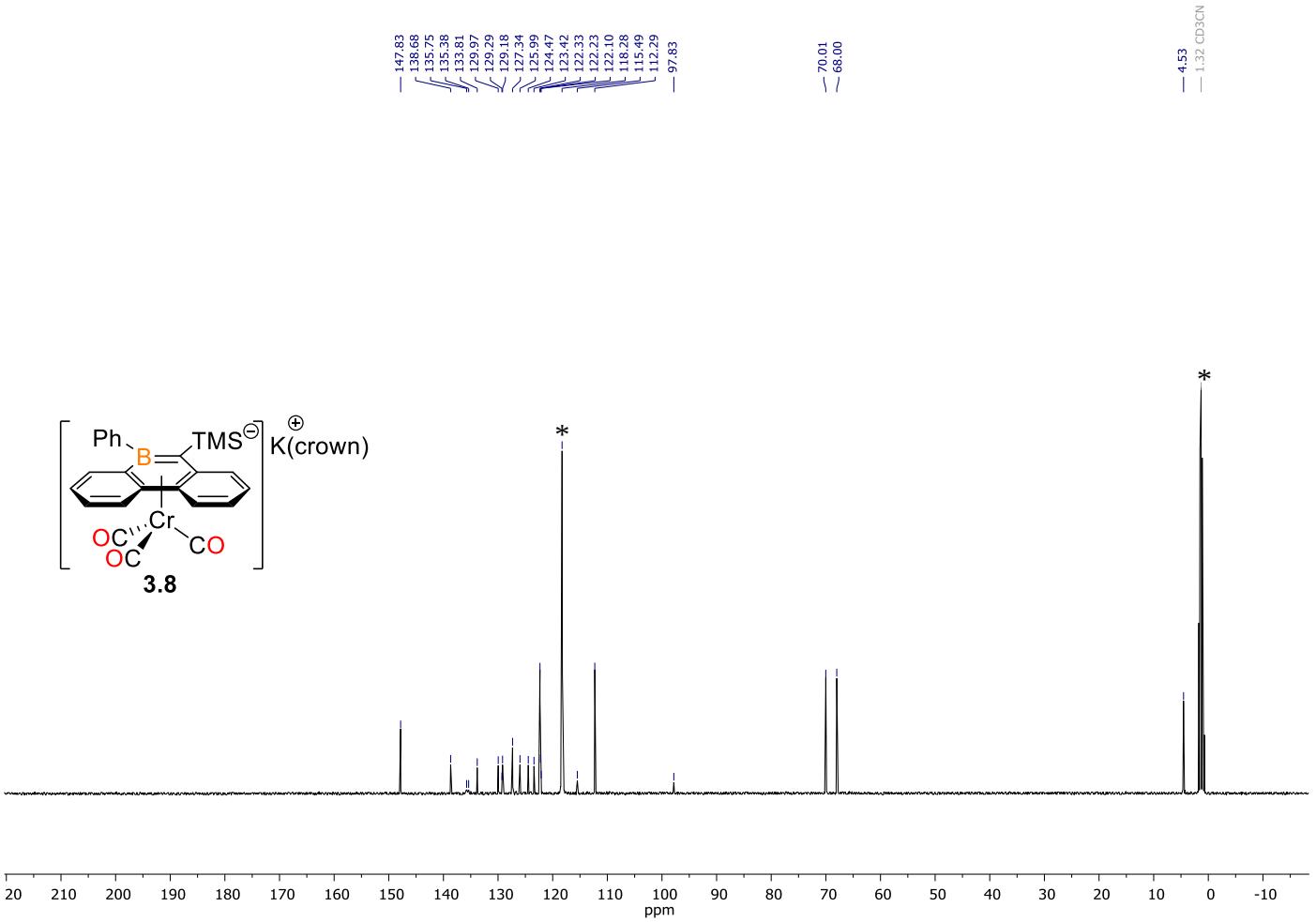

Figure B-54: $^{13}C\{^{1}H\}$ NMR spectrum of **3.8** in CD_3CN (* indicates CD_3CN).

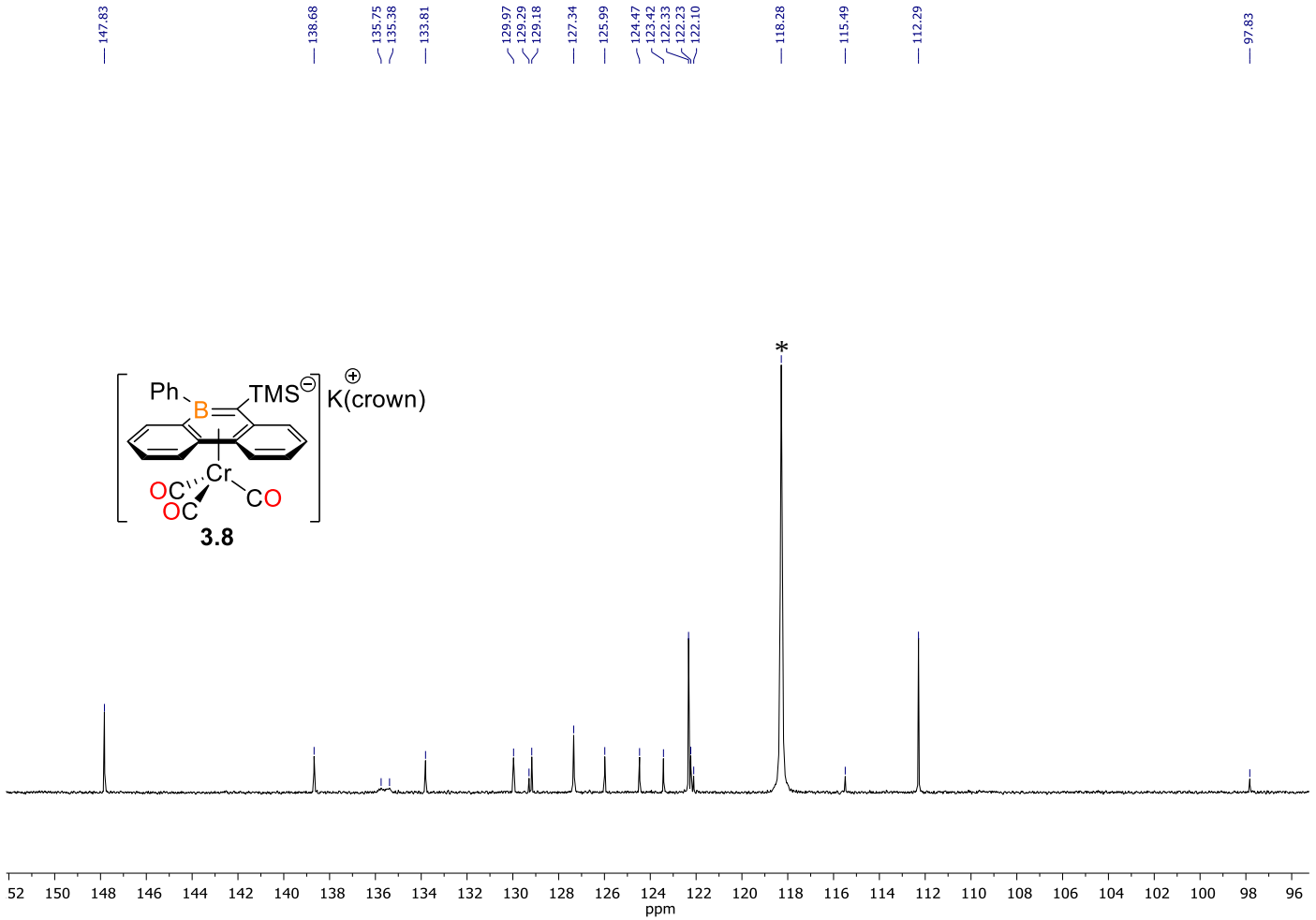

Figure B-55: Expansion of $^{13}C\{^{1}H\}$ NMR spectrum of **3.8** in CD_3CN (aryl region, * indicates CD_3CN).

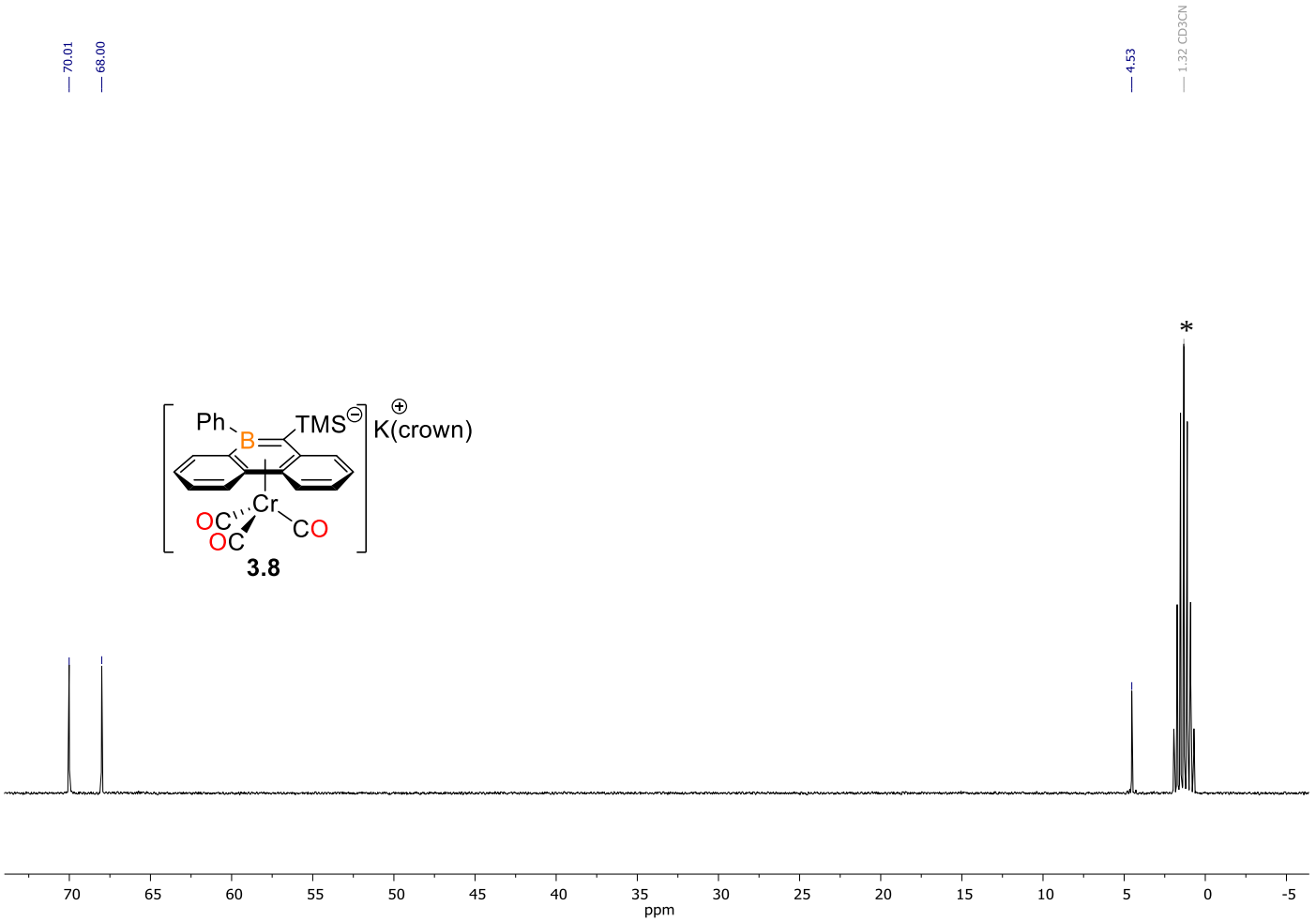

Figure B-56: Expansion of $^{13}C\{^{1}H\}$ NMR spectrum of **3.8** in CD_3CN (aliphatic region, * indicates CD_3CN).

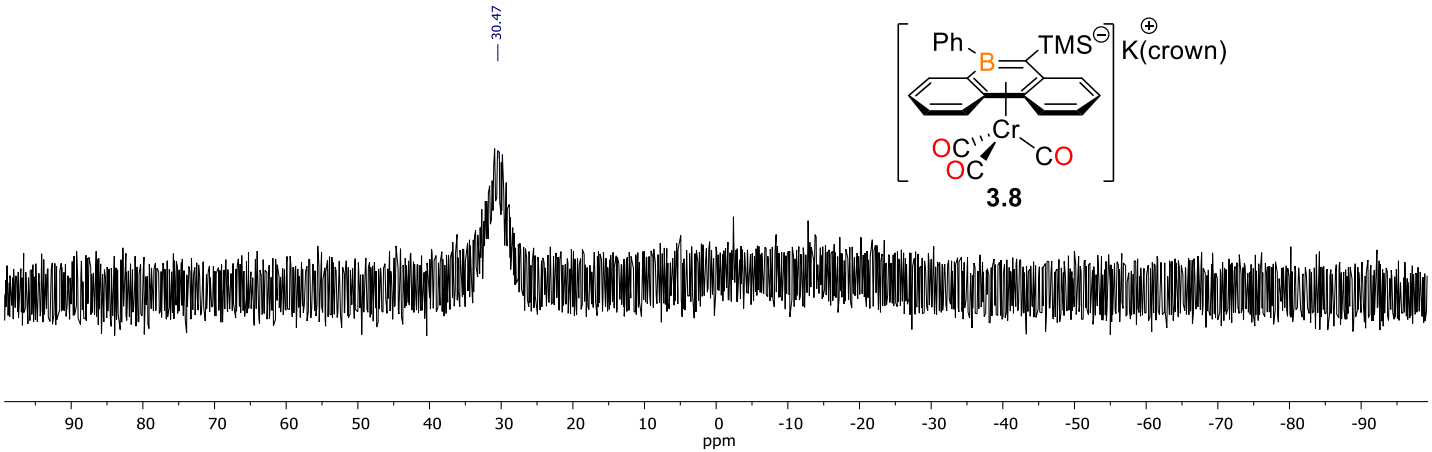

Figure B-57: ^{11}B NMR spectrum of **3.8** in CD_3CN.

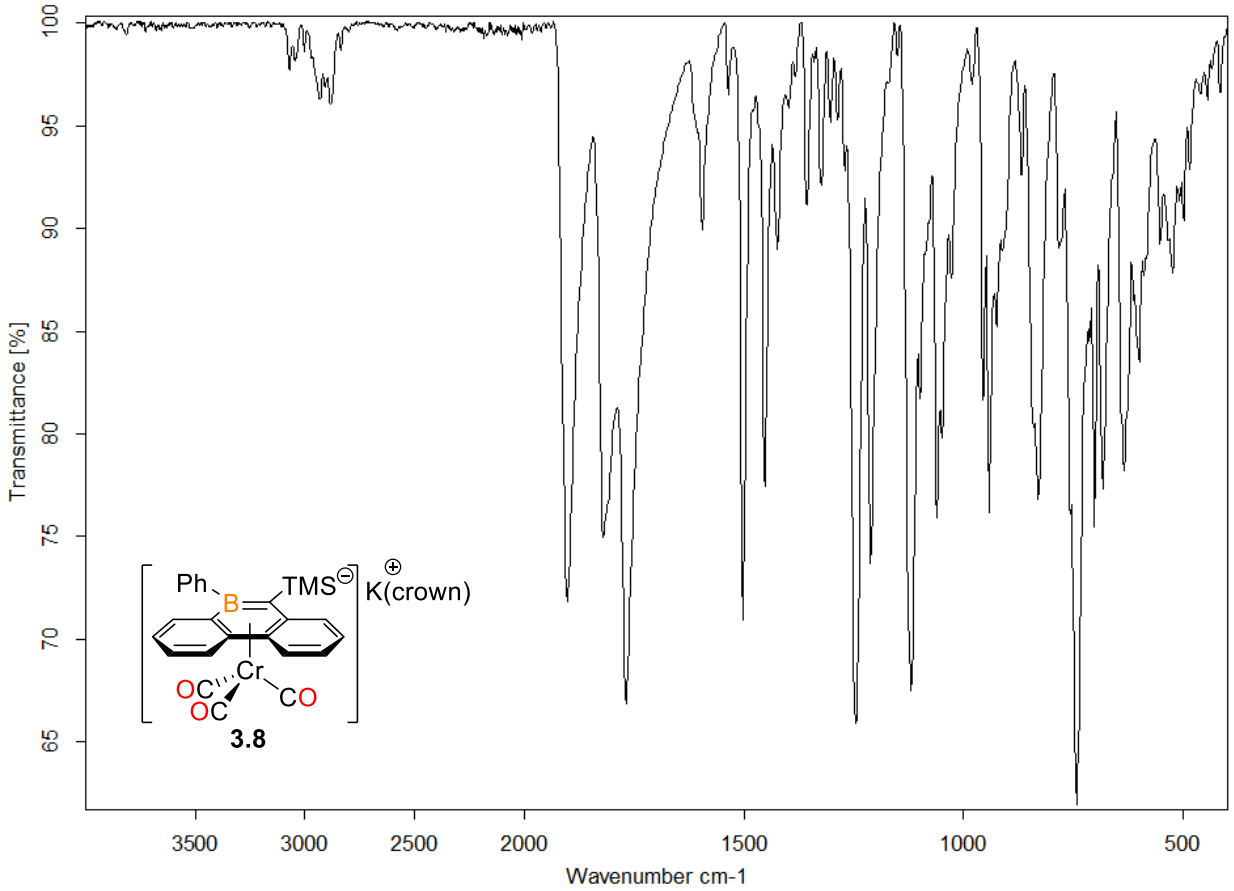

Figure B-58: FT-IR spectrum of **3.8**.

Table B-1: X-ray crystallographic details for **3.4•dioxane**, **3.4•THF**, **3.4•DME**, **3.5**, **3.6a**, **3.6b**, **3.7**, and **3.8**.

Compound	**3.4•dioxane**	**3.4•THF**	**3.4•DME**	**3.5**	**3.6a**	**3.6b**	**3.7**	**3.8**
CCDC	1981968	1981969	1981970	1981971	1981972	1981973	1981974	1981975
Empirical Formula	$C_{30}H_{38}BKO_4Si$	$C_{26}H_{30}BKOSi$	$C_{26}H_{32}BKO_2Si$	$C_{23}H_{25}BSi$	$C_{82}H_{104}B_4K_2O_6Si_2$	$C_{40}H_{59}B_2KO_5Si$	$C_{40}H_{37}AuBPSi$	$C_{46}H_{48}BCl_2CrKO_9Si$
FW (g/mol)	540.60	436.50	454.51	340.33	1363.27	708.68	784.53	945.74
Crystal System	Monoclinic	Orthorhombic	Monoclinic	Monoclinic	Monoclinic	Orthorhombic	Monoclinic	Monoclinic
Space Group	P 2_1/n	C 2 2 2_1	P 2_1/n	P 2_1/n	P 2_1/n	P n a 2_1	P 2_1/c	C c
a (Å)	10.9795(4)	11.8056(16)	11.2626(3)	10.9911(5)	14.6615(8)	18.6318(6)	17.6348(13)	14.3218(5)
b (Å)	10.4357(3)	17.5139(16)	13.5565(3)	12.8668(6)	12.7425(7)	22.1291(7)	11.9586(9)	32.2867(9)
c (Å)	25.2480(8)	23.592(3)	17.0667(4)	13.6970(6)	20.5645(11)	9.7488(3)	18.0192(13)	9.8202(13)
α (deg)	90	90	90	90	90	90	90	90
β (deg)	90.4046(12)	90	104.2659(8)	93.828(2)	91.322(22)	90	115.127(2)	103.1699(3)
γ (deg)	90	90	90	90	90	90	90	90
V (Å^3)	2892.81(16)	4877.9(10)	2525.41(11)	1932.71(15)	3840.9(4)	4019.5(2)	3440.4(4)	4421.5(2)
Z	4	8	4	4	2	4	4	4
D_c (g cm^{-3})	1.241	1.189	1.195	1.170	1.179	1.171	1.515	1.421
Radiation λ (Å)	0.71073	0.71073	0.71073	0.71073	0.71073	0.71073	0.71073	0.71073
Temp (K)	150	150	150	150	150	150	150	150
R1 [I>2(σ)I]^a	0.0496	0.0680	0.0431	0.0363	0.0452	0.0472	0.0587	0.0399
wR2 (F^2)^a	0.1198	0.1924	0.1139	0.1174	0.1302	0.1446	0.1602	0.1086
GOF (S)^a	1.040	1.135	1.039	1.127	1.086	1.069	1.188	1.147

^{a} $R1(F[I > 2(I)]) = \sum||F_o| - |F_c||/\sum|F_o|$; $wR2(F^2\text{ [all data]}) = [w(F_o^2 - F_c^2)^2]^{1/2}$; $S(\text{all data}) = [w(F_o^2 - F_c^2)^2/(n - p)]^{1/2}$ (n = no. of data; p = no. of parameters varied; $w = 1/[^2(F_o^2) + (aP)^2 + bP]$ where $P = (F_o^2 + 2F_c^2)/3$ and a and b are constants suggested by the refinement program.

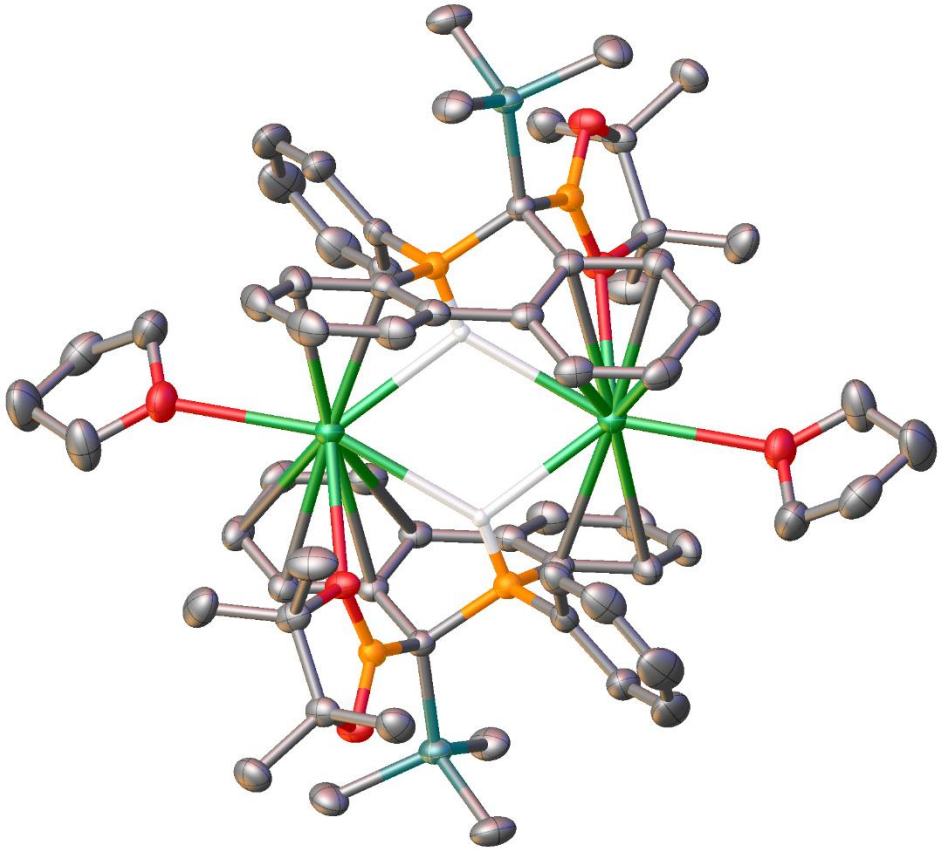

Figure B-59: Dimeric structure of **3.6a**. Hydrogen atoms (except for boron-bound hydrides) and non-coordinated solvates are omitted for clarity, and thermal ellipsoids are drawn at the 50% probability level.

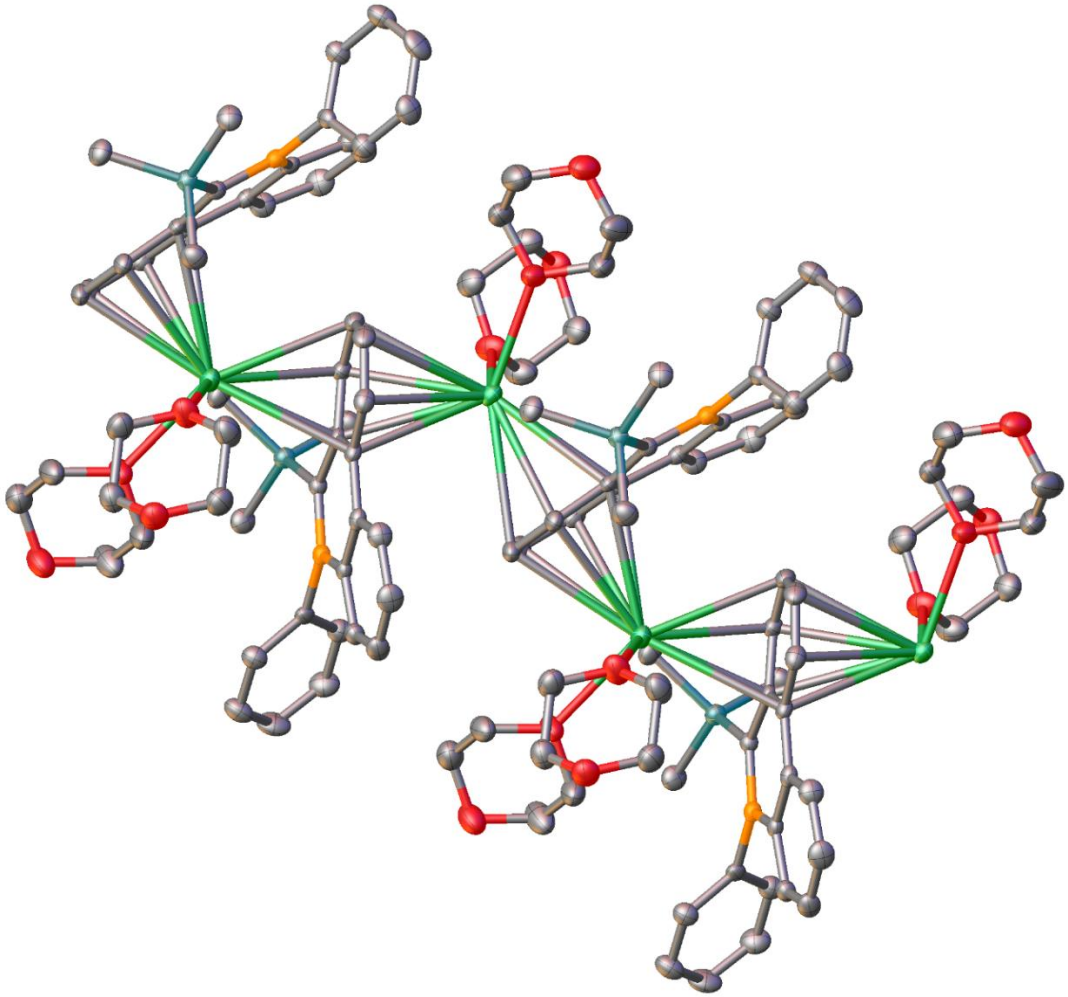

Figure B-60: Polymeric structure of **3.4•dioxane**. Hydrogen atoms are omitted for clarity, and thermal ellipsoids are drawn at the 50% probability level.

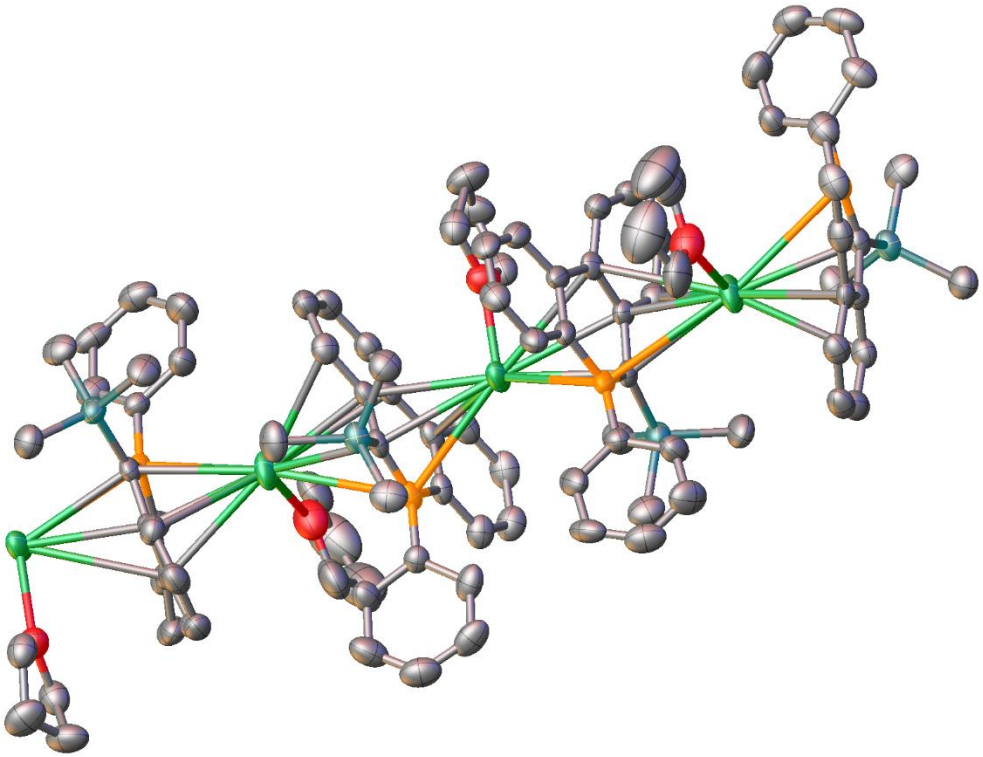

Figure B-61: Polymeric structure of **3.4•THF**. Hydrogen atoms are omitted for clarity, and thermal ellipsoids are drawn at the 50% probability level.

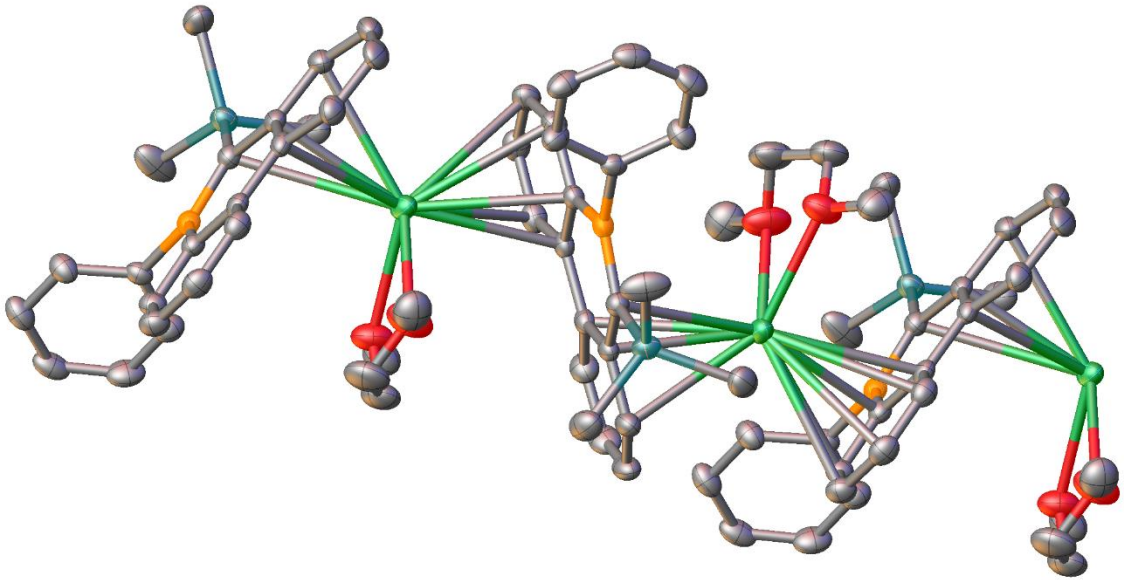

Figure B-62: Polymeric structure of **3.4•DME**. Hydrogen atoms are omitted for clarity, and thermal ellipsoids are drawn at the 50% probability level.

HOMO	**HOMO-1**	**HOMO-2**	**HOMO-3**
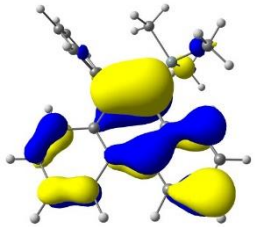	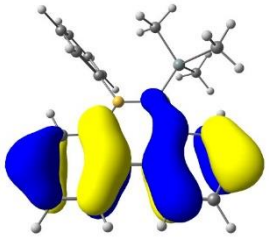	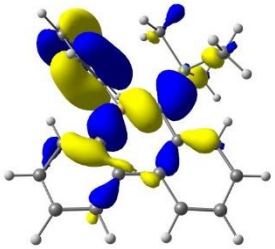	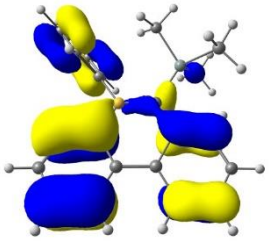
LUMO	**LUMO+1**	**LUMO+2**	**LUMO+3**
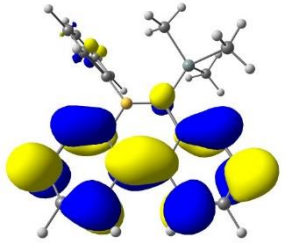	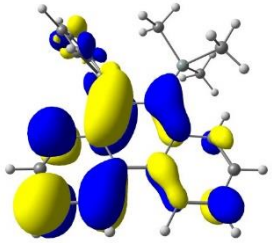	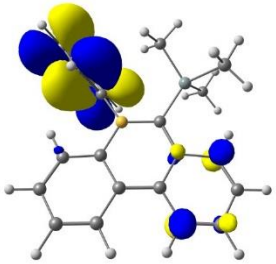	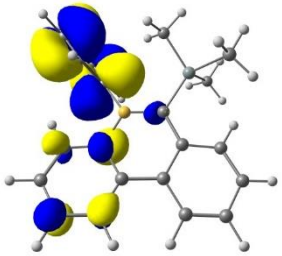

Figure B-63: Frontier molecular orbitals of **3.4**. B3LYP-D3(BJ)/def2-SVP in THF solvent.

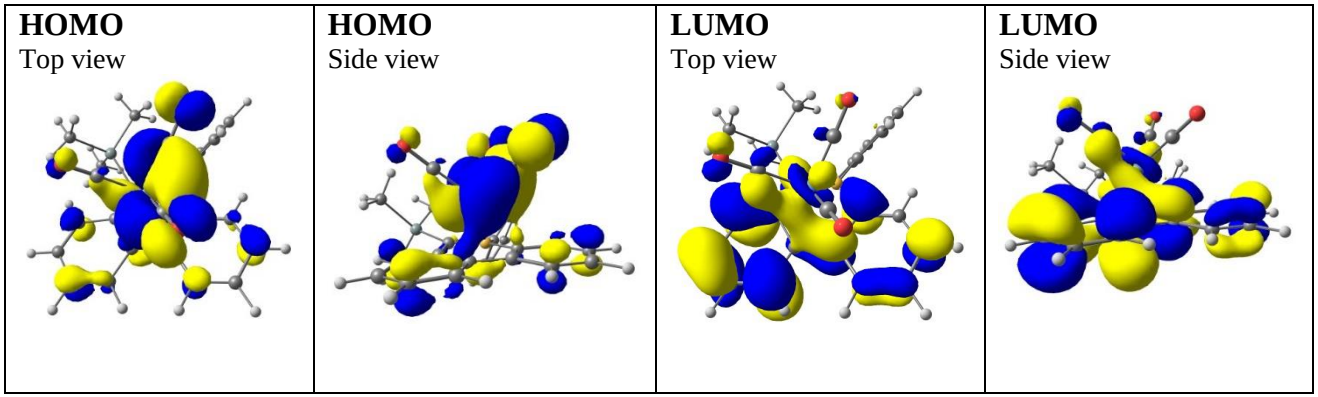

Figure B-64: Frontier molecular orbitals of **3.7**. B3LYP-D3(BJ)/def2-SVP in THF solvent.

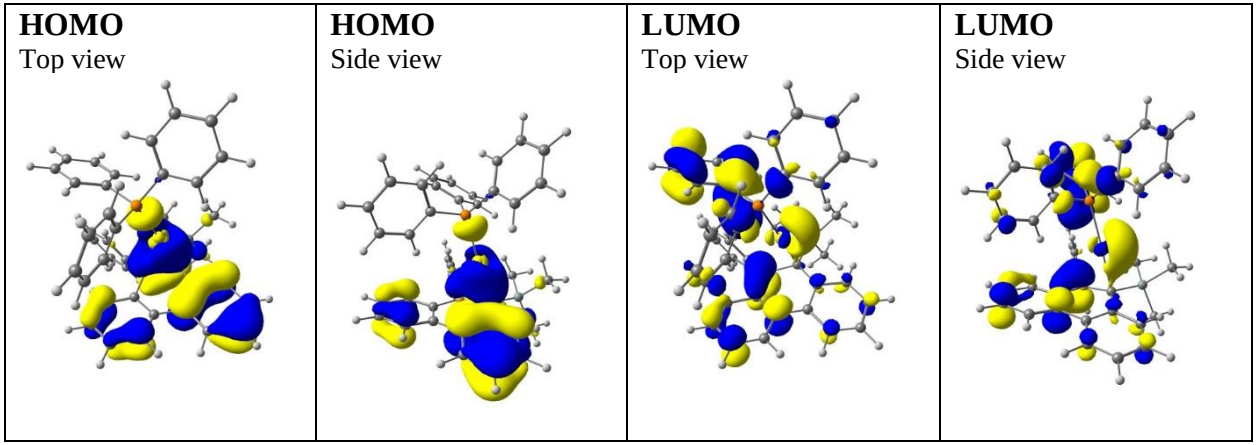

Figure B-65: Frontier molecular orbitals of **3.8**. B3LYP-D3(BJ)/def2-SVP in THF solvent.

APPENDIX C

Supplementary Information for Chapter Four

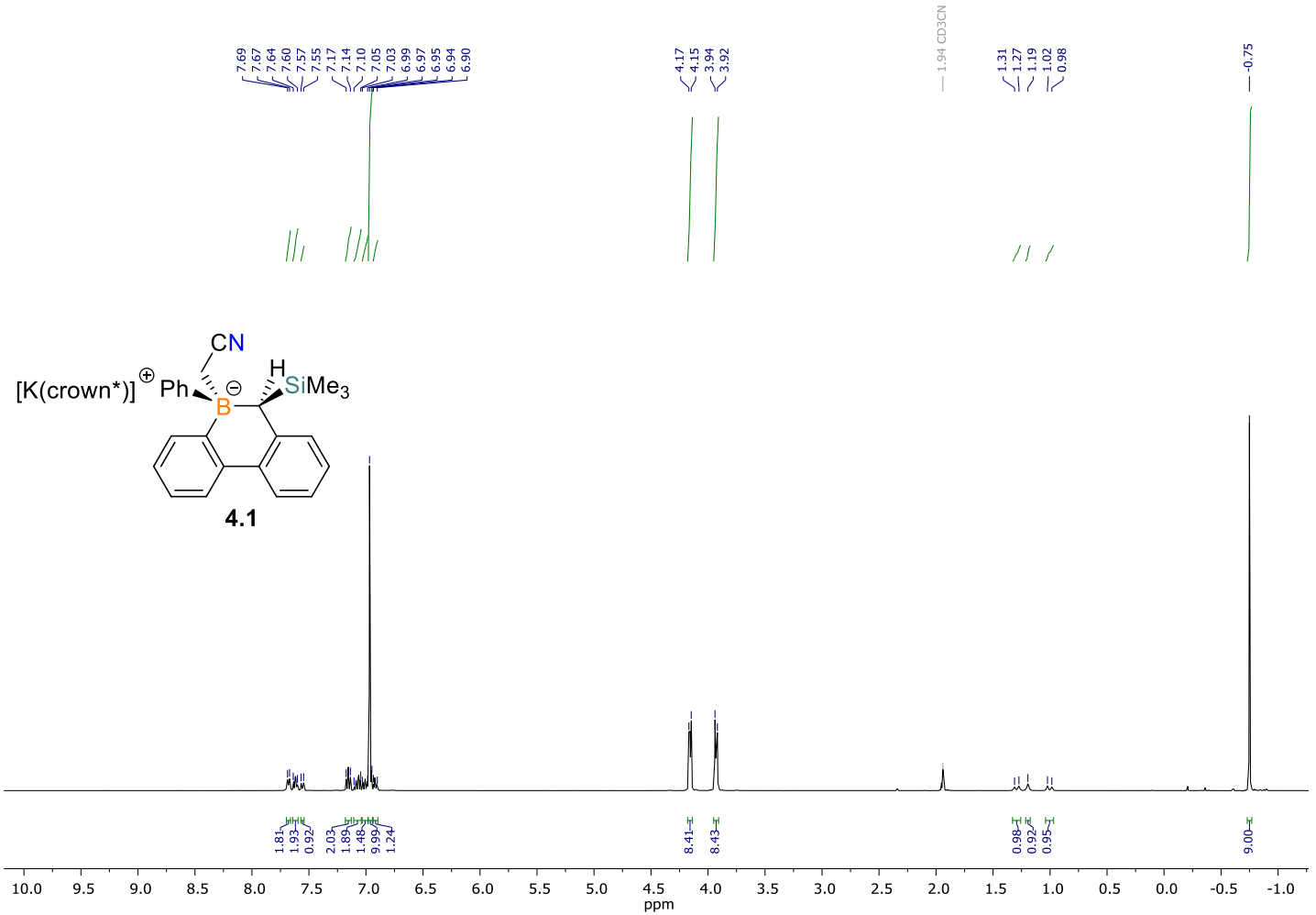

Figure C-1: ^{1}H NMR spectrum of **4.1** in CD_3CN.

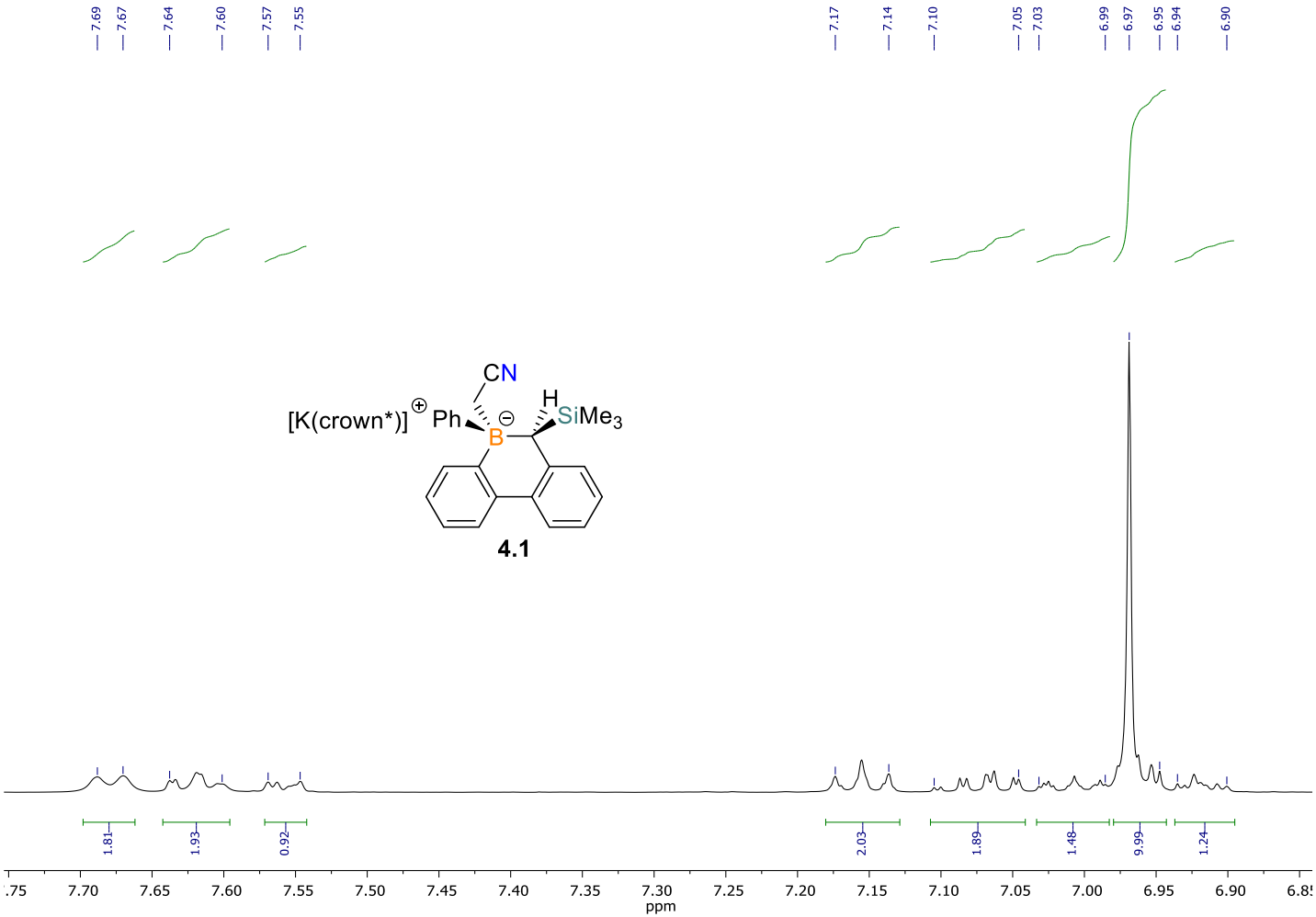

Figure C-2: Expansion of ^{1}H NMR spectrum of **4.1** in CD_3CN (aryl region).

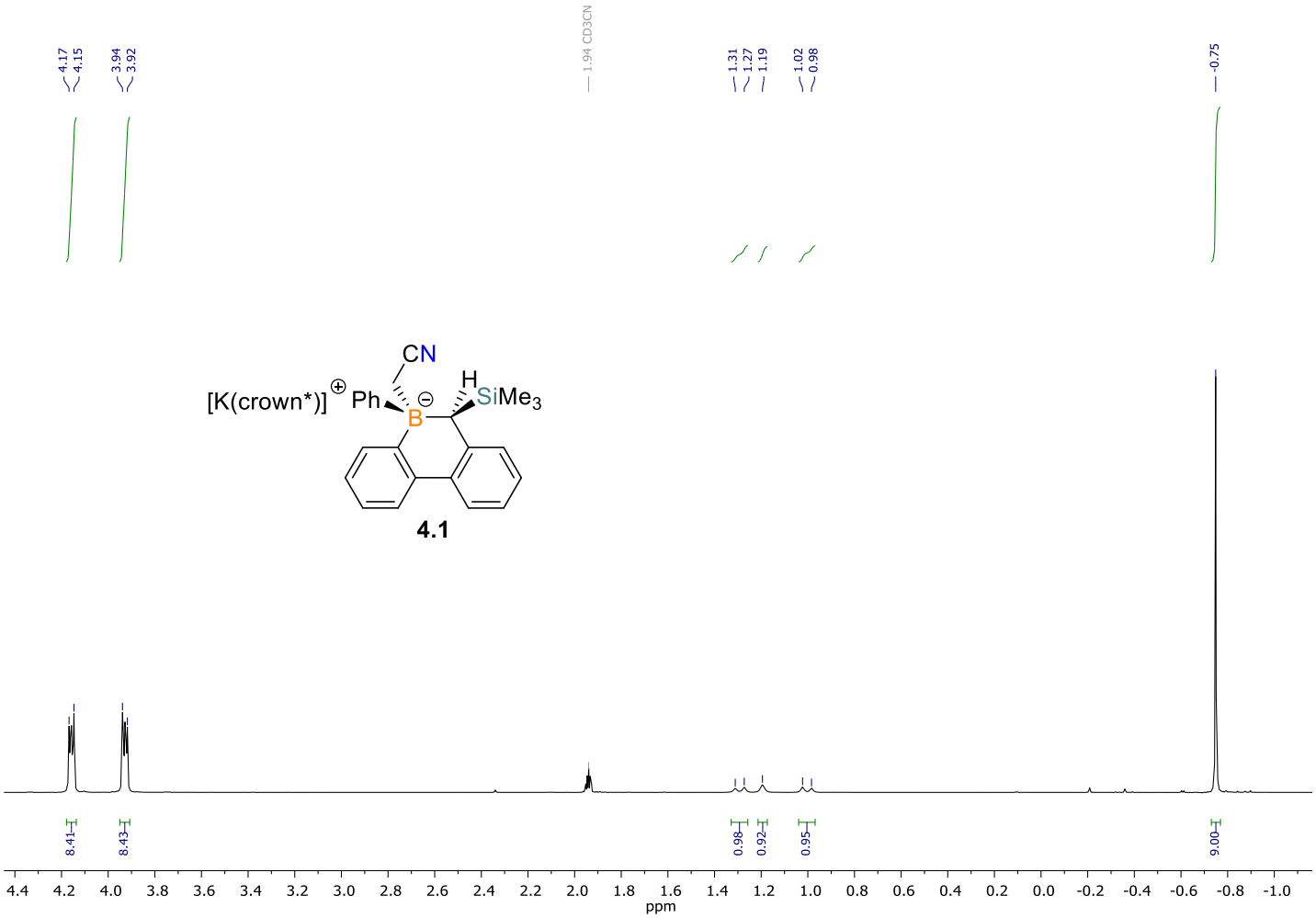

Figure C-3: Expansion of ^{1}H NMR spectrum of **4.1** in CD_3CN (aliphatic region).

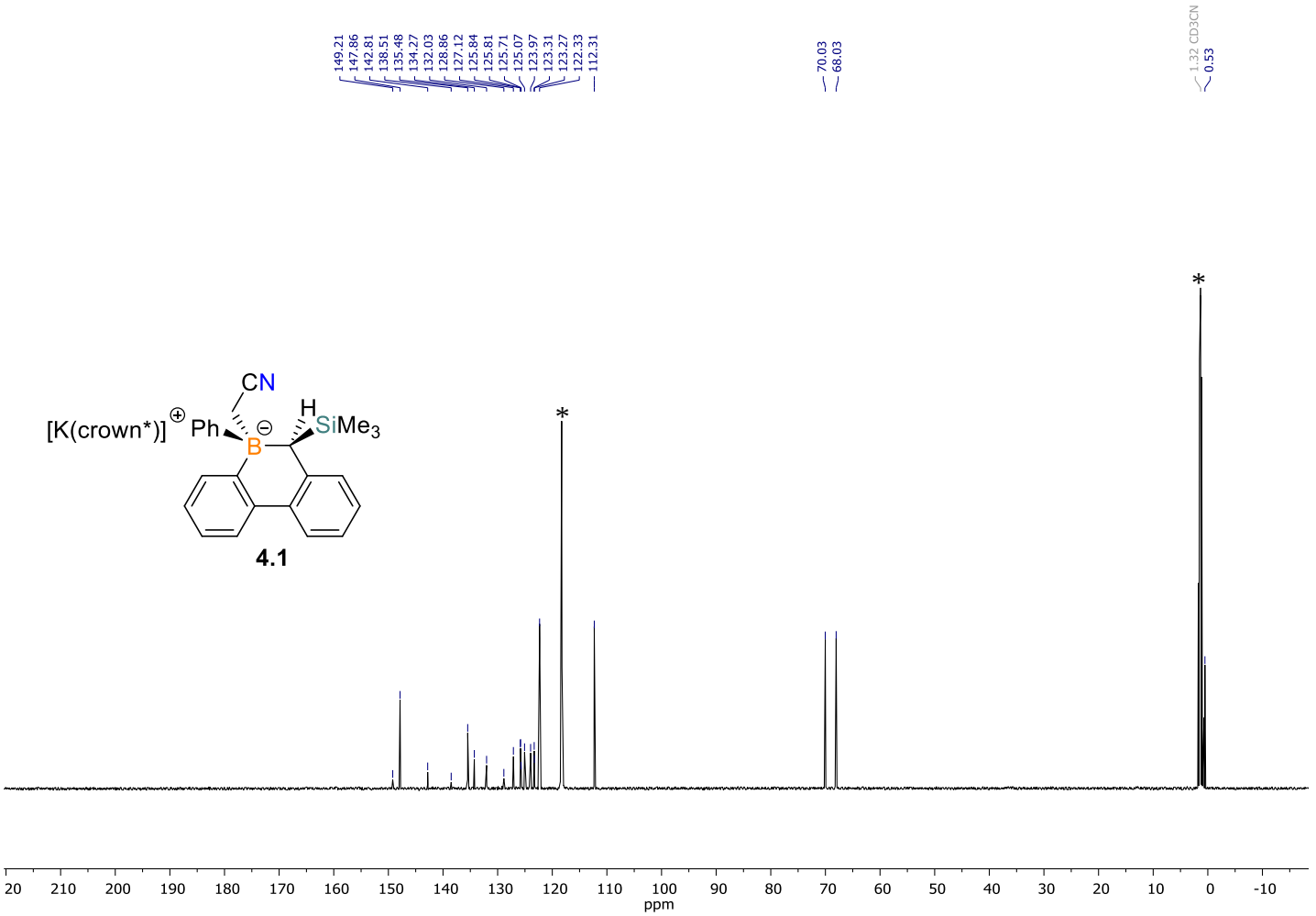

Figure C-4: $^{13}C\{^{1}H\}$ NMR spectrum of **4.1** in CD_3CN (* indicates CD_3CN).

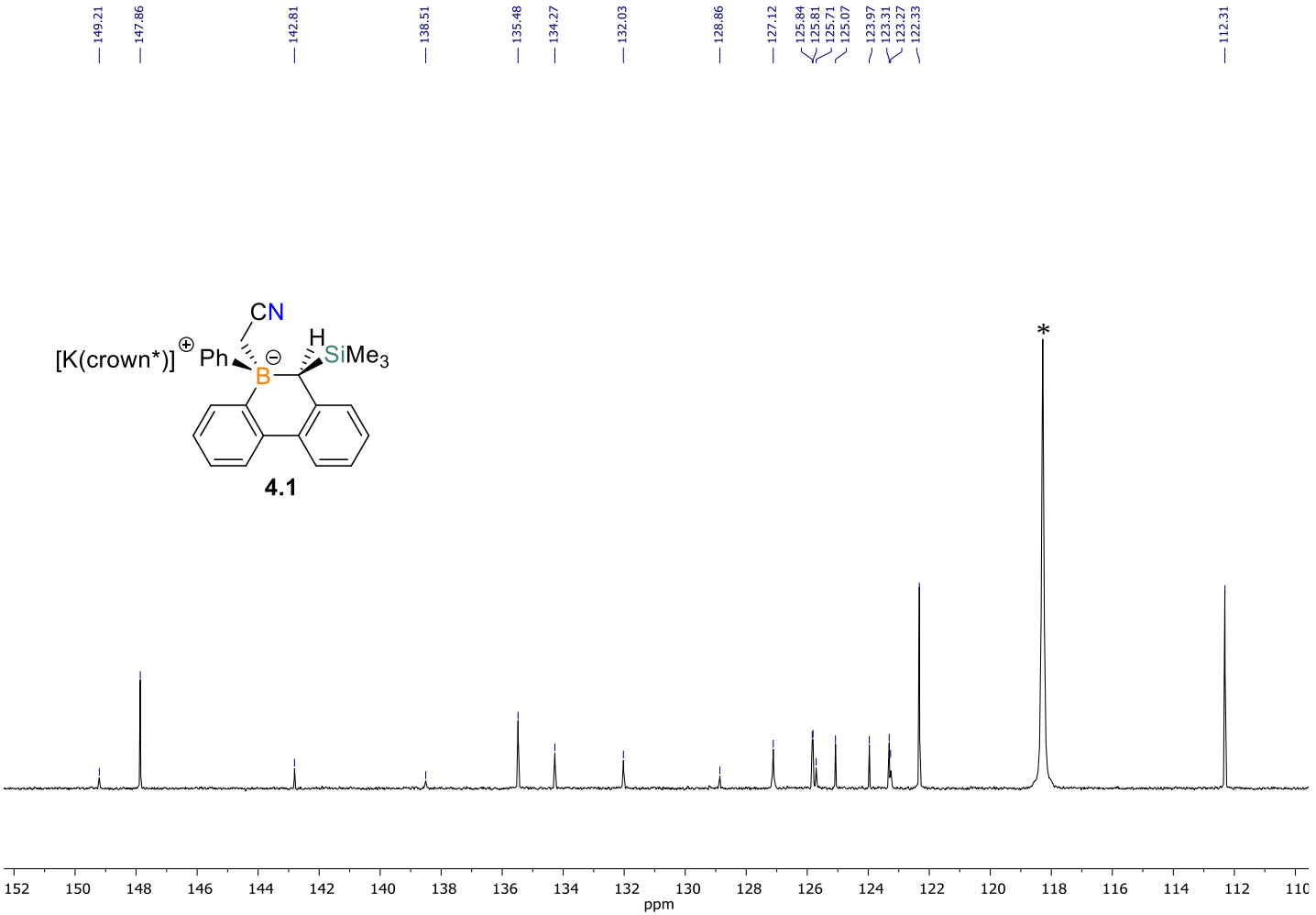

Figure C-5: Expansion of $^{13}C\{^{1}H\}$ NMR spectrum of **4.1** in CD_3CN (aryl region, * indicates CD_3CN).

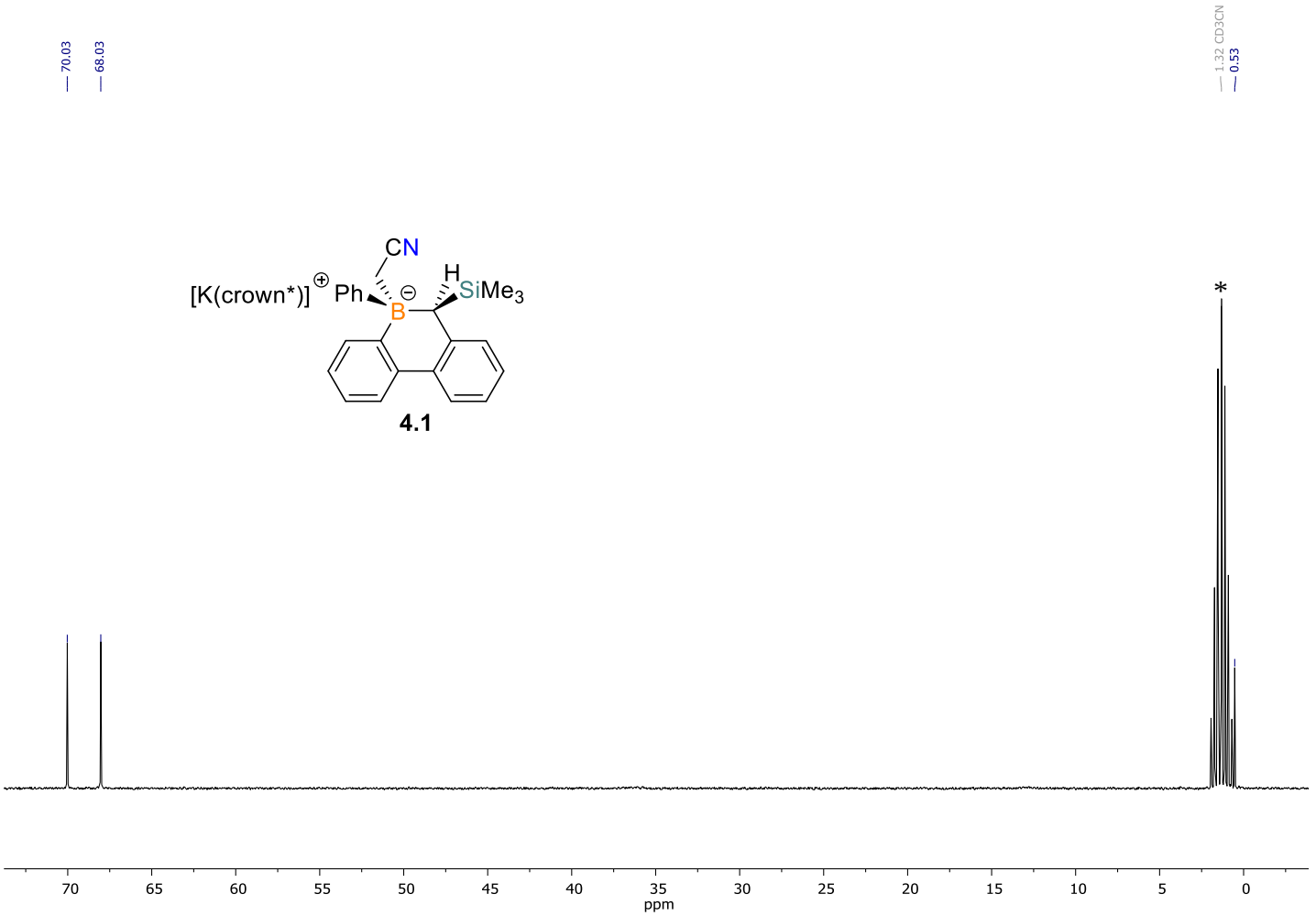

Figure C-6: Expansion of $^{13}C\{^{1}H\}$ NMR spectrum of **4.1** in CD_3CN (aliphatic region, * indicates CD_3CN).

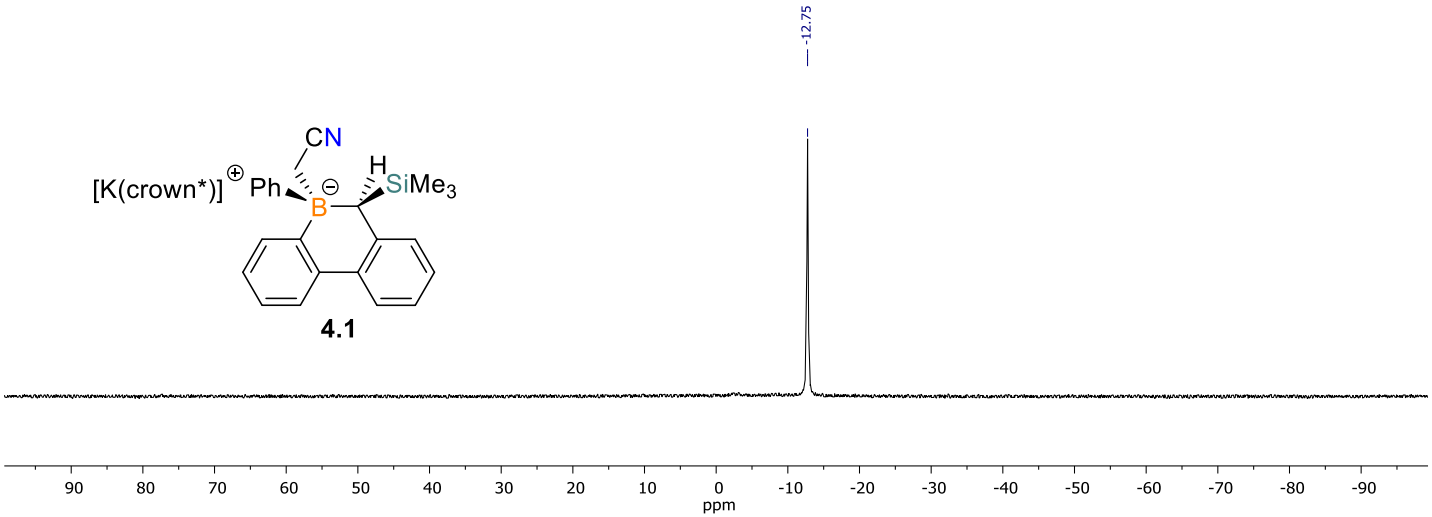

Figure C-7: ^{11}B NMR spectrum of **4.1** in CD_3CN.

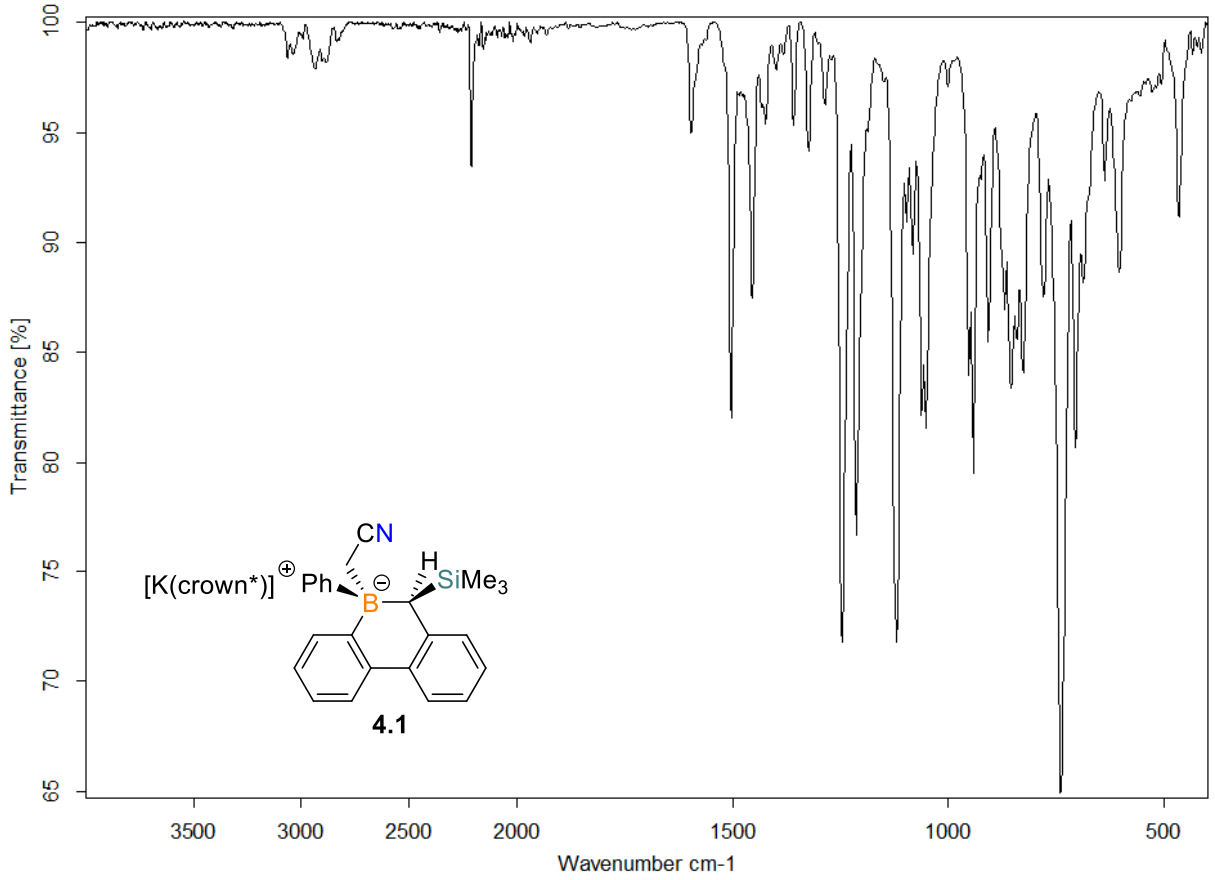

Figure C-8: FT-IR spectrum of **4.1**.

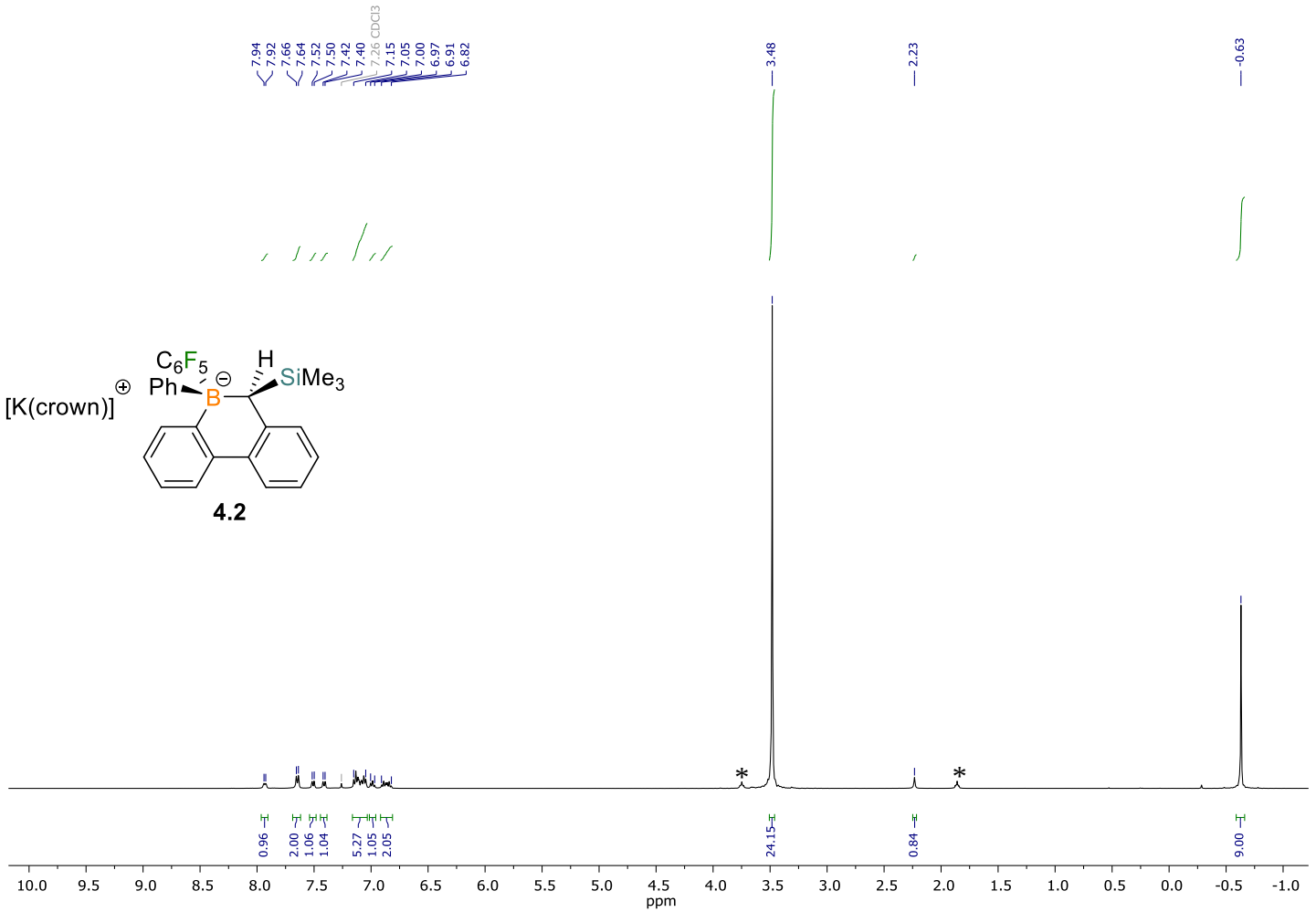

Figure C-9: ^{1}H NMR spectrum of **4.2** in $CDCl_3$ (* indicates THF).

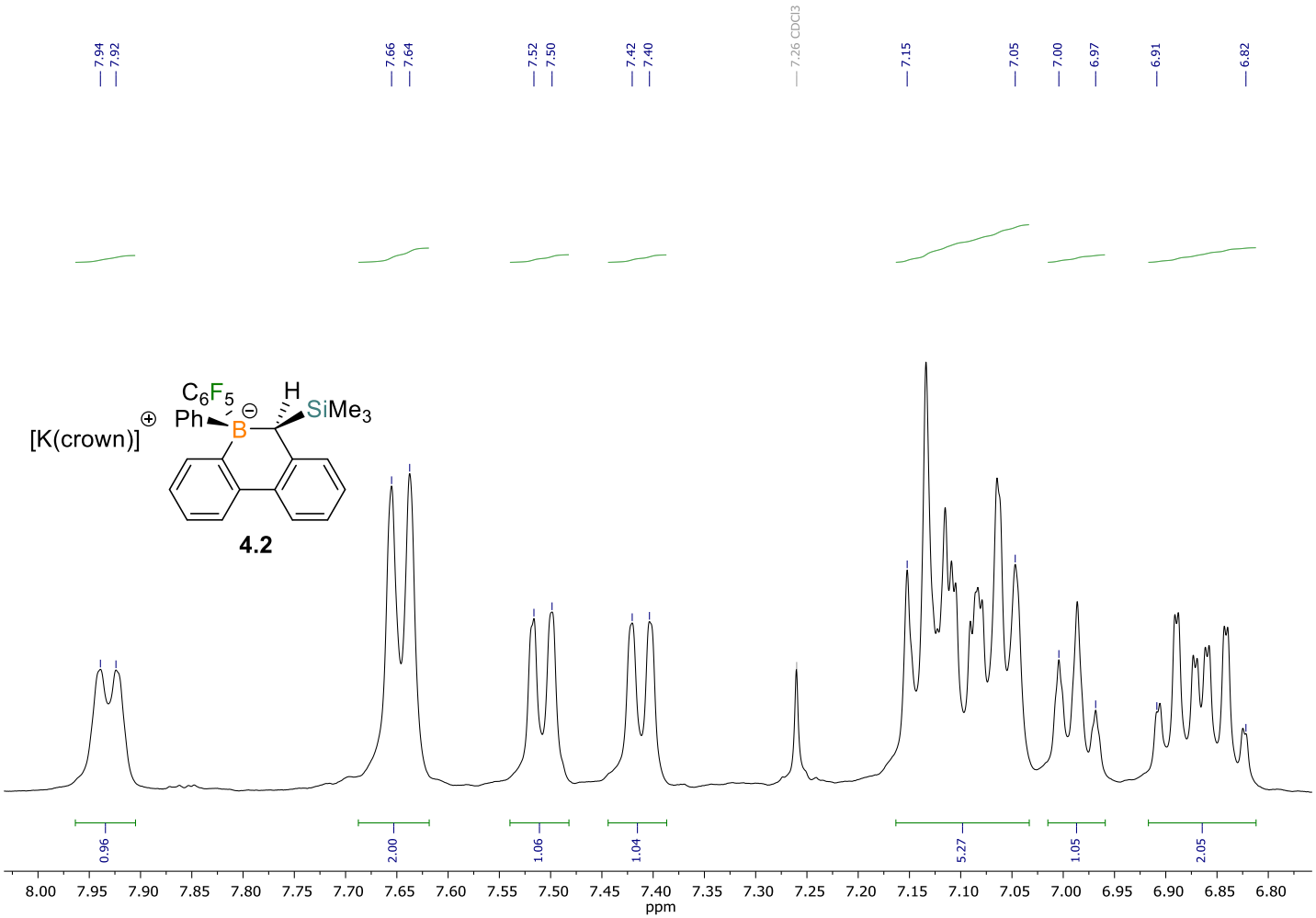

Figure C-10: Expansion of ^{1}H NMR spectrum of **4.2** in $CDCl_3$ (aryl region).

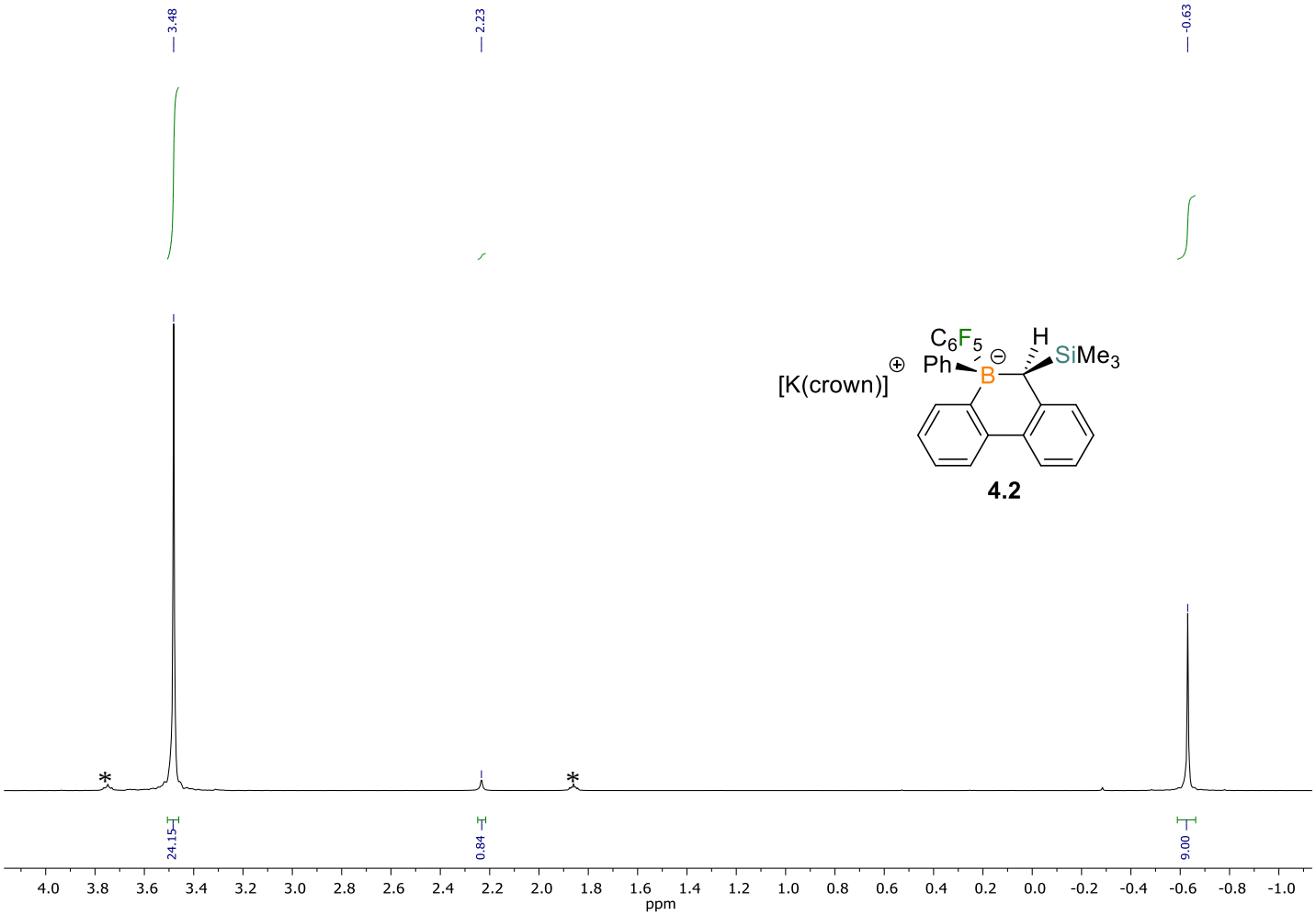

Figure C-11: Expansion of ^{1}H NMR spectrum of **4.2** in $CDCl_3$ (aliphatic region, * indicates THF).

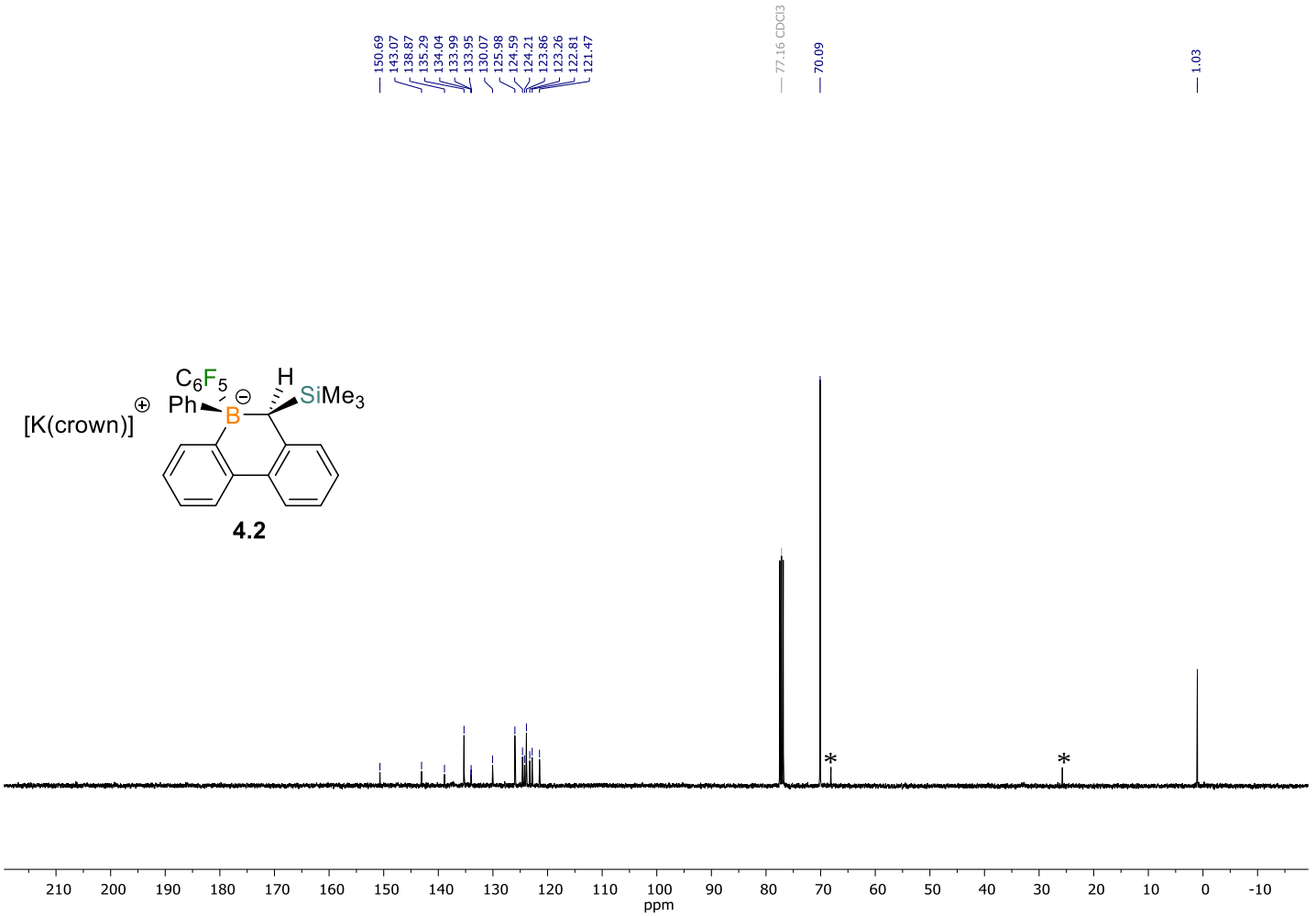

Figure C-12: $^{13}C\{^{1}H\}$ NMR spectrum of **4.2** in $CDCl_3$ (* indicates THF).

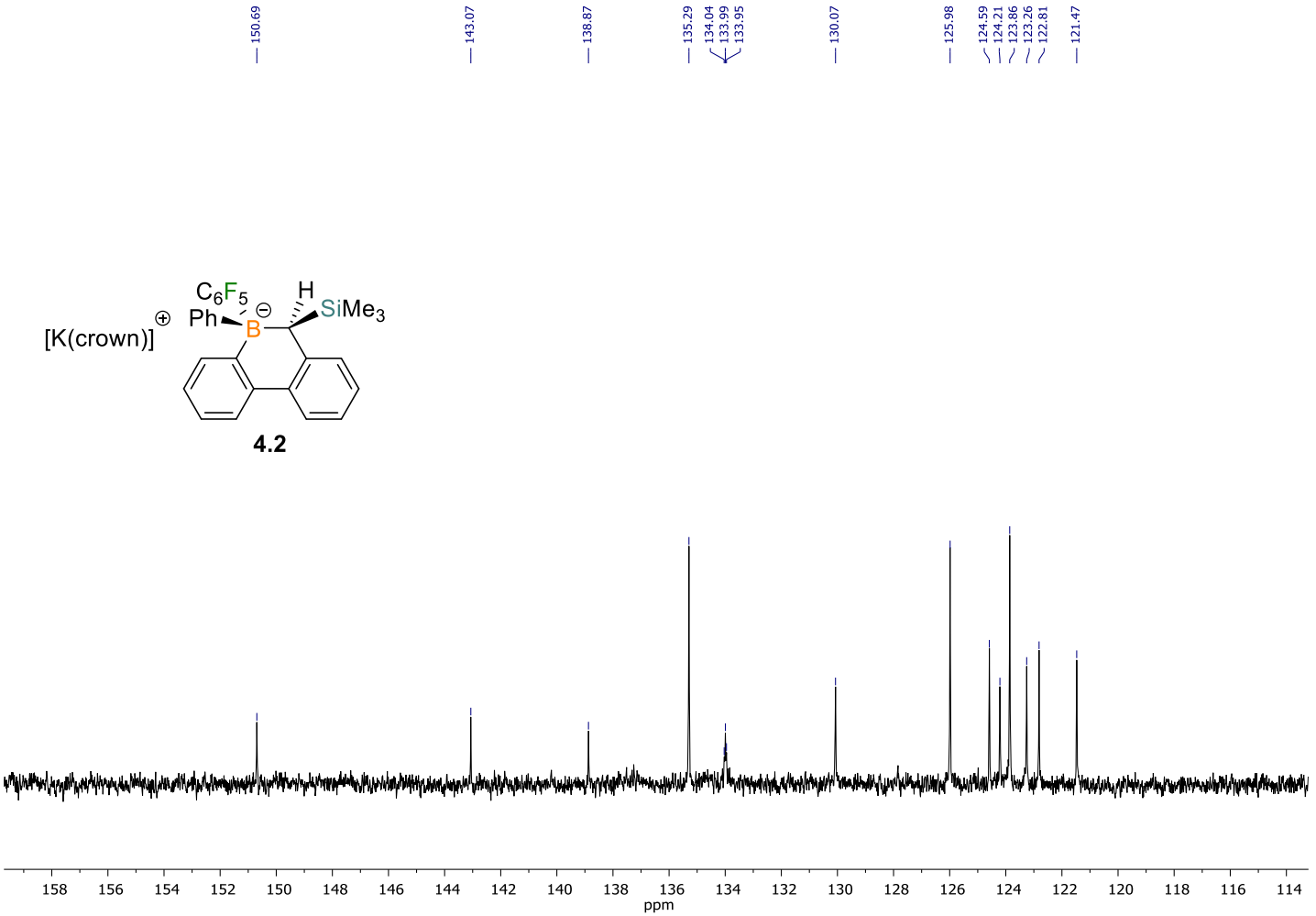

Figure C-13: Expansion of $^{13}C\{^{1}H\}$ NMR spectrum of **4.2** in $CDCl_3$ (aryl region).

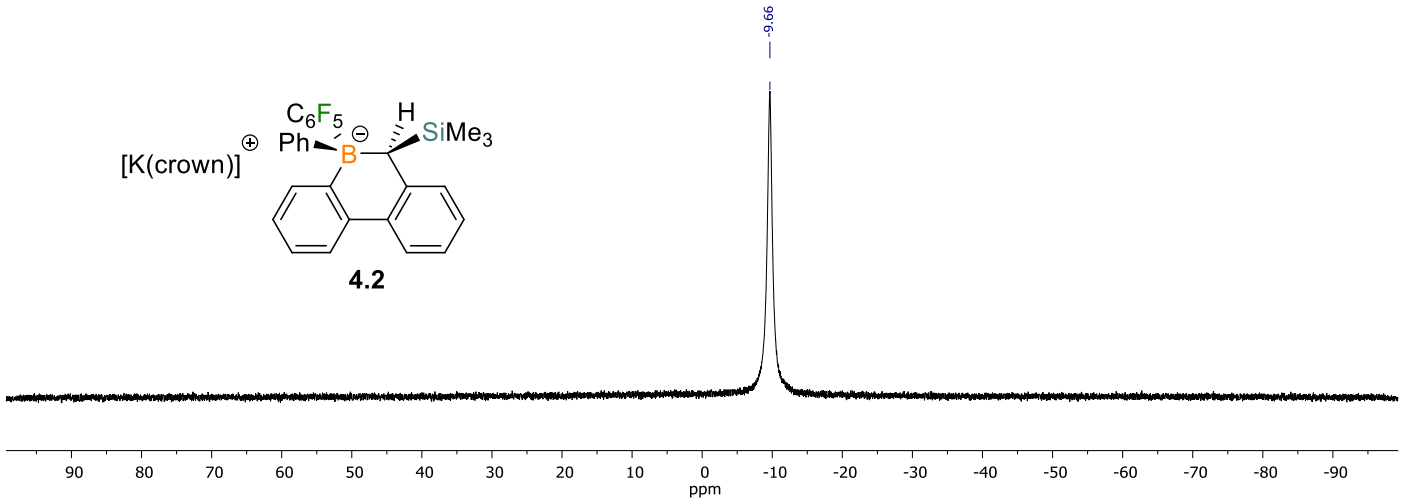

Figure C-14: ^{11}B NMR spectrum of **4.2** in $CDCl_3$.

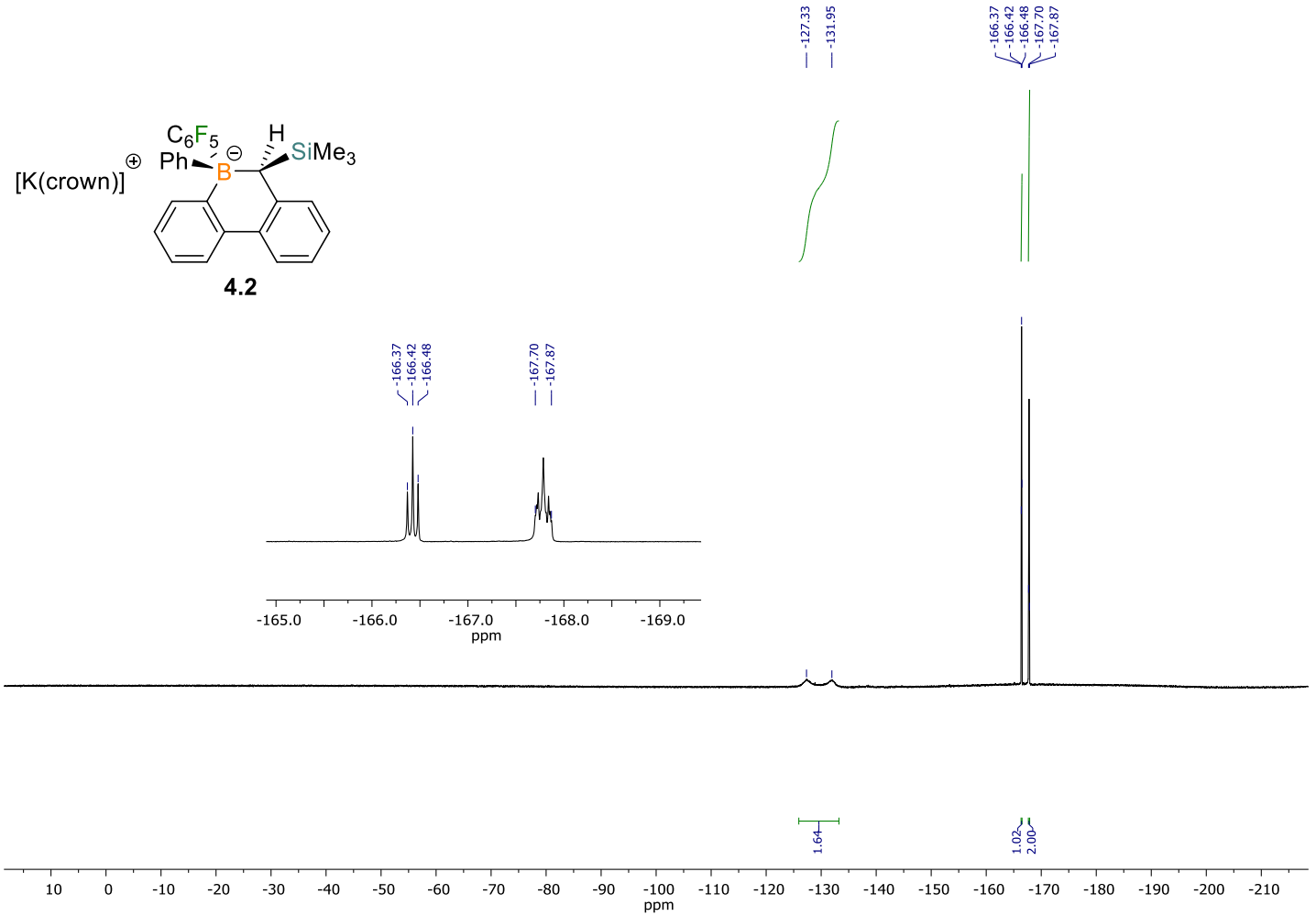

Figure C-15: $^{19}F\{^{1}H\}$ NMR spectrum of **4.2** in $CDCl_3$.

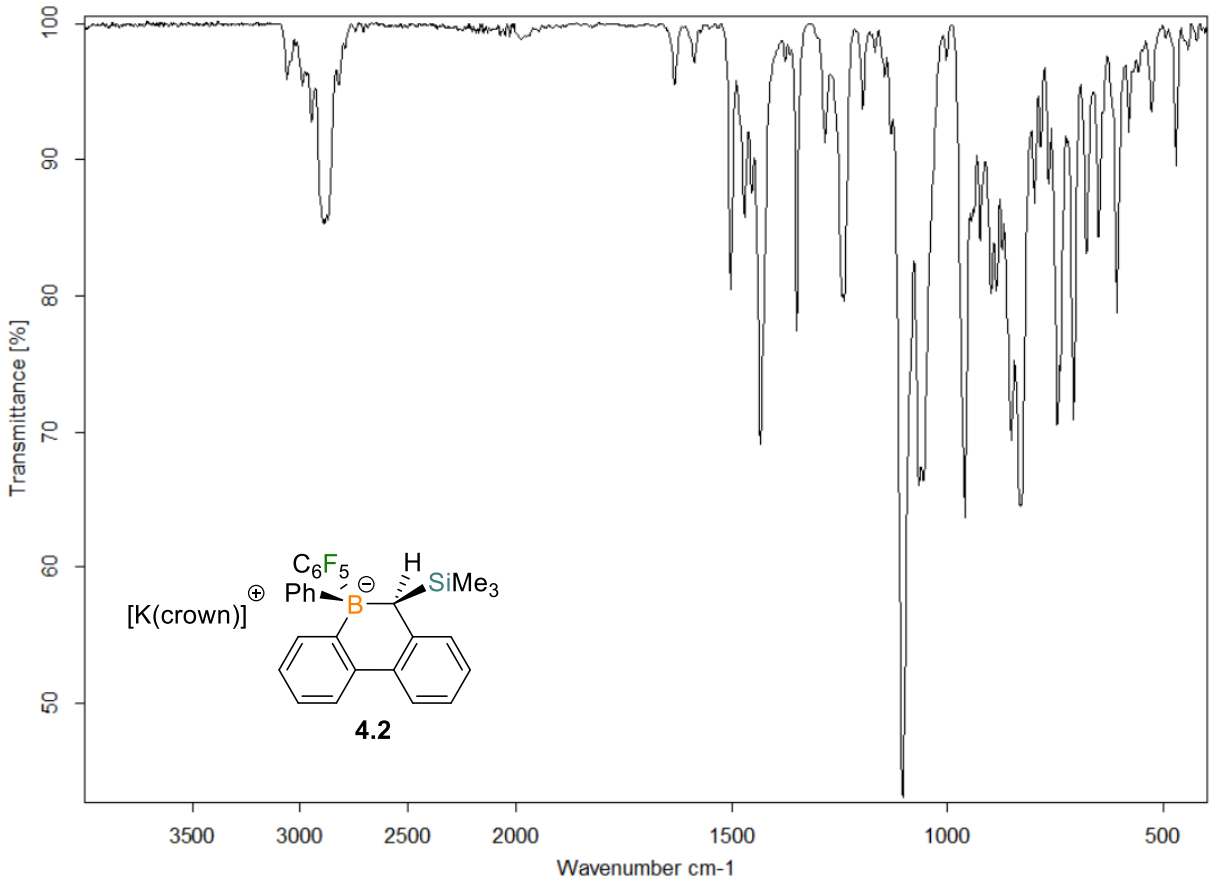

Figure C-16: FT-IR spectrum of **4.2**.

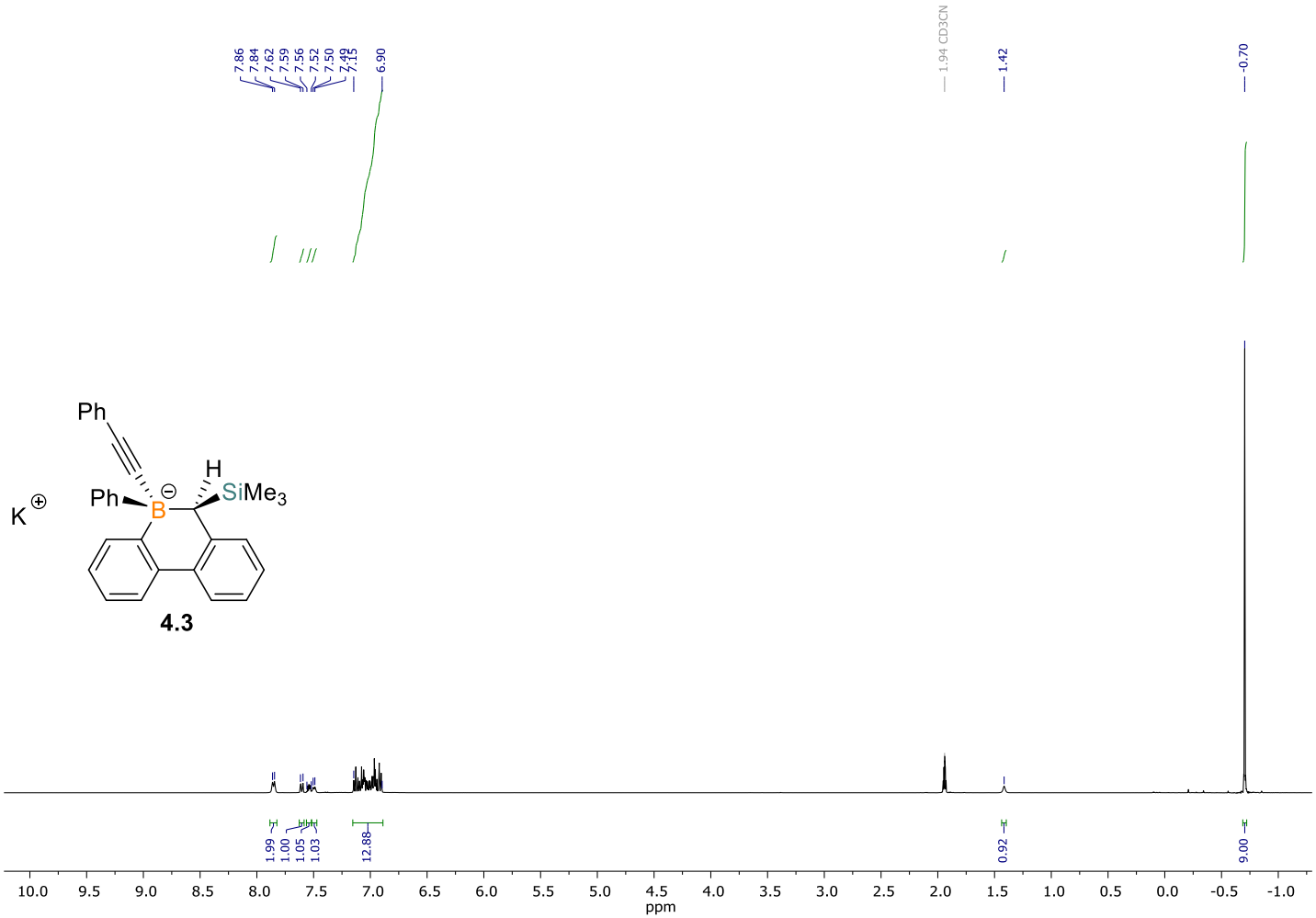

Figure C-17: ^{1}H NMR spectrum of **4.3** in CD_3CN.

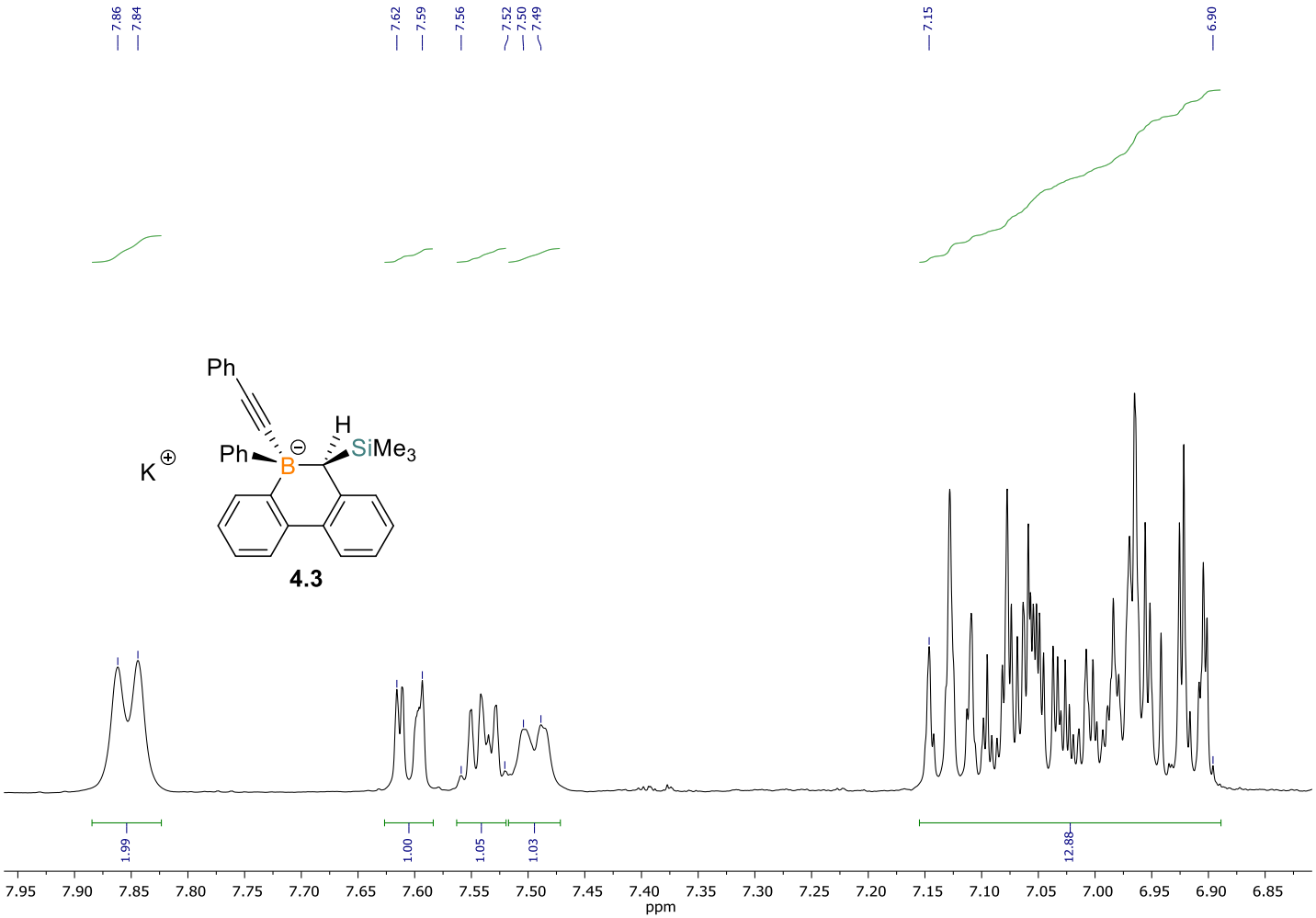

Figure C-18: Expansion of ^{1}H NMR spectrum of **4.3** in CD_3CN (aryl region).

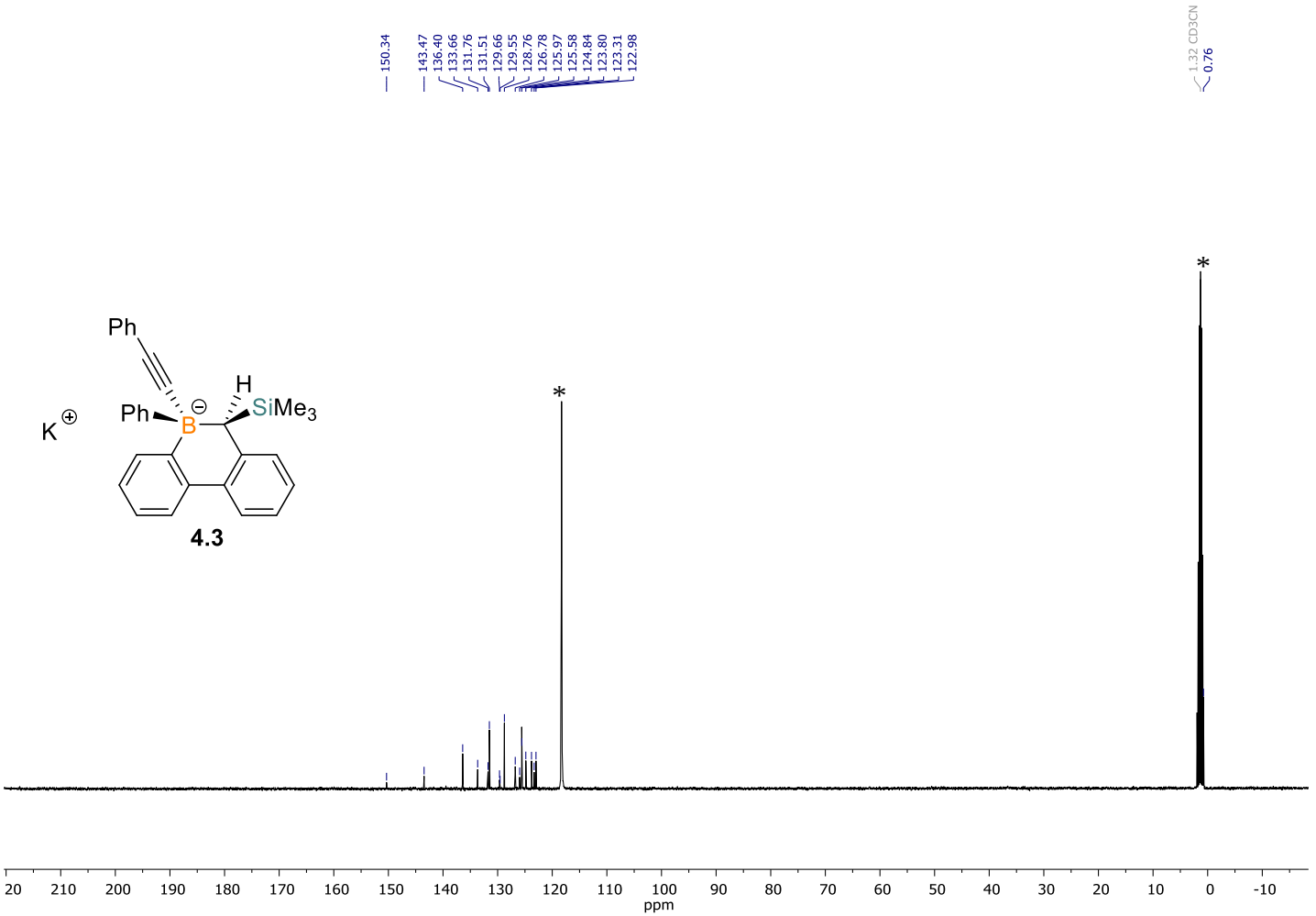

Figure C-19: $^{13}C\{^{1}H\}$ NMR spectrum of **4.3** in CD_3CN (* indicates CD_3CN).

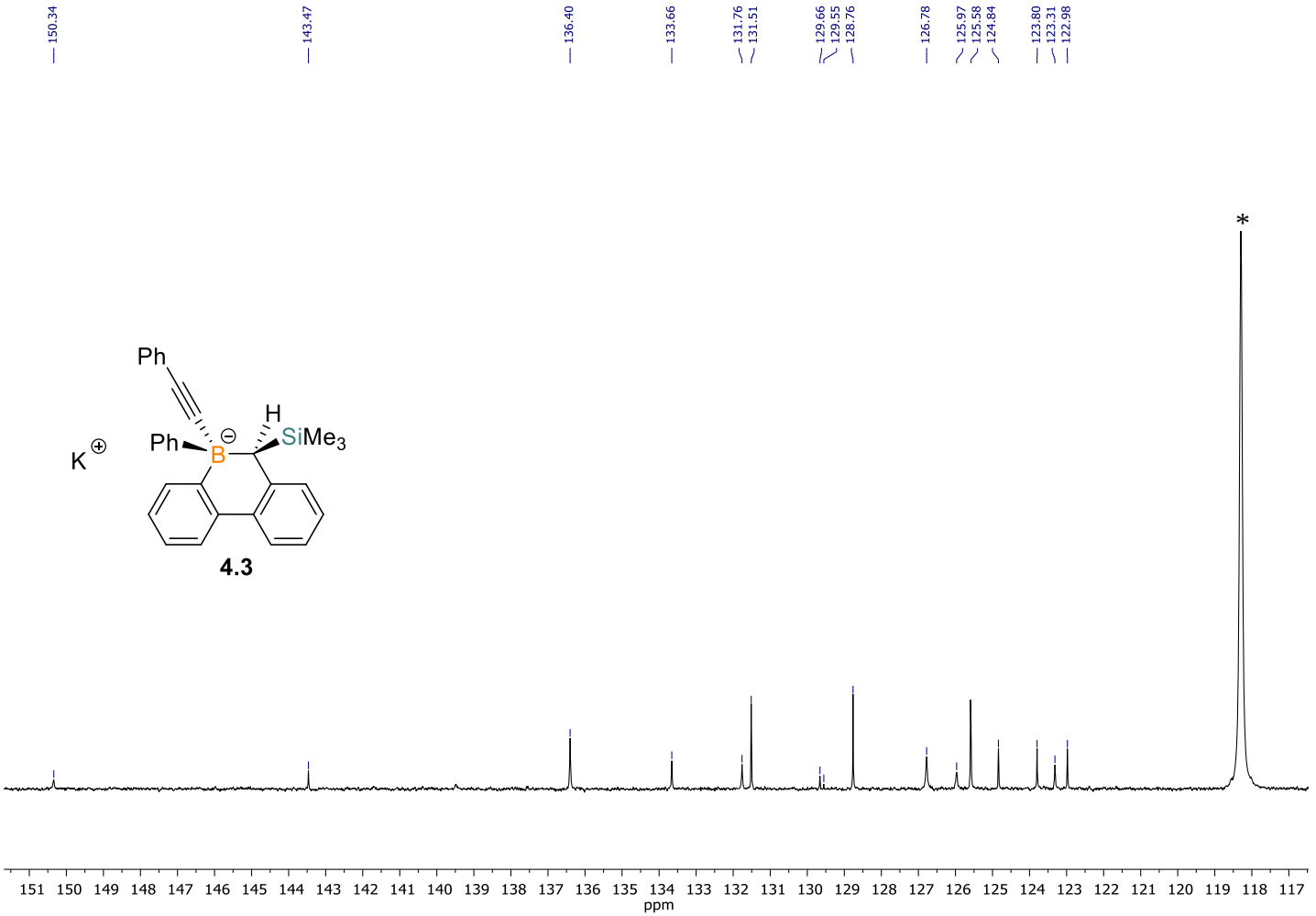

Figure C-20: Expansion of $^{13}C\{^{1}H\}$ NMR spectrum of **4.3** in CD_3CN (aryl region, * indicates CD_3CN).

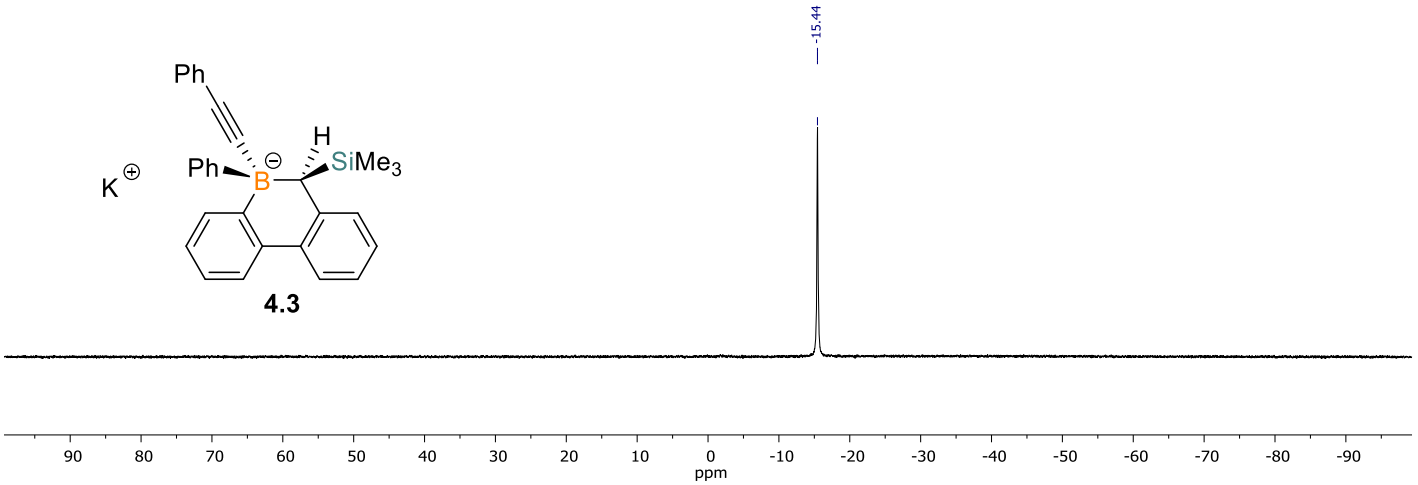

Figure C-21: ^{11}B NMR spectrum of **4.3** in CD_3CN.

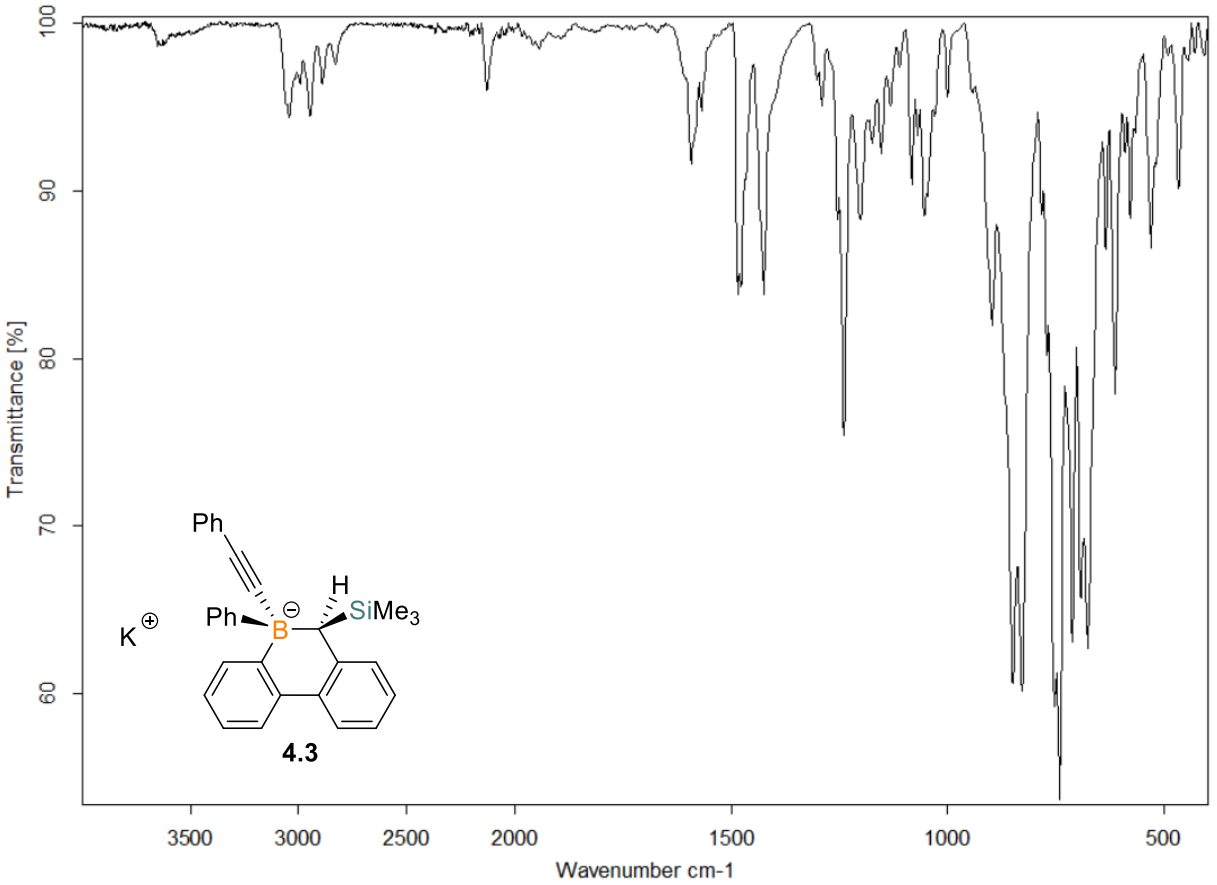

Figure C-22: FT-IR spectrum of **4.3**.

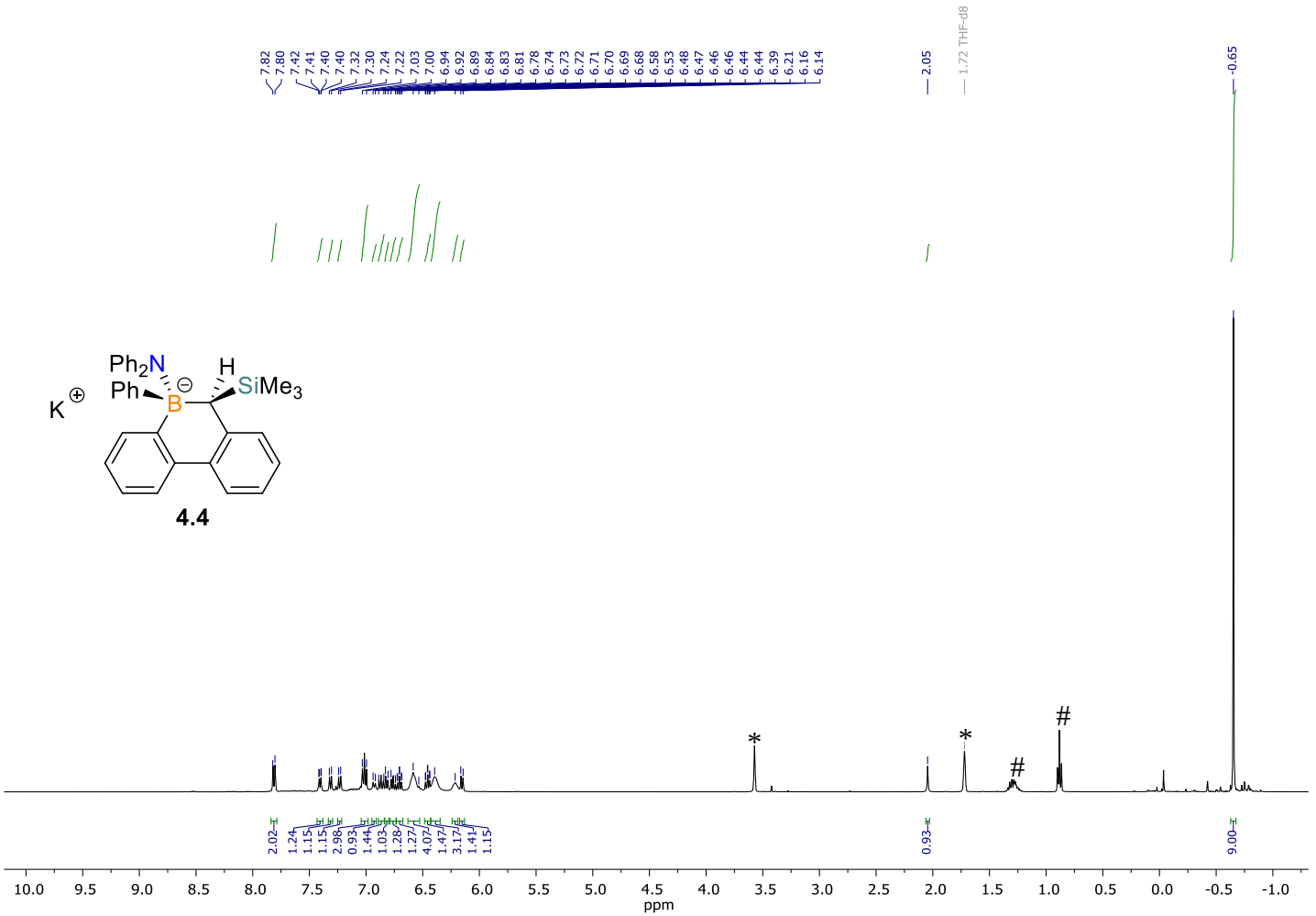

Figure C-23: ^{1}H NMR spectrum of **4.4** in THF-d_8 (* indicates THF-d_8, # indicates *n*-pentane).

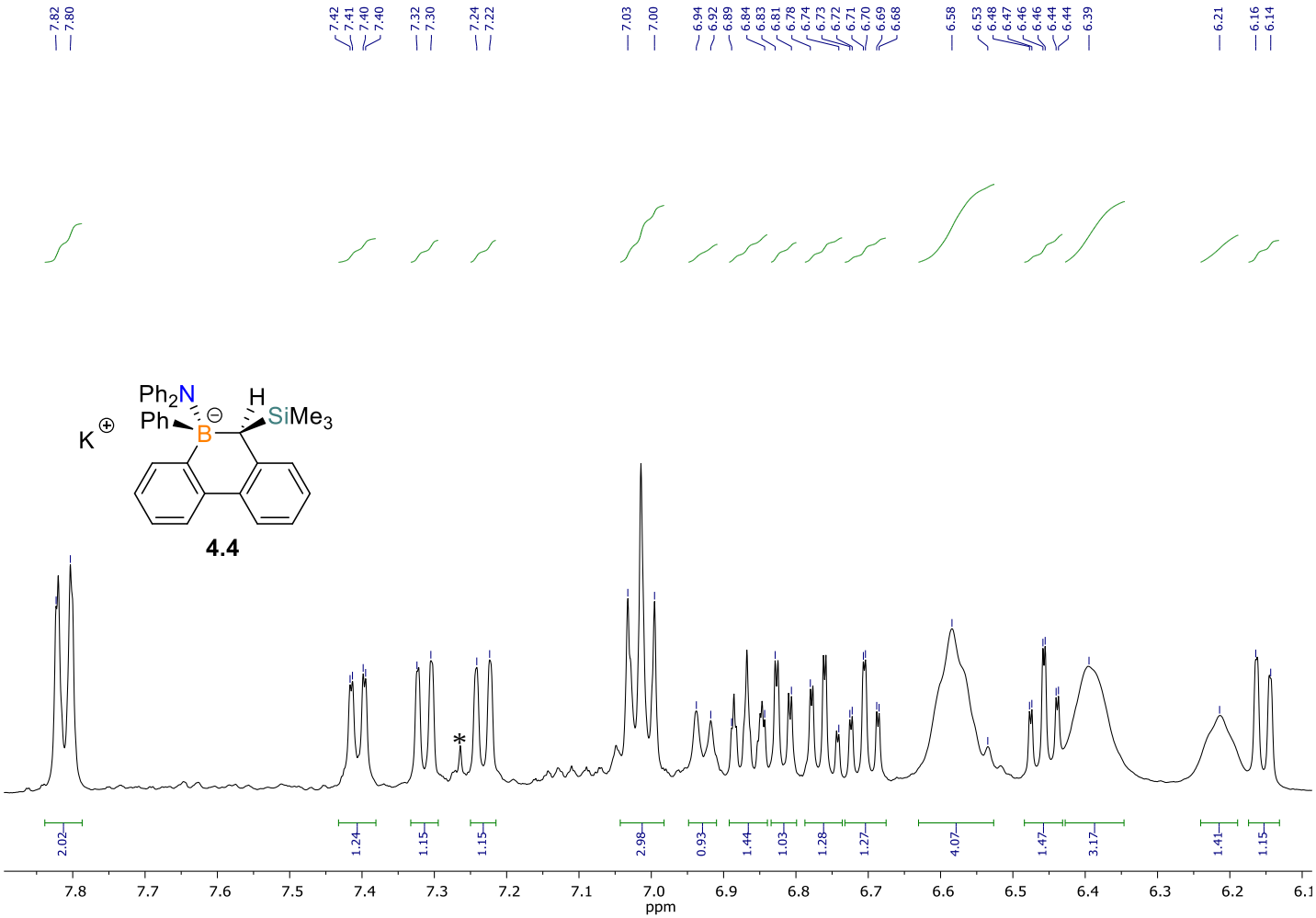

Figure C-24: Expansion of ^{1}H NMR spectrum of **4.4** in THF-d_8 (aryl region, * indicates benzene).

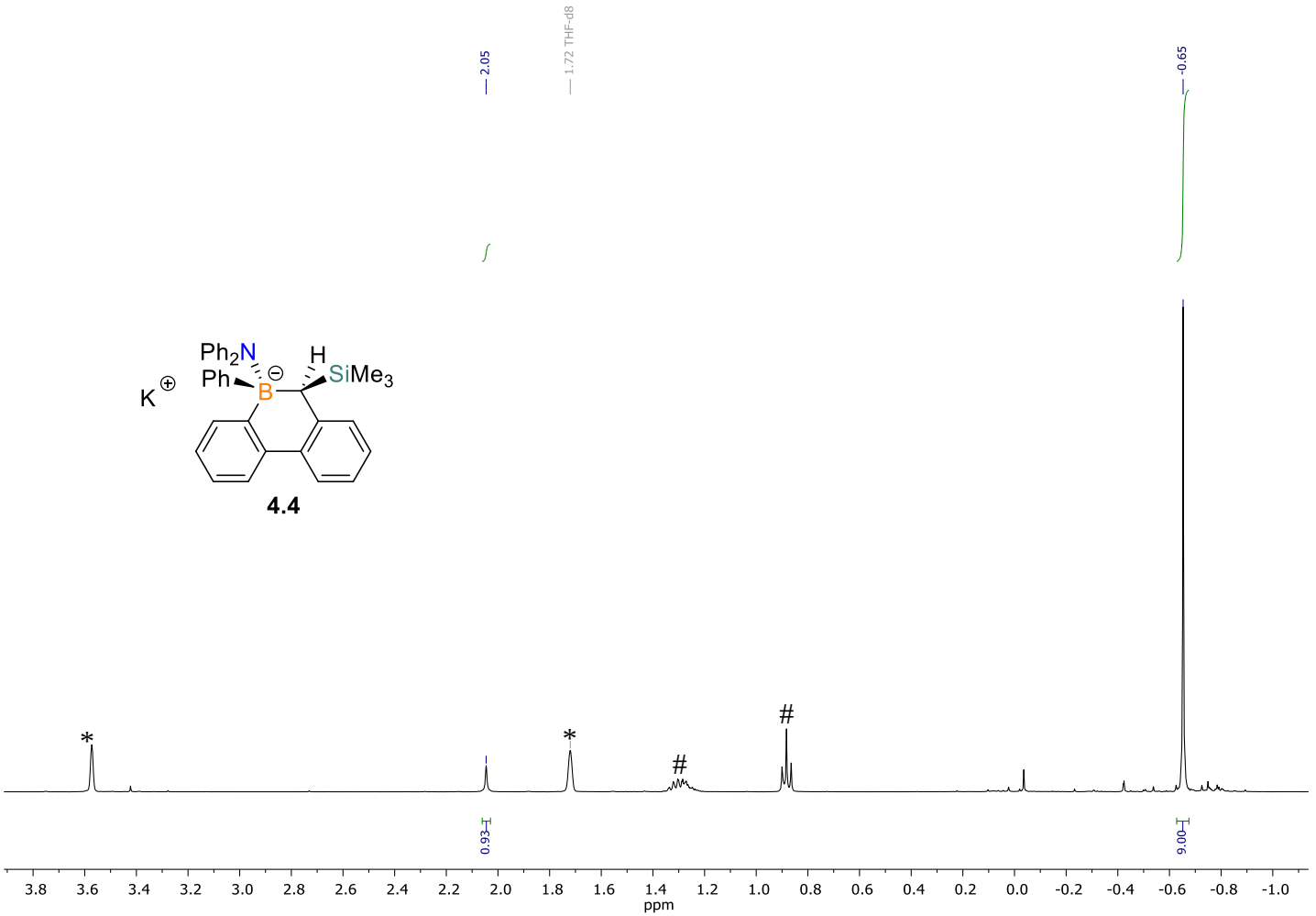

Figure C-25: Expansion of ^{1}H NMR spectrum of **4.4** in THF-d_8 (aliphatic region, * indicates THF-d_8, # indicates *n*-pentane).

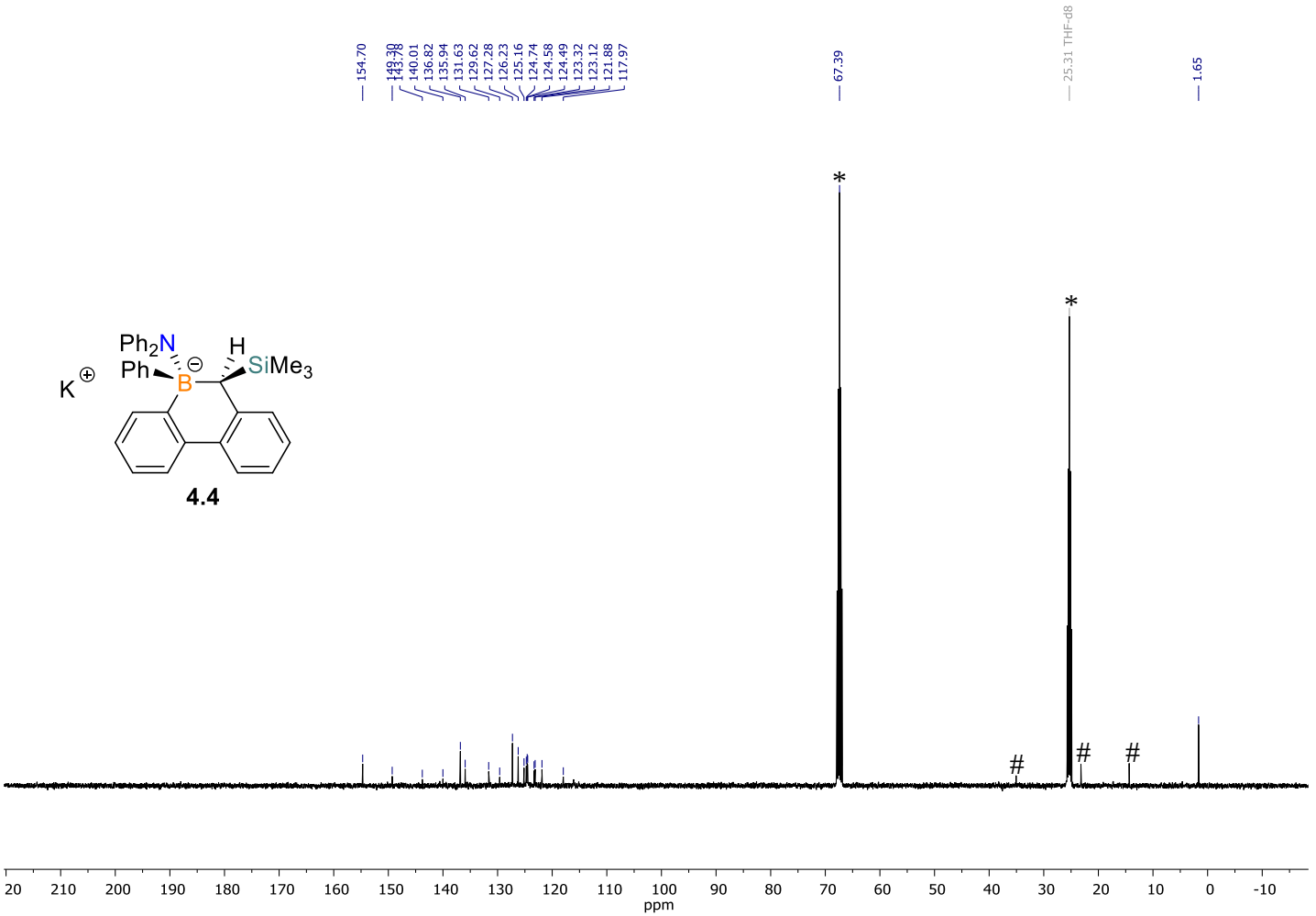

Figure C-26: $^{13}C\{^{1}H\}$ NMR spectrum of **4.4** in THF-d_8 (* indicates THF-d_8, # indicates *n*-pentane).

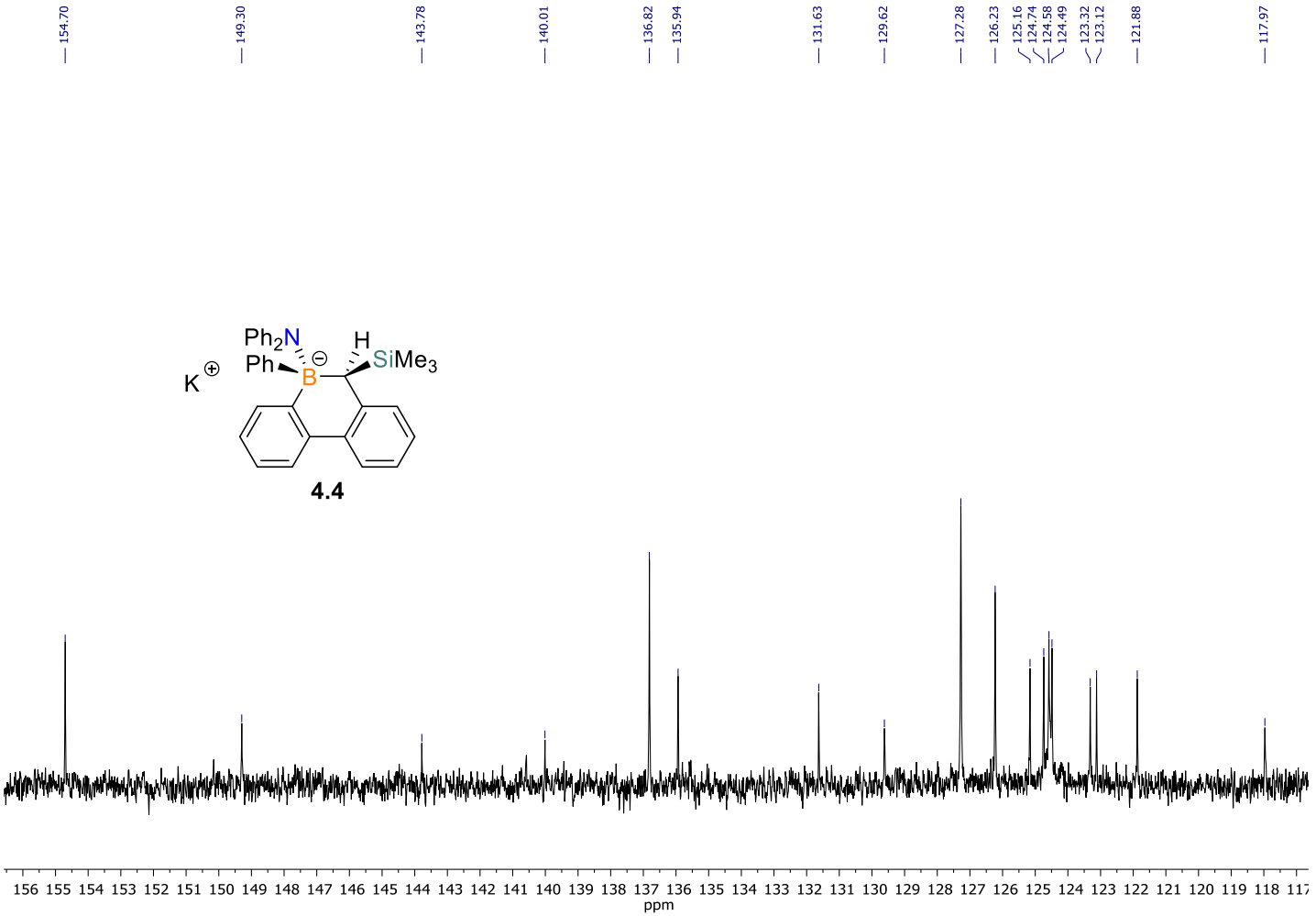

Figure C-27: Expansion of $^{13}C\{^{1}H\}$ NMR spectrum of **4.4** in THF-d_8 (aryl region).

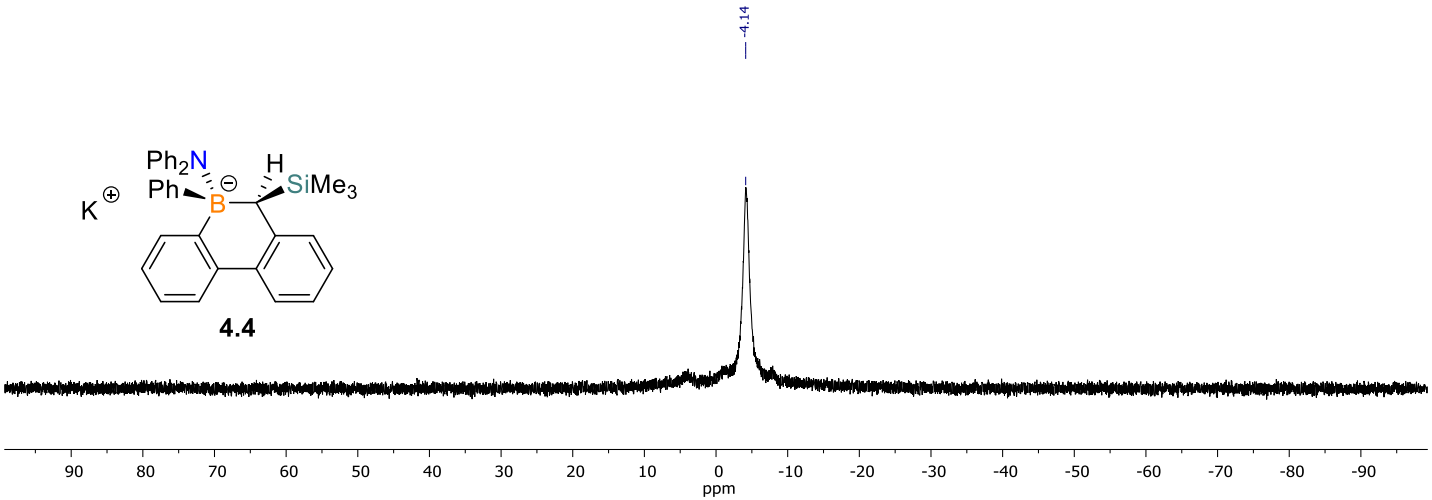

Figure C-28: ^{11}B NMR spectrum of **4.4** in THF-d_8.

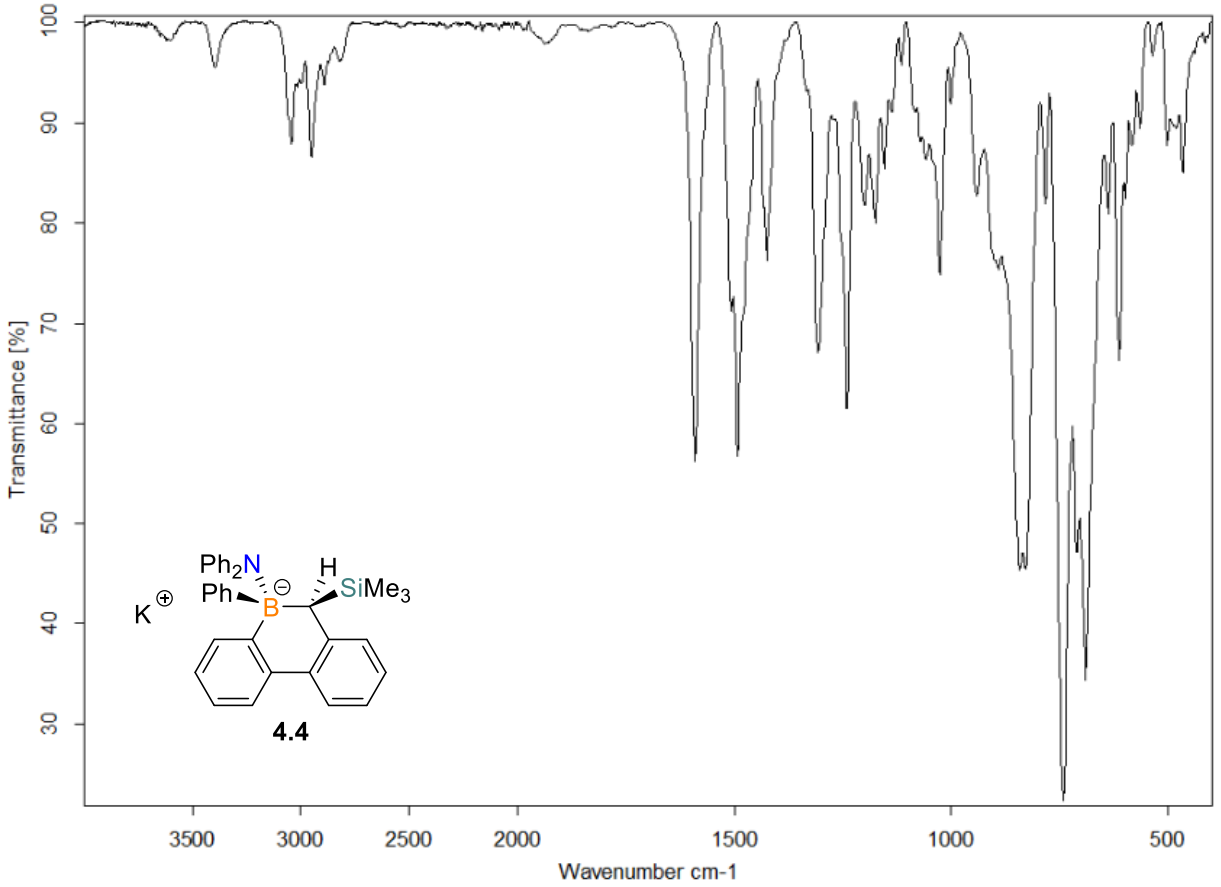

Figure C-29: FT-IR spectrum of **4.4**.

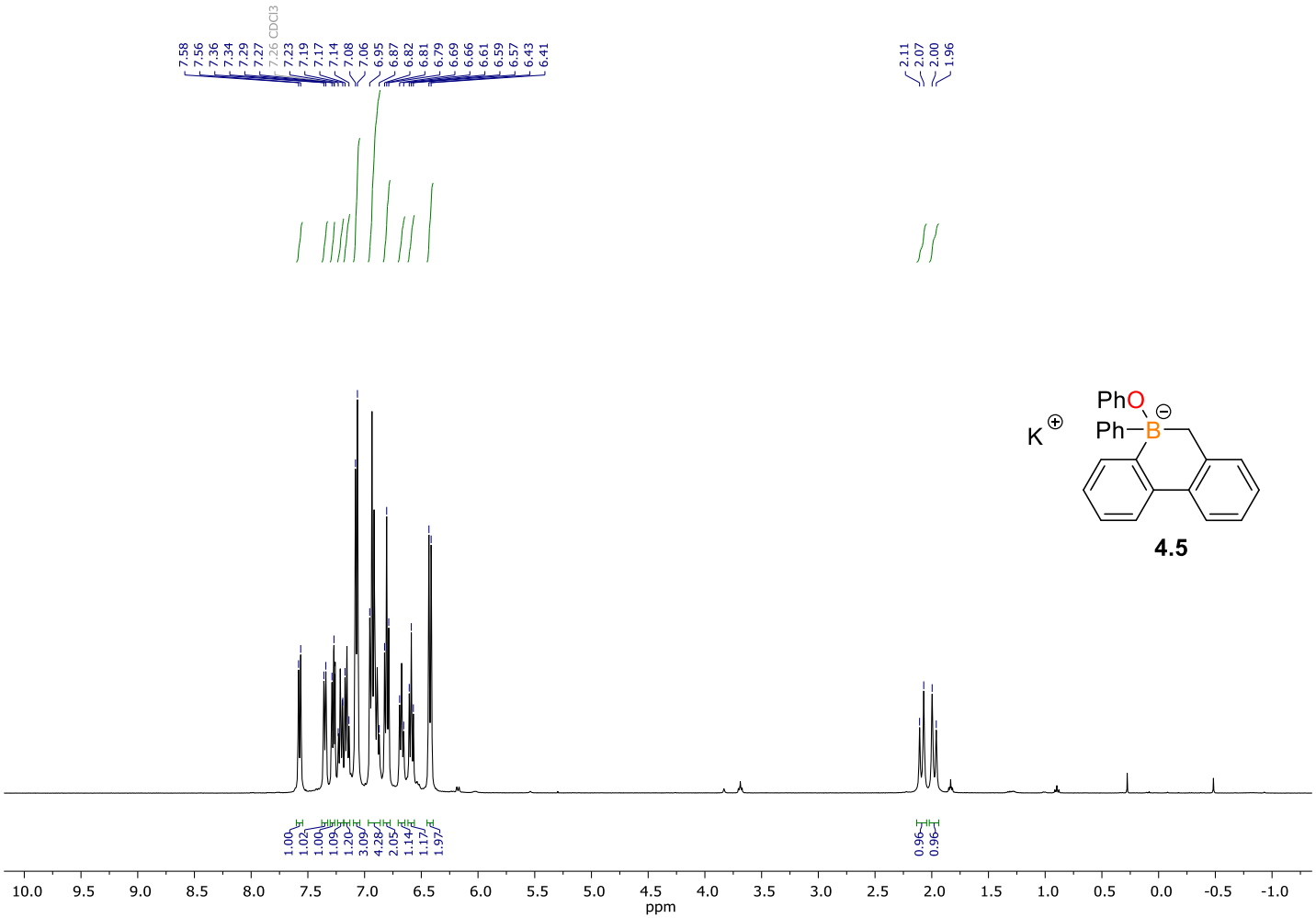

Figure C-30: ^{1}H NMR spectrum of **4.5** in $CDCl_3$.

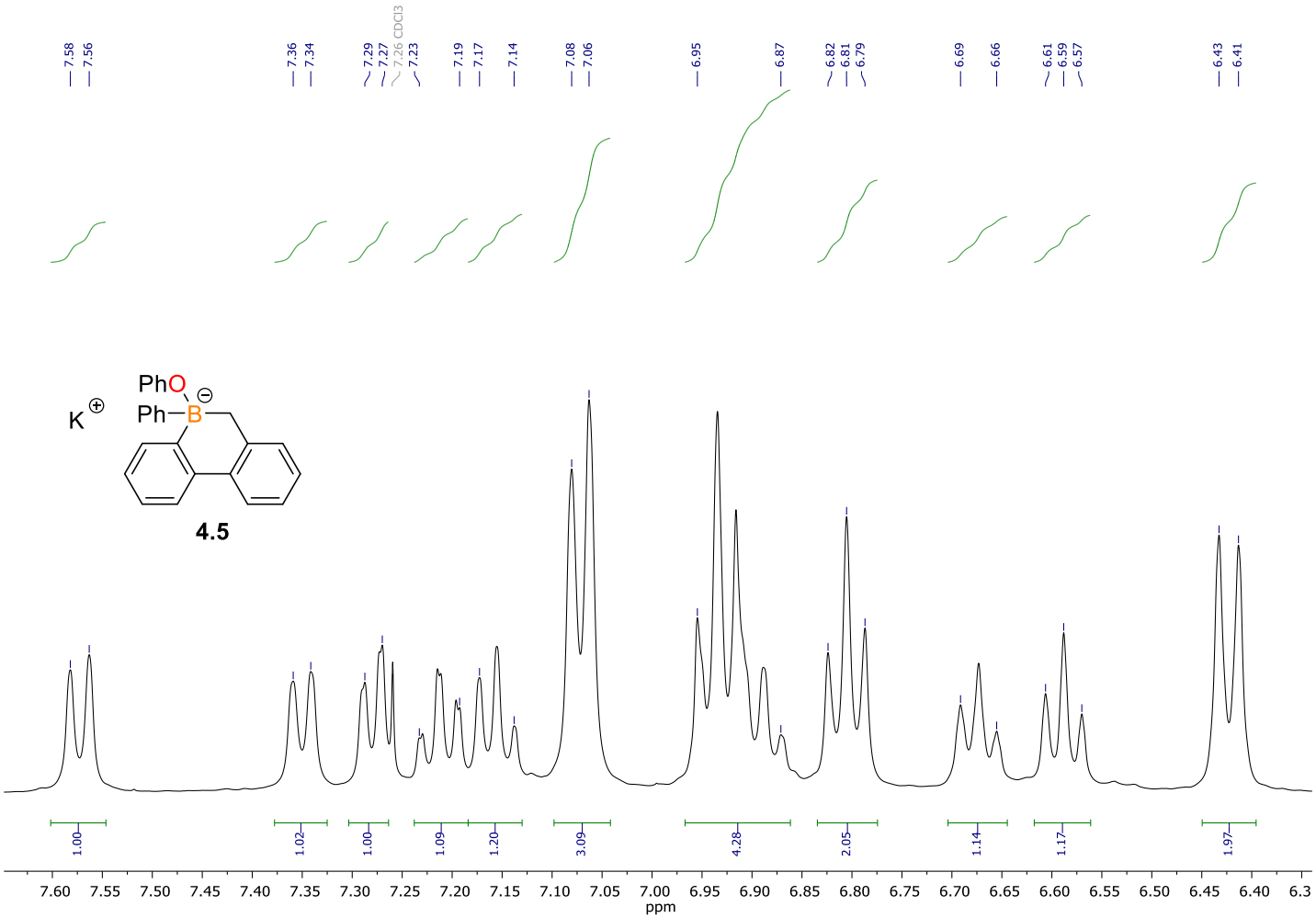

Figure C-31: Expansion of ^{1}H NMR spectrum of **4.5** in $CDCl_3$ (aryl region).

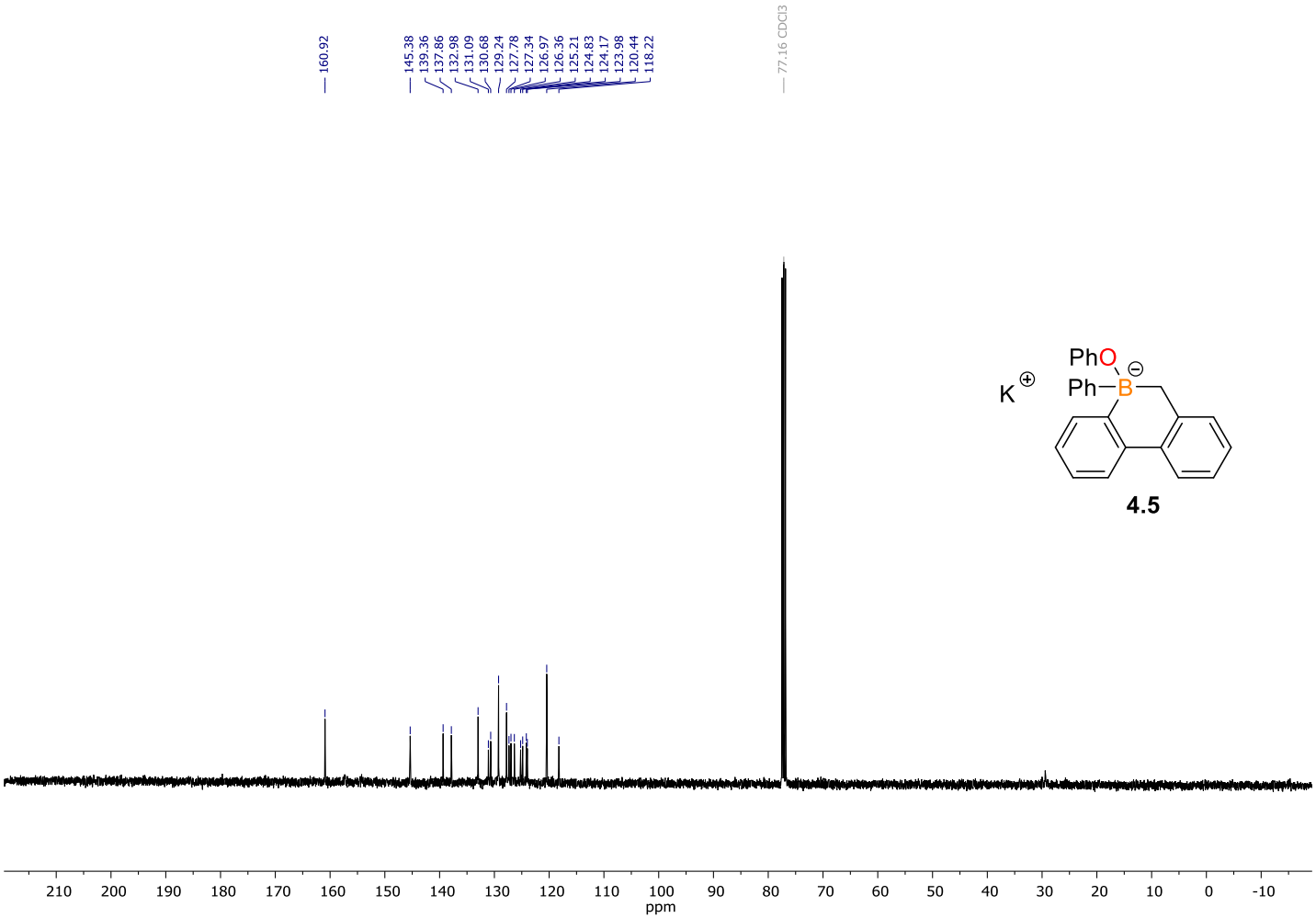

Figure C-32: $^{13}C\{^{1}H\}$ NMR spectrum of **4.5** in $CDCl_3$.

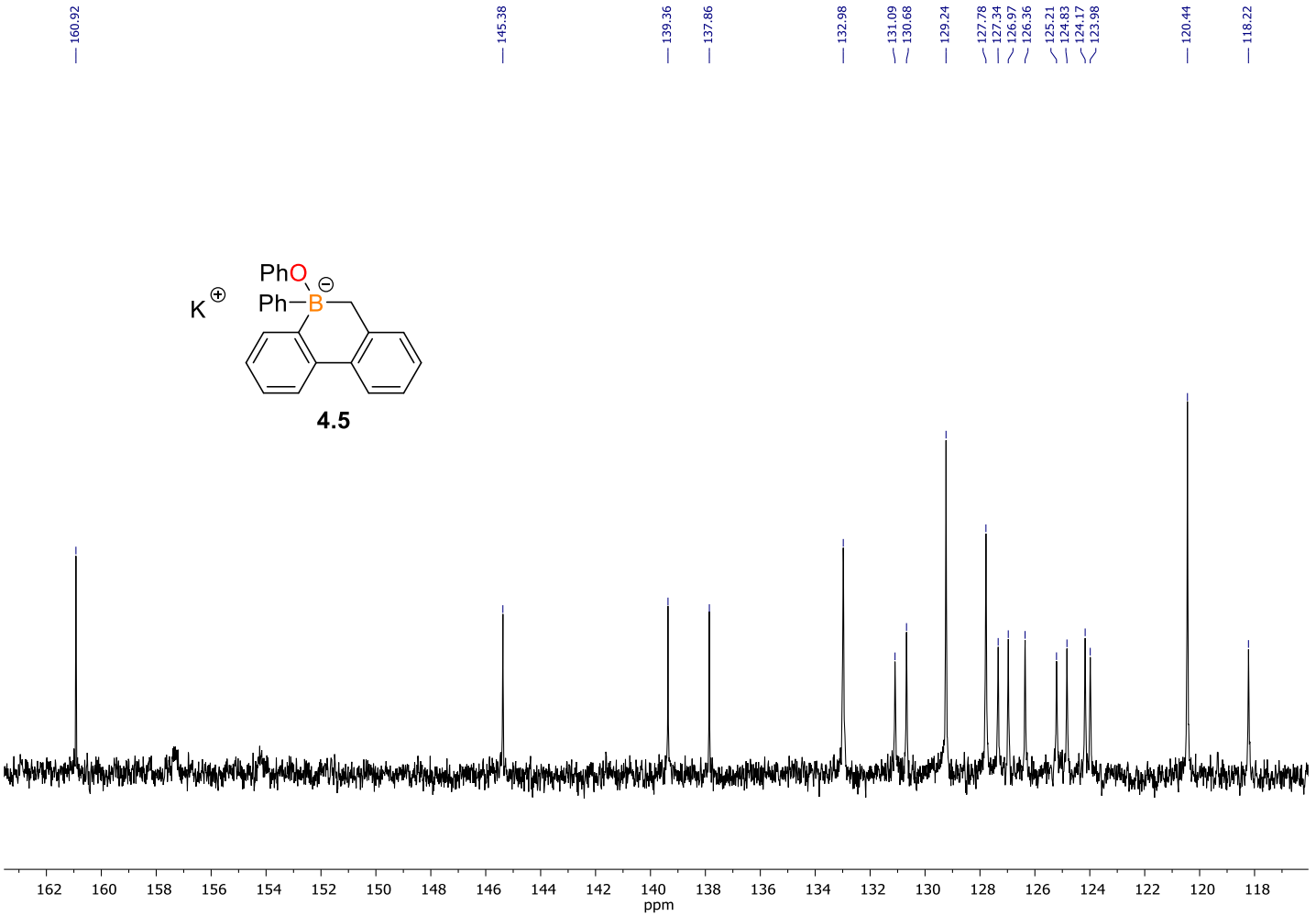

Figure C-33: Expansion of $^{13}C\{^{1}H\}$ NMR spectrum of **4.5** in $CDCl_3$ (aryl region).

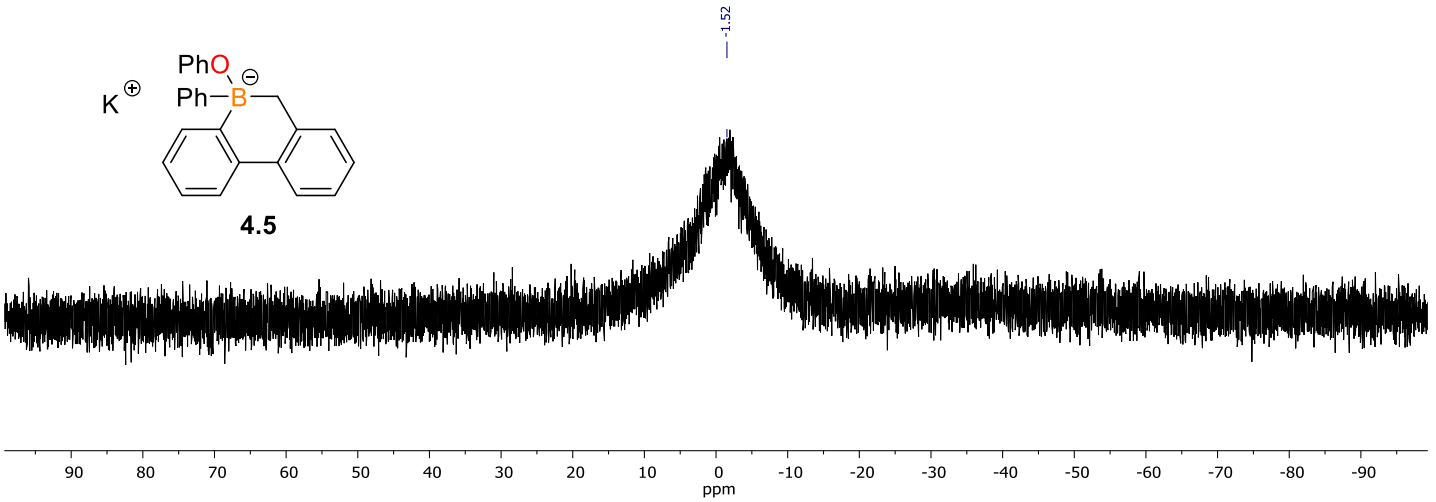

Figure C-34: ^{11}B NMR spectrum of **4.5** in $CDCl_3$.

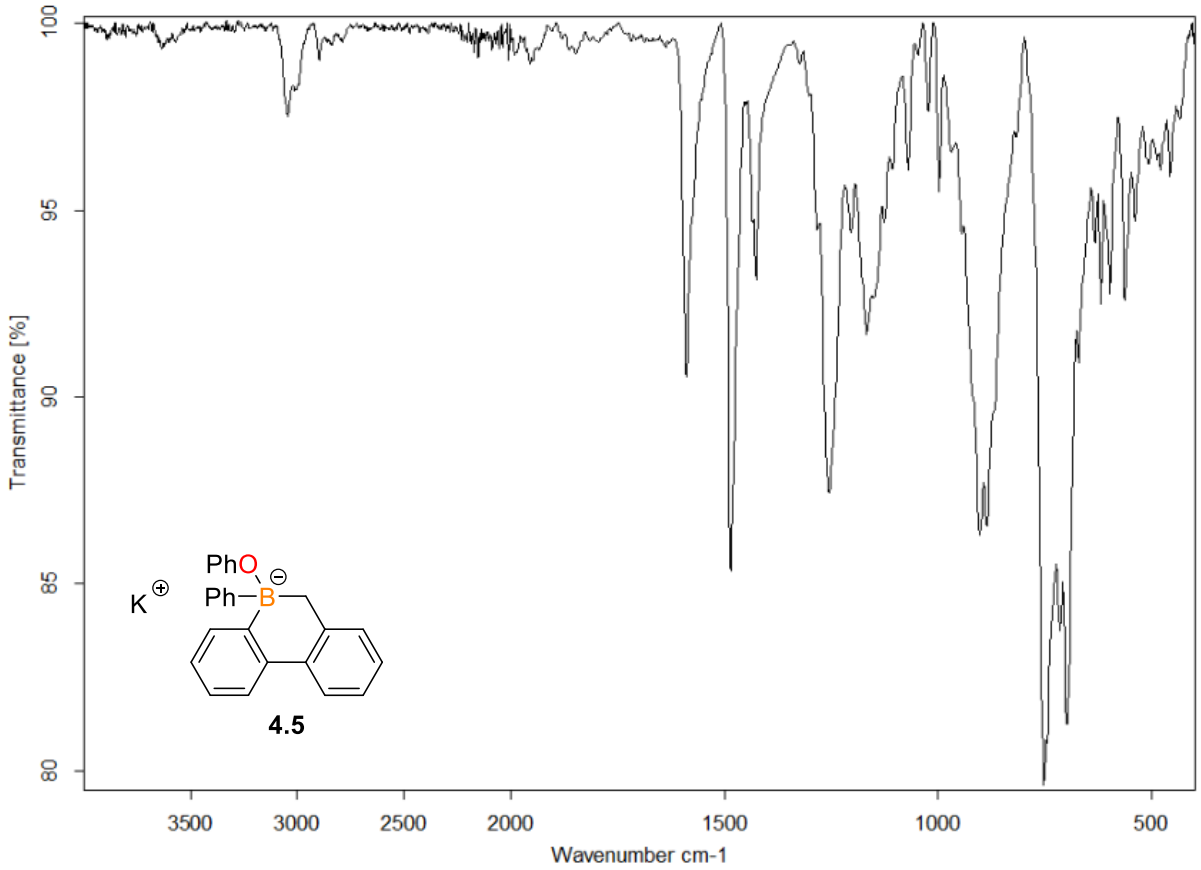

Figure C-35: FT-IR spectrum of **4.5**.

Table C-1: X-ray crystallographic details for **4.1**-**4.6**.

Compound	**4.1**	**4.2**	**4.3**	**4.4**	**4.5**	**4.6**
CCDC	2055588	2055589	2055590	2055591	2055592	2055593
Empirical Formula	$C_{48}H_{57}BKNO_8Si$	$C_{48}H_{63}BF_5KO_8Si$	$C_{31}H_{30}BCl_2KSi$	$C_{69}H_{68}B_2Cl_2K_2N_2Si_2$	$C_{51}H_{42}B_2Cl_2K_2O_2$	$C_{38}H_{32}B_2K_2O_2$
FW (g/mol)	853.94	940.98	551.45	1152.15	857.57	620.46
Crystal System	Triclinic	Triclinic	Triclinic	Orthorhombic	Monoclinic	Orthorhombic
Space Group	P -1	P -1	P -1	P b c n	C 2	P b c a
a (Å)	12.8450(6)	12.8356(9)	9.4582(6)	34.9192(11)	14.1976(4)	7.6101(3)
b (Å)	13.0893(6)	12.9157(10)	12.0005(7)	12.4926(3)	11.5651(3)	17.8756(7)
c (Å)	13.8502(6)	15.4217(11)	14.1845(10)	13.4223(4)	12.5866(3)	21.8496(9)
α (deg)	91.766(2)	95.417(3)	103.006(3)	90	90	90
β (deg)	92.514(2)	107.934(3)	91.479(3)	90	93.1742(11)	90
γ (deg)	100.196(2)	90.978(3)	111.154(2)	90	90	90
V ($Å^3$)	2287.92(18)	2418.7(3)	1452.79(16)	5855.2(3)	2063.51(9)	2972.3(2)
Z	2	2	2	4	2	4
D_c (g cm^{-3})	1.240	1.292	1.261	1.307	1.380	1.387
Radiation λ (Å)	0.71073	0.71073	0.71073	0.71073	0.71073	0.71073
Temp (K)	150	150	150	150	150	150
R1 [I>2(σ)I][a]	0.0765	0.0784	0.0813	0.0776	0.0417	0.0698
wR2 (F^2)[a]	0.2184	0.1860	0.2420	0.2137	0.1010	0.1932
GOF (S)[a]	1.095	1.076	1.148	1.079	1.035	1.072

[a] $R1(F[I > 2(I)]) = \sum||F_o| - |F_c||/\sum|F_o|$; $wR2(F^2\ [\text{all data}]) = [w(F_o^2 - F_c^2)^2]^{1/2}$; $S(\text{all data}) = [w(F_o^2 - F_c^2)^2/(n - p)]^{1/2}$ (n = no. of data; p = no. of parameters varied; $w = 1/[^2(F_o^2) + (aP)^2 + bP]$ where $P = (F_o^2 + 2F_c^2)/3$ and a and b are constants suggested by the refinement program.

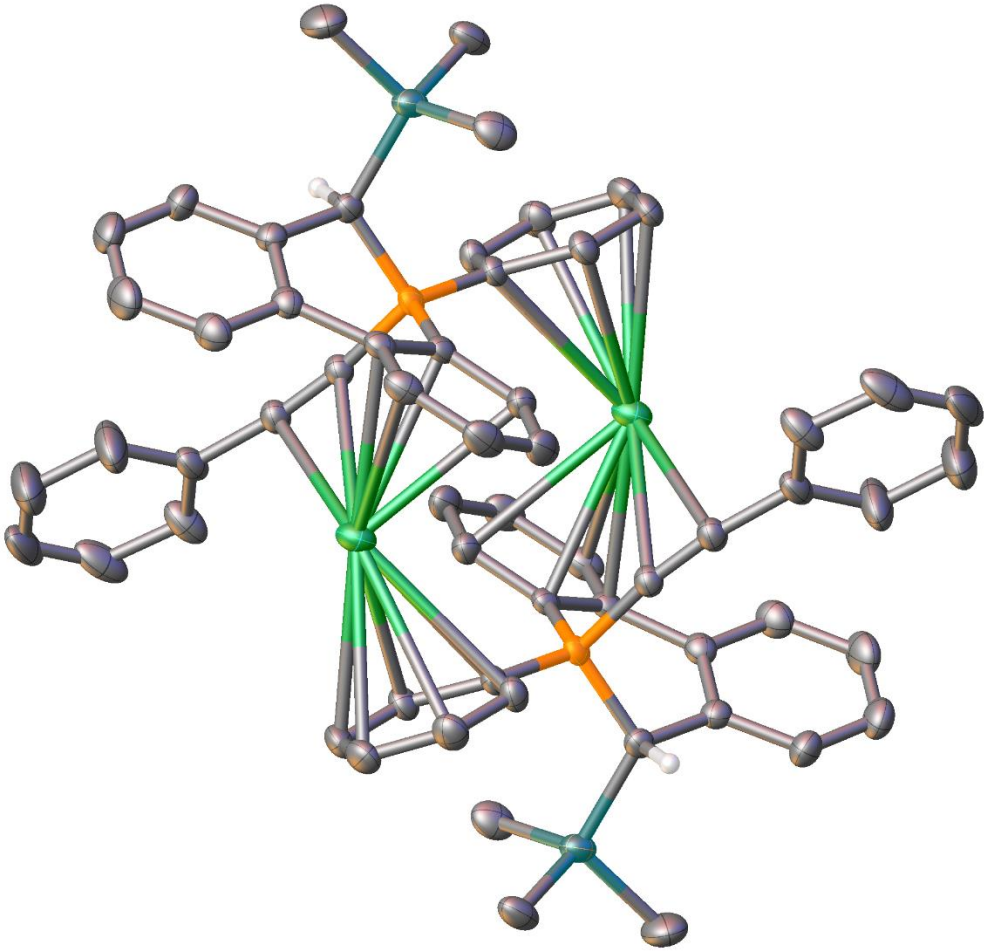

Figure C-36: Dimeric structure of **4.3**. Hydrogen atoms (except at the chiral center) and dichloromethane solvate are omitted for clarity, and thermal ellipsoids are drawn at the 50% probability level.

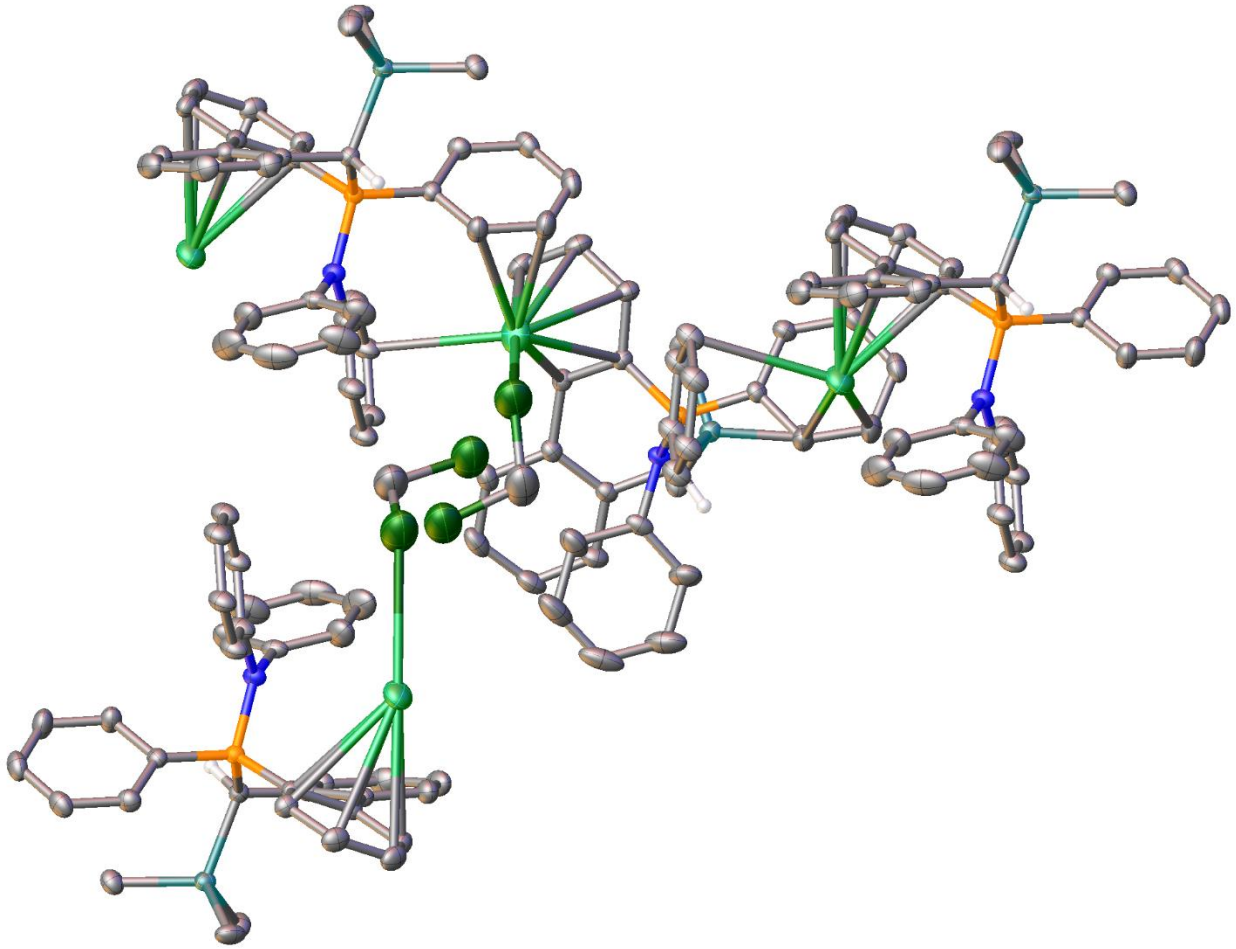

Figure C-37: Polymeric structure of **4.4**. Hydrogen atoms (except at the chiral center) are omitted for clarity, and thermal ellipsoids are drawn at the 50% probability level. For disordered atoms, only the component with the higher occupancy is shown.

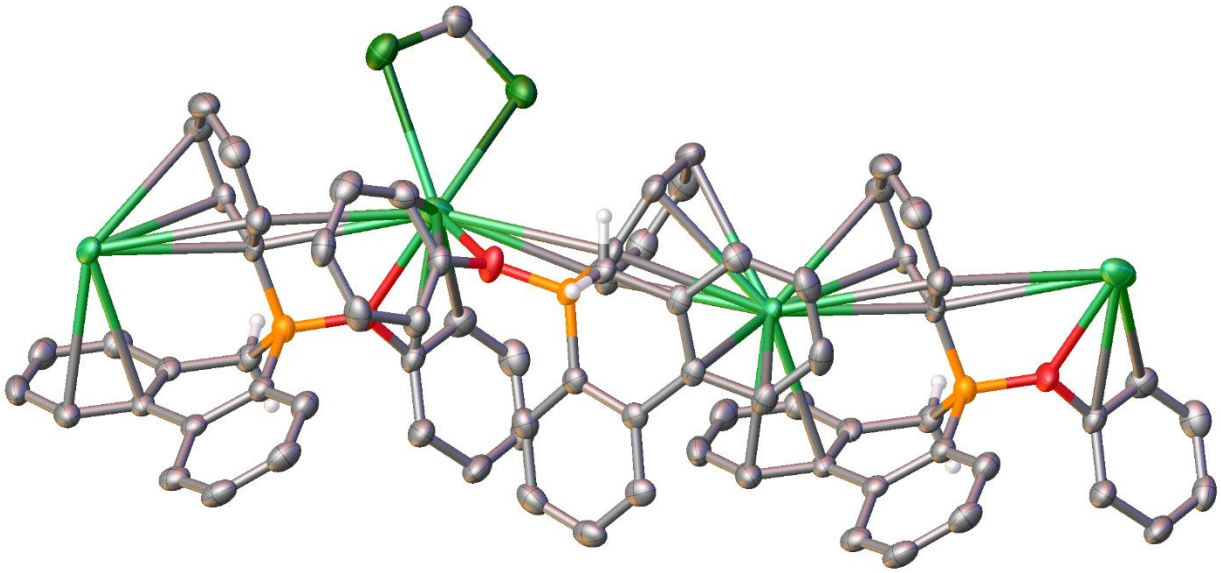

Figure C-38: Polymeric structure of **4.5**. Hydrogen atoms (except those derived from phenol) are omitted for clarity, and thermal ellipsoids are drawn at the 50% probability level.

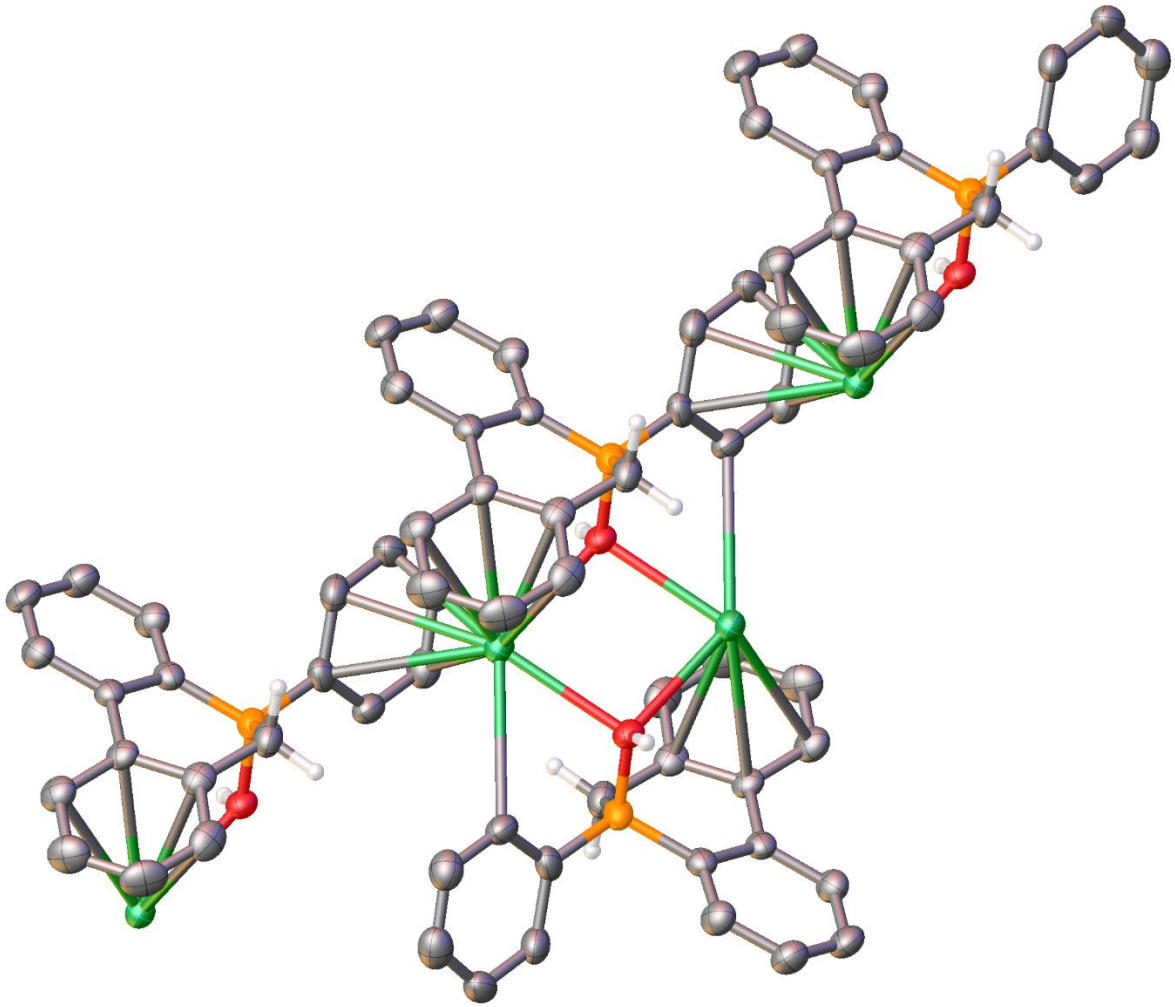

Figure C-39: Polymeric structure of **4.6**. Hydrogen atoms (except those derived from water) are omitted for clarity, and thermal ellipsoids are drawn at the 50% probability level.

Table C-2. B3LYP/def2-TZVP(THF) calculated barrier heights (Δ*G*, kJ/mol).

Substrate	TS4.1	TS4.2	TS4.3	Product
H_2O	86.5	48.0	120.5	2
CH_3CN	120.2	95.5	130.5	1
C_6F_5H	111.0	123.1	127.1	1
PhCCH	108.7	89.2	115.5	1
Ph_2NH	82.2	139.3	84.5	1
PhOH	48.2	80.9	46.4	2

Table C-3: Energies computed at the B3LYP-D3(BJ)/def2-SVP (IEFPCM, SMD, THF)

Compound	Energy (kJ/mol)
3.4	-1165.55421460
$(H_2O)_2$	-152.743310158
MeCN	-132.667514658
C_6F_5H	-727.337415642
PhCCH	-308.208784885
Ph_2NH	-518.352569587
PhOH	-307.281442745
TS4.1 (H_2O)	-1318.29337959
TS4.1 (MeCN)	-1298.19211679
TS4.1 (C_6F_5H)	-1893.40329788
TS4.1 (PhCCH)	-1473.73943369
TS4.1 (Ph_2NH)	-1683.90145245
TS4.1 (PhOH)	-1472.83931403
Int4.1	-1166.06303833
H_2O-OH^-	-152.188121414
CH_2CN^-	-132.125886503
$C_6F_5^-$	-727.337415642
$PhCC^-$	-307.681616751
Ph_2N^-	-517.829113879
PhO^-	-306.770767599
Prod4.1 (H_2O)	-1318.35836715
Prod4.1 (MeCN)	-1298.2525385
Prod4.1 (C_6F_5H)	-1893.46279723
Prod4.1 (PhCCH)	-1473.81138666
Prod4.1 (Ph_2NH)	-1683.94644368
Prod4.1 (PhOH)	-1472.89469177
TS4.2 (H_2O)	-1318.29034245
TS4.2 (MeCN)	-1298.18490614
TS4.2 (C_6F_5H)	-1893.39590947
TS4.2 (PhCCH)	-1473.73962424
TS4.2 (Ph_2NH)	-1683.8767599
TS4.2 (PhOH)	-1472.83830804
Int4.2	-757.017036425
H_2O-Me_3SiOH	-561.325331259
Me_3SiCH_2CN	-541.210408757
$Me_3SiC_6F_5$	-1136.41971913
$Me_3SiCCPh$	-716.767800908
Me_3SiNPh_2	-926.907630003
Me_3SiOPh	-715.857080536
TS4.3 (H_2O)	-909.744455199
TS4.3 (MeCN)	-889.646168021
TS4.3 (C_6F_5H)	-1484.8620052

Compound	Energy (kJ/mol)
TS4.3 (PhCCH)	-1065.19977133
TS4.3 (Ph_2NH)	-1275.35856519
TS4.3 (PhOH)	-1064.30057052
Int4.3	-757.508865028
Prod4.2 (H_2O)	-909.815225283
Prod4.2 (MeCN)	-889.708100393
Prod4.2 (C_6F_5H)	-1484.92061789
Prod4.2 (PhCCH)	-1065.26750032
Prod4.2 (Ph_2NH)	-1275.40304487
Prod4.2 (PhOH)	-1064.34962039

APPENDIX D

Supplementary Information for Chapter Five

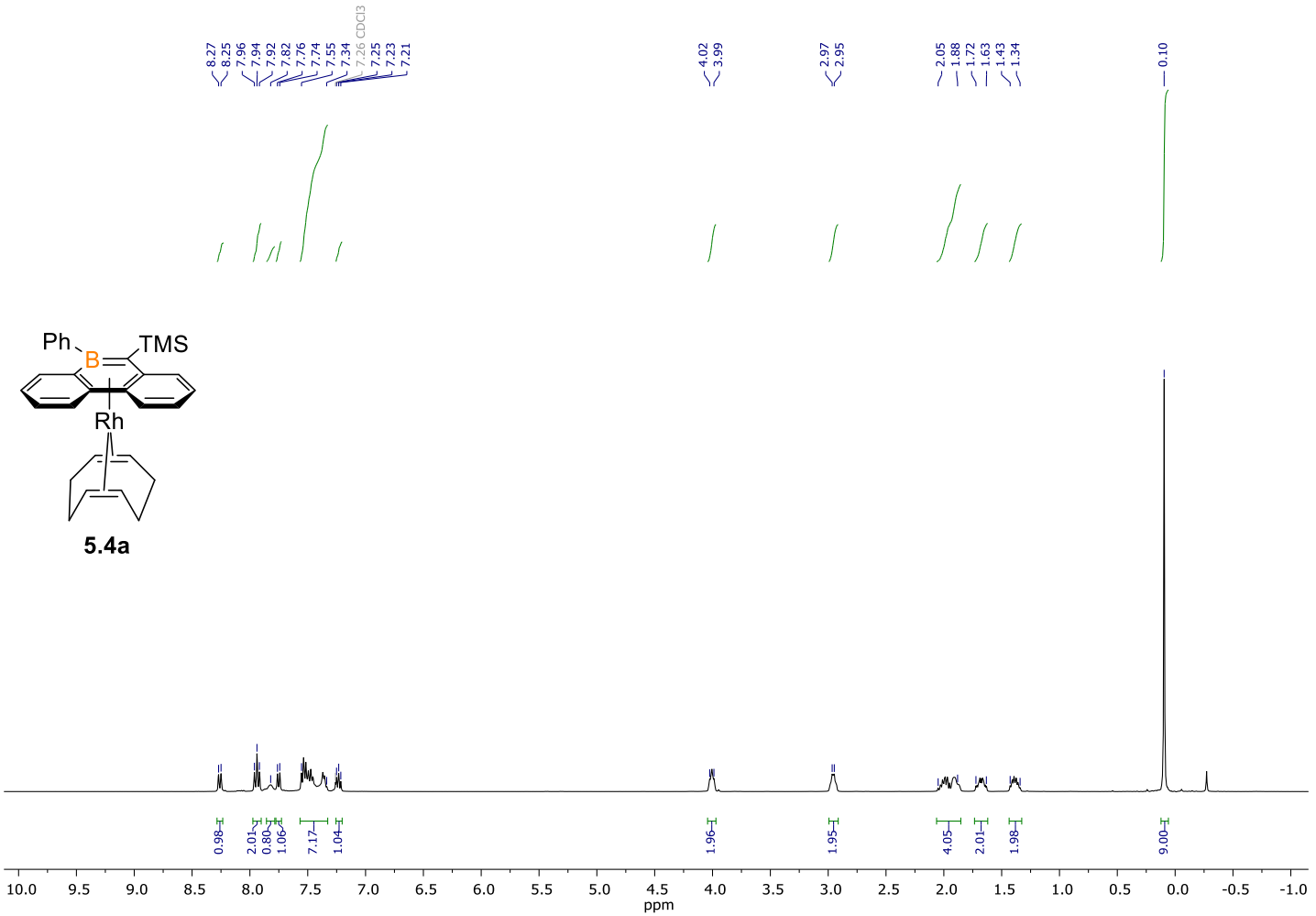

Figure D-1: ^{1}H NMR spectrum of **5.4a** in $CDCl_3$.

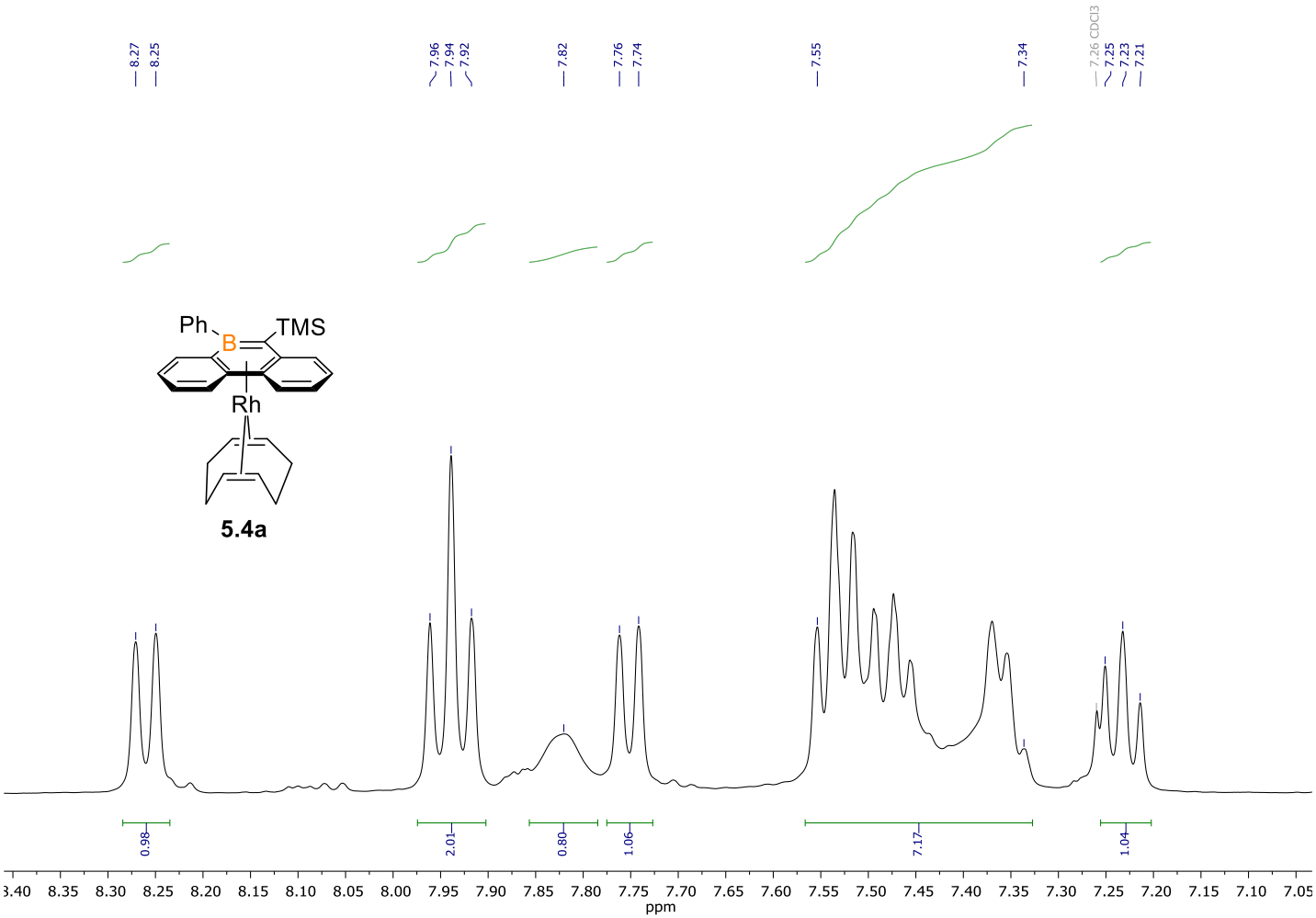

Figure D-2: Expansion of ^{1}H NMR spectrum of **5.4a** in $CDCl_3$ (aryl region).

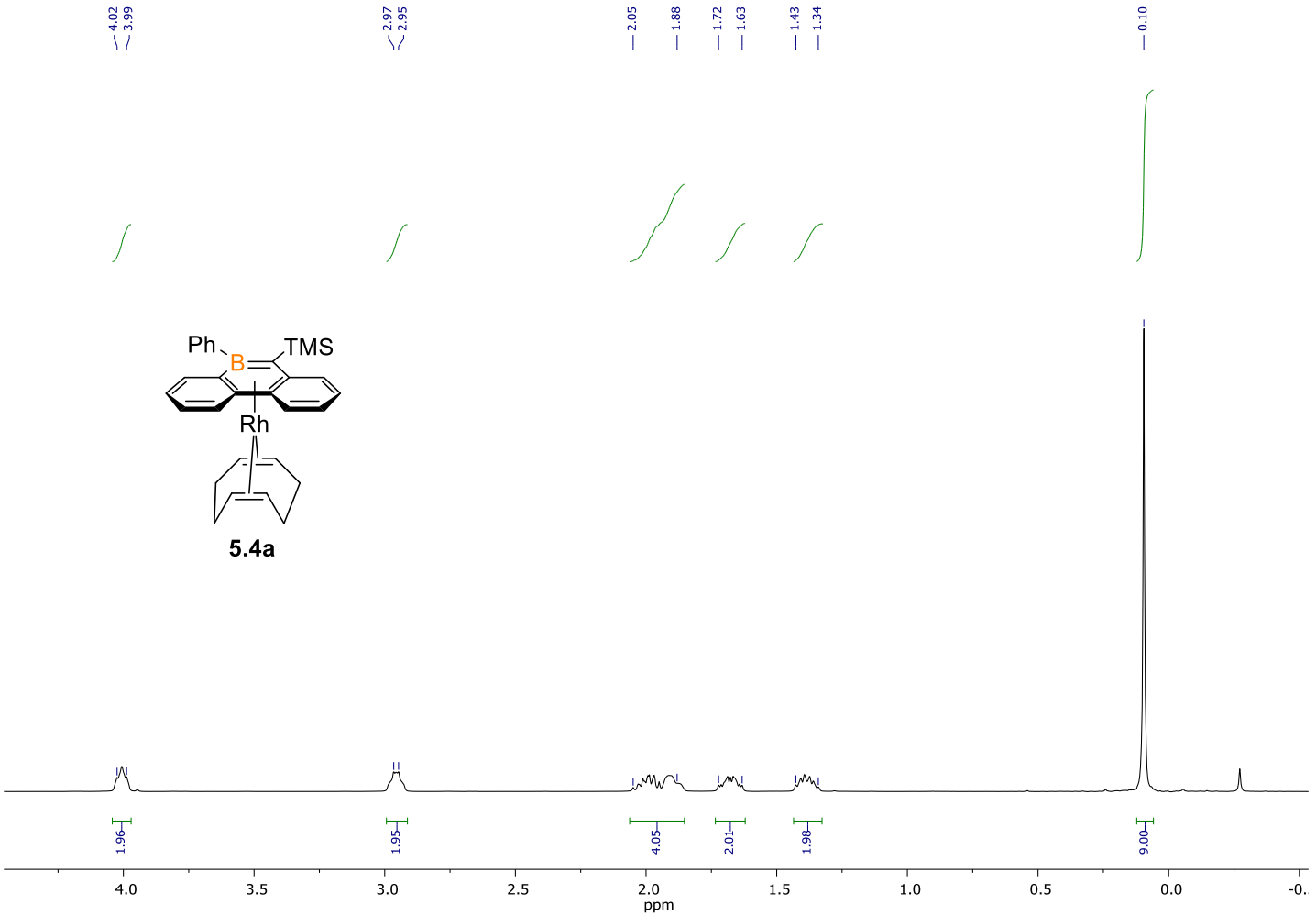

Figure D-3: Expansion of ^{1}H NMR spectrum of **5.4a** in $CDCl_3$ (aliphatic region).

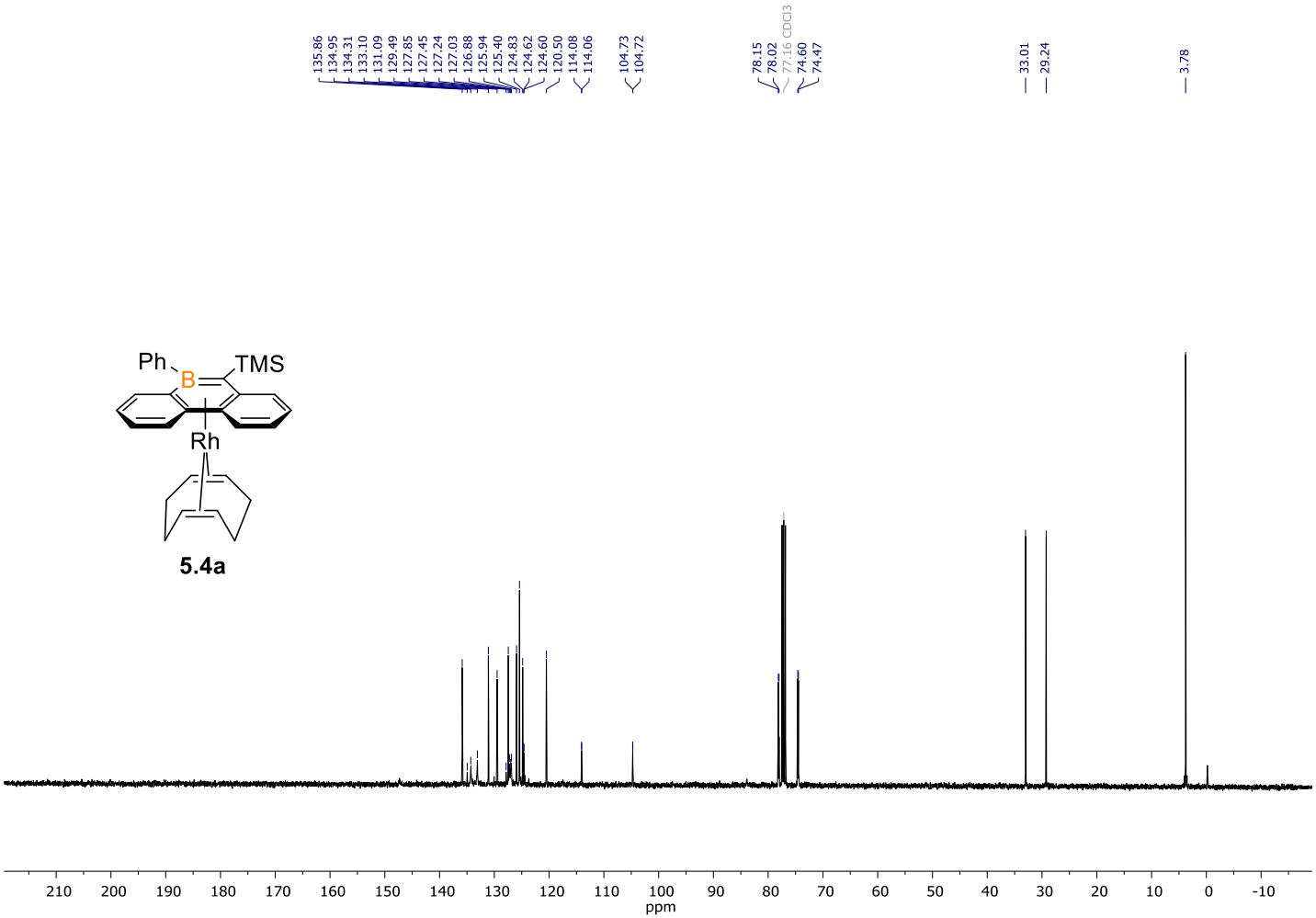

Figure D-4: $^{13}C\{^{1}H\}$ NMR spectrum of **5.4a** in $CDCl_3$.

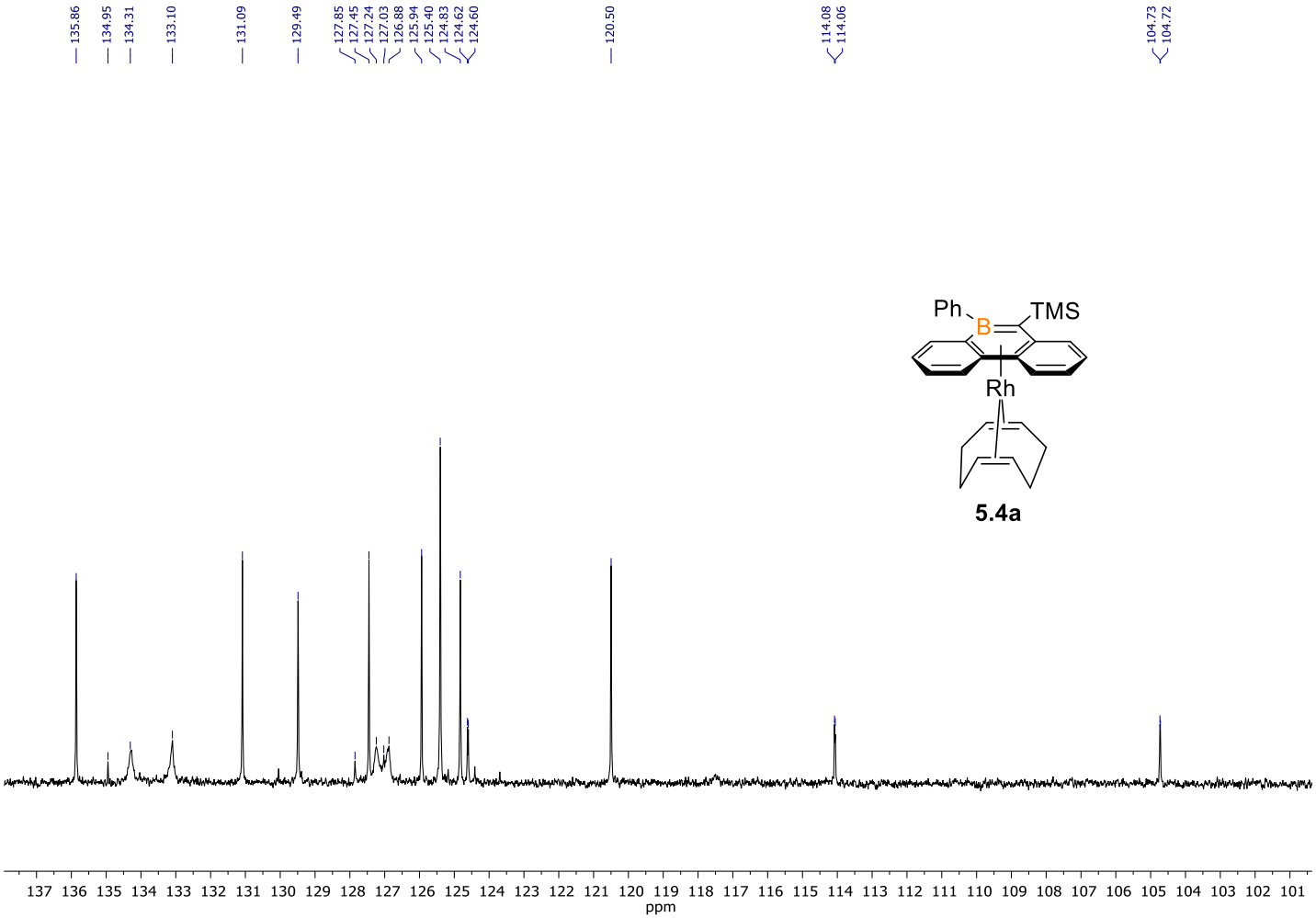

Figure D-5: Expansion of $^{13}C\{^{1}H\}$ NMR spectrum of **5.4a** in $CDCl_3$ (aryl region).

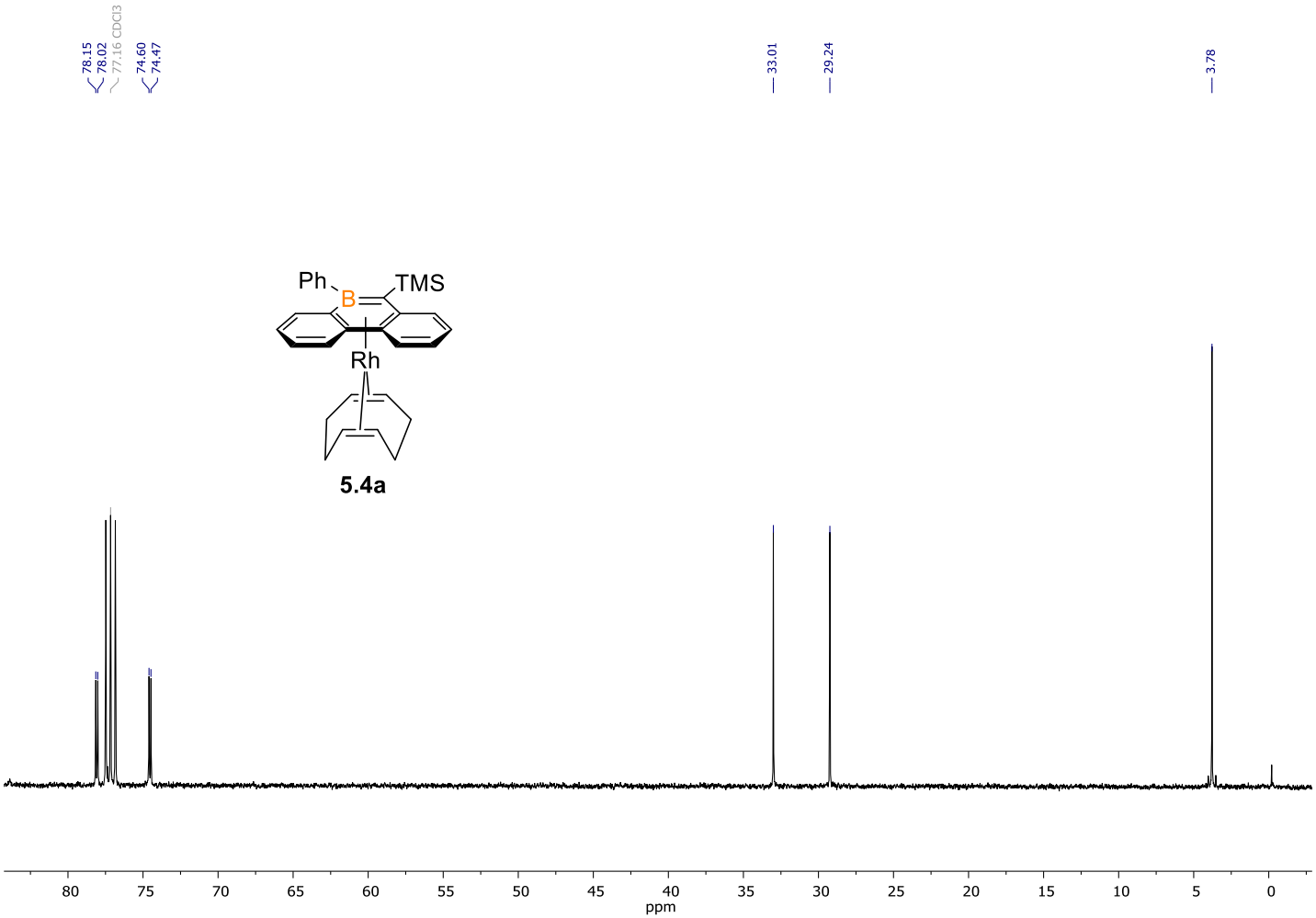

Figure D-6: Expansion of $^{13}C\{^{1}H\}$ NMR spectrum of **5.4a** in $CDCl_3$ (aliphatic region).

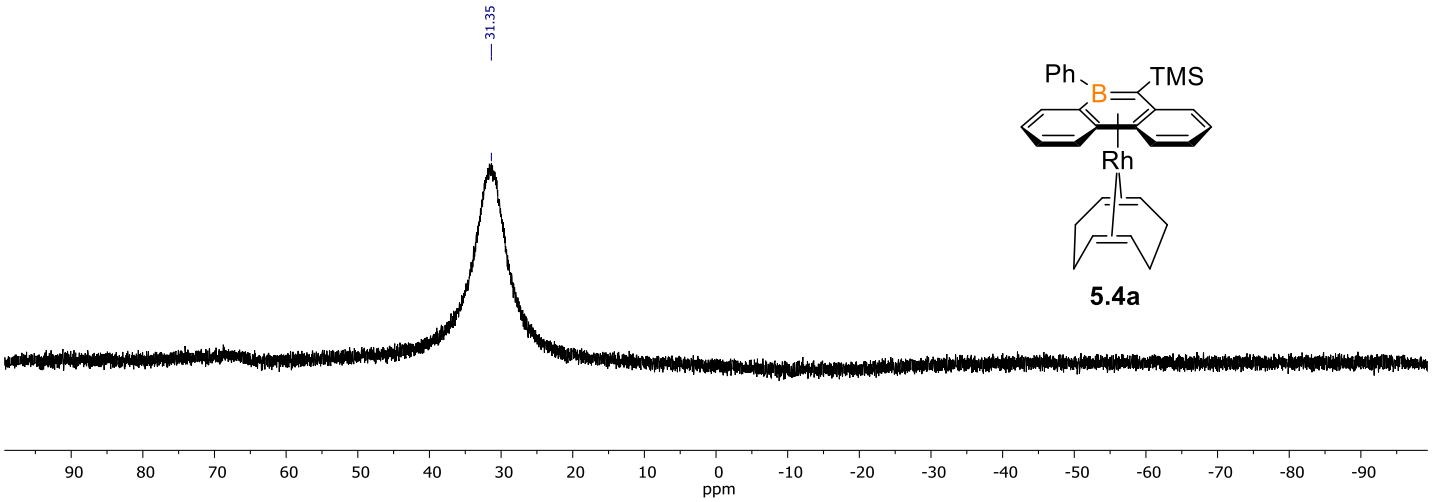

Figure D-7: ^{11}B NMR spectrum of **5.4a** in $CDCl_3$.

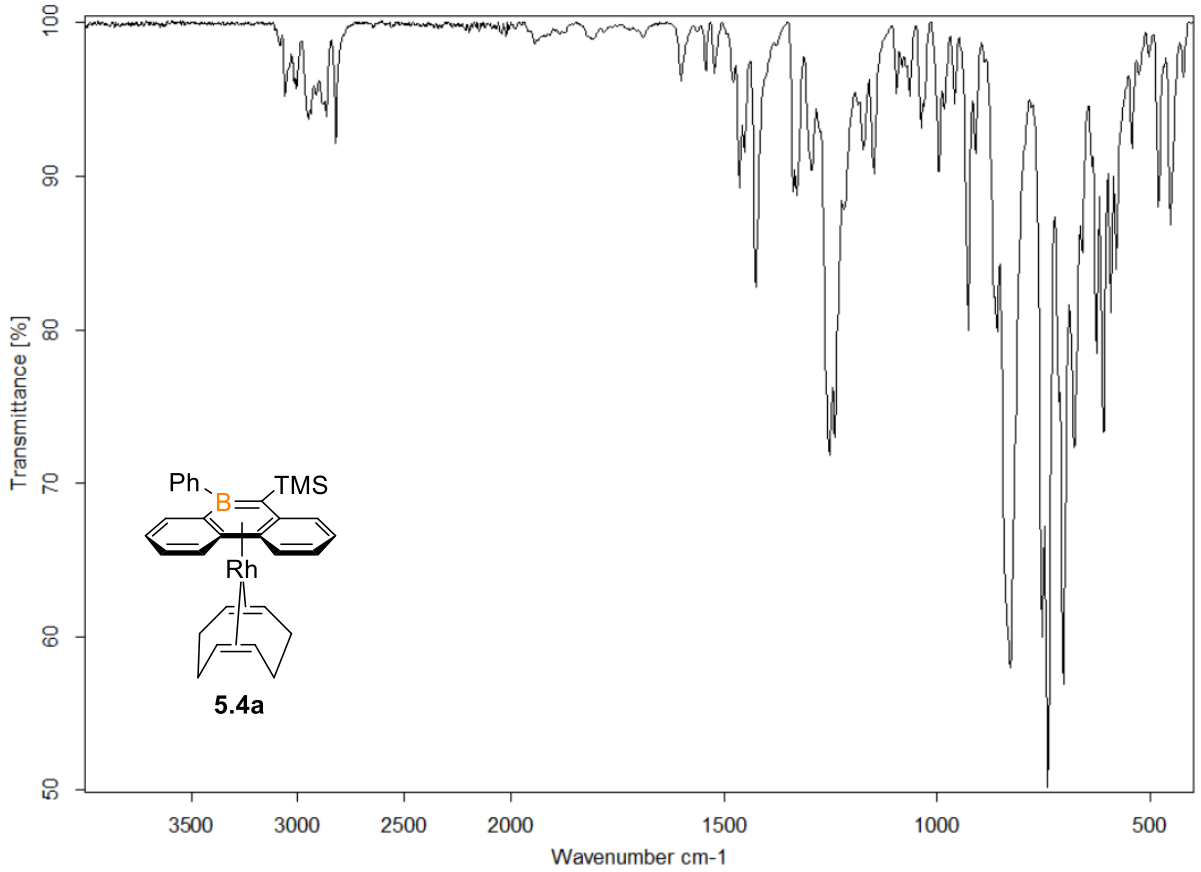

Figure D-8: FT-IR spectrum of **5.4a**.

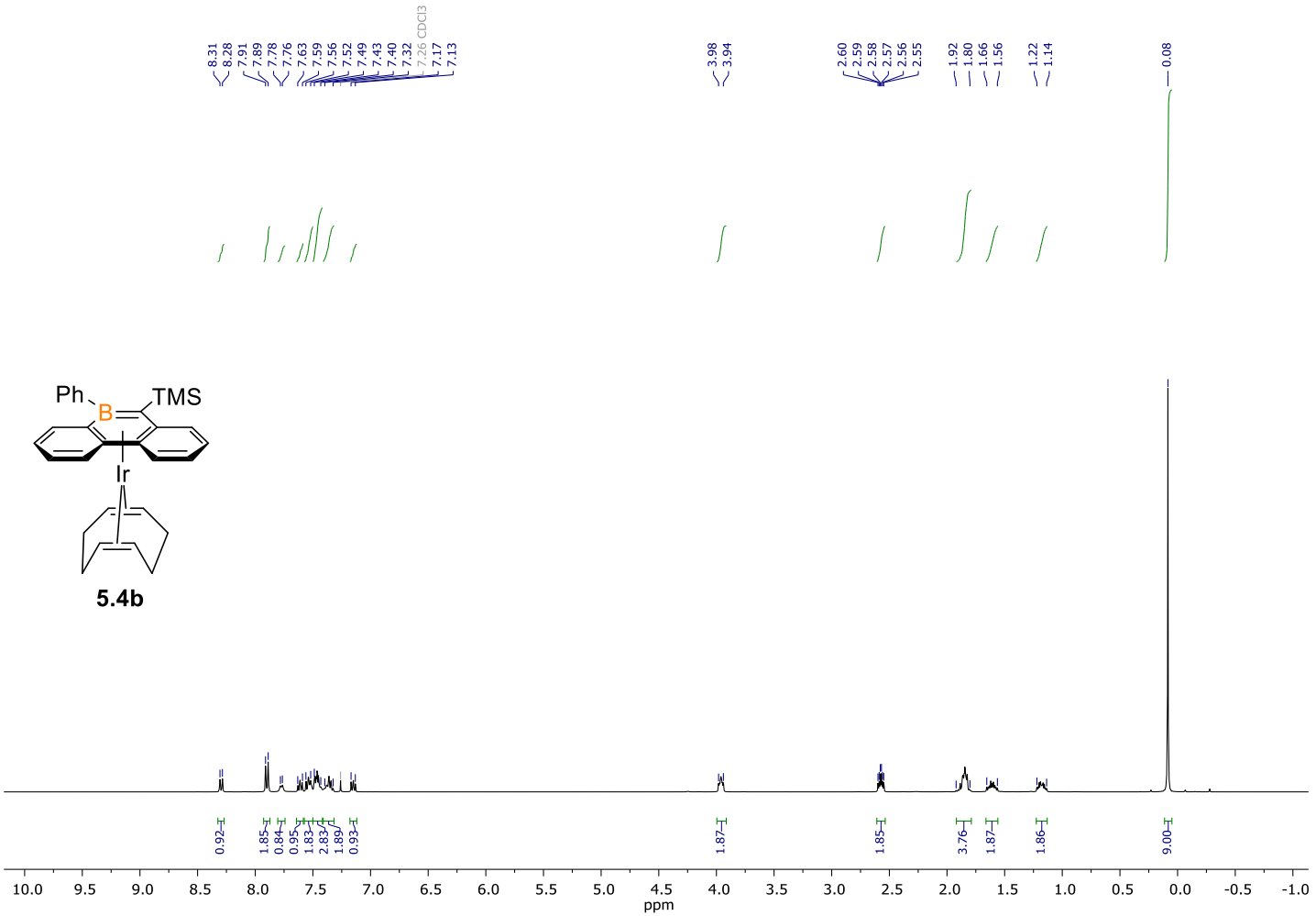

Figure D-9: ^{1}H NMR spectrum of **5.4b** in $CDCl_3$.

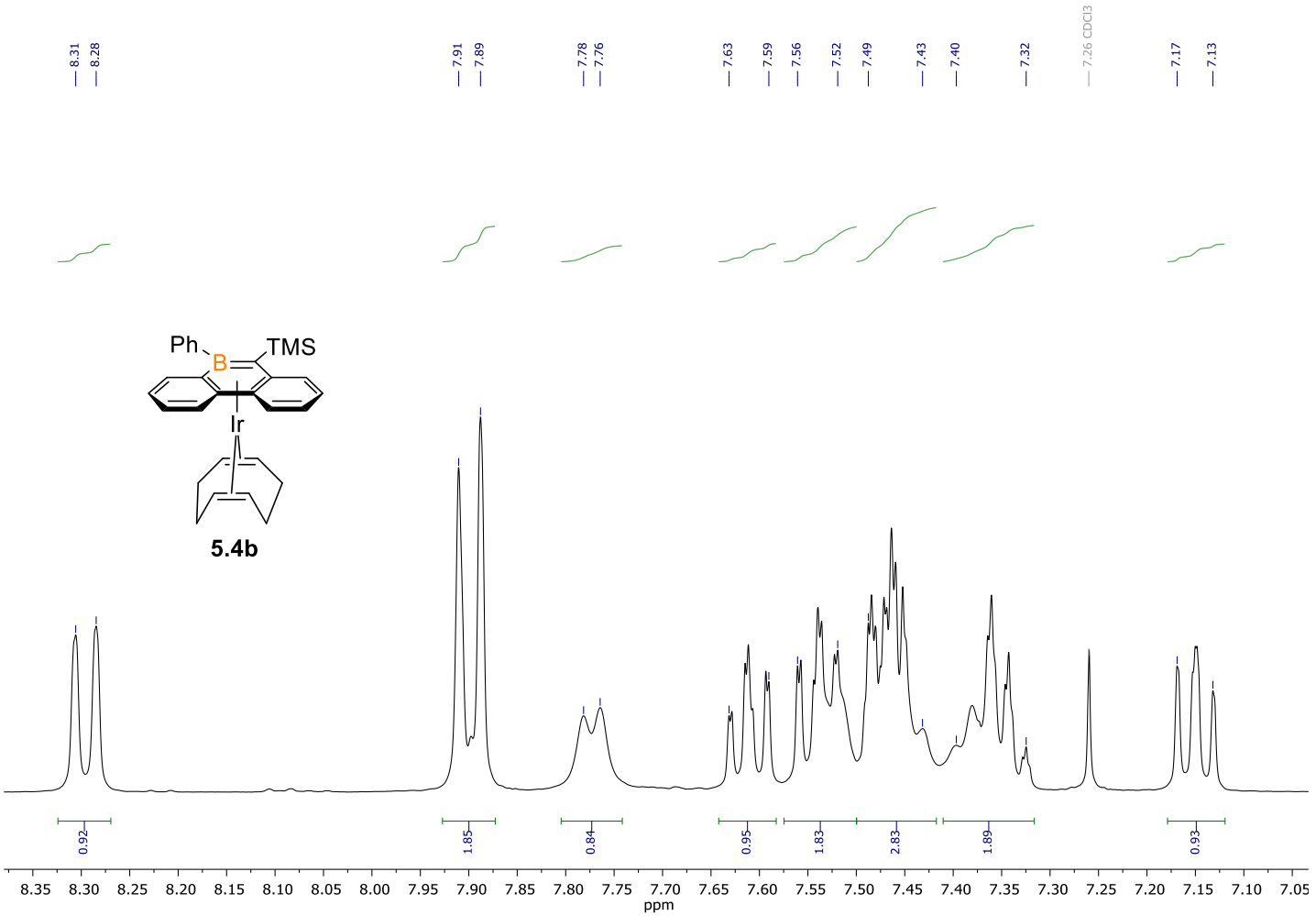

Figure D-10: Expansion of ^{1}H NMR spectrum of **5.4b** in $CDCl_3$ (aryl region).

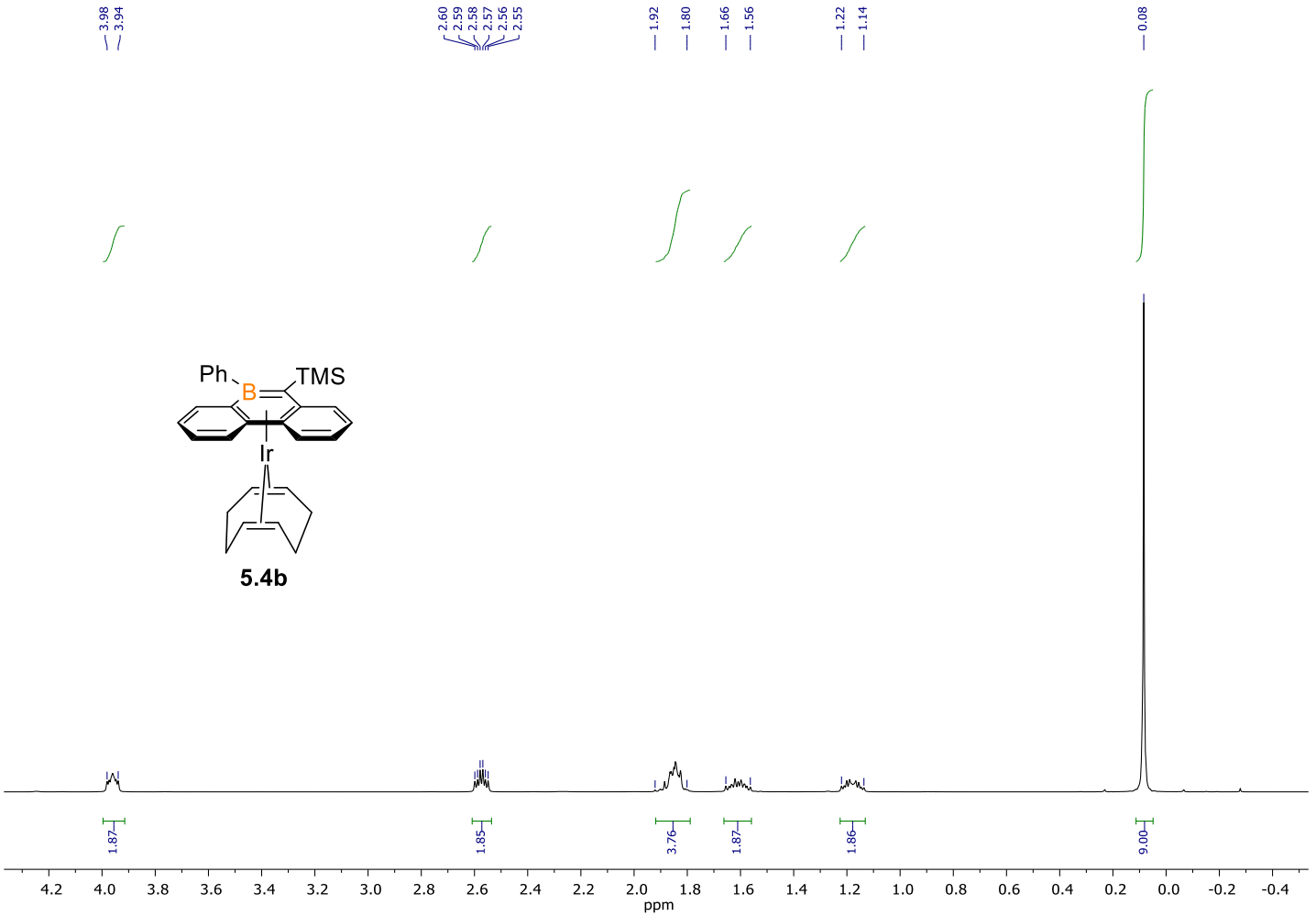

Figure D-11: Expansion of ^{1}H NMR spectrum of **5.4b** in $CDCl_3$ (aliphatic region).

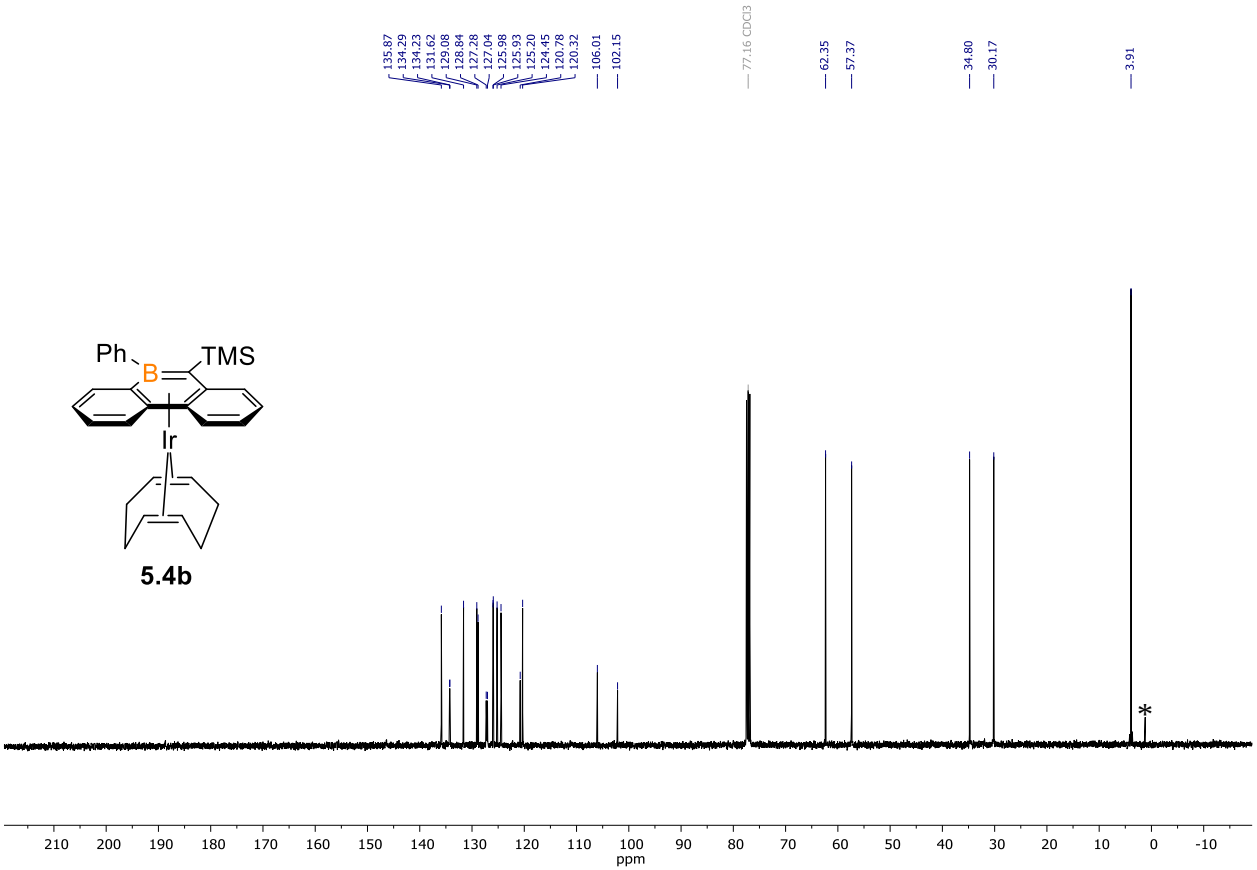

Figure D-12: $^{13}C\{^{1}H\}$ NMR spectrum of **5.4b** in $CDCl_3$ (* indicates grease).

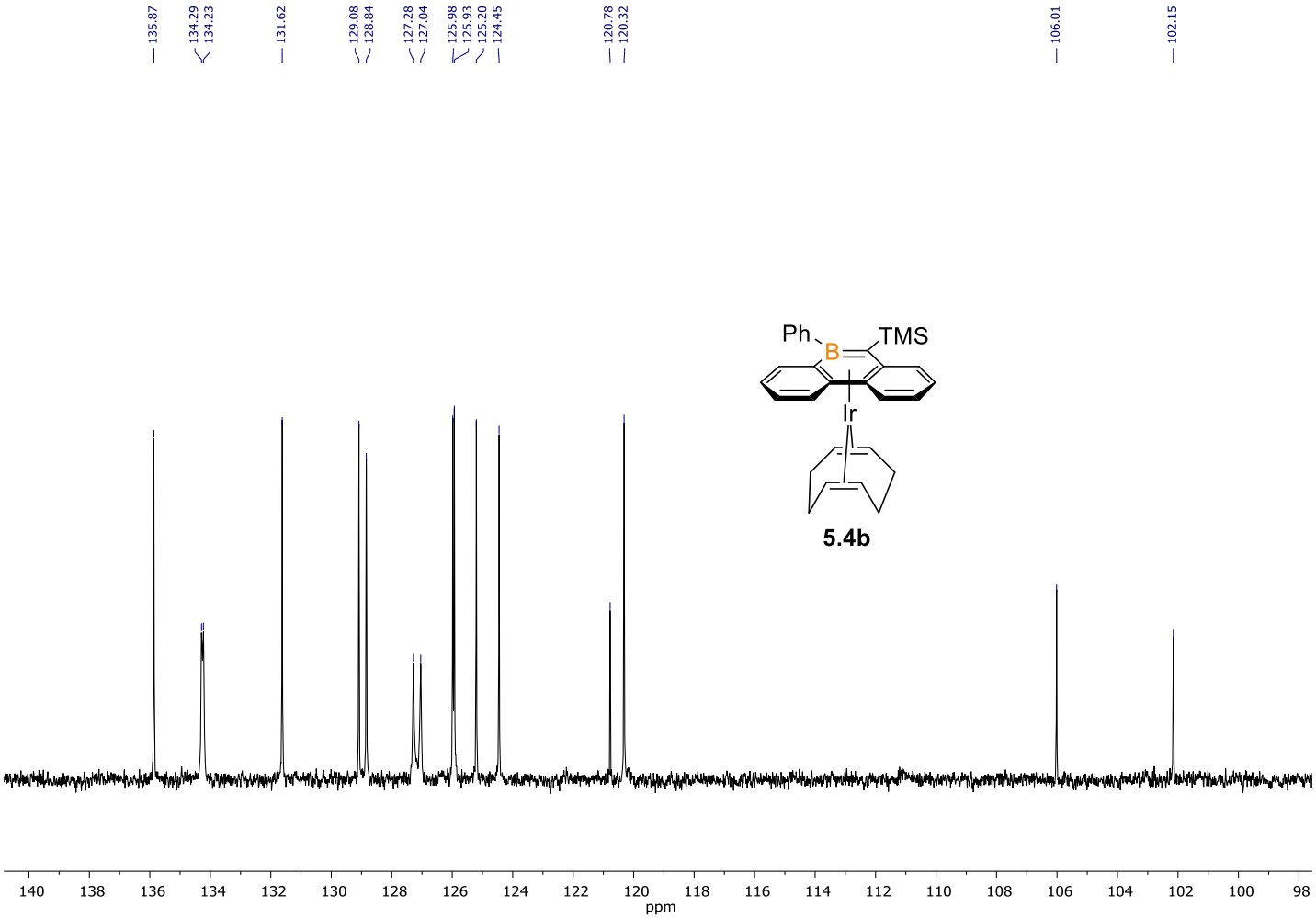

Figure D-13: Expansion of $^{13}C\{^{1}H\}$ NMR spectrum of **5.4b** in $CDCl_3$ (aryl region).

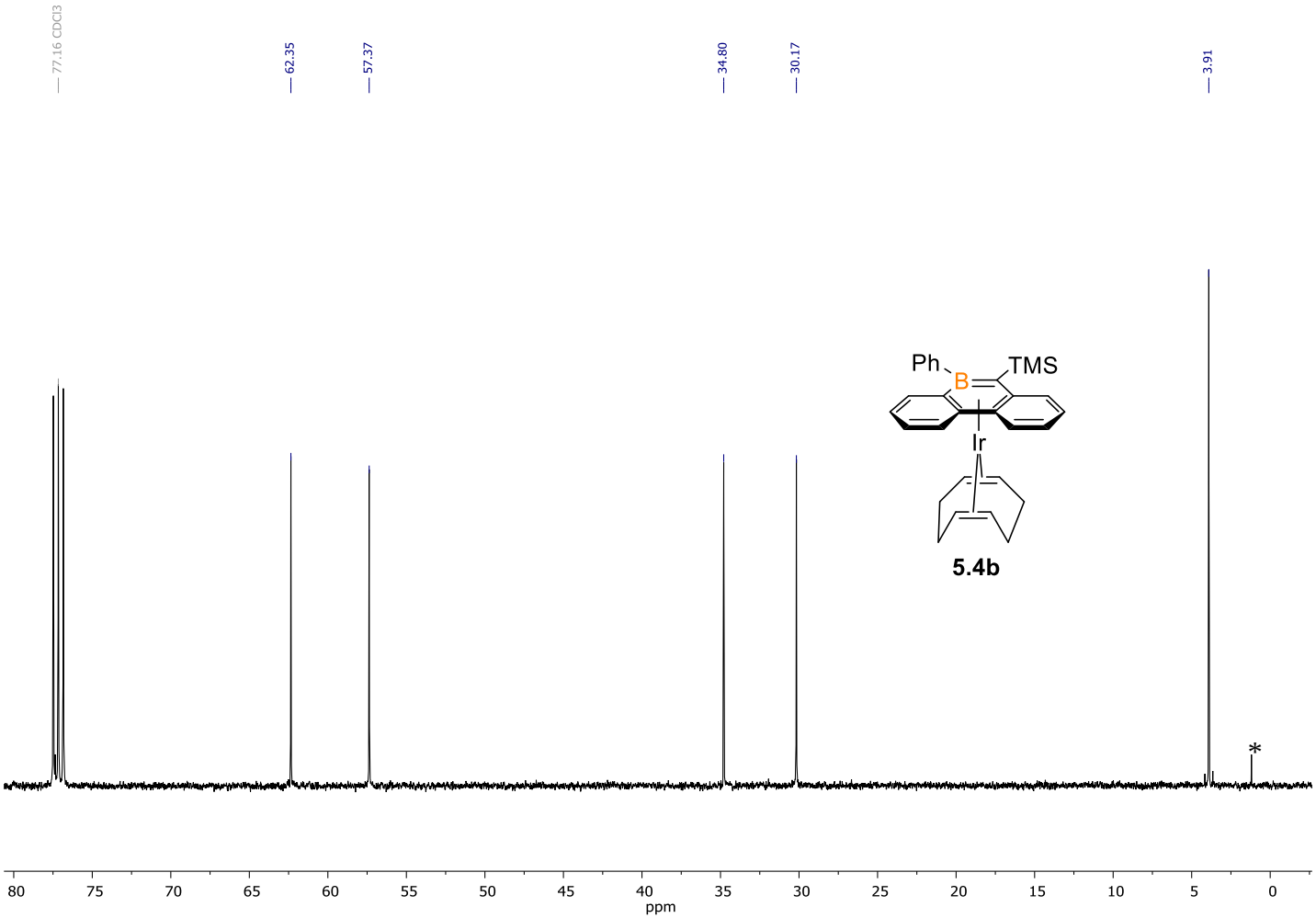

Figure D-14: Expansion of $^{13}C\{^{1}H\}$ NMR spectrum of **5.4b** in $CDCl_3$ (aliphatic region, * indicates grease).

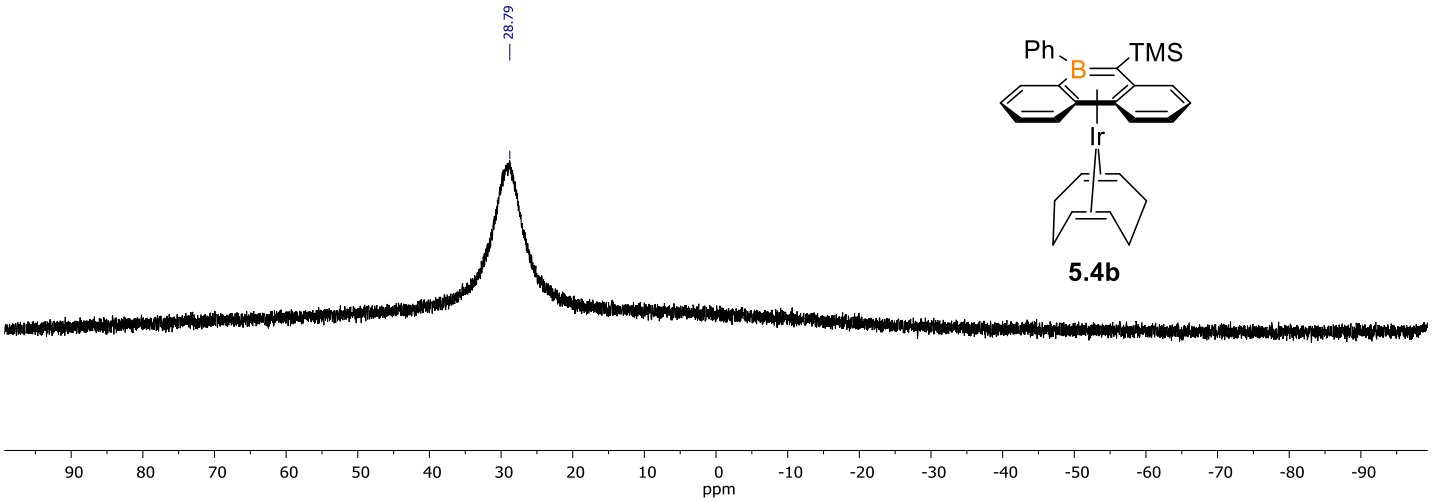

Figure D-15: ^{11}B NMR spectrum of **5.4b** in $CDCl_3$.

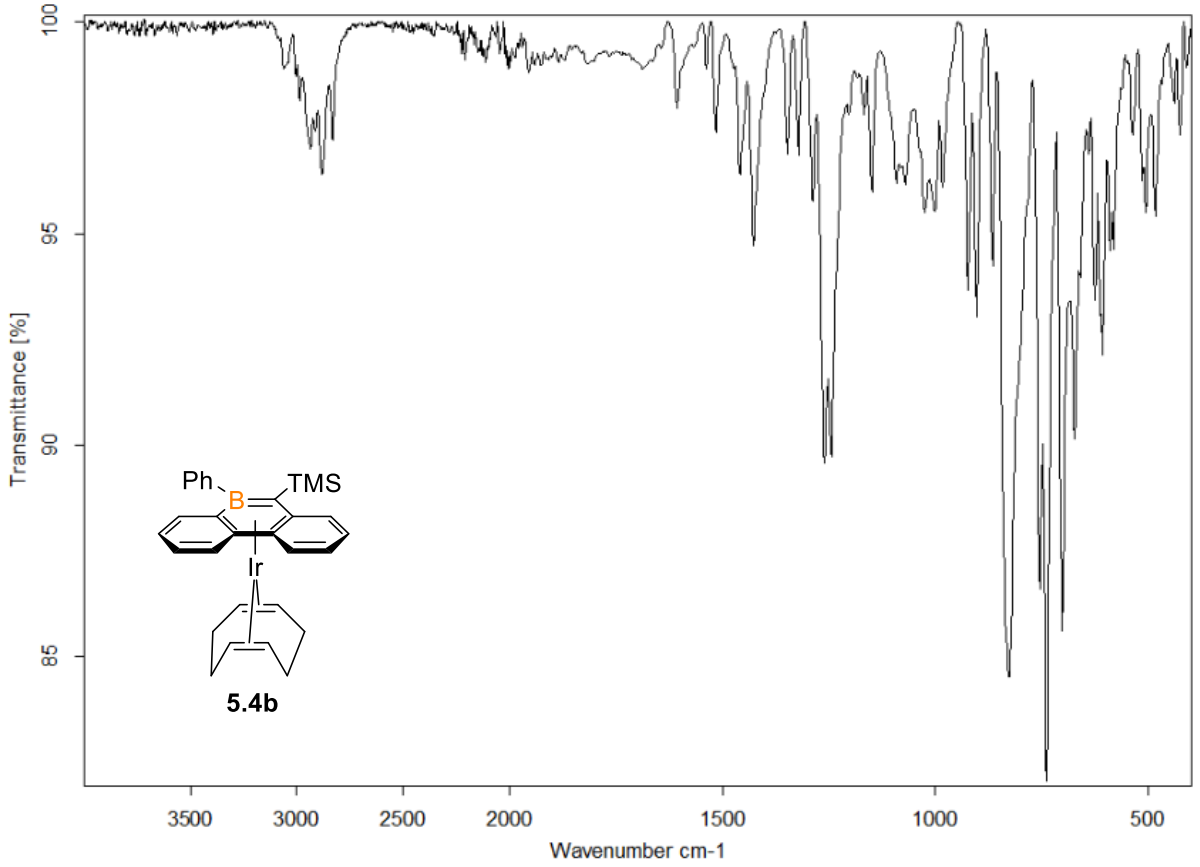

Figure D-16: FT-IR spectrum of **5.4b**.

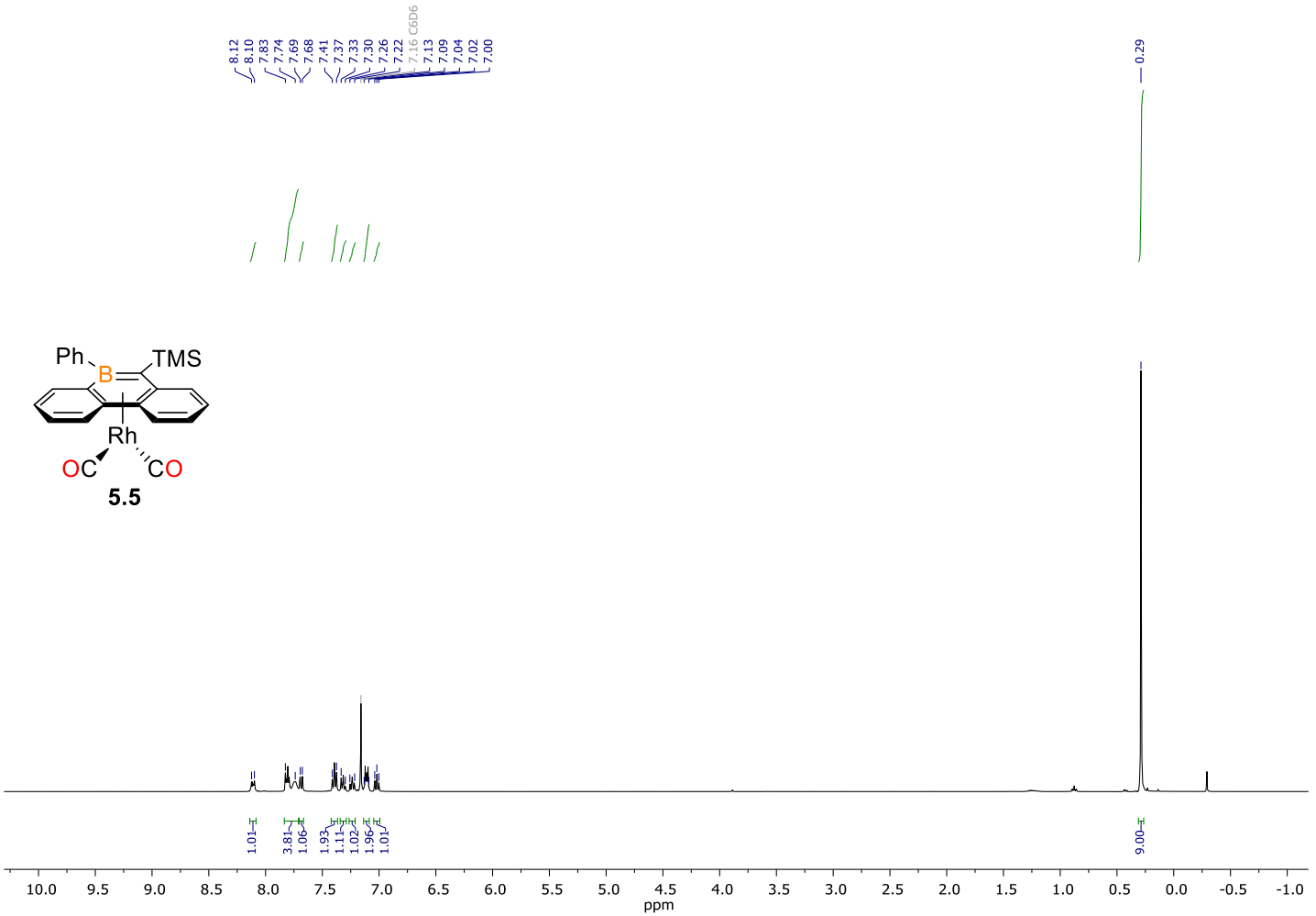

Figure D-17: ^{1}H NMR spectrum of **5.5** in C_6D_6.

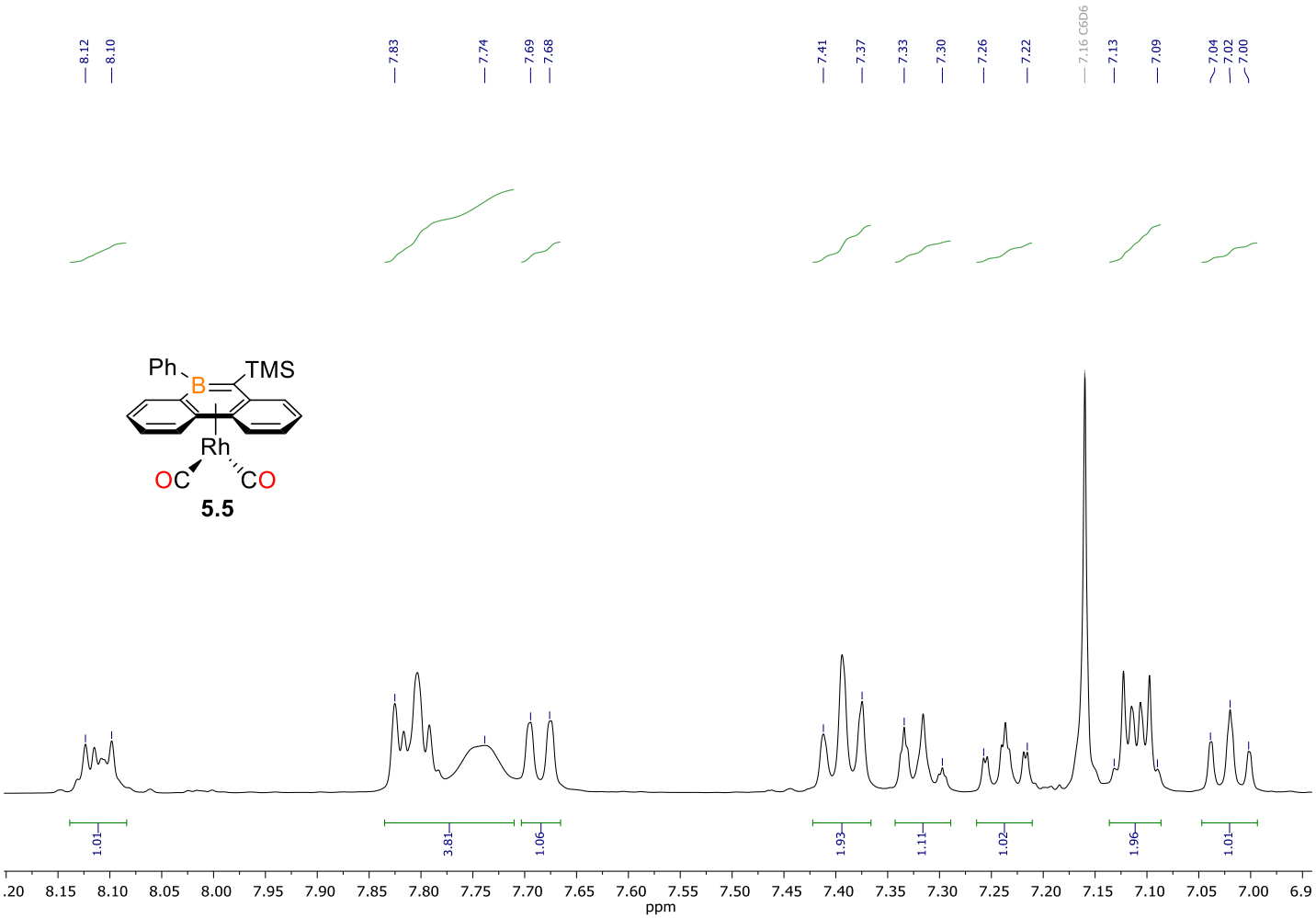

Figure D-18: Expansion of ^{1}H NMR spectrum of **5.5** in C_6D_6 (aryl region).

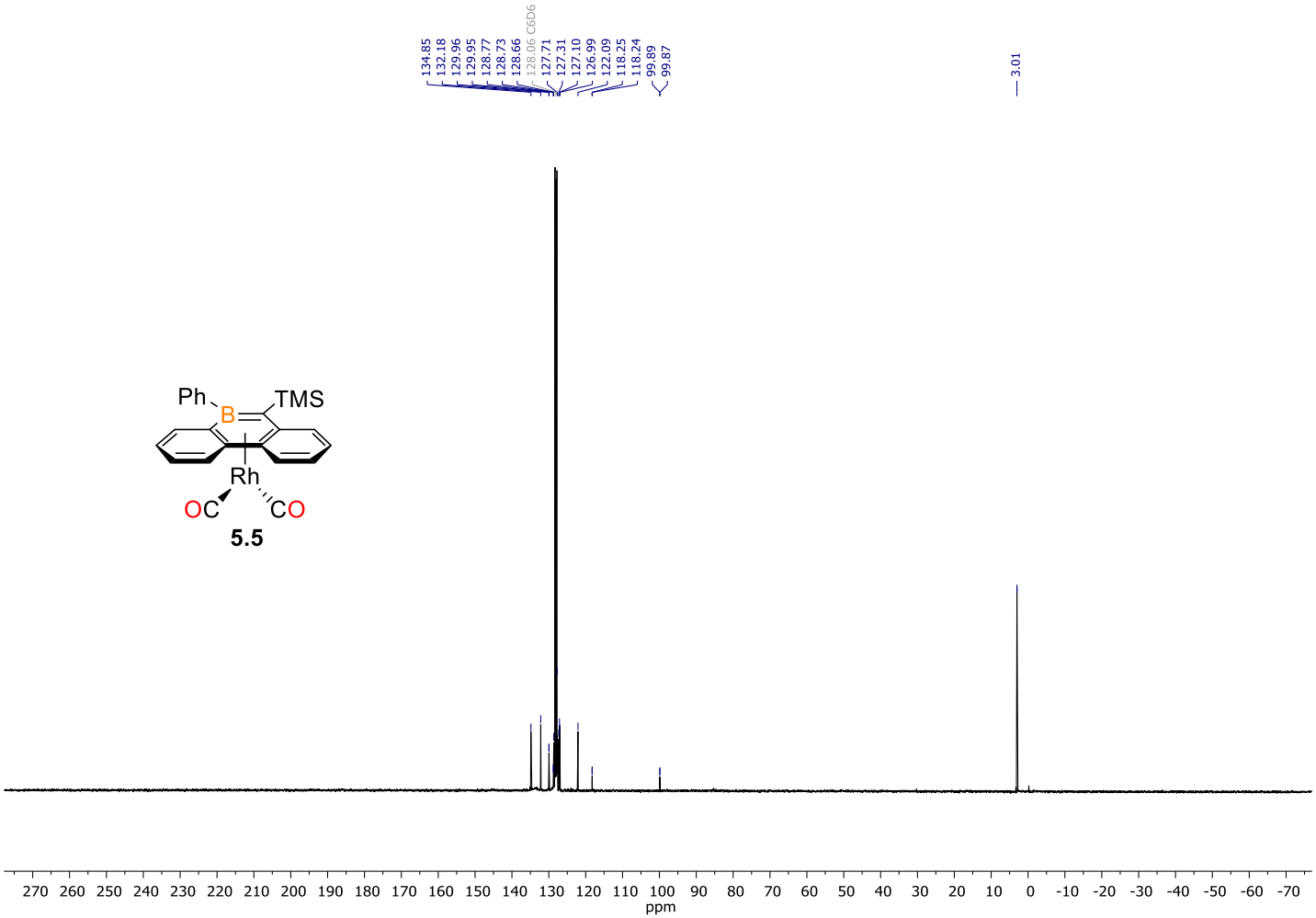

Figure D-19: $^{13}C\{^{1}H\}$ NMR spectrum of **5.5** in C_6D_6.

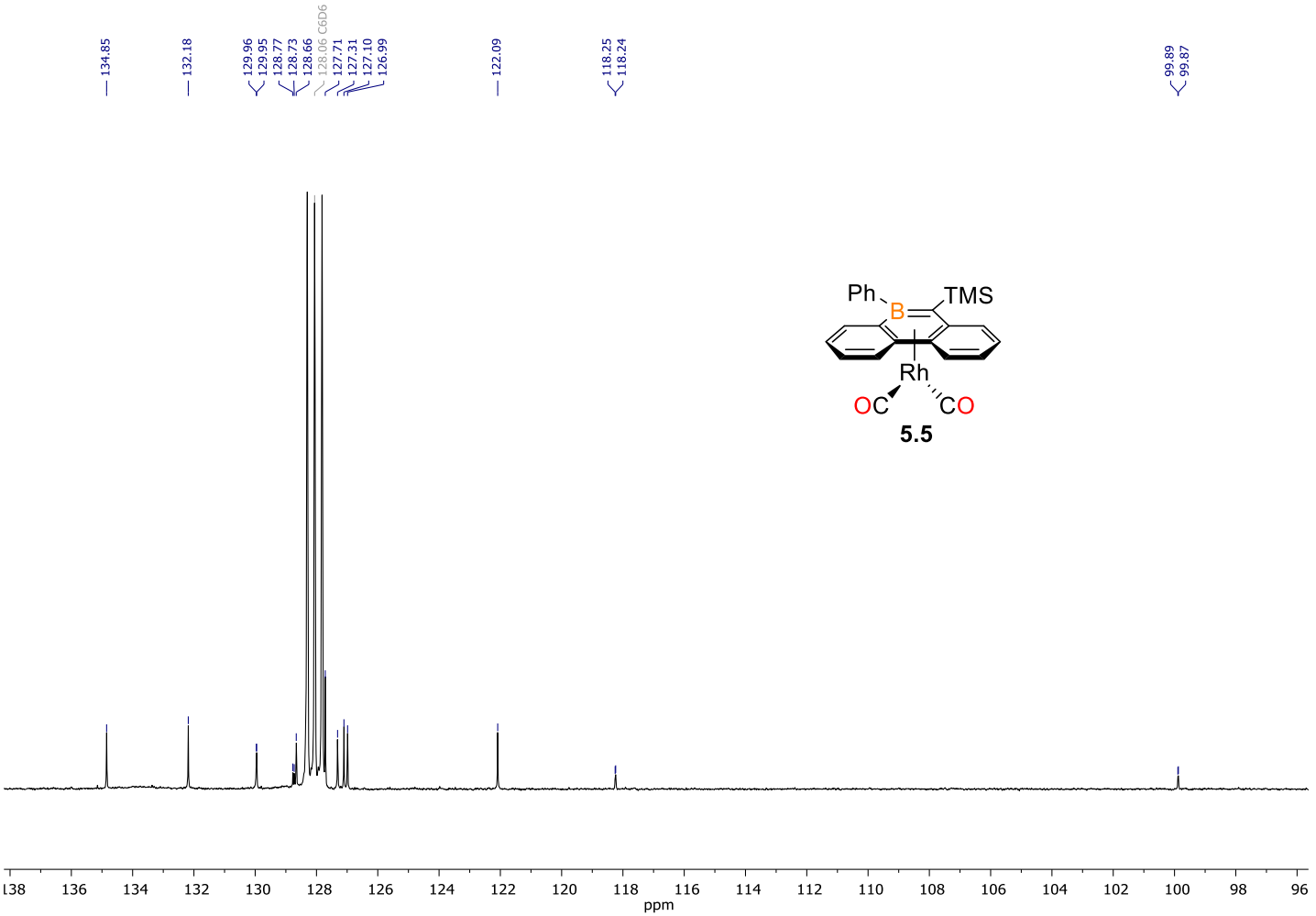

Figure D-20: Expansion of $^{13}C\{^{1}H\}$ NMR spectrum of **5.5** in C_6D_6 (aryl region).

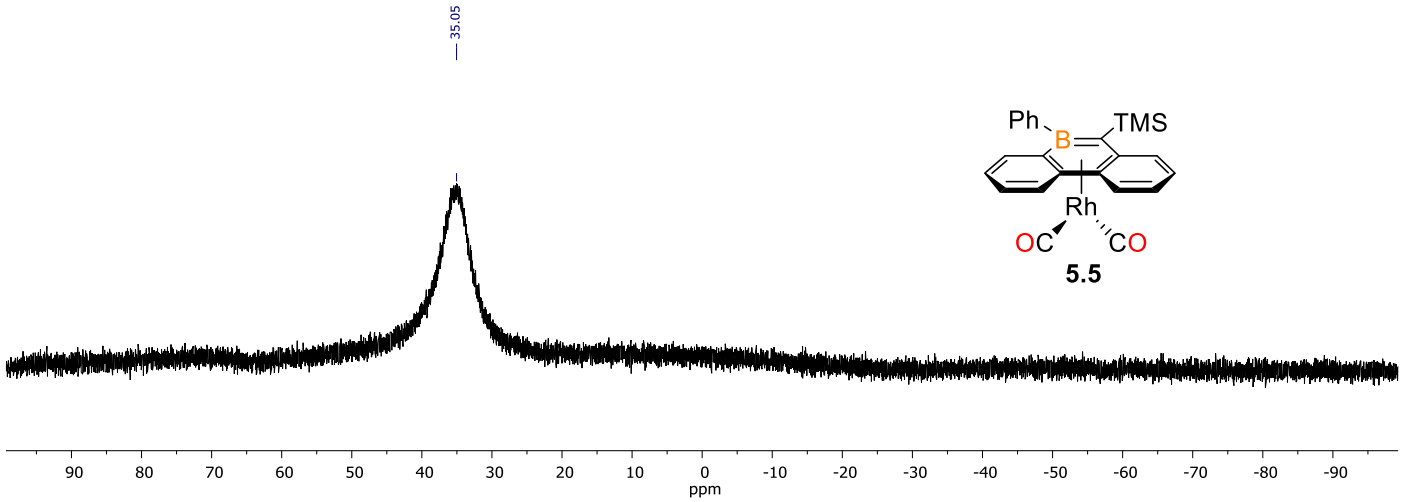

Figure D-21: ^{11}B NMR spectrum of **5.5** in C_6D_6.

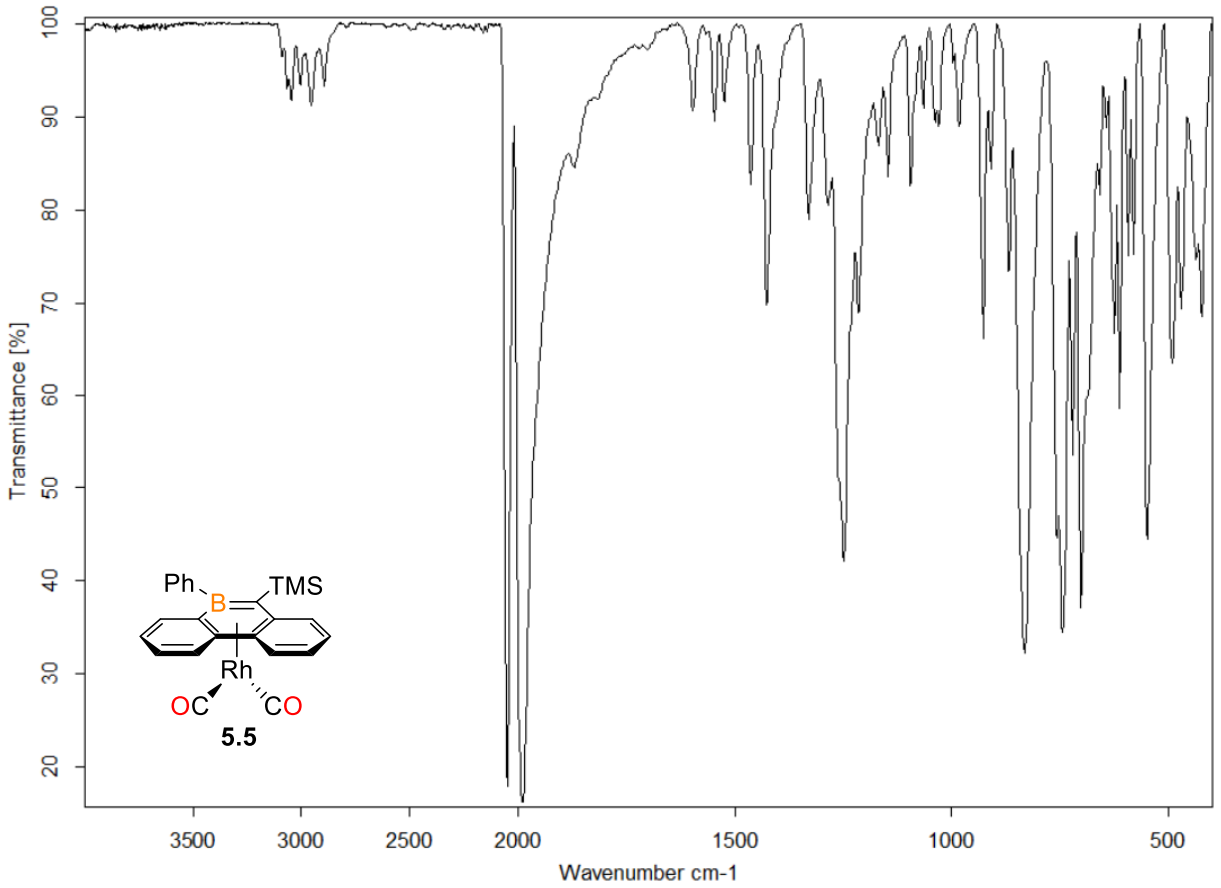

Figure D-22: FT-IR spectrum of **5.5**.

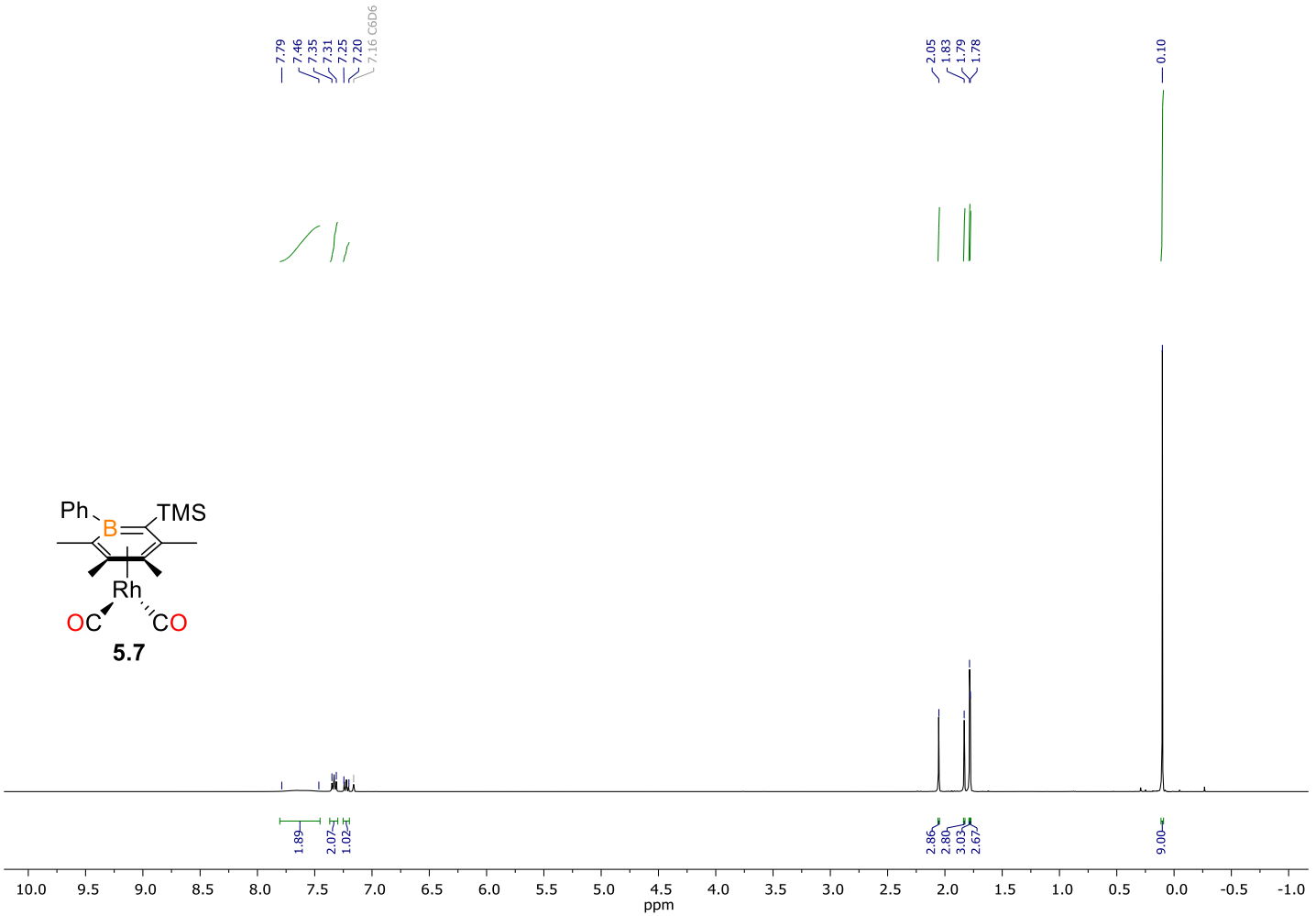

Figure D-23: ^{1}H NMR spectrum of **5.7** in C_6D_6.

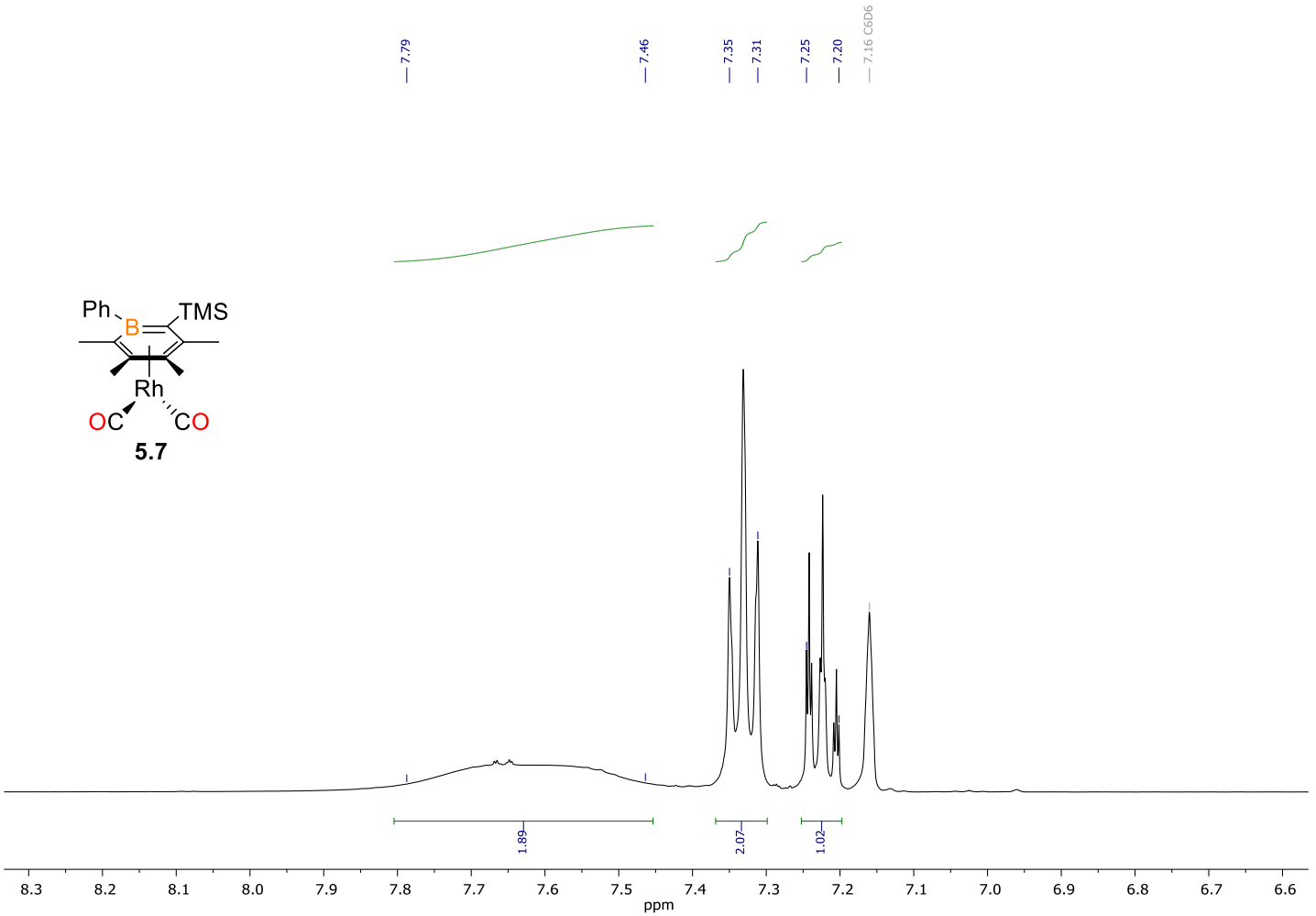

Figure D-24: Expansion of ^{1}H NMR spectrum of **5.7** in C_6D_6 (aryl region).

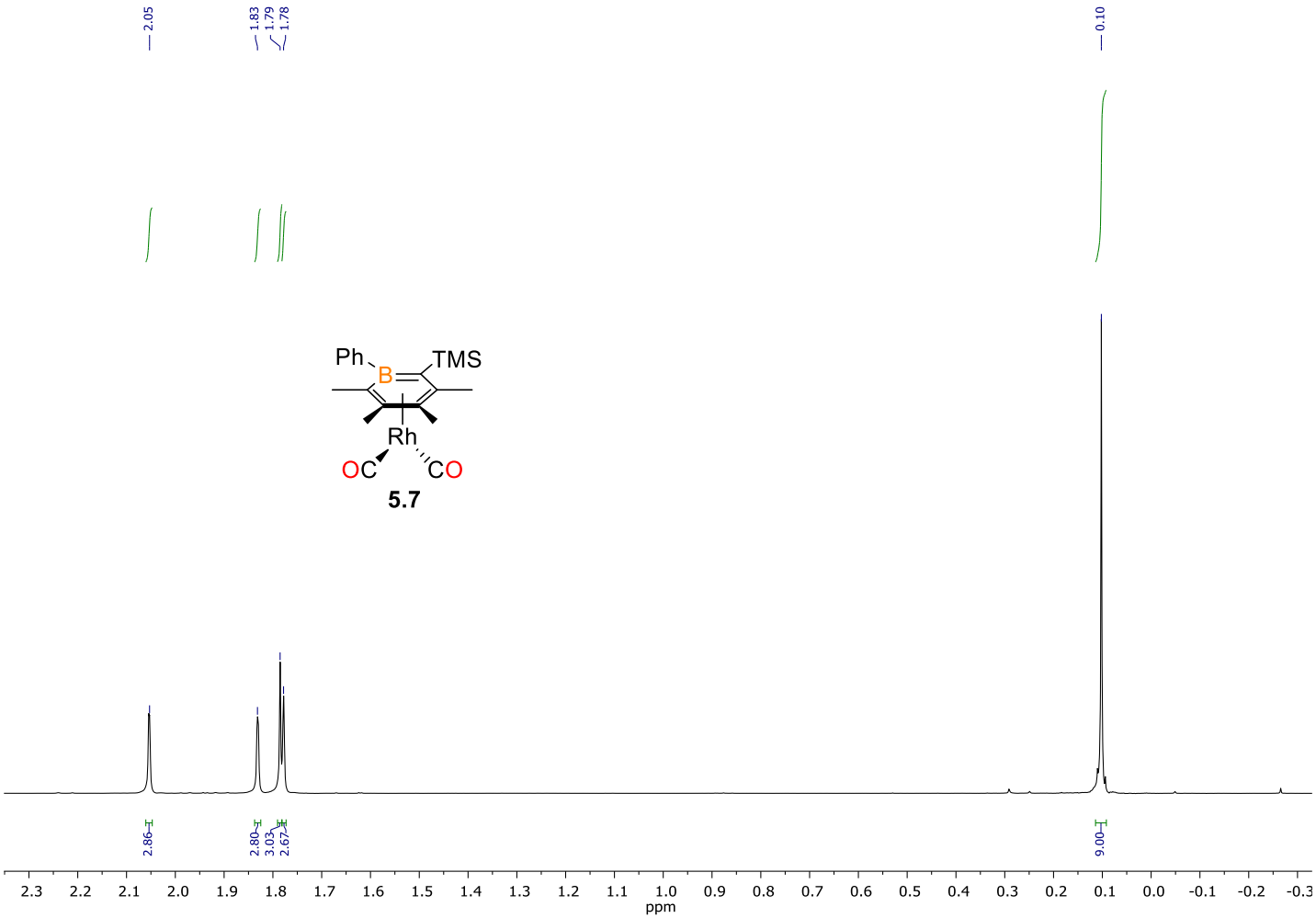

Figure D-25: Expansion of ^{1}H NMR spectrum of **5.7** in C_6D_6 (aliphatic region).

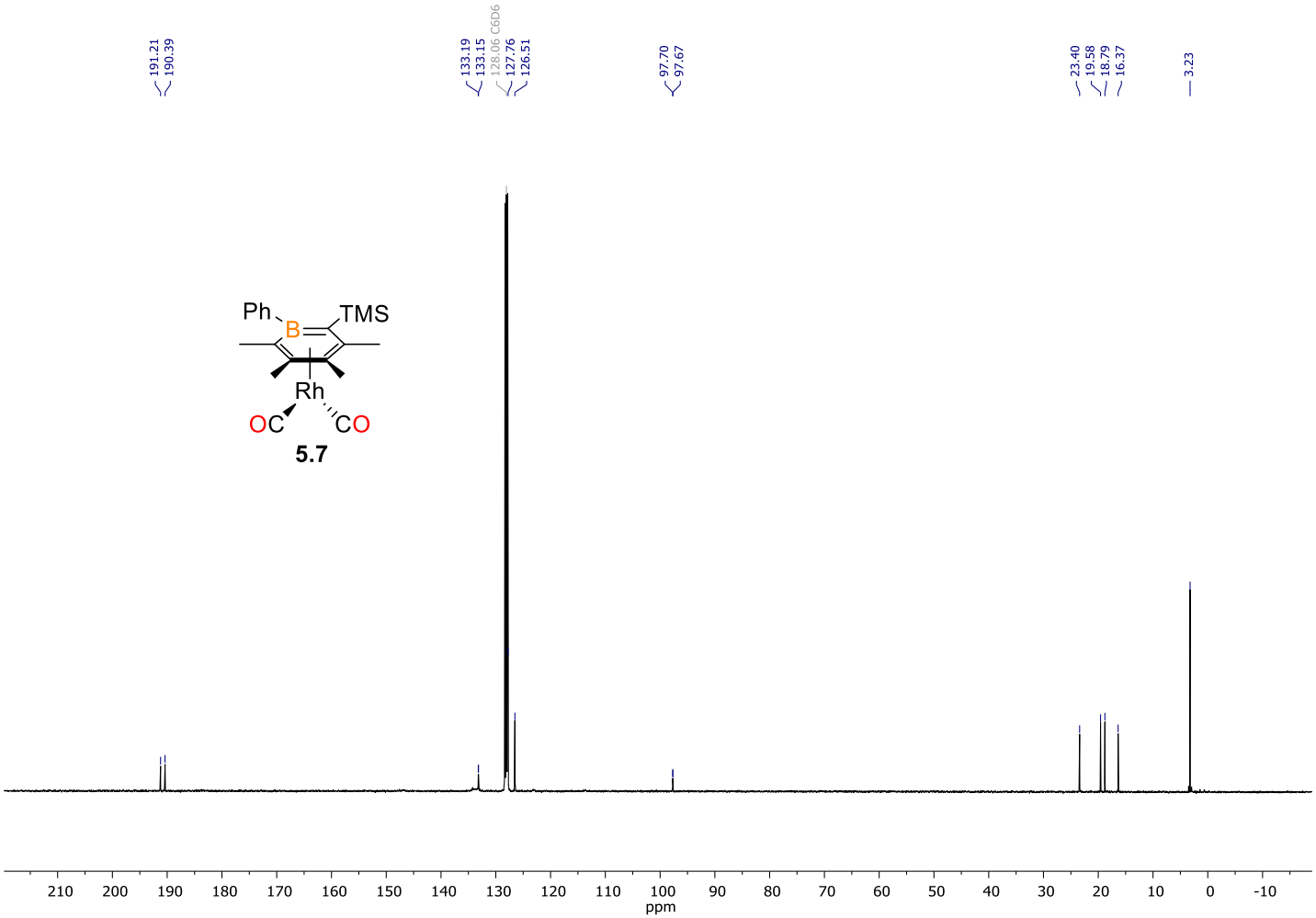

Figure D-26: $^{13}C\{^{1}H\}$ NMR spectrum of **5.7** in C_6D_6.

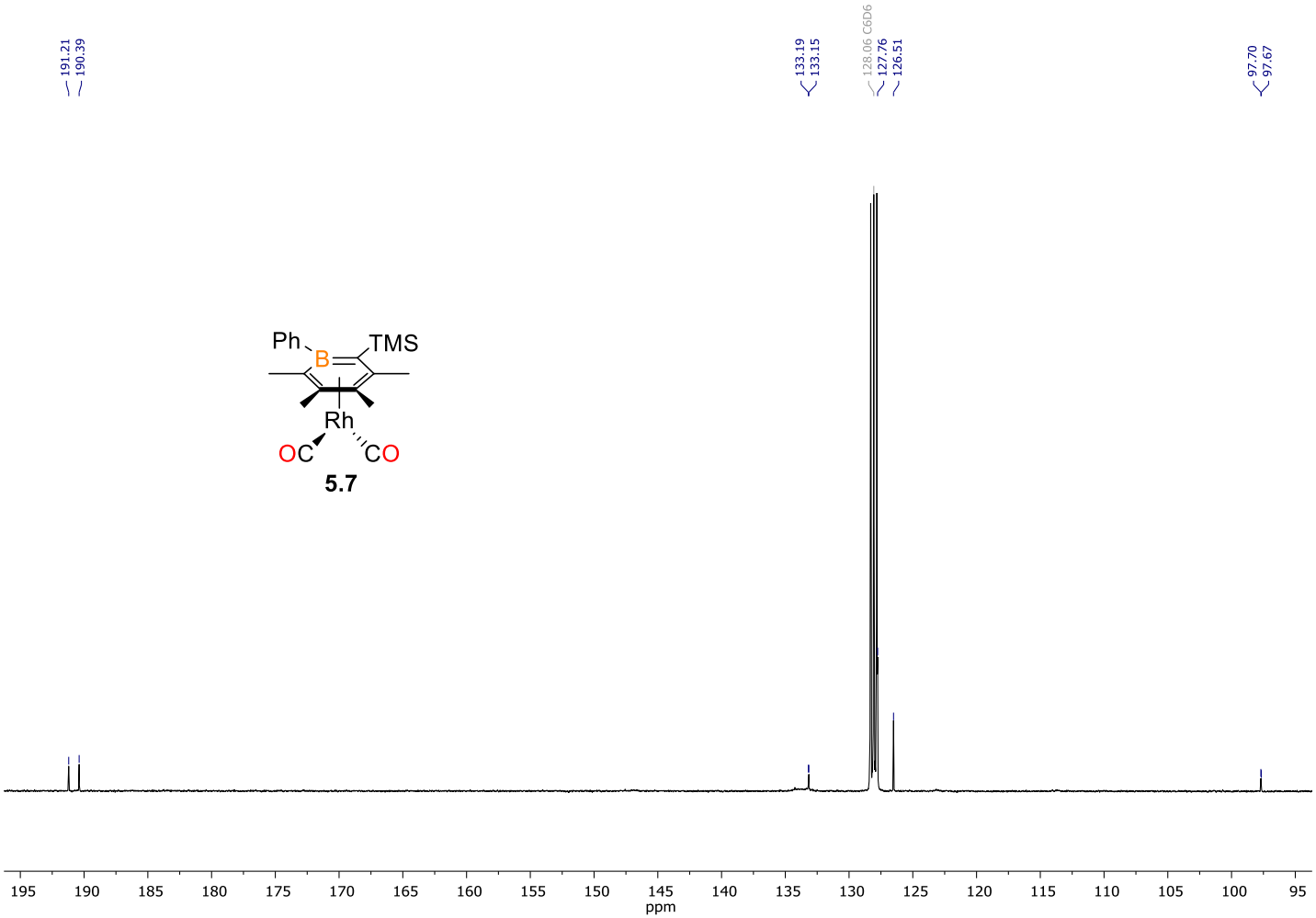

Figure D-27: Expansion of $^{13}C\{^{1}H\}$ NMR spectrum of **5.7** in C_6D_6 (aryl region).

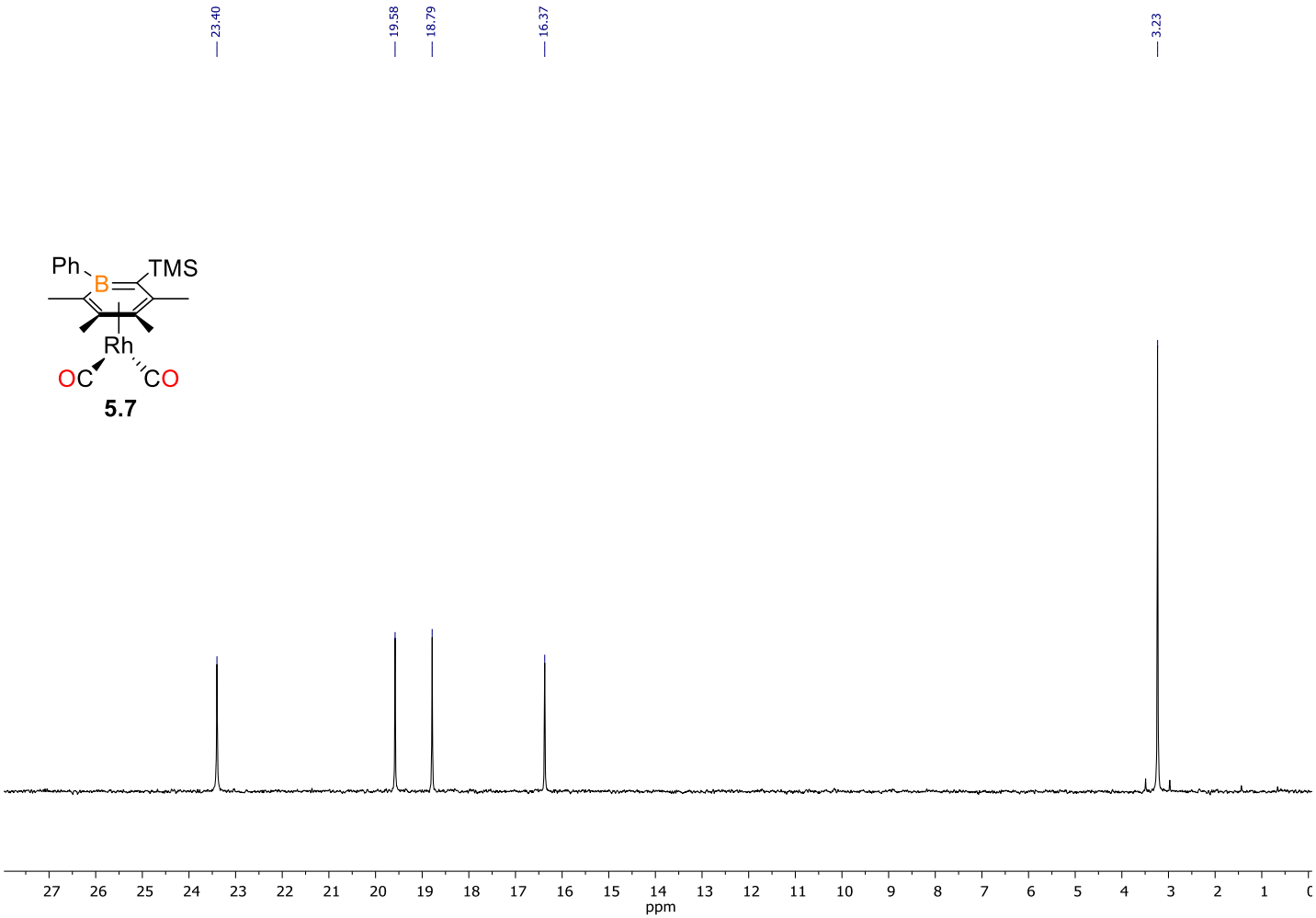

Figure D-28: Expansion of $^{13}C\{^{1}H\}$ NMR spectrum of **5.7** in C_6D_6 (aliphatic region).

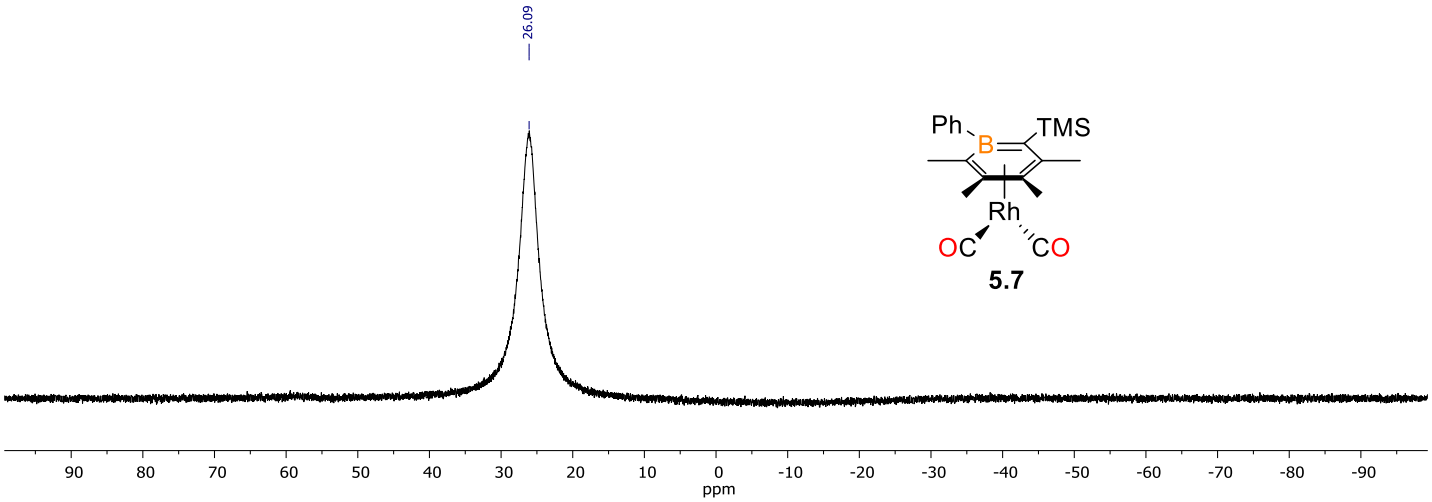

Figure D-29: ^{11}B NMR spectrum of **5.7** in C_6D_6.

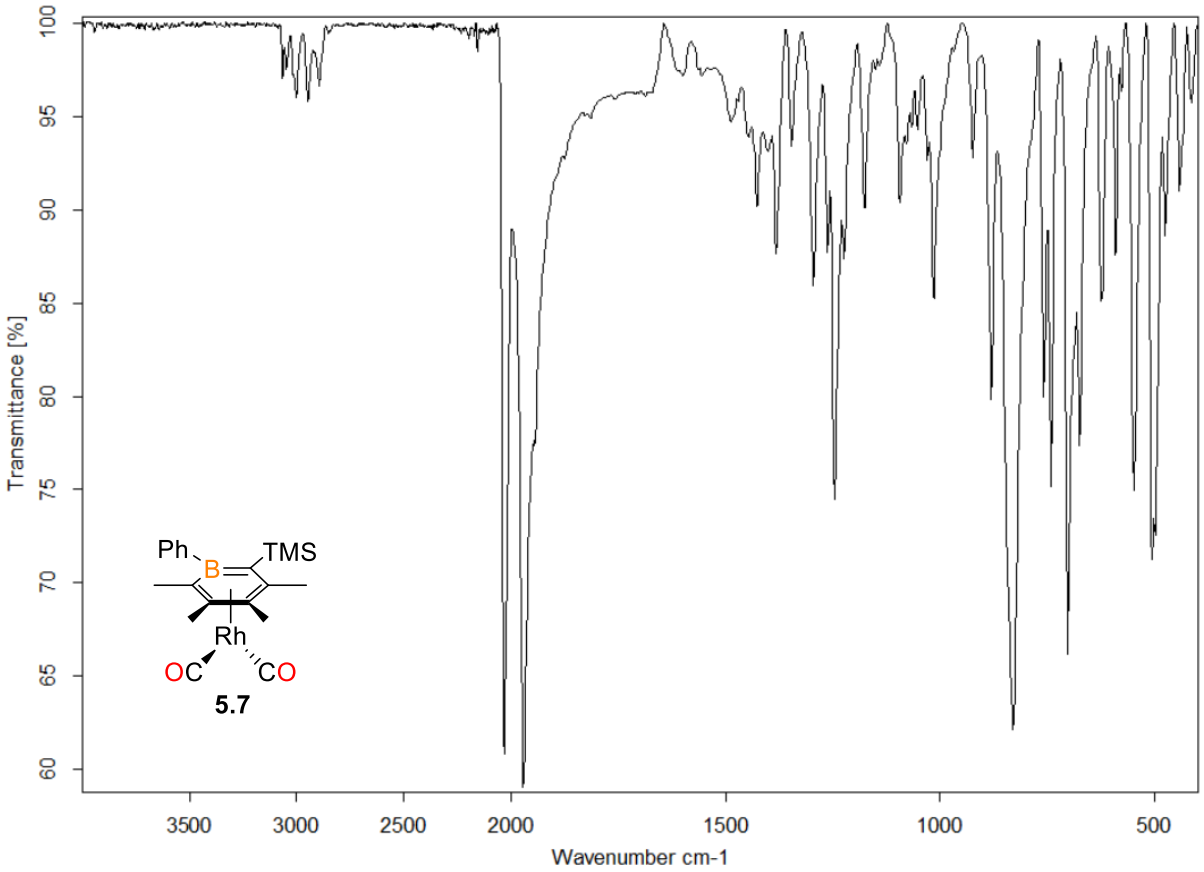

Figure D-30: FT-IR spectrum of **5.7**.

Table D-1: X-ray crystallographic details for **5.4a**, **5.4b**, **5.5**, **5.7**, **5.8**, **5.9**, and **5.10**.

Compound	**5.4a**	**5.4b**	**5.5**	**5.7**	**5.8**	**5.9**	**5.10**
CCDC							
Empirical Formula	$C_{30}H_{34}BRhSi$	$C_{30}H_{34}BIrSi$	$C_{24}H_{22}BO_2RhSi$	$C_{20}H_{26}BO_2RhSi$	$C_{50}H_{50}B_2FeSi_2$	$C_{48}H_{50}B_2FeN_2Si_2$	$C_{27}H_{27}BFeSi$
FW (g/mol)	536.38	625.67	484.22	440.22	784.55	788.55	446.23
Crystal System	Monoclinic	Monoclinic	Monoclinic	Monoclinic	Monoclinic	Triclinic	Orthorhombic
Space Group	P 2_1/n	P 2_1	P 2_1/n	P 2_1/c	P 2_1/n	P -1	P 2_1 2_1 2_1
a (Å)	8.0857(2)	8.1159(2)	12.3516(9)	17.3967(5)	13.2047(5)	11.811(1)	9.2649(10)
b (Å)	26.1897(8)	16.8603(4)	13.2338(9)	7.7875(2)	12.4134(4)	12.1808(9)	13.9458(15)
c (Å)	11.9546(4)	10.0230(3)	13.6808(9)	15.7760(4)	25.6818(8)	14.7978(12)	34.370(4)
α (deg)	90	90	90	90	90	80.932(3)	90
β (deg)	91.4112(10)	113.3504(8)	95.797(3)	105.7830(9)	96.7741(14)	79.441(3)	90
γ (deg)	90	90	90	90	90	76.351(3)	90
V (Å^3)	2530.76(13)	1259.18(6)	2224.8(3)	2056.70(10)	4180.2(2)	2019.1(3)	4440.8(9)
Z	4	2	4	4	4	2	8
D_c (g cm^{-3})	1.408	1.650	1.446	1.422	1.247	1.297	1.335
Radiation λ (Å)	0.71073	0.71073	0.71073	0.71073	0.71073	0.71073	0.71073
Temp (K)	150	150	150	150	150	150	150
R1 [I>2(σ)I][a]	0.0470	0.0297	0.0591	0.0181	0.0485	0.0639	0.1166
wR2 (F^2)[a]	0.1368	0.0892	0.1519	0.0460	0.1224	0.1703	0.2865
GOF (S)[a]	1.355	1.259	1.215	1.093	1.011	1.088	1.156

[a] $R1(F[I > 2(I)]) = \sum\|\|F_o| - |F_c\|\| / \sum |F_o|$; $wR2(F^2 \text{ [all data]}) = [w(F_o^2 - F_c^2)^2]^{1/2}$; $S(\text{all data}) = [w(F_o^2 - F_c^2)^2/(n - p)]^{1/2}$ (n = no. of data; p = no. of parameters varied; $w = 1/[^2(F_o^2) + (aP)^2 + bP]$ where $P = (F_o^2 + 2F_c^2)/3$ and a and b are constants suggested by the refinement program.

REFERENCES

1. Bosdet, M. J. D.; Piers, W. E., B-N as a C-C substitute in aromatic systems. *Can. J. Chem.* **2009**, *87*, 8-29.

2. Braunschweig, H.; Hörl, C.; Mailänder, L.; Radacki, K.; Wahler, J., Antiaromaticity to Aromaticity: From Boroles to 1,2-Azaborinines by Ring Expansion with Azides. *Chem. Eur. J.* **2014**, *20*, 9858-9861.

3. Escande, A.; Ingleson, M. J., Fused polycyclic aromatics incorporating boron in the core: fundamentals and applications. *Chem. Commun.* **2015**, *51*, 6257-6274.

4. Barnard, J. H.; Yruegas, S.; Huang, K.; Martin, C. D., Ring expansion reactions of anti-aromatic boroles: a promising synthetic avenue to unsaturated boracycles. *Chem. Commun.* **2016**, *52*, 9985-9991.

5. Bélanger-Chabot, G.; Braunschweig, H.; Roy, D. K., Recent Developments in Azaborinine Chemistry. *Eur. J. Inorg. Chem.* **2017**, 4353-4368.

6. Giustra, Z. X.; Liu, S.-Y., The State of the Art in Azaborine Chemistry: New Synthetic Methods and Applications. *J. Am. Chem. Soc.* **2018**, *140*, 1184-1194.

7. Eisch, J. J.; Hota, N. H.; Kozima, S., Synthesis of pentaphenylborole, a potentially antiaromatic system. *J. Am. Chem. Soc.* **1969**, *91*, 4575-4577.

8. Ashe III, A. J.; Shu, P., The 1-Phenylborabenzene Anion. *J. Am. Chem. Soc.* **1971**, *93*, 1804-1805.

9. Ashe III, A. J.; Al-Ahmad, S.; Fang, X., Boratabenzenes: from chemical curiosities to promising catalysts. *J. Organomet. Chem.* **1999**, *581*, 92-97.

10. Ashe III, A. J., Aromatic Borataheterocycles: Surrogates for Cyclopentadienyl in Transition-Metal Complexes. *Organometallics* **2009**, *28*, 4236-4248.

11. Fan, C.; Piers, W. E.; Parvez, M., Perfluoropentaphenylborole. *Angew. Chem. Int. Ed.* **2009**, *48*, 2955-2958.

12. Steffen, A.; Ward, R. M.; Jones, W. D.; Marder, T. B., Dibenzometallacyclopentadienes, boroles and selected transition metal and maingroup heterocyclopentadienes: Synthesis, catalytic and optical properties. *Coord. Chem. Rev.* **2010**, *254*, 1950-1976.

13. Cook, K. S.; Piers, W. E.; Woo, T. K.; McDonald, R., Reactions of Bis(pentafluorophenyl)borane with $Cp_2Ta(=CH_2)CH_3$: Generation and Trapping of Tantalocene Borataalkene Complexes. *Organometallics* **2001**, *20*, 3927-3937.

14. Cook, K. S.; Piers, W. E.; McDonald, R., Synthesis and Chemistry of Zwitterionic Tantala-3-boratacyclopentenes: Olefin-like Reactivity of a Borataalkene Ligand. *J. Am. Chem. Soc.* **2002**, *124*, 5411-5418.

15. Chiu, C.-W.; Gabbaï, F. P., Structural Changes Accompanying the Stepwise Population of a B-C π Bond. *Angew. Chem. Int. Ed.* **2007**, *46*, 6878-6881.

16. Olmstead, M. M.; Power, P. P.; Weese, K. J.; Doedens, R. J., Isolation and X-ray Crystal Structure of the Boron Methylidenide Ion $[Mes_2BCH_2]^-$ (Mes = 2,4,6-$Me_3C_6H_2$): A Boron-Carbon Double Bonded Alkene Analogue. *J. Am. Chem. Soc.* **1987**, *109*, 2541-2542.

17. Fan, C.; Piers, W. E.; Parvez, M.; McDonald, R., Divergent Reactivity of Perfluoropentaphenylborole with Alkynes. *Organometallics* **2010**, *29*, 5132-5139.

18. Fukazawa, A.; Dutton, J. L.; Fan, C.; Mercier, L. G.; Houghton, A. Y.; Wu, Q.; Piers, W. E.; Parvez, M., Reaction of pentaarylboroles with carbon monoxide: an isolable organoboron carbonyl complex. *Chem. Sci.* **2012**, *3*, 1814-1818.

19. Braunschweig, H.; Hupp, F.; Krummenacher, I.; Mailänder, L.; Rauch, F., Ring Expansions of Boroles with Diazo Compounds: Steric Control of C or N Insertion and Aromatic/Nonaromatic Products. *Chem. Eur. J.* **2015**, *21*, 17844-17849.

20. Huang, K.; Couchman, S. A.; Wilson, D. J. D.; Dutton, J. L.; Martin, C. D., Reactions of Imines, Nitriles, and Isocyanides with Pentaphenylborole: Coordination, Ring Expansion, C–H Bond Activation, and Hydrogen Migration Reactions. *Inorg. Chem.* **2015**, *54*, 8957-8968.

21. Huang, K.; Martin, C. D., Ring Expansion Reactions of Pentaphenylborole with Dipolar Molecules as a Route to Seven-Membered Boron Heterocycles. *Inorg. Chem.* **2015**, *54*, 1869-1875.

22. Barnard, J. H.; Yruegas, S.; Couchman, S. A.; Wilson, D. J. D.; Dutton, J. L.; Martin, C. D., Reactivity of a Phosphaalkyne with Pentaarylboroles. *Organometallics* **2016**, *35*, 929–931.

23. Caputo, B. C.; Manning, Z. J.; Barnard, J. H.; Martin, C. D., Reactions of pentaphenylborole with main group hydrides. *Polyhedron* **2016**, *114*, 273-277.

24. Huang, K.; Martin, C. D., Peculiar Reactivity of Isothiocyanates with Pentaphenylborole. *Inorg. Chem.* **2016**, *55*, 330-337.

25. Yruegas, S.; Martin, C. D., Expedient Synthesis of 1,2-Thiaborines via Sulfur Insertion into Boroles. *Chem. Eur. J.* **2016**, *22*, 18358-18361.

26. Yruegas, S.; Patterson, D. C.; Martin, C. D., Oxygen insertion into boroles as a route to 1,2-oxaborines. *Chem. Commun.* **2016**, *52*, 6658-6661.

27. Adiraju, V. A. K.; Martin, C. D., Isomer Dependence on the Reactivity of Diazenes with Pentaphenylborole. *Chem. Eur. J.* **2017**, *23*, 11437-11444.

28. Couchman, S. A.; Thompson, T. K.; Wilson, D. J. D.; Dutton, J. L.; Martin, C. D., Investigating the ring expansion reaction of pentaphenylborole and an azide. *Chem. Commun.* **2014**, *50*, 11724-11726.

29. Barnard, J. H.; Brown, P. A.; Shuford, K. L.; Martin, C. D., 1,2-Phosphaborines: Hybrid Inorganic/Organic P–B Analogues of Benzene. *Angew. Chem. Int. Ed.* **2015**, *54*, 12083-12086.

30. Baker, J. J.; Al-Furaiji, K. H. M.; Liyanage, O. T.; Wilson, D. J. D.; Dutton, J. L.; Martin, C. D., Diverse Reactivity of Dienes with Pentaphenylborole and 1-Phenyl-2,3,4,5-Tetramethylborole Dimer. *Chem. Eur. J.* **2019**, *25*, 1581-1587.

31. Herberich, G. E.; Ohst, H., Synthese von [1-(Diisopropylamino)borol]metall-Komplexen und das Diels-Alder-Dimere des 1-(Diisopropylamino)borols. *Chem. Ber.* **1985**, *118*, 4303-4313.

32. Fagan, P. J.; Burns, E. G.; Calabrese, J. C., Synthesis of boroles and their use in low-temperature Diels-Alder reactions with unactivated alkenes. *J. Am. Chem. Soc.* **1988**, *110*, 2979-2981.

33. Fagan, P. J.; Nugent, W. A.; Calabrese, J. C., Metallacycle Transfer from Zirconium to Main Group Elements: A Versatile Synthesis of Heterocycles. *J. Am. Chem. Soc.* **1994**, *116*, 1880-1889.

34. Su, X.; Baker, J. J.; Martin, C. D., Dimeric Boroles: Effective Sources of Monomeric Boroles for Heterocycle Synthesis. *Chem. Sci.* **2020**, *11*, 126-131.

35. Su, X.; Bartholome, T. A.; Tidwell, J. R.; Pujol, A.; Yruegas, S.; Martinez, J. J.; Martin, C. D., 9-Borafluorenes: Synthesis, Properties, and Reactivity. *Chem. Rev.* **2021**, *121*, 4147-4192.

36. Köster, R.; Benedikt, G., 9-Borafluorenes. *Angew. Chem. Int. Ed.* **1963**, *2*, 323-324.

37. Bluer, K. R.; Laperriere, L. E.; Pujol, A.; Yruegas, S.; Adiraju, V. A. K.; Martin, C. D., Coordination and Ring Expansion of 1,2-Dipolar Molecules with 9-Phenyl-9-borafluorene. *Organometallics* **2018**, *37*, 2917-2927.

38. Yruegas, S.; Martinez, J. J.; Martin, C. D., Intermolecular insertion reactions of azides into 9-borafluorenes to generate 9,10-B,N-phenanthrenes. *Chem. Commun.* **2018**, *54*, 6808-6811.

39. Zhang, W.; Li, G.; Xu, L.; Zhuo, Y.; Wan, W.; Yan, N.; He, G., 9,10-Azaboraphenanthrene-containing small molecules and conjugated polymers: synthesis and their application in chemodosimeters for the ratiometric detection of fluoride ions. *Chem. Sci.* **2018**, *9*, 4444-4450.

40. Narula, C. K.; Noeth, H., Contribution to the chemistry of boron. 150. Competition between adduct and cation formation in reactions between diorganylborane derivatives and pyridine or lutidines. *Inorg. Chem.* **1985**, *24*, 2532-9.

41. Laperriere, L. E.; Yruegas, S.; Martin, C. D., Investigating the reactivity of 9-phenyl-9-borafluorene with NH, OH, PH, and SH bonds. *Tetrahedron* **2019**, *75*, 937-943.

42. Chase, P. A.; Romero, P. E.; Piers, W. E.; Parvez, M.; Patrick, B. O., Fluorinated 9-borafluorenes vs. conventional perfluoroaryl boranes — Comparative Lewis acidity. *Can. J. Chem.* **2005**, *83*, 2098-2105.

43. Berger, C. J.; He, G.; Merten, C.; McDonald, R.; Ferguson, M. J.; Rivard, E., Synthesis and Luminescent Properties of Lewis Base-Appended Borafluorenes. *Inorg. Chem.* **2014**, *53*, 1475-1486.

44. Yang, W.; Krantz, K. E.; Freeman, L. A.; Dickie, D. A.; Molino, A.; Kaur, A.; Wilson, D. J. D.; Robert J. Gilliard, J., Stable Borepinium and Borafluorenium Heterocycles: A Reversible Thermochromic "Switch" Based on Boron-Oxygen Interactions. *Chem. Eur. J.* **2019**, *25*, 12512-12516.

45. Zhang, W.; Yu, D.; Wang, Z.; Zhang, B.; Xu, L.; Li, G.; Yan, N.; Rivard, E.; He, G., Dibora[10]annulenes: Construction, Properties, and Their Ring-Opening Reactions. *Org. Lett.* **2019**, *21*, 109-113.

46. Urban, M.; Durka, K.; Górka, P.; Wiosna-Sałyga, G.; Nawara, K.; Jankowski, P.; Luliński, S., The effect of locking π-conjugation in organoboron moieties in the structures of luminescent tetracoordinate boron complexes. *Dalton Trans.* **2019**, *48*, 8642-8663.

47. Matsumoto, T.; Ito, S.; Tanaka, K.; Chujo, Y., Synthesis, properties and structure of borafluorene-based conjugated polymers with kinetically and thermodynamically stabilized tetracoordinated boron atoms. *Polym. J.* **2018**, *50*, 197-202.

48. Cassidy, S. J.; Brettell-Adams, I.; McNamara, L. E.; Smith, M. F.; Bautista, M.; Cao, H.; Vasiliu, M.; Gerlach, D. L.; Qu, F.; Hammer, N. I.; Dixon, D. A.; Rupar, P. A., Boranes with Ultra-High Stokes Shift Fluorescence. *Organometallics* **2018**, *37*, 3732-3741.

49. Yamaguchi, S.; Shirasaka, T.; Akiyama, S.; Tamao, K., Dibenzoborole-Containing π-Electron Systems: Remarkable Fluorescence Change Based on the "On/Off" Control of the pπ−π* Conjugation. *J. Am. Chem. Soc.* **2002**, *124*, 8816-8817.

50. Adams, I. A.; Rupar, P. A., A Poly(9-Borafluorene) Homopolymer: An Electron-Deficient Polyfluorene with "Turn-On" Fluorescence Sensing of NH_3 Vapor. *Macromol. Rapid Commun.* **2015**, *36*, 1336-1340.

51. Matsumoto, T.; Takamine, H.; Tanaka, K.; Chujo, Y., Design of bond-cleavage-induced intramolecular charge transfer emission with dibenzoboroles and their application to ratiometric sensors for discriminating chain lengths of alkanes. *Mater. Chem. Front.* **2017**, *1*, 2368-2375.

52. Herberich, G. E.; Greiss, G.; Heil, H. F., A Novel Aromatic Boron Heterocycle as Ligand in a Transition Metal π-Complex. *Angew. Chem. Int. Ed.* **1970**, *9*, 805-806.

53. Herberich, G. E.; Greiss, G.; Heil, H. F.; Müller, J., Paramagnetic Borabenzene Cobalt Complexes. *Chem. Commun.* **1971**, 1328-1329.

54. Huttner, G.; Krieg, B., Structure of $(CH_3OBC_5H_5)_2Co$, a Derivative of the Aromatic Hydridoborinate Anion. *Angew. Chem. Int. Ed.* **1972**, *11*, 42-43.

55. Huttner, G.; Krieg, B.; Gartzke, W., Kristall- und Molekülstrukturen von zwei "Borabenzol"-Derivaten: Bis(1-methoxyborinato)kobalt und Bis(1-methylborinato)kobalt. *Chem. Ber.* **1972**, *105*, 3424-3436.

56. Herberich, G. E.; Becker, H. J., Tricarbonyl-(1-phenylborinato)manganese. *Angew. Chem. Int. Ed.* **1973**, *12*, 764-765.

57. Ashe III, A. J.; Meyers, E.; Shu, P.; Lehmann, T. V.; Bastide, J., Bis(1-substituted-borabenzene)iron Complexes. *J. Am. Chem. Soc.* **1975**, *97*, 6865-6866.

58. Herberich, G. E.; Becker, H. J.; Carsten, K.; Engelke, C.; Koch, W., Ein neuer Weg zu Alkalimetallborinaten. Synthesen von Ruthenium-, Osmium-, Rhodium- und Platin-Verbindungen mit Borinat-Liganden. *Chem. Ber.* **1976**, *109*, 2382-2388.

59. Herberich, G. E.; Koch, W., Paramagnetische Chrom-Komplexe des 1-Methyl- und 1-Phenylborinat-Ions. *Chem. Ber.* **1977**, *110*, 816-819.

60. Herberich, G. E.; Carsten, K., Derivate des Borabenzols XI. Neuartige Ringumwandlungen von Borinatoeisen-Komplexen. *J. Organomet. Chem.* **1978**, *144*, C1-C5.

61. Herberich, G. E.; Hessner, B.; Kho, T. T., Derivate des Borabenzols XV. Friedel-Crafts-Acetylierung Versus Ringgliedsubstitution an Tricarbonyl(1-methylborinato)mangan. *J. Organomet. Chem.* **1980**, *197*, 1-5.

62. Herberich, G. E.; Söhnen, D., Derivate des Borabenzols XVII. Tricarbonyl(1-methylborinato)chrom-Derivate. *J. Organomet. Chem.* **1983**, *254*, 143-147.

63. Herberich, G. E.; Boveleth, W.; Hessner, B.; Koch, W.; Raabe, E.; Schmitz, D., Derivate des Borabenzols XVIII. Vanadium-Komplexe des 1-Methyl- und 1-Phenylborinat-Ions. *J. Organomet. Chem.* **1984**, *265*, 225-235.

64. Herberich, G. E.; Becker, H. J.; Hessner, B.; Zelenka, L., Derivate des Borabenzols XIX. Die Darstellung von Dicarbonyl(1-methylborinato)cobalt, von Zwei (Borinato)(cyclobutadien)cobalt-Komplexen mit Unsubstituiertem Cyclobutadien-Liganden und von Di-μ-carbonyl-bis[(1-methylborinato)nickel]. *J. Organomet. Chem.* **1985**, *280*, 147-151.

65. Herberich, G. E.; Ohst, H., Borabenzene Metal Complexes. *Adv. Organomet. Chem.* **1986**, *25*, 199-236.

66. Paetzold, P.; Finke, N.; Wennek, P.; Schmid, G.; Boese, R., 2-Boratanaphthalin-Anion als hexahapto-gebundener Ligand. *Z. Naturforsch.* **1986**, *41b*, 167-174.

67. Bazan, G. C.; Rodriguez, G.; Ashe III, A. J.; Al-Ahmad, S.; Müller, C., Aminoboratabenzene Derivatives of Zirconium: A New Class of Olefin Polymerization Catalysts. *J. Am. Chem. Soc.* **1996**, *118*, 2291-2292.

68. Bazan, G. C.; Rodriguez, G.; Ashe III, A. J.; Al-Ahmad, S.; Kampf, J. W., (Phenylboratabenzene)zirconium Complexes: Tuning the Reactivity of an Olefin Polymerization Catalyst. *Organometallics* **1997**, *16*, 2492-2494.

69. Barnhart, R. W.; Bazan, G. C.; Mourey, T., Synthesis of Branched Polyolefins Using a Combination of Homogeneous Metallocene Mimics. *J. Am. Chem. Soc.* **1998**, *120*, 1082-1083.

70. Lee, R. A.; Lachicotte, R. J.; Bazan, G. C., Zirconium Complexes of 9-Phenyl-9-borataanthracene. Synthesis, Structural Characterization, and Reactivity. *J. Am. Chem. Soc.* **1998**, *120*, 6037-6046.

71. Herberich, G. E.; Englert, U.; Fischer, A.; Ni, J.; Schmitz, A., Borabenzene Derivatives. 29. Synthesis and Structural Diversity of Bis(boratabenzene)scandium Complexes. Structures of $[ScCl(C_5H_5BMe)_2]_2$, $[ScCl(3,5\text{-}Me_2C_5H_3BNMe_2)_2]_2$, and $ScCl[3,5\text{-}Me_2C_5H_3BN(SiMe_3)_2]_2$. *Organometallics* **1999**, *18*, 5496-5501.

72. Herberich, G. E.; Zheng, X.; Rosenplänter, J.; Englert, U., Borabenzene Derivatives. 30. Bis(1-methylboratabenzene) Compounds of Germanium, Tin, and Lead. First Structural Characterization of Facial Bonding of a Boratabenzene to a p-Element and the Structures of $Pb(C_5H_5BMe)_2$ and Its 2,2'-Bipyridine Adduct. *Organometallics* **1999**, *18*, 4747-4752.

73. Rogers, J. S.; Bu, X.; Bazan, G. C., Boratabenzene Complexes of Cr(III). *J. Am. Chem. Soc.* **2000**, *122*, 730-731.

74. Rogers, J. S.; Bu, X.; Bazan, G. C., Synthesis, Characterization, and Reactivity of Chromium Boratabenzene Complexes. *Organometallics* **2000**, *19*, 3948-3956.

75. Braunstein, P.; Cura, E.; Herberich, G. E., Heterometallic complexes and clusters with 2-boratanaphthalene ligands. *J. Chem. Soc., Dalton Trans.* **2001**, 1754-1760.

76. Fu, G. C., The Chemistry of Borabenzenes (1986-2000). *Adv. Organomet. Chem.* **2001**, *47*, 101-119.

77. Zheng, X.; Wang, B.; Englert, U.; Herberich, G. E., Three Conformational Polymorphs of Di-μ-chlorotetrakis(1-methylboratabenzene)diyttrium: Synthesis, X-ray Structures, Quantum Chemical Calculations, and Lattice Energy Minimizations. *Inorg. Chem.* **2001**, *40*, 3117-3123.

78. Cui, P.; Chen, Y.; Zeng, X.; Sun, J.; Li, G.; Xia, W., Boratabenzene Derivatives of Divalent Samarium: Synthesis, Structures and Catalytic Reactivities of $(C_5H_5BXPh_2)_2Sm(THF)_2$ (X = N, P). *Organometallics* **2007**, *26*, 6519-6521.

79. Cui, P.; Chen, Y.; Li, G.; Xia, W., An ansa-Heteroborabenzene Divalent Lanthanide Amide through C-H Bond Cleavage. *Angew. Chem. Int. Ed.* **2008**, *47*, 9944-9947.

80. Yuan, Y.; Chen, Y.; Li, G.; Xia, W., Reactions of Boratabenzene Yttrium Complexes with $KN(SiMe_3)_2$: Salt Elimination and π-Ligand Displacement. *Organometallics* **2008**, *27*, 6307-6312.

81. Languérand, A.; Barnes, S. S.; Bélanger-Chabot, G.; Maron, L.; Berrouard, P.; Audet, P.; Fontaine, F. G., [(IMes)2Pt(H)(ClBC5H4SiMe3)]: a Borabenzene–Platinum Adduct with an Unusual Pt-Cl-B Interaction. *Angew. Chem. Int. Ed.* **2009**, *48*, 6695-6698.

82. Cui, P.; Chen, Y.; Zhang, Q.; Li, G.; Xia, W., Synthesis, and structural characterization of solvent-free divalent ytterbium bis(boratabenzene) and (cyclopentadienyl)(boratabenzene) complexes. *J. Organomet. Chem.* **2010**, *695*, 2713-2719.

83. Cui, P.; Chen, Y.; Li, G.; Xia, W., Versatile Reactivities of *ansa*-Heteroborabenzene Divalent Ytterbium Amide toward Alkali-Metal Salts and the Generation of Heterometallic Ytterbium--Alkali-Metal Boratabenzene Complexes. *Organometallics* **2011**, *30*, 2012-2017.

84. Pammer, F.; Lalancette, R. A.; Jäkle, F., Metallopolymers Featuring Boratabenzene Iron Complexes. *Chem. Eur. J.* **2011**, *17*, 11280-11289.

85. Yuan, Y.; Wang, X.; Li, Y.; Fan, L.; Xu, X.; Chen, Y.; Li, G.; Xia, W., Rapid Entry to Functionalized Boratabenzene Complexes through Metal-Induced Hydroboration at the Anionic 1-H-Boratabenzene Ligand. *Organometallics* **2011**, *30*, 4330-4341.

86. Wang, X.; Peng, W.; Cui, P.; Leng, X.; Xia, W.; Chen, Y., Synthesis and Catalytic Activity of Amido-Boratabenzene Complexes of Rare-Earth Metals and Zirconium and Chromium. *Organometallics* **2013**, *32*, 6166-6169.

87. Mushtaq, A.; Bi, W.; Légaré, M.-A.; Fontaine, F.-G., Synthesis and Reactivity of Novel Mesityl Boratabenzene Ligands and Their Coordination to Transition Metals. *Organometallics* **2014**, *33*, 3173-3181.

88. Pérez, V.; Barnes, S. S.; Fontaine, F.-G., Generation of Group VI Piano-Stool and Triple-Decker Complexes from [$(IMes)_2$PtH(Cl-boratabenzene)] Species. *Eur. J. Inorg. Chem.* **2014**, 5698-5702.

89. Cui, P.; Chen, Y., Boratabenzene rare-earth metal complexes. *Coord. Chem. Rev.* **2016**, *314*, 2-13.

90. Meng, Y.-S.; Wang, C.-H.; Zhang, Y.-Q.; Leng, X.-B.; Wang, B.-W.; Chen, Y.-F.; Gao, S., (Boratabenzene)(cyclooctatetraenyl) lanthanide complexes: a new type of organometallic single-ion magnet. *Inorg. Chem. Front.* **2016**, *3*, 828-835.

91. Perez, V.; Audet, P.; Bi, W.; Fontaine, F.-G., Phosphidoboratabenzene-rhodium(I) complexes as precatalysts for the hydrogenation of alkenes at room temperature and atmospheric pressure. *Dalton Trans.* **2016**, *45*, 2130-2137.

92. Krummenacher, I.; Schuster, J. K.; Braunschweig, H., Synthesis and Reactivity of Bora- and Borata-Benzenes. In *Patai's Chemistry of Functional Groups*, Marek, I.; Gandelman, M., Eds. 2019.

93. Ashe III, A. J.; Fang, X.; Kampf, J. W., Synthesis and Properties of 1-Substituted 1-Boratanaphthalenes. *Organometallics* **1999**, *18*, 466-473.

94. Rathke, M. W.; Kow, R., Generation of Boron-Stabilized Carbanions. *J. Am. Chem. Soc.* **1972**, *94*, 6854-6856.

95. Cook, K. S.; Piers, W. E.; Rettig, S. J., Reactions of Bis(pentafluorophenyl)borane with $Cp_2Ta(=CH_2)CH_3$. *Organometallics* **1999**, *18*, 1575-1577.

96. Pelter, A., Some chemistry of hindered organoboranes. *Pure Appl. Chem.* **1994**, *66*, 223-233.

97. Pelter, A.; Singaram, B.; Wilson, J. W., The Dimesitylboron Group in Organic Synthesis. 4. The 'Boron Wittig' Reaction. *Tetrahedron Lett.* **1983**, *24*, 635-636.

98. Pelter, A.; Bugden, G.; Rosser, R., The Dimesitylboron Group in Organic Synthesis 8. Preparations of 1,3-Diols from Oxiranes. *Tetrahedron Lett.* **1985**, *26*, 5097-5100.

99. Pelter, A.; Williams, L.; Wilson, J. W., The Dimesitylboron Group in Organic Synthesis 2. The C-Alkylation of Alkyldimesitylboranes. *Tetrahedron Lett.* **1983**, *24*, 627-630.

100. Kawashima, T.; Yamashita, N.; Okazaki, R., Synthesis, Structure, and Thermolysis of a Tetracoordinate 1,2-Oxaboretanide: An Intermediate of the Boron-Wittig Reaction under Basic Conditions. *J. Am. Chem. Soc.* **1995**, *117*, 6142-6143.

101. Wang, T.; Kohrt, S.; Daniliuc, C. G.; Kehr, G.; Erker, G., Borata-Wittig olefination reactions of ketones, carboxylic esters and amides with bis(pentafluorophenyl)borata-alkene reagents. *Org. Biomol. Chem.* **2017**, *15*, 6223-6232.

102. Su, B.; Kinjo, R., Construction of Boron-Containing Aromatic Heterocycles. *Synthesis* **2017**, *49*, 2985-3034.

103. Brière, J.-F.; Côté, M., Electronic, Structural, and Optical Properties of Conjugated Polymers Based on Carbazole, Fluorene, and Borafluorene. *J. Phys. Chem. B* **2004**, *108*, 3123-3129.

104. Lorenz-Rothe, M.; Schellhammer, K. S.; Jägeler-Hoheisel, T.; Meerheim, R.; Kraner, S.; Hein, M. P.; Schünemann, C.; Tietze, M. L.; Hummert, M.; Ortmann, F.; Cuniberti, G.; Körner, C.; Leo, K., From Fluorine to Fluorene—A Route to Thermally Stable aza-BODIPYs for Organic Solar Cell Application. *Adv. Electron. Mater.* **2016**, *2*, 1600152.

105. Muhammad, S.; Janjua, M. R. S. A.; Su, Z., Investigation of Dibenzoboroles Having *J. Phys. Chem. C* **2009**, *113*.

106. Thanthiriwatte, K. S.; Gwaltney, S. R., Excitation Spectra of Dibenzoborole Containing π-Electron Systems: Controlling the Electronic Spectra by Changing the pπ−π* Conjugation. *J. Phys. Chem. A* **2006**, *110*, 2434-2439.

107. Yamaguchi, S.; Wakamiya, A., Boron as a key component for new π-electron materials. *Pure Appl. Chem.* **2006**, *78*, 1413.

108. Romero, P. E.; Piers, W. E.; Decker, S. A.; Chau, D.; Woo, T. K.; Parvez, M., η^1 versus η^5 Bonding Modes in Cp*Al(I) Adducts of 9-Borafluorenes. *Organometallics* **2003**, *22*, 1266-1274.

109. Berger, C. J.; He, G.; Merten, C.; McDonald, R.; Ferguson, M. J.; Rivard, E., Synthesis and Luminescent Properties of Lewis Base-Appended Borafluorenes. *Inorg. Chem.* **2014**, *53*, 1475-1486.

110. Smith, M. F.; Cassidy, S. J.; Adams, I. A.; Vasiliu, M.; Gerlach, D. L.; Dixon, D. A.; Rupar, P. A., Substituent Effects on the Properties of Borafluorenes. *Organometallics* **2016**, *35*, 3182-3191.

111. Braunschweig, H.; Celik, M. A.; Hupp, F.; Krummenacher, I.; Mailänder, L., Formation of BN Isosteres of Azo Dyes by Ring Expansion of Boroles with Azides. *Angew. Chem. Int. Ed.* **2015**, *54*, 6347-6351.

112. Braunschweig, H.; Krummenacher, I.; Mailänder, L.; Rauch, F., O,N,B-Containing eight-membered heterocycles by ring expansion of boroles with nitrones. *Chem. Commun.* **2015**, *51*, 14513-14515.

113. Braunschweig, H.; Celik, M.; Dellermann, T.; Frenking, G.; Hammond, K.; Hupp, F.; Kelch, H.; Krummenacher, I.; Lindl, F.; Mailänder, L.; Müssig, J.; Ruppert, A., Scope of the Thermal Ring Expansion Reaction of Boroles with Organoazides. *Chem. Eur. J.* **2017**, *23*, 8006-8013.

114. Wang, Z.; Zhou, Y.; Zhang, J.-X.; Krummenacher, I.; Braunschweig, H.; Lin, Z., DFT Studies on the Reactions of Boroles with Alkynes. *Chem. Eur. J.* **2018**, *24*, 9612-9621.

115. Eisch, J. J.; Galle, J. E.; Shafii, B.; Rheingold, A. L., Thermal generation and transformation of the borepin ring system; a paradigm of pericyclic processes. *Organometallics* **1990**, *9*, 2342-2349.

116. Yruegas, S.; Wilson, C.; Dutton, J. L.; Martin, C. D., Ring Opening of Epoxides Induced by Pentaphenylborole. *Organometallics* **2017**, *36*, 2581-2587.

117. Lindl, F.; Lin, S.; Krummenacher, I.; Lenczyk, C.; Stoy, A.; Müller, M.; Lin, Z.; Braunschweig, H., 1,2,3-Diazaborinine: A BN Analogue of Pyridine Obtained by Ring Expansion of a Borole with an Organic Azide. *Angew. Chem. Int. Ed.* **2019**, *58*, 338-342.

118. Li, Y.; Siwatch, R. K.; Mondal, T.; Li, Y.; Ganguly, R.; Koley, D.; So, C.-W., Diverse Bonding Activations in the Reactivity of a Pentaphenylborole toward Sodium Phosphaethynolate: Heterocycle Synthesis and Mechanistic Studies. *Inorg. Chem.* **2017**, *56*, 4112-4120.

119. Braunschweig, H.; Maier, J.; Radacki, K.; Wahler, J., Ring Expansion of 7-Boranorbornadienes by Coordination with an N-Heterocyclic Carbene. *Organometallics* **2013**, *32*, 6353-6359.

120. Shoji, Y.; Hwang, M.; Sugiyama, H.; Ishiwari, F.; Takenouchi, K.; Osuga, R.; Kondo, J. N.; Fujikawa, S.; Fukushima, T., Highly efficient transformation of linear poly(phenylene ethynylene)s into zigzag-shaped π-conjugated microporous polymers through boron-mediated alkyne benzannulation. *Mater. Chem. Front.* **2018**, *2*, 807-814.

121. Yruegas, S.; Barnard, J. H.; Al-Furaiji, K.; Dutton, J. L.; Wilson, D. J. D.; Martin, C. D., Boraphosphaalkene Synthesis via Phosphaalkyne Insertion into 9-Borafluorene. *Organometallics* **2018**, *37*, 1515-1518.

122. Kashida, J.; Shoji, Y.; Fukushima, T., Synthesis and Reactivity of Cyclic Borane-Amidine Conjugated Molecules Formed by Direct 1,2-Carboboration of Carbodiimides with 9-Borafluorenes. *Chem. Asian J.* **2019**, *14*, 1879-1885.

123. Shoji, Y.; Shigeno, N.; Takenouchi, K.; Sugimoto, M.; Fukushima, T., Mechanistic Study of Highly Efficient Direct 1,2-Carboboration of Alkynes with 9-Borafluorenes. *Chem. Eur. J.* **2018**, *24*, 13223-13230.

124. Özen, C.; Shoji, Y.; Fukushima, T.; Maeda, S., A Theoretical Study on the Mechanism of the Oxidative Deborylation/C–C Coupling Reaction of Borepin Derivatives. *J. Org. Chem.* **2019**, *84*, 1941-1950.

125. Shoji, Y.; Tanaka, N.; Muranaka, S.; Shigeno, N.; Sugiyama, H.; Takenouchi, K.; Hajjaj, F.; Fukushima, T., Boron-mediated sequential alkyne insertion and C–C coupling reactions affording extended π-conjugated molecules. *Nat. Commun.* **2016**, *7*, 12704.

126. Matteson, D. S.; Majumdar, D., Homologation of boronic esters to .alpha.-chloro boronic esters. *Organometallics* **1983**, *2*, 1529-1535.

127. Sadhu, K. M.; Matteson, D. S., (Chloromethyl)lithium: efficient generation and capture by boronic esters and a simple preparation of diisopropyl (chloromethyl)boronate. *Organometallics* **1985**, *4*, 1687-1689.

128. Matteson, D. S.; Majumdar, D., α-Chloro boronic esters from homologation of boronic esters. *J. Am. Chem. Soc.* **1980**, *102*, 7588-7590.

129. Brown, H. C.; Naik, R. G.; Bakshi, R. K.; Pyun, C.; Singaram, B., Chiral synthesis via organoboranes. 4. Synthetic utility of boronic esters of essentially 100% optical purity. Synthesis of homologated boronic acids and esters of very high enantiomeric purities. *J. Org. Chem.* **1985**, *50*, 5586-5592.

130. Brown, H. C.; Singh, S. M.; Rangaishenvi, M. V., Organoboranes. 46. New procedures for the homologation of boronic esters. A critical examination of the available procedures to achieve convenient homologation of boronic esters. *J. Org. Chem.* **1986**, *51*, 3150-3155.

131. Brown, H. C.; Phadke, A. S.; Rangaishenvi, M. V., Ring enlargement of boracyclanes via sequential one carbon homologation. The first synthesis of boracyclanes in the strained medium ring range. *J. Am. Chem. Soc.* **1988**, *110*, 6263-6264.

132. Ashe III, A. J.; Kampf, J. W.; Waas, J. R., 4-Methyl-1,4-Thiaborin, an Aromatic Boron-Sulfur Heterocycle. *Organometallics* **1995**, *14*, 3141-3142.

133. Ashe III, A. J.; Fang, X.; Fang, X.; Kampf, J. W., Synthesis of 1,2-Dihydro-1,2-azaborines and Their Conversion to Tricarbonyl Chromium and Molybdenum Complexes. *Organometallics* **2001**, *20*, 5413-5418.

134. Chen, J.; Bajko, Z.; Kampf, J. W.; Ashe III, A. J., 1,2-Dihydro-1,2-oxaborine: A Boron−Oxygen Heterocycle Isoelectronic with Benzene. *Organometallics* **2007**, *26*, 1563-1564.

135. Melen, R. L., A Step Closer to Metal-Free Dinitrogen Activation: A New Chapter in the Chemistry of Frustrated Lewis Pairs. *Angew. Chem. Int. Ed.* **2018**, *57*, 880-882.

136. Ruddy, A. J.; Ould, D. M. C.; Newman, P. D.; Melen, R. L., Push and pull: the potential role of boron in N_2 activation. *Dalton Trans.* **2018**, *47*, 10377-10381.

137. Schneider, C.; LaFortune, J. H. W.; Melen, R. L.; Stephan, D. W., Lewis and Brønsted basicity of phosphine-diazomethane derivatives. *Dalton Trans.* **2018**, *47*, 12742-12749.

138. Neu, R. C.; Stephan, D. W., Insertion Reactions of Diazomethanes and Electrophilic Boranes. *Organometallics* **2012**, *31*, 46-49.

139. Neu, R. C.; Jiang, C.; Stephan, D. W., Bulky derivatives of boranes, boronic acids and boronate esters via reaction with diazomethanes. *Dalton Trans.* **2013**, *42*, 726-736.

140. Lam, J.; Günther, B. A. R.; Farrell, J. M.; Eisenberger, P.; Bestvater, B. P.; Newman, P. D.; Melen, R. L.; Crudden, C. M.; Stephan, D. W., Chiral carbene–borane adducts: precursors for borenium catalysts for asymmetric FLP hydrogenations. *Dalton Trans.* **2016**, *45*, 15303-15316.

141. Tang, C.; Liang, Q.; Jupp, A. R.; Johnstone, T. C.; Neu, R. C.; Song, D.; Grimme, S.; Stephan, D. W., 1,1-Hydroboration and a Borane Adduct of Diphenyldiazomethane: A Potential Prelude to FLP-N_2 Chemistry. *Angew. Chem. Int. Ed.* **2017**, *56*, 16588-16592.

142. From the experiments it is not clear if the observed *meso* isomer is the kinetic or thermodynamic product

143. A variable temperature ^{1}H NMR spectroscopy experiment from -60 °C to 90 °C in toluene-d_8 did not reveal any signs of coalescence of the signals.

144. Campbell, P. G.; Marwitz, A. J. V.; Liu, S.-Y., Recent Advances in Azaborine Chemistry. *Angew. Chem. Int. Ed.* **2012**, *51*, 6074-6092.

145. Brown, P. A.; Martin, C. D.; Shuford, K. L., Aromaticity of unsaturated BEC_4 heterocycles (E = N, P, As, Sb, O, S, Se, Te). *Phys. Chem. Chem. Phys.* **2019**, *21*, 18458-18466.

146. Noguchi, M.; Suzuki, K.; Kobayashi, J.; Yurino, T.; Tsurugi, H.; Mashima, K.; Yamashita, M., Planar and Bent BN-Embedded p-Quinodimethanes Synthesized by Transmetalation of Bis(trimethylsilyl)-1,4-dihydropyrazines with Chloroborane. *Organometallics* **2018**, *37*, 1833-1836.

147. Marwitz, A. J. V.; Matus, M. H.; Zakharov, L. N.; Dixon, D. A.; Liu, S.-Y., A Hybrid Organic/Inorganic Benzene. *Angew. Chem. Int. Ed.* **2009**, *48*, 972-977.

148. Janiak, C., Metallocene and related catalysts for olefin, alkyne and silane dimerization and oligomerization. *Coord. Chem. Rev.* **2006**, *250*, 66-94.

149. Tweddell, J.; Hoic, D. A.; Fu, G. C., First Synthesis and Structural Characterization of an Enantiomerically Pure Planar-Chiral Lewis Acid Complex. *J. Org. Chem.* **1997**, *62*, 8286-8287.

150. Herberich, G. E.; Ganter, B.; Pons, M., Borabenzene Derivatives. 27. From (-)-α-Pinene to the First Chiral Boratabenzene Salt. *Organometallics* **1998**, *17*, 1254-1256.

151. Herberich, G. E.; Englert, U.; Ganter, B.; Pons, M.; Wang, R., Borabenzene Derivatives. 28. Pinene-Fused Dihydroborinines, Boratabenzenes, and a Borabenzene-Pyridine Adduct. *Organometallics* **1999**, *18*, 3406-3413.

152. Herberich, G. E.; Cura, E.; Ni, J., A new synthetic route to 2-boratanaphthalenes. *Inorg. Chem. Commun.* **1999**, *2*, 503-506.

153. van Veen, R.; Bickelhaupt, F., The 9-mesityl-9-boraanthracene anion. *J. Organomet. Chem.* **1971**, *30*, C51-C53.

154. van Veen, R.; Bickelhaupt, F., Reactions of the 9-Mesityl-9-boraanthracene Anion. *J. Organomet. Chem.* **1974**, *77*, 153-165.

155. van Veen, R.; Bickelhaupt, F., Equilibrium CH-Acidity in Cyclohexylamine: The Aromatic 9-Mesityl-9-boraanthracene Anion. *J. Organomet. Chem.* **1974**, *74*, 393-403.

156. Mason, S. F., Reactivities of Aromatic Hydrocarbons. Part I. Bromination. *J. Chem. Soc.* **1958**, 4329-4333.

157. Bailey, P. S., The Ozonolysis of Phenanthrene in Methanol. *J. Am. Chem. Soc.* **1956**, *78*, 3811-3816.

158. Bailey, P. S.; Erickson, R. E., Diphenaldehyde. *Org. Synth.* **1961**, *41*, 41.

159. Copeland, P. G.; Dean, R. E.; McNeil, D., The Ozonolysis of Polycyclic Hydrocarbons. Part II. *J. Chem. Soc.* **1961**, 1232-1238.

160. Stanger, A., Nucleus-Independent Chemical Shifts (NICS): Distance Dependence and Revised Criteria for Aromaticity and Antiaromaticity. *J. Org. Chem.* **2006**, *71*, 883-893.

161. A 2-boratanaphthalene anion was generated as an intermediate, but not characterized, in the following manuscript: R. Boese, N. Finke, J. Henkelmann, G. Maier, P. Paetzold, H. P. Reisenauer, G. Schmid, *Chem. Ber.* **1985**, *118*, 1644–1654.

162. Bartholome, T. A.; Bluer, K. R.; Martin, C. D., Successive Carbene Insertion into 9-Phenyl-9-Borafluorene. *Dalton Trans.* **2019**, *48*, 6319-6322.

163. Herberich, G. E.; Schmidt, B.; Englert, U., Borabenzene Derivatives. 22. Synthesis of Boratabenzene Salts from 2,4-Pentadienylboranes. Structure of $[NMe_3Ph][C_5H_5BMe]$. *Organometallics* **1995**, *14*, 471-480.

164. Yu, J.; Kehr, G.; Daniliuc, C. G.; Erker, G., A Unique Frustrated Lewis Pair Pathway to Remarkably Stable Borata-Alkene Systems. *Eur. J. Inorg. Chem.* **2013**, 3312-3315.

165. Möbus, J.; Kehr, G.; Daniliuc, C. G.; Fröhlich, R.; Erker, G., Borata-alkene derivatives conveniently made by frustrated Lewis pair chemistry. *Dalton Trans.* **2014**, *43*, 632-638.

166. Kohrt, S.; Dachwitz, S.; Daniliuc, C. G.; Kehr, G.; Erker, G., Stabilized borata-alkene formation: structural features, reactions and the role of the counter cation. *Dalton Trans.* **2015**, *44*, 21032-21040.

167. Hoic, D. A.; Davis, W. M.; Fu, G. C., A Boron Analogue of Benzene: Synthesis, Structure, and Reactivity of 1-*H*-Boratabenzene. *J. Am. Chem. Soc.* **1995**, *117*, 8480-8481.

168. Bauer, J.; Braunschweig, H.; Hörl, C.; Radacki, K.; Wahler, J., Synthesis of Zwitterionic Cobaltocenium Borate and Borata-alkene Derivatives from a Borole-Radical Anion. *Chem. Eur. J.* **2013**, *19*, 13396-13401.

169. Kobayashi, A.; Suzuki, K.; Kitamura, R.; Yamashita, M., Formation of BCBH/BCBCl Four-Membered Rings by Complexation of Boron- and Nitrogen-Substituted Acetylene with Hydro-/Chloroboranes. *Organometallics* **2020**, *39*, 383-387.

170. Moquist, P.; Chen, G.-Q.; Mück-Lichtenfeld, C.; Bussmann, K.; Daniliuc, C. G.; Kehr, G.; Erker, G., α-CH acidity of alkyl-$B(C_6F_5)_2$ compounds - the role of stabilized borata-alkene formation in frustrated Lewis pair chemistry. *Chem. Sci.* **2015**, *6*, 816-825.

171. Wang, T.; Kehr, G.; Liu, L.; Grimme, S.; Daniliuc, C. G.; Erker, G., Selective Oxidation of an Active Intramolecular Amine/Borane Frustrated Lewis Pair with Dioxygen. *J. Am. Chem. Soc.* **2016**, *138*, 4302-4305.

172. Pelter, A.; Warren, L.; Wilson, J. W., Hindered Organoboron Groups in Organic Chemistry. 20. Alkylations and Acylations of Dimesitylboron Stabilised Carbanions. *Tetrahedron* **1993**, *49*, 2988-3006.

173. Dávila, R. M.; Staples, R. J.; Fackler Jr., J. P., Synthesis and Structural Characterization of $Au_4(MNT)(dppee)_2Cl_2 \bullet 1/4\ CH_2Cl_2$ (MNT = 1,2-Dicyanoethene-1,2-dithiolate-*S,S'*; dppee = *cis*-Bis(diphenylphosphino)ethylene): A Gold(I) Metal-Olefin Complex in Which the Olefin Orientation Relative to the Coordination Plane Involving the Metal Is Defined. *Organometallics* **1994**, *13*, 418-420.

174. Chambrier, I.; Rocchigiani, L.; Hughes, D. L.; Budzelaar, P. M. H.; Bochmann, M., Thermally Stable Gold(III) Alkene and Alkyne Complexes: Synthesis, Structures, and Assessment of the *trans*-Influence on Gold-Ligand Bond Enthalpies. *Chem. Eur. J.* **2018**, *24*, 11467-11474.

175. Cinellu, M. A.; Arca, M.; Ortu, F.; Stoccoro, S.; Zucca, A.; Pintus, A.; Maiore, L., Structural, Theoretical and Spectroscopic Characterisation of a Series of Novel Gold(I)-Norbornene Complexes Supported by Phenanthrolines: Effects of the Supporting Ligand. *Eur. J. Inorg. Chem.* **2019**, 4784-4795.

176. Emslie, D. J. H.; Cowie, B. E.; Kolpin, K. B., Acyclic boron-containing π-ligand complexes: η^2- and η^3-coordination modes. *Dalton Trans.* **2012**, *41*, 1101-1117.

177. Bruce, M. I.; Nicholson, B. K.; Shawkataly, O. B., Synthesis of Gold-Containing Mixed-Metal Cluster Complexes. *Inorg. Synth.* **1989**, *26*, 324-328.

178. Frisch, M. J.; Trucks, G. W.; Schlegel, H. B.; Scuseria, G. E.; Robb, M. A.; Cheeseman, J. R.; Scalmani, G.; Barone, V.; Petersson, G. A.; Nakatsuji, H.; Li, X.; Caricato, M.; Marenich, A. V.; Bloino, J.; Janesko, B. G.; Gomperts, R.; Mennucci, B.; Hratchian, H. P.; Ortiz, J. V.; Izmaylov, A. F.; Sonnenberg, J. L.; Williams-Young, D.; Ding, F.; Lipparini, F.; Egidi, F.; Goings, J.; Peng, B.; Petrone, A.; Henderson, T.; Ranasinghe, D.; Zakrzewski, V. G.; Gao, J.; Rega, N.; Zheng, G.; Liang, W.; Hada, M.; Ehara, M.; Toyota, K.; Fukuda, R.; Hasegawa, J.; Ishida, M.; Nakajima, T.; Honda, Y.; Kitao, O.; Nakai, H.; Vreven, T.; Throssell, K.; Montgomery Jr., J. A.; Peralta, J. E.; Ogliaro, F.; Bearpark, M. J.; Heyd, J. J.; Brothers, E. N.; Kudin, K. N.; Staroverov, V. N.; Keith, T. A.; Kobayashi, R.; Normand, J.; Raghavachari, K.; Rendell, A. P.; Burant, J. C.; Iyengar, S. S.; Tomasi, J.; Cossi, M.; Millam, J. M.; Klene, M.; Adamo, C.; Cammi, R.; Ochterski, J. W.; Martin, R. L.; Morokuma, K.; Farkas, O.; Foresman, J. B.; Fox, D. J. *Gaussian 16 Rev. C.01*, Wallingford, CT, 2016.

179. Grimme, S.; Ehrlich, S.; Goerigk, L., Effect of the damping function in dispersion corrected density functional theory. *J. Comput. Chem.* **2011**, *32*, 1456-1465.

180. Weigend, F.; Ahlrichs, R., Balanced basis sets of split valence, triple zeta valence and quadruple zeta valence quality for H to Rn: Design and assessment of accuracy. *Phys. Chem. Chem. Phys.* **2005**, *7*, 3297-3305.

181. Glendening, E. D.; Landis, C. R.; Weinhold, F., NBO 6.0: Natural bond orbital analysis program. *J. Comput. Chem.* **2013**, *34*, 1429-1437.

182. Rahalkar, A.; Stanger, A. Aroma. https://chemistry.technion.ac.il/members/amnon-stanger/.

183. Stanger, A., Obtaining Relative Induced Ring Currents Quantitatively from NICS. *J. Org. Chem.* **2010**, *75*, 2281-2288.

184. Gershoni-Poranne, R.; Stanger, A., The NICS-XY-Scan: Identification of Local and Global Ring Currents in Multi-Ring Systems. *Chem. Eur. J.* **2014**, *20*, 5673-5688.

185. Lee, C.; Yang, W.; Parr, R. G., Development of the Colle-Salvetti correlation-energy formula into a functional of the electron density. *Phys. Rev. B* **1988**, *37*, 785-789.

186. Becke, A. D., Density-functional thermochemistry. III. The role of exact exchange. *J. Chem. Phys.* **1993**, *98*, 5648-5652.

187. Beller, M.; Seayad, J.; Tillack, A.; Jiao, H., Catalytic Markovnikov and anti-Markovnikov Functionalization of Alkenes and Alkynes: Recent Developments and Trends. *Angew. Chem. Int. Ed.* **2004**, *43*, 3368-3398.

188. Rodriguez-Ruiz, V.; Carlino, R.; Bezzenine-Lafollée, S.; Gil, R.; Prim, D.; Schulz, E.; Hannedouche, J., Recent developments in alkene hydro-functionalisation promoted by homogeneous catalysts based on earth abundant elements: formation of C–N, C–O and C–P bond. *Dalton Trans.* **2015**, *44*, 12029-12059.

189. Liu, C.; Bender, C. F.; Han, X.; Widenhoefer, R. A., Platinum-catalyzed hydrofunctionalization of unactivated alkenes with carbon, nitrogen and oxygen nucleophiles. *Chem. Commun.* **2007**, 3607-3618.

190. Chen, J.; Lu, Z., Asymmetric hydrofunctionalization of minimally functionalized alkenes *via* earth abundant transition metal catalysis. *Org. Chem. Front.* **2018**, *5*, 260-272.

191. Obligacion, J. V.; Chirik, P. J., Earth-abundant transition metal catalysts for alkene hydrosilylation and hydroboration. *Nat. Rev. Chem.* **2018**, *2*, 15-34.

192. Li, G.; Huo, X.; Jiang, X.; Zhang, W., Asymmetric synthesis of allylic compounds *via* hydrofunctionalisation and difunctionalisation of dienes, allenes, and alkynes. *Chem. Soc. Rev.* **2020**, *49*, 2060-2118.

193. Wang, X.-X.; Lu, X.; Li, Y.; Wang, J.-W.; Fu, Y., Recent advances in nickel-catalyzed reductive hydroalkylation and hydroarylation of electronically unbiased alkenes. *Sci. China Chem.* **2020**, *63*, 1586-1600.

194. Burgess, K.; Ohlmeyer, M. J., Transition-Metal-Promoted Hydroborations of Alkenes, Emerging Methodology for Organic Transformations. *Chem. Rev.* **1991**, *91*, 1179-1191.

195. Tamang, S. R.; Bedi, D.; Shafiei-Haghighi, S.; Smith, C. R.; Crawford, C.; Findlater, M., Cobalt-Catalyzed Hydroboration of Alkenes, Aldehydes, and Ketones. *Org. Lett.* **2018**, *20*, 6695-6700.

196. Bismuto, A.; Cowley, M. J.; Thomas, S. P., Aluminum-Catalyzed Hydroboration of Alkenes. *ACS Catal.* **2018**, *8*, 2001-2005.

197. Beletskaya, I.; Pelter, A., Hydroborations Catalysed by Transition Metal Complexes. *Tetrahedron* **1997**, *53*, 4957-5026.

198. Thomas, S. P.; Aggarwal, V. K., Asymmetric Hydroboration of 1,1-Disubstituted Alkenes. *Angew. Chem. Int. Ed.* **2009**, *48*, 1896-1898.

199. Tamang, S. R.; Findlater, M., Emergence and Applications of Base Metals (Fe, Co, and Ni) in Hydroboration and Hydrosilylation. *Molecules* **2019**, *24*, 3194.

200. DiBenedetto, T. A.; Parsons, A. M.; Jones, W. D., Markovnikov-Selective Hydroboration of Olefins Catalyzed by a Copper N-Heterocyclic Carbene Complex. *Organometallics* **2019**, *38*, 3322-3326.

201. Bosnich, B., Asymmetric Catalysis. A Comparative Study of the Mechanisms of Intramolecular Hydroacylation and Hydrosilation. *Acc. Chem. Res.* **1998**, *31*, 667-674.

202. Pérez, M.; Hounjet, L. J.; Caputo, C. B.; Dobrovetsky, R.; Stephan, D. W., Olefin Isomerization and Hydrosilylation Catalysis by Lewis Acidic Organofluorophosphonium Salts. *J. Am. Chem. Soc.* **2013**, *135*, 18308-18310.

203. Andrews, R. J.; Chitnis, S. S.; Stephan, D. W., Carbonyl and olefin hydrosilylation mediated by an air-stable phosphorus(III) dication under mild conditions. *Chem. Commun.* **2019**, *55*, 5599-5602.

204. Du, X.; Huang, Z., Advances in Base-Metal-Catalyzed Alkene Hydrosilylation. *ACS Catal.* **2017**, *7*, 1227-1243.

205. Müller, T. E.; Beller, M., Metal-Initiated Amination of Alkenes and Alkynes. *Chem. Rev.* **1998**, *98*, 675-703.

206. Huang, L.; Arndt, M.; Gooßen, K.; Heydt, H.; Gooßen, L. J., Late Transition Metal-Catalyzed Hydroamination and Hydroamidation. *Chem. Rev.* **2015**, *115*, 2596-2697.

207. Streiff, S.; Jérôme, F., Hydroamination of non-activated alkenes with ammonia: a holy grail in catalysis. *Chem. Soc. Rev.* **2021**, *50*, 1512-1521.

208. Hannedouche, J.; Schulz, E., Asymmetric Hydroamination: A Survey of the Most Recent Developments. *Chem. Eur. J.* **2013**, *19*, 4972-4985.

209. Barreiro, E. M.; Adrio, L. A.; Hii, K. K. M.; Brazier, J. B., Coinage Metal Catalysts for the Addition of O–H to C=C Bonds. *Eur. J. Org. Chem.* **2013**, 1027-1039.

210. Xie, W.-B.; Li, Z., Asymmetric Synthesis of Ethers by Catalytic Alkene Hydroalkoxylation. *Synthesis* **2020**, *52*, 2127-2146.

211. Willis, M. C., Transition Metal Catalyzed Alkene and Alkyne Hydroacylation. *Chem. Rev.* **2010**, *110*, 725-748.

212. Pei, T.; Widenhoefer, R. A., Palladium-Catalyzed Intramolecular Addition of 1,3-Diones to Unactivated Olefins. *J. Am. Chem. Soc.* **2001**, *123*, 11290-11291.

213. DiRocco, D. A.; Rovis, T., Organocatalytic Hydroacylation of Unactivated Alkenes. *Angew. Chem. Int. Ed.* **2011**, *50*, 7982-7983.

214. Murphy, S. K.; Dong, V. M., Enantioselective hydroacylation of olefins with rhodium catalysts. *Chem. Commun.* **2014**, *50*, 13645-13649.

215. Espelt, L. R.; Wiensch, E. M.; Yoon, T. P., Brønsted Acid Cocatalysts in Photocatalytic Radical Addition of α-Amino C−H Bonds across Michael Acceptors. *J. Org. Chem.* **2013**, *78*, 4107-4114.

216. Chen, X.; Rao, W.; Yang, T.; Koh, M. J., Alkyl halides as both hydride and alkyl sources in catalytic regioselective reductive olefin hydroalkylation. *Nat. Commun.* **2020**, *11*, 5857.

217. Andreatta, J. R.; McKeown, B. A.; Gunnoe, T. B., Transition metal catalyzed hydroarylation of olefins using unactivated substrates: Recent developments and challenges. *J. Organomet. Chem.* **2011**, *696*, 305-315.

218. Wang, Z.-X.; Bai, X.-Y.; Li, B.-J., Recent Progress of Transition-Metal-Catalyzed Enantioselective Hydroalkynylation of Alkenes. *Synlett* **2017**, *28*, 509-514.

219. Shirakura, M.; Suginome, M., Nickel-Catalyzed Regioselective Hydroalkynylation of Styrenes: Improved Catalyst System, Reaction Scope, and Mechanism. *Org. Lett.* **2009**, *11*, 523-526.

220. Bai, X.-Y.; Wang, Z.-X.; Li, B.-J., Iridium-Catalyzed Enantioselective Hydroalkynylation of Enamides for the Synthesis of Homopropargyl Amides. *Angew. Chem. Int. Ed.* **2016**, *55*, 9007-9011.

221. Fan, B.-M.; Yang, Q.-j.; Hu, J.; Fan, C.-l.; Li, S.-f.; Yu, L.; Huang, C.; Tsang, W. W.; Kwong, F. Y., Asymmetric Hydroalkynylation of Norbornadienes Promoted by Chiral Iridium Catalysts. *Angew. Chem. Int. Ed.* **2012**, *51*, 7821-7824.

222. Braunschweig, H.; Hörl, C., Unexpected cluster formation upon hydroboration of a neutral diborene with 9-BBN. *Chem. Commun.* **2014**, *50*, 10983-10985.

223. Brückner, T.; Heß, M.; Stennett, T. E.; Rempel, A.; Braunschweig, H., Synthesis of Boron Analogues of Enamines via Hydroamination of a Boron-Boron Triple Bond. *Angew. Chem. Int. Ed.* **2021**, *60*, 736-741.

224. Brückner, T.; Stennett, T. E.; Heß, M.; Braunschweig, H., Single and Double Hydroboration of B−B Triple Bonds and Convergent Routes to a Cationic Tetraborane. *J. Am. Chem. Soc.* **2019**, *141*, 14898-14903.

225. Stennett, T. E.; Jayaraman, A.; Brückner, T.; Schneider, L.; Braunschweig, H., Hydrophosphination of boron–boron multiple bonds. *Chem. Sci.* **2020**, *11*, 1335-1341.

226. Braunschweig, H.; Dewhurst, R. D.; Hörl, C.; Phukan, A. K.; Pinzner, F.; Ullrich, S., Direct Hydroboration of B=B Bonds: A Mild Strategy for the Proliferation of B-B Bonds. *Angew. Chem. Int. Ed.* **2014**, *53*, 3241-3244.

227. Hoefelmeyer, J. D.; Solé, S.; Gabbaï, F. P., Reactivity of the dimesityl-1,8-naphthalenediylborate anion: isolation of the borataalkene isomer and synthesis of 1,8-diborylnaphthalenes. *Dalton Trans.* **2004**, 1254-1258.

228. Pardasani, R. T., Studies on the Synthesis and Properties of Boron Stabilised Carbanions. *J. Indian Chem. Soc.* **1997**, *74*, 433-439.

229. Pelter, A.; Vaughan-Williams, G. F.; Rosser, R. M., Hindered Organoboron Groups in Organic Chemistry. 21. The Reactions of Dimesitylboron Stabilised Carbanions with Oxiranes. *Tetrahedron* **1993**, *49*, 3007-3034.

230. Bartholome, T. A.; Kaur, A.; Wilson, D. J. D.; Dutton, J. L.; Martin, C. D., The 9-Borataphenanthrene Anion. *Angew. Chem. Int. Ed.* **2020**, *59*, 11470-11476.

231. A cyclic alkyl amino carbene (CAAC)-borylene adduct that has allenic character and can be described as a B=C bond was shown to undergo hydrogenation with H_2 in the following paper: Dahcheh, F.; Martin, D.; Stephan, D. W.; Bertrand, G., Synthesis and Reactivity of a CAAC–Aminoborylene Adduct: A Hetero-Allene or an Organoboron Isoelectronic with Singlet Carbenes, *Angew. Chem. Int. Ed.*, **2014**, *53*, 13159-13163.

232. Hitchcock, P. B.; Lappert, M. F.; Liu, D.-S., Transformation of the Bis(trimethylsilyl)methyl into Aza-allyl and β-Diketinimato Ligands; the X-Ray Structures of $[Li\{N(R)C(Bu^t)CH(R)\}]_2$ and $[Zr\{N(R)C(Bu^t)CHC(Ph)N(R)\}Cl_3]$(R = $SiMe_3$). *J. Chem. Soc., Chem. Commun.* **1994**, 2637-2638.

233. Hitchcock, P. B.; Lappert, M. F.; Layh, M., Synthesis and structures of tin(II) and lead(II) 1-aza-allyls; the $[N(SiMe_3)C(Ph)C(SiMe_3)_2]^-$ ligand. *Inorg. Chim. Acta* **1998**, *269*, 181-190.

234. While the presence of impurities in the crude product indicates that the occurrence of C-F activation in the reaction with C_6F_5H cannot be ruled out, compound **4.2** was found to be the clear major product by ^1H, $^{19}F\{^1H\}$, and ^{11}B NMR spectroscopy.

235. Compound A was dissolved in THF, 1,4-dioxane, and dimethoxyethane and showed no reaction at room temperature over 24 h. THF solutions of **3.4** did not show any signs of reaction with H_2 and 2,3,4,5,6-pentafluorotoluene at room temperature over 24 h.

236. Matthews, W. S.; Bares, J. E.; Bartmess, J. E.; Bordwell, F. G.; Cornforth, F. J.; Drucker, G. E.; Margolin, Z.; McCallum, R. J.; McCollum, G. J.; Vanier, N. R., Equilibrium Acidities of Carbon Acids. VI. Establishment of an Absolute Scale of Acidities in Dimethyl Sulfoxide Solution. *J. Am. Chem. Soc.* **1975**, *97*, 7006-7014.

237. Bordwell, F. G.; Branca, J. C.; Hughes, D. L.; Olmstead, W. N., Equilibria Involving Organic Anions in Dimethyl Sulfoxide and *N*-Methylpyrrolidin-2-one: Acidities, Ion Pairing, and Hydrogen Bonding. *J. Org. Chem.* **1980**, *45*, 3305-3313.

238. Olmstead, W. N.; Margolin, Z.; Bordwell, F. G., Acidities of Water and Simple Alcohols in Dimethyl Sulfoxide Solution. *J. Org. Chem.* **1980**, *45*, 3295-3299.

239. Bordwell, F. G.; McCallum, R. J.; Olmstead, W. N., Acidities and Hydrogen Bonding of Phenols in Dimethyl Sulfoxide. *J. Org. Chem.* **1984**, *49*, 1424-1427.

240. Bordwell, F. G.; Drucker, G. E.; Andersen, N. H.; Denniston, A. D., Acidities of Hydrocarbons and Sulfur-Containing Hydrocarbons in Dimethyl Sulfoxide Solution. *J. Am. Chem. Soc.* **1986**, *108*, 7310-7313.

241. Shen, K.; Fu, Y.; Li, J.-N.; Liu, L.; Guo, Q.-X., What are the pK_a values of C–H bonds in aromatic heterocyclic compounds in DMSO? *Tetrahedron* **2007**, *63*, 1568-1576.

242. Becke, A. D., A new mixing of Hartree–Fock and local density-functional theories. *J. Chem. Phys.* **1993**, *98*, 1372-1377.

243. Grimme, S.; Antony, J.; Ehrlich, S.; Krieg, H., A consistent and accurate ab initio parametrization of density functional dispersion correction (DFT-D) for the 94 elements H-Pu. *J. Chem. Phys.* **2010**, *132*, 154104.

244. Marenich, A. V.; Cramer, C. J.; Truhlar, D. G., Universal Solvation Model Based on Solute Electron Density and on a Continuum Model of the Solvent Defined by the Bulk Dielectric Constant and Atomic Surface Tensions. *J. Phys. Chem. B* **2009**, *113*, 6378-6396.

245. Marenich, A. V.; Jerome, S. V.; Cramer, C. J.; Truhlar, D. G., Charge Model 5: An Extension of Hirshfeld Population Analysis for the Accurate Description of Molecular Interactions in Gaseous and Condensed Phases. *J. Chem. Theory Comput.* **2012**, *8*, 527-541.

246. Chai, J.-D.; Head-Gordon, M., Long-range corrected hybrid density functionals with damped atom–atom dispersion corrections. *Phys. Chem. Chem. Phys.* **2008**, *10*, 6615-6620.

247. The portions of this chapter detailing the syntheses of **5.5** and **5.7** are to be included in the following manuscript: Rojales, K.; Bartholome, T. A.; Martin, C. D., Evaluating the Donor Abilities of Boratabenzene and 9-Borataphenanthrene Ligands.

248. Giordano, G.; Crabtree, R. H., Di-μ-Chloro-Bis(η^4-1,5-Cyclooctadiene)-Dirhodium(I). *Inorg. Synth.* **1990**, *28*, 88-90.

249. $Rh_2Cl_2(cod)_2$ was obtained courtesy of Dr. F. Gordon A. Stone

250. Herde, J. L.; Lambert, J. C.; Senoff, C. V., Cyclooctene and 1,5-Cyclooctadiene Complexes of Iridium(I). *Inorg. Synth.* **1974**, *15*, 18-20.

251. Wisofsky, G. K.; Rojales, K.; Su, X.; Bartholome, T. A.; Molino, A.; Kaur, A.; Wilson, D. J. D.; Dutton, J. L.; Martin, C. D., Coordination of Boratabenzene and 9-Borataphenanthrene to Coinage Metals. *Unpublished work*.

252. Spek, A. L., *PLATON* SQUEEZE: a tool for the calculation of the disordered solvent contribution to the calculated structure factors. *Acta Cryst.* **2015**, *C71*, 9-18.

253. Zhukhovitskiy, A. V.; Kobylianskii, I. J.; Wu, C.-Y.; Toste, F. D., Migratory Insertion of Carbenes into Au(III)-C Bonds. *J. Am. Chem. Soc.* **2018**, *140*, 466-474.

254. Sheldrick, G. M., A short history of SHELX. *Acta Cryst.* **2008**, *A64*, 112-122.

255. Dolomanov, O. V.; Bourhis, L. J.; Gildea, R. J.; Howard, J. A. K.; Puschmann, H., OLEX2: a complete structure solution, refinement and analysis program. *J. Appl. Crystallogr.* **2009**, *42*, 339-341.